Sulfur Release during Alternative fuels Combustion in Cement Rotary Kilns

Cortada Mut, Maria del Mar; Dam-Johansen, Kim; Glarborg, Peter; Nørskov, Linda Kaare

Publication date:
2014

Document Version
Publisher's PDF, also known as Version of record

Sulfur Release during Alternative Fuels Combustion in Cement Rotary Kilns

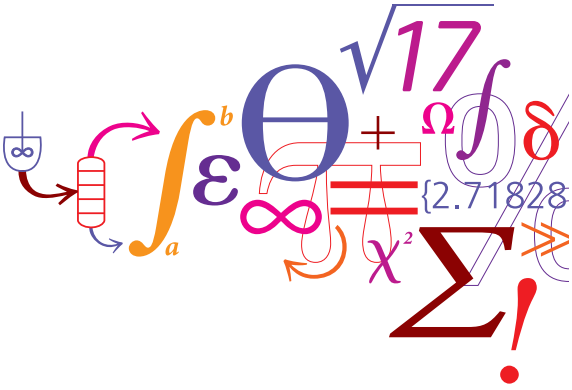

Maria del Mar Cortada Mut

Ph.D. Thesis

August 2014

Sulfur Release during Alternative Fuels Combustion in Cement Rotary Kilns

Maria del Mar Cortada Mut

Ph.D. Thesis

August, 2014

DTU Chemical Engineering
Department of Chemical and Biochemical Engineering

Address: Centre of Combustion and Harmful Emission Control
Department of Chemical and
Biochemical Engineering
Technical University of Denmark
Søltofts Plads, Building 229
DK-2800 Kgs. Lyngby
Denmark
Phone: +45 4525 2800
Fax: +45 4525 4588
Web: www.chec.kt.dtu.dk

Print: J&R Frydenberg A/S
København
November 2014

ISBN: 978-87-93054-48-6

Preface

This dissertation summarizes the outcome of 3 years of research and is submitted partial fulfillment of the requirements for obtaining the Ph.D. degree at the Technical University of Denmark (DTU). The work has been carried out at the research center CHEC at the Department of Chemical and Biochemical Engineering at the Technical University of Denmark (DTU) in close collaboration with FLSmidth A/S. The project is part of the research platform "New Cement Production Technology", financially supported by the Technical University of Denmark, FLSmidth A/S, and The Danish National Advanced Technology Foundation.

First of all, I would like to thank my supervisors Kim Dam-Johansen (DTU), Peter Glarborg (DTU) and Linda Kaare Nørskov (FLSmidth A/S) for their guidance and support during the supervision of this project. Thanks also to Anders Rooma Nielsen and Kim Hougaard Pedersen, who were involved in the supervision at some point during the 3 years. I would like to express my gratitude to all of them for their time, ideas, feedback, support, and fruitful discussions during the project.

Furthermore, I would like to thank current and former employees from DTU and FLSmidth that directly or indirectly have been involved in the project, especial thanks to Flemming Frandsen, Stig Wedel, and Ebbe Jøns for their help, patience, and knowledge sharing. Thanks to Erik Benzen for the collaboration and the great opportunity, and to his team for their assistance taking samples. Thanks to the PhD comics, which are always true in a cheer up way, and to the participants in 8th CemFuels conference for the big interest in my project, which gave me extra motivation to complete this project. Thanks to Søren Henkel and Tobias Hansen for their contribution to the project, to Nezam Azizaddini for the help with some figures, to the CHEC technicians group, the workshop at DTU and to the people at FLSmidth's research center Dania and Valby, who have also been involved and helped in this project.

Finally, I would also like to thank to the Ph.D. students at CHEC, especially David Bøgh, Claus Maarup, and Thomas Klint, for providing a pleasant working atmosphere, and of course for enjoyable lunches, fruitful discussions, and the social activities we have had.

At last but not least, thanks to my family and friends for all their support through the last 3 years, *Moltes Gràcies!*, and big thanks to Per, who has been there in all moments.

Maria del Mar Cortada Mut

Kgs. Lyngby, August 2014.

Abstract

Cement production is an energy-intensive process, which has traditionally been dependent on fossil fuels. However, the usage of selected waste, biomass, and by-products with recoverable calorific value, defined as alternative fuels, is increasing and their combustion is more challenging compared to fossil fuels, due to the lack of experience in handling the different and varying combustion characteristics caused by different chemical and physical properties, e.g. higher moisture content and larger particle sizes.

When full combustion of alternative fuels in the calciner and/or main burner is not achieved, partially or unburned solid fuels may drop into the material bed in direct contact with the bed material of the rotary kiln. The combustion of alternative fuels in direct contact with the bed material of the rotary kiln causes local reducing conditions and may alter the input and the behavior of minor elements into the kiln system.

The minor elements of concern are sulfur, chlorine, sodium, and potassium, which are known to be circulating or volatile elements in the kiln system. Compounds containing these elements evaporate, when exposed to high temperatures, and may subsequently condense in cooler parts of the plant. High internal circulation seriously affects the process stability and operation of the cement kiln system, such as material build-ups in the cyclones and/or in the rotary kiln as rings, and on a longer time-scale by shell corrosion.

This thesis provides a detailed analysis of the circulation of the volatile elements and the transformation of different species containing these elements at different locations in the cement plant. This is complemented by thermodynamic calculations for a better understanding of the inorganic chemistry in the rotary kiln. The main focus is given to SO_2 release due to decomposition of calcium sulfate in the kiln inlet and the modification of the sulfur circulation during alternative fuel combustion, because sulfur is the most affected element by reducing combustion conditions.

Sulfur release from cement raw materials during alternative fuel combustion is experimentally investigated using pine wood and tire rubber particles in a pilot scale set-up, which is able to simulate the process conditions in the material inlet end of an industrial rotary kiln. The SO_2 release increases with decreasing fuel particle size, oxygen content in the freeboard gas, and increasing sulfur content in the bed material. Experiments with wood with different degree of volatiles show that the sulfur release mainly takes place during devolatilization. This is supported by the finding of the industrial investigation on sulfur released, where no clear relationship is observed between the carbon from the fuel, mainly expected to be in the form of char, entering in the rotary kiln and the sulfur recirculation.

The effect of different concentrations and binary mixtures of the main reducing agents released from fuels on sulfur release are investigated experimentally in order to separate the influence of the simultaneous phenomena occurring in the experimental set-up, such as mixing the fuel with the bed material, heating up of a particle,

devolatilization, char combustion, the reactions between $CaSO_4$ and the different reducing agents, and the oxidation of the volatiles gases in the freeboard. The main reducing agents are CO, CH_4 and H_2, which are introduced under the bed material in the high temperature rotary drum to characterize the SO_2 release under variation of temperature, oxygen content in the gas, and time of exposure. A threshold concentration for each reducing gas, below which no SO_2 release occurs, is found. The reducing concentration and the time of exposure are of high importance for SO_2 release because it is shown that introducing the same total amount of gas, the highest reducing agent concentration for a short period released a higher total SO_2 amount compared to the lowest concentration during a long period.

A mathematical reaction based model for predicting sulfur release caused by volatiles from wood particles fired in the material kiln inlet is developed and evaluated against pilot scale data, which shows that the model follows the experimental data tendency. The model can predict SO_2 release varying particle size, fill degree, and firing degree but the effect of sulfur content in the bed cannot be predicted. Further development regarding particle motion according to the rotational speed may be needed. Furthermore, a model for predicting the tendency of build-ups for a kiln system is developed based on the prediction of SO_3 and Cl concentrations in the hot meal. The predictions can be performed for a kiln system operating only with fuel in the calciner and kiln burner, and the influence of bypass operation can be added as well as alternative fuels substitution in the kiln inlet.

The sulfur release in the inlet of the rotary kiln can be minimized if the fuel combustion takes place at temperatures lower than 800 ^{o}C and can be avoided when the volatile gases from fuels are not released in contact with the bed material.

Dansk resumé

Cementproduktion er en energikrævende proces, som traditionelt har været afhængig af fossile brændstoffer. Brugen af udvalgt affald, biomasse og biprodukter med genindvindingsværdi, defineret som alternative brændstoffer, er imidlertid stigende, og forbrændingen er mere udfordrende end fossile brændsel, på grund af manglende erfaring i håndtering af den anderledes og varierende udbrændingskarakteristik, som skyldes forskellige kemiske og fysiske egenskaber, f.eks. højere vandindhold og større partikelstørrelser.

Ved ufuldstændig forbrænding af brændsler i kalcineren og/eller brænderen, kan uforbrændt eller delvis udbrændt brændsler havne i roterovnsfyldningen i direkte kontakt med fyldningsmaterialet. Forbrænding af alternative brændsler i direkte kontakt med roterovnens fyldningsmateriale medfører lokale reducerende betingelser og kan ændre input og adfærd af mindre elementer i ovnsystemet. Disse elementer, er svovl, klor, natrium og kalium, som er kendt for at cirkulere i ovnsystemet pga. deres flygtighed. Forbindelser, der indeholder disse elementer, fordamper når de udsættes for høje temperaturer, og kan senere kondensere i køligere dele af anlægget. En høj intern cirkulation kan skade processtabiliteten og driften alvorligt i form af materialeopbygninger, ringdannelse og på længere sigt ved ovnskalskorrosion.

Denne afhandling indeholder en detaljeret beskrivelse af cirkulationen af de flygtige elementer og omdannelsen af forskellige forbindelser af disse elementer under fremstillingen af klinker. Dette suppleres af termodynamiske beregninger for forbedret forståelse af den uorganiske kemi i roterovnen. Resultaterne stemmer godt overens med stabiliteten af sulfater i roterovnens ovnindløb beskrevet i litteraturen. Afhandlingen fokuserer på SO_2 frigivelse på grund af nedbrydning af kalciumsulfat i ovnindløb og ændring af svovlcirkulationen ved forbrænding af alternative brændsler, fordi svovl er det mest påvirkede element under reducerende forbrændingsbetingelser.

Svovlfrigivelse fra cement råmaterialer under forbrænding af alternative brændsler, repræsenteret af fyrretræ og gummipartikler af dæk, er undersøgt eksperimentelt i en pilotskala opstilling, som er i stand til at simulere procesbetingelserne i materieindløbet af en industriel roterovn. SO_2 frigivelsen stiger med faldende brændeselpartikelstørrelse, iltindhold i atmosfæren og stigende indhold af svovl i fyldningsmaterialet. Forsøg med træ med forskellig indhold af flygtige stoffer viste, at frigivelsen af svovl hovedsageligt fandt sted under afgasningen. Dette er i god overensstemmelse med resultaterne af den industrielle undersøgelse om frigivelse af svovl udført i dette projekt, hvor ingen direkte sammenhæng mellem kulstof fra brændsel, hovedsagelig forventet at være i form af koks, som ender i ovnindløbet og svovlcirkulationen kunne påvises.

Virkningen af forskellige koncentrationer af de vigtigste reduktionsmidler og binære blandinger heraf som frigøres fra brændstoffer er undersøgt eksperimentelt for at adskille indflydelsen af de samtidige fænomener i den eksperimentelle opsætning, såsom opblanding af brændstoffet med fyldningsmaterialet,

partikelopvarmning, pyrolyse, koksforbrænding, reaktionerne mellem $CaSO_4$ og de forskellige reduktionsmidler, og oxidation af flygtige gasser i gasfasen. De vigtigste reduktionsmidler er CO, CH_4 og H_2, som blev indført under fyldningsmaterialet i en roterende højtemperaturtromle for at karakterisere SO_2 frigivelse under varierende temperaturer, iltindhold og eksponeringstid. En grænseværdi for koncentrationen af hver reducerende gas, hvorunder der ikke forekommer SO_2 frigivelse, blev fundet. Koncentration af den reducerende specie og eksponeringstiden er af stor betydning for den totale SO_2 frigivelse, fordi det blev påvist ved indførelse af den samme samlede mængde gas, at en høj reducerende koncentration i løbet af en kort periode medførte en højere samlet SO_2 frigivelse i forhold til en lav koncentration i en længere periode.

En matematisk reaktionsbaseret model til forudsigelse af svovlfrigivelse forårsaget af flygtige stoffer fra træpartikler fyret i ovnindløbet er blevet udviklet og valideret mod pilotskala data, hvilket viste, at modellen følger tendensen for de eksperimentelle data. Modellen kan forudsige SO_2 frigivelse for varierende partikelstørrelse, fyldningsgrad og fyringsgrad, men effekten af svovlindholdet i fyldningen kan ikke forudsiges. Yderligere udvikling vedrørende partikelbevægelse som funktion af rotationshastigheden kan være nødvendig. Herudover er en model til forudsigelse af materialeopbygningstendens for en ovn blevet udviklet, baseret på forudsigelse af SO_3 og Cl koncentrationer i ovnindløbsmaterialet. Forudsigelserne kan udføres for et ovnsystem med brændselsfyring kun i kalcinatoren og roterovnensbrænderen, og derudover kan indflydelsen af bypass og alternative brændslesfyring i ovnindløbet tilføjes.

Svovlfrigivelsen i ovnindløbet af roterovnen kan minimeres, hvis forbrændingen sker ved temperature lavere end 800 ^oC, og kan udgås hvis afgasningen af de flygtige forbindelser fra brændslerne ikke sker i direkte kontakt med fyldningsmaterialet.

Table of Contents

1. Introduction 1

1.1 Background 1

1.2 Project Objectives 2

1.3 Structure of the Ph.D. Thesis 2

1.4 References 3

2. Cement Chemistry and Production 5

2.1 Introduction 5

2.2 Cement Chemistry 5

2.2.1 Raw Materials 6

2.2.2 Calcination 6

2.2.3 Clinker Reactions 7

2.3 Cement Production 8

2.3.1 Preparation of Raw Materials 9

2.3.2 Pyro Processing 10

2.3.3 Clinker Processing 12

2.3.4 Process Data Overview 12

2.4 Conclusions 13

2.5 References 13

3. Alternatives Fuels in the Cement Production 17

3.1 Introduction 17

3.2 Combustion of Alternative Fuels 21

3.2.1 Combustion Studies of Alternative Fuels 24

3.2.2 Volatile Gases from Fuels 25

3.3 Technologies for Alternative Fuels Combustion 28

3.3.1 External reactors 29

3.3.2 Kiln burners 30

3.3.3 Emerging technologies 31

3.4 Conclusions 32

3.5 References 33

4. Circulation of Inorganic Elements in the Kiln System 39

4.1 Circulation of Volatiles Elements 39

4.1.1 Reaction Affinity between Volatile Elements 40

4.1.2 Circulation of Sulfur ... 40
4.1.3 Circulation of Chlorine ... 47
4.1.4 Circulation of Alkalis ... 50
4.2 Consequences of High Volatile Circulation ... 53
4.2.1 Deposit Build-up Formation ... 53
4.2.2 Coating and Ring Formation in Rotary Kilns ... 57
4.2.3 Shell Corrosion and Refractory Deterioration ... 61
4.3 Circulation of Volatile Elements due to Combustion of Alternative Fuels ... 63
4.3.1 Introduction or Increase of Elements in the Cement Chemistry ... 64
4.3.2 Local Reducing Conditions ... 64
4.3.3 Increase of Circulation Phenomena in the Kiln System ... 65
4.4 Thermodynamic Calculations ... 67
4.4.1 System considering inorganic chemistry with clinker chemistry ... 67
4.4.2 System considering inorganic chemistry ... 71
4.4.3 Concluding Remarks about Thermodynamic Equilibrium Calculations ... 78
4.5 Conclusions ... 79
4.6 References ... 80
5. Sulfur Release during Combustion of Alternative Fuels Particles ... 87
5.1 Literature Study on Sulfur Release in the Kiln System ... 87
5.1.1 Phase Diagrams for $CaSO_4$-CaO-CaS system ... 87
5.1.2 Sulfur Release during Combustion of Solid Fuels ... 89
5.1.3 Pre-experimental Considerations ... 92
5.2 Experimental ... 93
5.2.1 Experimental Set-up ... 93
5.2.2 Experimental Method ... 95
5.2.3 Fuel Samples ... 96
5.2.4 Wood Char Preparation ... 97
5.3 Results and Discussion ... 98
5.3.1 General Observations ... 98
5.3.2 Effect of Particle Size of Different Fuel Types ... 100
5.3.3 Effect of Degree of Devolatilization of Wood Particles ... 103
5.3.4 Effect of Sulfur Concentration in the Bed Material ... 107
5.3.5 Effect of Moisture Content ... 108
5.3.6 Discussion ... 110
5.4 Conclusions ... 111
5.5 References ... 111

6. Effect of Different Pyrolized Gases on Sulfur Release 115
6.1 Literature Study of the $CaSO_4$ Reductive Decomposition 115
6.1.1 Carbon Monoxide 115
6.1.2 Hydrogen 118
6.1.3 Methane 118
6.1.4 Alternating Oxidizing and Reducing conditions 119
6.1.5 Pre-experimental Considerations 120
6.2 Experimental 121
6.3 Results and Discussion 122
6.3.1 Carbon Monoxide 123
6.3.2 Methane 132
6.3.3 Hydrogen 135
6.3.4 Carbon Monoxide, Hydrogen, and Methane Comparison 141
6.3.5 Binary Mixtures 143
6.3.6 Thermal Decomposition of $CaSO_4$ 146
6.4 Conclusions 146
6.5 References 147
7. Modeling the Sulfur Release in the Inlet of the Rotary Kiln 151
7.1 Literature Study on Rotary Kiln Models for the Cement Industry 151
7.1.1 Review of Rotary Kilns Models 151
7.1.2 Kiln System Models including Alternative Fuels Usage 152
7.2 System Description and Modeling approach 154
7.3 Assumptions 156
7.4 Mathematical Development 157
7.4.1 Calculation of the Particle Temperature Profile 157
7.4.2 Calculation of Pyrolysis 158
7.4.3 Rotary Kiln Model 158
7.5 Results 162
7.5.1 Substitution 10 % Energy with Alternative Fuels fired in the Kiln Inlet 162
7.5.2 Effect of Firing Degree in the Kiln Inlet 171
7.5.3 Sensitivity analysis 172
7.6 Model Validation 173
7.7 Conclusions 177
7.8 References 178

8. Model on Build-ups Tendency in the Kiln System 183
8.1 Introduction 183
8.2 Kiln System without Alternative Fuel Substitution in the Kiln Inlet 185
8.2.1 Model Development 185
8.2.2 Results 188
8.3 Kiln System with Alternative Fuel Substitution in the Kiln Inlet 191
8.3.1 Model Modification 191
8.3.2 Results 193
8.4 Model Limitations 195
8.5 Conclusions 195
8.6 References 196
9. Industrial Experience on Sulfur Release 197
9.1 Background 197
9.2 Gas Measurements 200
9.2.1 Comparison between Two Measurements Systems 200
9.3 Investigation of Sulfur Evaporation on the Process 205
9.3.1 Fuel Conversion in the Calciner 208
9.3.2 Tendency of Build-ups 210
9.3.3 Sulfur Volatility 211
9.4 Conclusions for the Industrial Experience and Challenges 212
10. Final Conclusions 215
10.1 Main Results and Conclusions 215
10.2 Recommendations 217
10.3 Suggestions for Future Work 219
10.4 References 219
List of Symbols 221
Appendixes 225
Appendix A: Equilibrium Calculations 227
Appendix B: Species included in the Thermodynamic Calculations 229
Appendix C: Data from the Experiments using Reducing Agents 233
Appendix D: Kinetic Studies of $CaSO_4$ Reductive Decomposition 239
Appendix E: $CaSO_4$ Particle Analysis 241
Appendix F: Mass balance in basis of loss of ignition free 243
Appendix G: Industrial gas measurement system principles 245

Appendix H: Clinker composition for the industrial investigation 247
Publication 249

1. Introduction

1.1 Background

Cement production is an energy-intensive process, which requires approximate 3 MJ/kg cement clinker produced, equivalent to 60-130 kg coal/ton of cement clinker depending on the type of coal (VDZ, 2009). The energy consumed by the cement industry is estimated to constitute about 2 % of the global primary energy consumption (Rubenstein, 2010; Worrell et al., 2001).

During the last decades, an interest in replacing fossil fuels with selected waste, biomass, and by-products with recoverable calorific value, defined as alternative fuels, has arisen in order to minimize production cost and due to environmental concerns (Lechtenberg and Diller, 2012). The introduction of alternative fuels is however not straight forward because it may influence emissions, product quality, process efficiency, and process stability of the cement production plant.

Furthermore, alternative fuels may be partly or fully CO_2-neutral, which may be important from an environmental point of view. The European cement industry recovers a substantial amount of waste-derived fuels, which replace fossil fuels up to a level of more than 80 % in some individual plants (European IPPC, 2013). The change in energy sources is illustrated in Figure 1-1 and Figure 1-2, which show the type of the fuels used in average by the cement industry in Europe in 1990 and 2011, respectively.

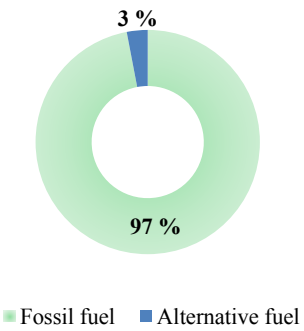

Figure 1-1: Percentage of fossil fuels and alternative fuels used in Europe in 1990 (CW Group, 2013).

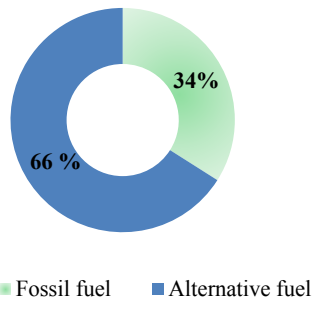

Figure 1-2: Percentage of fossil fuels and alternative fuels used in Europe in 2011 (CW Group, 2013).

In comparison with fossil fuels, alternative fuels typically consist of relatively large particles, which are difficult to downsize, and may have different chemical and physical properties. This will be elaborated in Chapter 3. Despite these differences, alternative fuels are fired at the traditional firing points of a cement plant (calciner and kiln burner) or directly in the rotary kiln. The combustion of alternative fuels at these location may have some consequences (Nielsen, 2011), which are:

- Direct physical contact between the solid fuel and the cement raw materials.
- Local reducing conditions in the material bed of the rotary kiln.
- Potential of increase internal circulation of sulfur, chlorine and alkali metal species.

These consequences lead to modification of process conditions and may affect the clinker quality and the process operation, causing build-ups, blockages, and/or corrosion.

1.2 Project Objectives

The main objective of this thesis is to obtain a scientifically based knowledge about the release of sulfur due to combustion of solid alternative fuels in cement production. This is achieved via a combination of theoretical considerations and experimental investigations coupled with mathematical modeling.

The main technical subject of this Ph.D. project has been to investigate the consequences of the combustion of solid alternative fuels on the process operation and process stability of a cement plant. The project has focused on the sulfur release from the bed material close to the inlet of the rotary kiln. The strategy is first to provide a detailed analysis of the inorganic chemistry in the kiln system and how it may be affected by utilization of alternative fuels in the material inlet end. Experiments with solid fuels and reducing gases have been conducted in a pilot-scale rotary drum in order to understand the behavior of the sulfur release at the inlet of the rotary kiln. The experimental data were also used for the validation of a mathematical model capable of qualitatively predicting the SO_2 release from the bed material. The tendency of build-ups when using alternative fuels can be predicted on basis of the model and consequently operational problems may be avoided.

The knowledge obtained may be used to improve the design basis of cement plants, redesign of existing technology or to develop new technology in order to minimize the sulfur release, and operational problems such as build-ups, due to the combustion of solid alternative fuels in the calciner and/or in the inlet of the rotary kiln.

1.3 Structure of the Ph.D. Thesis

Chapter 2 provides an introduction to the cement chemistry and production.

Chapter 3 introduces the general characteristics of alternative fuels in cement production and reviews the current status regarding combustion of solid alternative fuels and the available technologies.

The inorganic chemistry consisting of the volatile elements (S, Cl, K, and Na) in the kiln system is described in details in Chapter 4. The consequences related to the combustion of alternative fuels are also reviewed; special attention is given to the modification of the sulfur circulation. Furthermore, the inorganic chemistry along the rotary kiln is studied by thermodynamic equilibrium calculations.

Chapter 5 describes the experiments with sulfur release from raw materials during solid fuel combustion, focusing on fuel particle size, degree of fuel devolatilization, and moisture content.

Experiments quantifying the sulfur release from raw materials by introduction of CO, CH_4, and H_2, and their mixtures under the bed material are explained in Chapter 6.

Chapter 7 contains the development of a mathematical model for predicting sulfur release in the inlet of the rotary kiln. The results are further used to predict the tendency of build-ups, which is described in Chapter 8.

An analysis of industrial experience with focus on sulfur release is provided in Chapter 9. The chapter determines the calciner fuel conversion, the tendency of build-ups and the sulfur volatility. An analysis of the current challenges with monitoring and controlling sulfur release in the cement plants is also provided.

Finally, the overall conclusions regarding the sulfur release during combustion of alternative fuels in the rotary kiln material inlet end and suggestions for further work are provided in Chapter 10.

1.4 References

CW Group. Alternative fuels in Spain and in the rest of Europe. *CemWeek Magazine Issue 17.* October-November 2013. Available at http://www.cemweek.com/magazine/cemweek-magazine.

Lechtenberg, D., and Diller, H.; Alternative fuels and raw materials handbook for the cement and lime industry. MVW Lechtenberg & Partner, Düsseldorf, Germany. 2012. ISBN: 978-3-7640-0550-4.

Nielsen, A.R., Larsen, M.B., Glarborg, P., Dam-Johansen, K.; High-Temperature Release of SO_2 from Calcined Cement Raw Materials. Energy & Fuels, 25, 2917-2926, 2011.

Rubenstein, M.; The GNCS factsheets: Mitigating emissions from cement. Columbia Climate Cementer. Earth Institute, Columbia University, 2010.

VDZ (Verein Deutscher Zementwerke); Activity report 2007-2009. Available at http://www.vdz.de.

Worrell, E., Price, L., Martin, N., Hendriks, C., and Meida, L. O.; Carbon dioxide emissions from the global cement industry. Annual Review of Energy and the Environment, 26, 303-29, 2001.

European IPPC; Best available techniques (BAT) reference document for the production of cement, lime and magnesium oxide- European Integrated Pollution Prevention and Control Bureau. 2013.

2. Cement Chemistry and Production

This chapter seeks to provide a fundamental understanding of the cement chemistry and the cement production, which is necessary for the understanding of the subsequent chapters.

2.1 Introduction

Cement has been known as a binder material since ancient times, but the manufacturing process has evolved greatly since then. Nowadays, cement is one of the most important materials, used for production of concrete and mortar in the construction sector. Cement and mortar are used for bonding of natural and artificial aggregates in infrastructure and in many building materials (Cembureau, 2009). The most commonly used type of cement is the so-called Portland cement. Several other types of cement with other characteristics are also produced for specific purposes. However, this thesis will focus on the Portland cement.

The industrial production of cement started in the middle of the 19th century with the development of the continuous kiln. One of the first continuous kilns was the shaft kiln, which bears a high degree of resemblance to a blast furnace. In the end of the 19th century, the shaft kiln was replaced by the rotary kiln, which is still an important part of a modern cement plant (Schneider et al., 2011).

Cement production is a very energy-consuming process. The energy costs account typically for 30-40 % of the total costs of the cement production. Cement production is an industrial sectors that have been growing steadily since the end of World War II. The annual global cement production grew from 100 million tons in 1950 (van Oss, 2005), to 2600 million tons in 2006 (U.S. Geological Survey, 2007). After a decrease in production due to the global economic down of 2007-2009, the cement production has recovered and in 2013 a total of 4 billion tons cement was estimated to be manufactured worldwide (U.S. Geological Survey, 2014). The cement industry accounts for around 5 % of the global CO_2 emissions (World Energy Council, 2008), making it one of the more greenhouse emissions-intense industries.

2.2 Cement Chemistry

Portland cement is a hydraulic binder that sets and hardens by hydration (Hewlett, 1998) and is manufactured from Portland cement clinker, which consists of a mixture of burned limestone, sand, and clay. The clinker is ground and mixed with gypsum (calcium sulfates) and other minerals may be added to obtain cement with the desired performance in terms of setting time and strength development (Cochez and Wouter, 2010).

Portland clinker consists mainly of belite, alite, ferrite and aluminate, comprising more than 90 wt. % of the product. The typical content of these minerals are displayed in Table 2-1. Subsequently, 3-6 wt. % of gypsum is added to the clinker and the mixture is finely ground to form the finished cement (Theisen, 2007).

Table 2-1: Main constituents of Portland cement clinker (Hewlett, 1998; Taylor, 1997).

Name	Chemical composition	Nomenclature	Approximate content [wt. %]
Belite	$(CaO)_2 \cdot SiO_2$	C_2S	15-30
Alite	$(CaO)_3 \cdot SiO_2$	C_3S	50-70
Ferrite	$(CaO)_4 \cdot Al_2O_3 \cdot Fe_2O_3$	C_4AF	5-10
Aluminate	$(CaO)_3 \cdot Al_2O_3$	C_3A	5-15

The major mineral phase in the Portland cement is tricalciumsilicate, often referred to as alite. Alite is responsible for setting and development of *early* strength, because it is relatively fast reacting. Dicalcium silicate, belite, controls the *late* strength due to its slow reactivity properties. Ferrite and aluminate are present due to the need to obtain a liquid at the peak kiln temperature (1400-1450 °C), facilitating the formation of the desired silicate phases during the clinker reactions. Besides these phases, cement contains from 0.5 to 1.5 % of free lime (CaO), and 1 % of SO_3, and a small proportion of MgO. Clinker has typically a mass content of 67 % CaO, 22 % SiO_2, 5 % Al_2O_3, 3 % Fe_2O_3, and 3 % other components (Taylor, 1997).

2.2.1 Raw Materials

The typical mixture of raw materials used for Portland cement contains ground limestone, clay, shale, and sand, introducing the various elements needed for clinker formation. Calcium is mainly provided by raw materials such as limestone, marl, or chalk and constitutes approximately 75-80 wt. % of the raw materials. Silica, aluminum, and iron components, as well as other elements, are provided by clay, shale, and other materials. Small amounts of additives such as iron ore, bauxite, and shale may be needed to provide additional iron oxide (Fe_2O_3), alumina (Al_2O_3) and silica (SiO_2) to adjust the chemical composition of the raw mix to the process and product requirements (Hewlett, 1998; Bye, 1999). The different kinds of raw materials needed to achieve the required cement composition are ground and mixed to produce a homogeneous blend, which is processed in the kiln (CSI, 2005).

Selected waste and by-products, such as blast furnace slag and fly ash, containing useful minerals are also used in the production of cement. The usage of waste as a replacement for conventional raw materials decreases the demands on local landfills. Hence, the overall environmental impact is reduced (CSI, 2005).

2.2.2 Calcination

Calcination is the first major chemical change in the thermal treatment of the raw materials and consists of the thermal decomposition of calcium carbonate into calcium oxide and carbon dioxide as shown in reaction (2-1). The calcination occurs in the temperature range of 700-900 °C.

$$CaCO_3(s) \rightarrow CO_2(g) + CaO(s) \qquad \Delta H° = 1782 \text{ kJ/kg } CaCO_3 \qquad (2\text{-}1)$$

The reaction is highly endothermic and consumes around 60 % of the total energy required for the production of cement (Hewlett, 1998). The energy required by the calcination process comes from the combustion of fuels in the calciner, which is the furnace where calcination takes place (see Figure 2-2 and Figure 2-3). The degree of calcination, which is the degree of dissociation of the calcium carbonate, is typically around 90-95 % in a modern calciner kiln system (Taylor, 1997).

2.2.3 Clinker Reactions

Clinker reactions occur at temperatures between 700 and 1450 °C. The reactions may be affected by minor compounds and involve intermediate compounds before the formation of the final clinker product. A general description of the overall clinker reactions are presented in reactions (2-2) to (2-5). A detailed overview of the chemistry, phase relations, etc. is provided elsewhere (Hewlett, 1998; Bye, 1999).

The formation of belite from lime and silica, reaction (2-2), starts at temperatures above 700 °C.

$$2CaO(s) + SiO_2(s) \rightarrow (CaO)_2 \cdot SiO_2(s) \quad (2\text{-}2)$$

Above 1300 °C, the proportion of clinker liquid increases and nodules are formed. At the same time, intermediate phases dissociate to form liquid and belite. The belite reacts with free lime to form alite, according to reaction (2-3). A clinker temperature of about 1450 °C is required in order to obtain a proper product quality. A proper clinker quality has an alite content of minimum 50 wt. % and a free lime content of maximum of 1.5 wt. % (Taylor, 1997).

$$CaO(s) + (CaO)_2 \cdot SiO_2(s) \rightarrow (CaO)_3 \cdot SiO_2(s) \quad (2\text{-}3)$$

The formation of solid aluminate and ferrite from the liquid phase takes place when the temperature drops to 1230 °C, according to reactions (2-4) and (2-5).

$$3CaO(s) + Al_2O_3(l) \rightarrow (CaO)_3 \cdot Al_2O_3(s) \quad (2\text{-}4)$$

$$4CaO(s) + Al_2O_3(l) + Fe_2O_3(l) \rightarrow (CaO)_4 \cdot Al_2O_3 \cdot Fe_2O_3(s) \quad (2\text{-}5)$$

Figure 2-1 shows the distribution of the different phases in the temperature range 300-1500 °C during heating and for 1500 to 1100 °C during cooling.

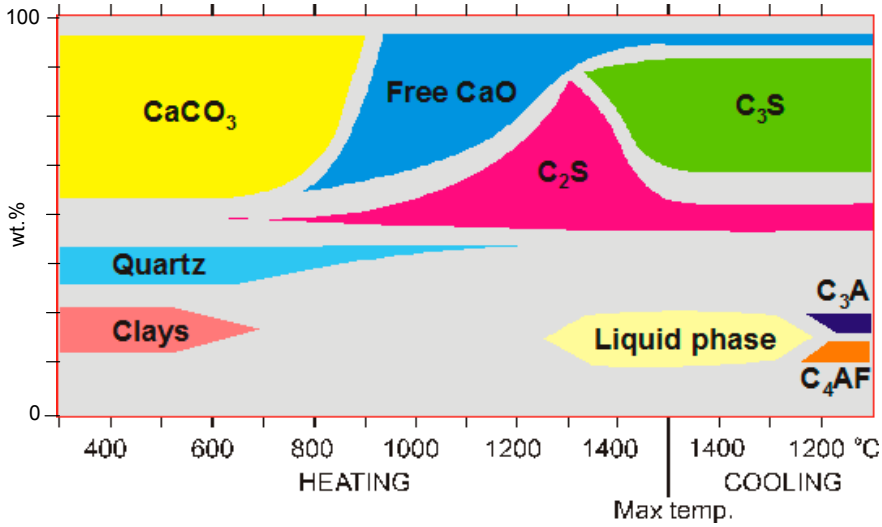

Figure 2-1: Phases distributed by weight, as a function of material temperature. Abbreviations are: C=CaO, A=Al_2O_3, S=SiO_2, and F=Fe_2O_3 (Theisen, 2007).

2.3 Cement Production

Cement is produced in a continuous process and can be produced by at least four different methods, respectively referred to as wet, semi-wet, semi-dry and dry. This thesis will focus on the dry process because it is the most common production process nowadays. A more comprehensive description of the different types of production processes can be found elsewhere (Labahn and Kohlaas, 1983; Peray and Waddell, 1972).

The cement production process can be divided into three consecutive parts: [1)] Preparation of the raw materials, [2)] pyro-processing, and [3)] clinker processing. A flow diagram for the pyro processing stage, consisting of the kiln system is shown in Figure 2-2.

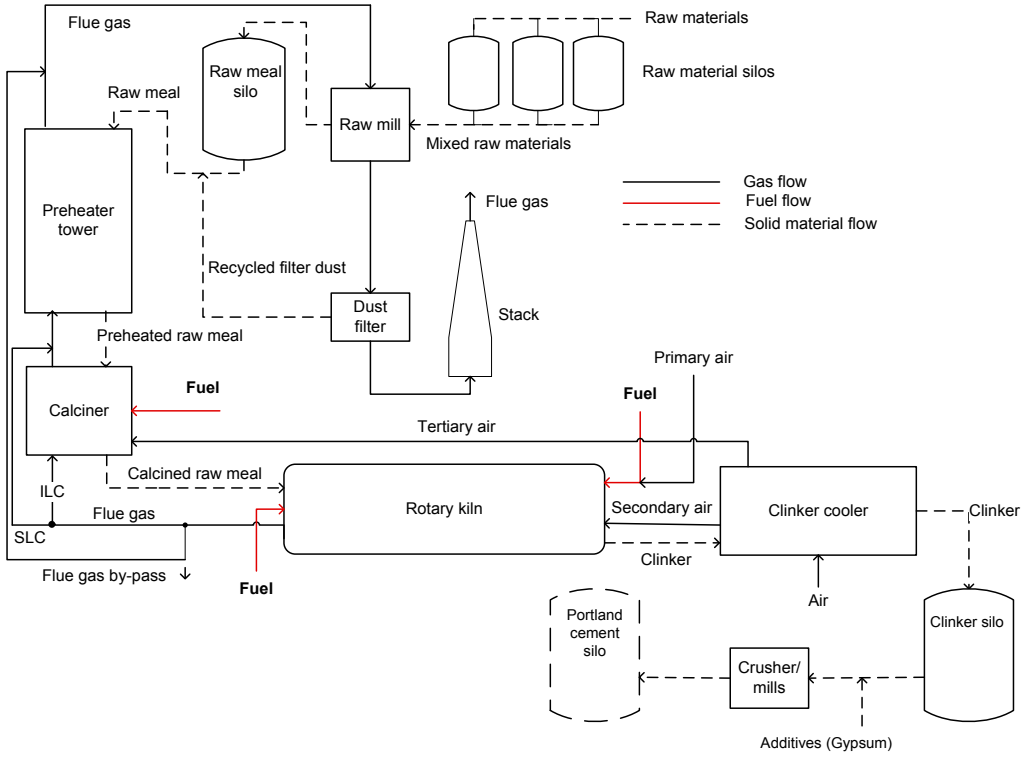

Figure 2-2: Flow diagram of modern kiln system for cement production. The abbreviations ILC and SLC refer to In-Line Calciner and Separate-Line Calciner, respectively (Nielsen, 2012).

2.3.1 Preparation of Raw Materials

The first step in the production of cement is the crushing of the raw materials to a particle size of about 25-100 mm. The raw materials are subsequently stored in separate tanks according to their composition. This facilitates and controls the continuous delivery of raw materials to the raw mill with the desired composition. In the raw mill, the raw materials are dried by hot flue gasses from the kiln system and ground together in a defined and well controlled proportion to produce the raw meal. The particle size of the ground raw material can vary from 5 to 125 µm (Bye, 1999). The fineness of the particles is important for reaching the desired reactivity and ensuring a good heating and calcination (Bhatty et al., 2011; Cembureau, 1999). The blended raw materials are stored in a silo before being fed into the kiln system. The silo can typically store raw material for several production days in order to provide a buffer to ensure a continuous cement production (Cembureau, 1999).

2.3.2 Pyro Processing

The pyro-processing step is the heart of cement production, and covers the thermal treatment of the raw material, necessary to obtain the cement clinker. It involves preheating of raw materials, calcination, clinker reactions, and cooling of the clinker. These steps take place in the kiln system, which consists of a preheater tower, a calciner, a rotary kiln, and a clinker cooler. A typical modern kiln system and its parts are schematically illustrated in Figure 2-3.

The raw materials, which are referred to as raw meal in the kiln system, are introduced to the preheater tower. A preheater tower consists of a series of 4-6 vertical cyclones and is arranged in a 50-120 m high tower structure. By direct contact with hot exhaust gases from the kiln flowing counter currently, the raw meal is heated. Thus, a part of the thermal energy is recovered in the system. The most common preheater tower is the five staged, meaning with 5 cyclones, where the first cyclone has a temperature of approximately 300 °C and the final cyclone has a temperature around 800-900 °C. The residence time in each cyclone step is approximately 8 seconds for the raw materials and 1-2 seconds for the hot flue gases. Overall, the raw materials pass through the preheating tower in less than a minute (Hewlett, 1998; Taylor, 1997).

The preheated raw meal is admitted to the calciner, which has a temperature of 850-900 °C and under these conditions the majority of the $CaCO_3$ will thermally decompose into CaO and CO_2. Hot air from the clinker cooler, so-called tertiary air, is utilized as combustion air in the calciner. The fuel consumption for calcination can account for up to 60 % of the fuel needed for cement production (Madlool et al., 2011). The calciner can be integrated into the kiln system as an In-Line Calciner (ILC), where the flue gas from the rotary kiln passes through the calciner, or as a Separate-Line Calciner (SLC), where the flue gas from the rotary kiln bypasses the calciner, and enters the preheater. The ILC-system minimizes the amount of gas flow through the rotary kiln and hence rotary kiln size reduction. In addition, good conditions for reduction of NO_x produced in the rotary kiln are achieved (Jensen, 1999). On the other hand, in a SLC-configuration, fuel combustion takes place more rapidly, due to a higher O_2 concentration, and a smaller calciner volume is needed compared to the ILC-system, for a fixed residence time, since the amount of gas through the calciner is smaller (Jensen, 1999). However, the solid residence time is lower in a SLC-system and the mass and the particle behaviours lowers heat transfer from gas to fuel particle (Larsen, 2007). This thesis will refer only to the ILC-configuration because it is the preferred and most common design nowadays.

The hot meal, i.e. calcined raw meal after the 5^{th} stage cyclone, enters into the rotary kiln, and flows counter currently to the hot flue gases, that are produced by the kiln burner flame. The rotary kiln is a long tube which is inclined 1-4° with horizontal and rotates 1-5 rpm to ease mass transport (Taylor, 1997). The rotary kiln can be divided into three different zones, as illustrated in Figure 2-3. The material cold end is the inlet of hot meal into the rotary kiln. In the transition zone, the materials start to melt, and form the clinker nodules. The clinker

reactions take place in the burning zone, or the hot end of the rotary kiln, where the clinker achieves a temperature of up to 1450 °C.

The clinker is cooled down by atmospheric air in the clinker cooler, which is typically a grate cooler (Hewlett, 1998). In this manner, preheated combustion air is produced and returned to the process through the rotary kiln (for combustion of the main burner fuel as secondary air) and the calciner (for combustion of the calciner fuel, as tertiary air). Grate coolers provide the most efficient and most flexible heat recovery system for modern cement plants (Cembureau, 1999). Experience has shown that a rapid cooling down from 1450 to 1200 ºC is advantageous in order to minimize the formation of secondary belite and free lime (Taylor, 1997; Hewlett 1998).

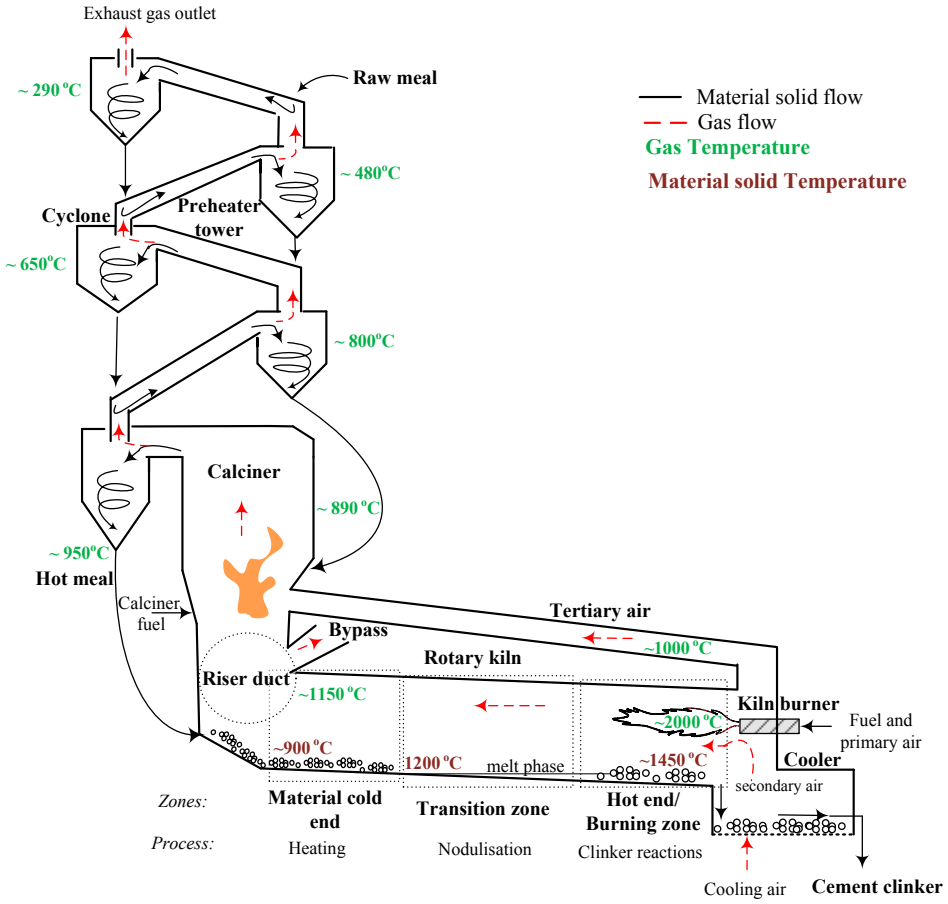

Figure 2-3: Scheme of a typical kiln system, specifying the nomenclature used for different parts.

Modern cement plants can have a bypass system for the process gases, in order to reduce the chloride concentration the kiln. The bypass system comprises the steps of extracting a portion of kiln exhaust gases, cooling the extracted exhaust gases and separating the dust. The bypass starts at the gas extraction point, which is located at the kiln side of the riser duct. At this position, the kiln gases have a low dust concentration and high gaseous concentration of Cl (FLSmidth A/S, 2008). The extracted kiln gases containing Cl and kiln dust, are quenched by air, in order to initiate condensation of the chlorides, and facilitate the subsequent separation of chlorides from the gas. This separation takes place in an electrostatic precipitator or a baghouse filter (FLSmidth A/S, 2008). Typical bypass rates are of up to 15 % for chlorine bypass (European IPPC, 2013). The installation of the bypass requires additional capital investment and increases heat and material losses. The removal of hot gas by the bypass leads to higher specific heat consumption of about 6–12 MJ/ton clinker per cent of removed kiln inlet gas (European IPPC, 2013).

2.3.3 Clinker Processing

The cooled clinker has a variable particle size, typically a diameter between 3-25 mm (Taylor, 1997). The clinker may be stored in a clinker silo or it can be directly ground in a ball mill, which is a rotating horizontal steel tube filled with steel balls, or in a vertical mill. When the tube rotates, the steel balls tumble and crush the clinker into a fine power with a particle size ranging mainly from 3 to 30 μm (Taylor, 1997). A small amount of gypsum is added during the final grinding to control the setting properties. Additives such as coal fly ash, sand or raw material may also be added in order to improve the strength properties of the cement or to make the cement production more sustainable (Hewlett, 1998). The final cement product is transported to a cement silo until it is packed and distributed.

2.3.4 Process Data Overview

Table 2-2 provides an overview of typical process data, for a modern calciner kiln, representative for an ILC-system. The process data consists of the temperatures and residence times for both the gas and solids, and the O_2 concentration in the gas phase.

Table 2-2: Typical temperatures, residence times, and O_2 concentration range in a modern calciner kiln (Cembureau, 1999).

	Preheater	**Calciner**	**Rotary kiln**	**Cooler**
Gas temperature [°C]	350-880	880-1100	1100-2000	1100-25
Gas residence time [s]	~ 5-10	~ 3-4	~ 5-10	~ 1
Material temperature [°C]	100-780	780-900	900-1450	1400-100
Material residence time [s]	~ 50	~ 5	15-30 min	~ 30 min
Gas O_2 concentration [vol. %]	~3-12	11-12	2-7	~ 21

The data for the temperatures of the gas and the materials is a consequence of the counter current flow. The solid material is heated from 100 °C in the preheater to 1450 °C in the burning zone of the rotary kiln, while the gas that flows in the opposite direction, enters at ambient temperature in the cooler and reaches 2000 °C in the rotary kiln. The gas temperature gradually decreases until 350 °C in the preheater. The cooled gas is usually used to preheat the cement raw materials in the raw mill and leaves to the stack at a temperature around 100 °C.

Atmospheric air, which contains 21 vol. % O_2, is introduced into the cooler and further used in the kiln system. The oxygen concentration decreases to 2-7 vol. % in the rotary kiln as the combustion proceeds. However, a fraction of the cooling combustion air is bypassed via the tertiary air duct from the cooler to the lower part of the calciner, where the oxygen content is around 11-12 vol. %. In the lower part of the calciner, the fuel is introduced without combustion air, which contributes to a low oxygen level. The oxygen level decreases in the rotary kiln due to the combustion process and the dilution with the CO_2 formed during the calcination. In the preheater section, the oxygen concentration is affected slightly by oxidation reactions in the raw meal. The reactions include formation of SO_2 from pyrite, recarbonation of CaO, formation of $CaCO_3$ and combustion of organic bound carbon.

2.4 Conclusions

The production of Portland cement is a highly energy-consuming process which consists of a three step process. The process can be divided into preparation of raw materials, clinker production, and cement grinding. The clinker production, which takes place in the kiln system, requires that the raw materials, which consist typically of a mixture of limestone, clay and sand, are heated up to approx. 1450 ºC in order to calcine limestone and facilitate the clinker reactions. The calcination is a very endothermic process which normally uses 50-60 % of the total energy required for the production of cement. Gas temperatures in the kiln system range from ambient temperatures up to 2000 ºC and the oxygen levels range from 2 to 21 vol. %, depending on the position in the kiln system.

Portland clinker consists mainly of four different minerals, which are alite, belite, ferrite, and aluminate. A proper clinker quality has an alite content of minimum 50 wt. % and a free lime content of maximum of 1.5 wt. %. The main strength giving compounds in Portland cement are alite and belite.

2.5 References

Bhatty, J. I., Miller, F. M., and Kosmathka, S. K.; Innovations in Portland cement manufacturing. Illinois, USA. 2011. ISBN: 978-0893122713.

Bye, G. C.; Portland cement. Second Edition. Thomas Telford, London, 1999. ISBN: 0-7277-2766-4.

Cembureau; Best available techniques for the cement industry, 1999. Available at http://cembureau.be/.

Cembureau; Sustainable cement production: Co-processing of alternative fuels and raw materials in the cement industry, 2009. Available at http://cembureau.be/.

CSI (Cement Sustainability Initiative); Guidelines for the selection and use of fuels and raw materials in the cement manufacturing process. World Business Council for Sustainable Development, Switzerland, 2005.

Cochez, E., and Wouter, N.; Cement production. IEA-Energy Technology Network, Issue IEA ETSAP-Technology Brief I03, 2010.

European IPPC; Best available techniques (BAT) reference document for the production of cement, lime and magnesium oxide- European Integrated Pollution Prevention and Control Bureau. 2013.

FLSmidth A/S; Overcoming side effects of alternative fuels on pyro process. Highlights, 28, November, 2008.

Hewlett, P. C.; Lea's chemistry of cement and concrete. Fourth edition. New York, 1998. ISBN: 978-0-7506-6256-7.

Jensen, L. S.; NO_x from cement production- reduction by primary measures. Ph.D. thesis, Technical University of Denmark, Department of Chemical and Biochemical Engineering, 1999. ISBN: 87-90142-55-1.

Labahn, O., and Kohlaas, B.; Cement engineer's handbook. Third Edition. Bauvelarg GmbH, 1983. ISBN: 978-3-7625-0975-2.

Madlool, N. A., Saidur, R., Hossain, M. S., and Rahim, N. A.; A critical review on energy use and savings in the cement industries. Renewable & Sustainable Energy Reviews, 15, 2042-60, 2011.

Nielsen, A. R.; Combustion of large solid fuels in cement rotary kilns. Ph.D. thesis, Technical University of Denmark, Department of Chemical and Biochemical Engineering, 2012. ISBN: 978-87-92481-66-5.

Peray, K. E., and Waddell, J. J.; The rotary cement kiln. Chemical Publishing Co., New York, 1972. ISBN: 978-08-20603-67-4.

Schneider, M., Romer, M., Tschudin, M., and Bolio, H.; Sustainable cement production-present and future. Cement and Concrete Research, 41, 642-650, 2011.

Taylor, H. F. W.; Cement chemistry. Second Edition. Academic Press Thomas Telford., London, 1997. ISBN: 978-0727725929.

Theisen, K.; The international cement production seminar 2007. FLSmidth A/S, Valby, Denmark, Volume II, 2007.

U.S. Geological Survey; Minerals yearbook 2007, cement. U.S. Geological Survey and U.S. Department of the Interior prepared by van Oss, H.G., 2007. Available at http://minerals.usgs.gov/minerals/pubs/commodity/cement/index.html.

U.S. Geological Survey; Mineral commodity summaries- cement. U.S. Geological Survey and U.S. Department of the Interior prepared by van Oss, H.G., 2014. Available at http://minerals.usgs.gov/minerals/pubs/commodity/cement/index.html.

van Oss, H. G.; Background facts and issues concerning cement and cement data. U.S. Geological Survey and U.S. Department of the Interior, U.S. Geological Survey Open-File Report 2005-11522005. Available at http://pubs.usgs.gov/of/2005/1152/index.htm

World Energy Council; Energy efficiency policies around the world: Review and evaluation, 2008. ISBN: 0-946121-30-3. Available at http://www.worldenergy.org/

VDZ (Verein Deutscher Zementwerke); Activity Report 2007-2009, 2009. Available at http://www.vdz.de

3. Alternatives Fuels in the Cement Production

This chapter provides an insight in the use of alternative fuels in cement production. Sections 3.1 and 3.2 describe the general characteristics of alternative fuels and their combustion. Finally, section 3.3 outlines the existing technologies for combustion of alternative fuels.

3.1 Introduction

Cement production has depended mainly on the use of fossil fuels such as coal and petcoke. However, the utilization of secondary fuels or alternative fuels, such as car tires (Trezza and Scian, 2009), plastic waste, sewage sludge (Zabaniotou and Theofilou, 2008) and wood waste (Mackes and Lightburn, 2003), is continuously increasing due to environmental concerns and the increase of conventional fuels prices. One of the leading countries with respect to replacement of fossil fuels is Germany, where 61.1 % of the thermal energy came from alternative fuel sources in 2011 (VDZ, 2012). Individual cement plants are reported to have alternative fuels energy shares higher than 80 % (European IPPC, 2013). Alternative fuels cover a wide range of fuels ranging from fossil fuel based (e.g. waste oil and natural gas) and all non-fossil fuels, such as biomass based, and waste from other industries.

Alternative fuels can have different chemical and physical properties compared to fossil fuels. The most important fuel characteristics to consider, when selecting alternative fuels, are the heating value, the ash content and composition, the particle size, and the moisture content. The heterogeneity amongst the physical and chemical properties of alternative fuels affect both the thermal energy input and the process stability, such as possible fuel spillage and modification of the input of minor elements. Fuel spillage is considered when unburned fuel drops into the material bed and this can happen in the kiln flame and in the calciner. The fuel ash, which is incorporated into the clinker chemistry, may modify the minor elements input, thus the composition balance of the raw materials needs to be readjusted. The different types of typical alternative fuels used in the cement industry can be grouped as shown in Table 3-1. Some of the most common alternative fuels are industrial and municipal waste, tire derived fuels, meat and bone meal, and wood waste.

Table 3-1: Grouping of typical alternatives fuels used in cement production (Larsen, 2007; Murray and Price, 2008; Nielsen, 2012).

Solid alternative fuels	Liquid alternative fuels	Gas alternative fuels
Sewage sludge	Tar waste oil	Landfill gas
Meat and bone meal	Paint residues	Pyrolysis gas
Refuse derived fuel (RDF)	Waste solvents	Refinery waste gas
Waste wood/saw dust	Wax suspension	Biogas
Tire derived fuel (TDF)		Petrochemical wastes
Agricultural waste		
Plastic/paper/textile waste		

There are numerous advantages of using alternative fuels, both for the cement industry, and from society's point of view in relation to the general waste problems (Pizant and Gauthier, 1997; Mokrzycki and Uliasz-Bochenczyk, 2003; Greco and Enfil, 2006). Some benefits of the substitution of fossil fuels by alternative fuels are:

- Reduction of fuel and production costs.
- Alternative fuels may be partly or fully CO_2-neutral.
- Waste is effectively utilized as energy.
- The ash residue is incorporated into the cement clinker.

However, the usage of alternative fuels has some general requirements, such as availability of large amounts, legislation and permissions before a specific alternative fuel can be used, logistics for transport and handling of the specific fuel. The usage of alternative fuels varies widely across regions and countries and depends on local conditions.

Fuel analyses of fossil fuels and some commonly used alternative fuels are presented in Table 3-2. The presented values are approximate and may deviate depending on source, local conditions, water content, pre-treatment, etc. However, the tabulated values reflect the diversity amongst typical fuels utilized and give an estimation of heating value and elemental composition. The fraction of volatile matter and fixed carbon are important for the combustion characteristics. The most important differences between alternative fuels and fossil fuels are listed below, because these differences may have a significant impact on the combustion and cement production.

- Alternative fuels may have a significantly higher content of volatiles compared to the solid fossil fuels. In general, alternative fuels contain less sulfur, fixed carbon, and fuel-bound nitrogen, and have a higher oxygen and hydrogen content than fossil fuels.
- The ash content of alternative fuels is typically higher than for fossil fuels. The ash may introduce some new elements, which can interfere with the chemistry of the cement materials and affect the operation of the system. Furthermore, alternative fuels may contain different amounts of volatile elements, such as S, Cl, Na, K, and Hg.
- Alternative fuels often have high moisture content, which may increase the combustion time needed. Furthermore, some energy is consumed for heating and evaporation of water and the flue gas volume is increased. This may decrease the production capacity and negatively affect the process efficiency.
- The heating value of some alternative fuels may be significantly lower than typical fossil fuels, due to ash and moisture content and the chemical composition. This implies that higher fuel mass flows are needed to provide the same thermal input. The increase of volume (if the density of the fuel is low) together with the increased mass flow can cause handling and feeding problems.

- Alternative fuels may have different devolatilization and char oxidation kinetics than conventional fuels due to different chemical composition and structure. This may influence the fuel combustion time and NO_x emissions.

Moreover, the composition of alternative fuels is rarely constant, which will be reflected by inhomogeneous physical and chemical properties. These variations can affect emissions, process stability, and clinker quality. Another important difference with respect to fossil fuels is that alternative fuels may be introduced to the kiln system in the form of large particles in the range of millimetres and centimetres, while fossil fuels are typically introduced with a particle sieve residue of 2-20 % on a 90 μm sieve (Nørskov, 2012).

The use of alternative fuels has been shown not to increase the total emissions of pollutants compared to fossil fuels (Lemarchand, 2000; Karstensen, 2008; Lee et al., 2007; Prisciandaro et al., 2003; Realff et al., 2005; Wurst and Prey, 2003). However, the use of alternative fuels may have positive as well as negative effects on the emissions of gas pollutants (Tokheim, 2012). The cement plants located in the European Union, which are using alternative fuels, are subject to Directive 2010/75/EU about industrial emissions (Directive 2010/75/EU). The important emissions are SO_2, NO_x, HCl, HF, Hg, Tl, dioxins and furans, total organic carbon, and CO. Further information about the legislation of emissions and the emission limit of each compound can be found in the aforementioned European Directive, except CO emission limit, which is set by local authorities.

Table 3-2: Typical composition, proximate analysis and heating values of fossil and alternative fuels used in the cement production. Notes: [1] VM: Volatile matter, [2] FC: fixed carbon, [3]RDF: Refuse derived fuel, [4] TDF: Tire Derived fuel, [5] MBM: Meat and Bone Meal, [6] PE: Polyethylene, [7] PVC: Poly-Vinyl-Chloride, [a] lower heating value calculated from the higher heating value, * Concentration in ppm weight dry basis, [#] Chemical ash composition as wt. % Na_2O and K_2O, n.a.: not available

	Fuel	Proximate analysis [wt. % dry]			Ultimate analysis [wt. % dry]								LHV [MJ/kg]	Reference
		VM[1]	FC[2]	Ash	C	H	N	O	Cl	S	Na	K		
Fossil fuels	Anthracite Coal	1.7-11	67-98	3.8-20	64-87	0.4-3.4	0.2-1.5	0.7-2.2	300-380*	0.7-2.2	0.09-2.9[#]	0.29-4.15[#]	30.23-34.89	(Tsubouchi et al., 2005) (Weston, 1992) (Singer, 1991) (Zevenhoven and Kilpinen, 2004) (Vassilev et al.,2010)
	Bituminous coal	14-40	33-86	3.7-12	55-85	3.8-5.9	1.0-2.0	1.8-13	100-340*	0.3-4.3			19.77-34.89	
	Lignite coal	26-47	29-40	4.2-18	42-65	2.8-6.2	0.7-1.6	12-31	100-140*	0.5-6.7			9.30-19.30	
	Petcoke	10-20	71-88	0.2-3.0	81-90	3.1-3.7	0.9-1.7	0.8-4.3	~ 0	2.9-7.4	40-70*	20-50*	29.5-34	(Singer, 1991)(AFPM, 2012) (US Department of Energy, 2012) (Milenkova et al., 2003)
	Crude oil	n.a.	n.a.	~0	81-87	10-15	n.a.	0-3.8	~ 0	0-5.7	n.a.	n.a.	39-42.7	(US Department of Energy, 2012) (Babcock & Wilcox Co., 2007)
	Natural gas	100	0	0	65-75	20-24	0-1.5	0-1.5	~ 0	0-10	n.a.	n.a.	46.8-53.8	(Weston, 1992) (Zevenhoven and Kilpinen, 2004)
Alternative fuels	Pine wood	79-83	15-17	0.3-0.5	49-51	5.8-6.0	0.1-5.9	36-44	< 0.1	~ 0	n.a.	~ 1000*	19.7-19.8[a]	(Hassan et al., 2009) (Weston, 1992) (BioBank, 2013)
	Straw	64.3-80.5	13-19.5	4.7-20.1	46-50	5.6-6.4	0.5-2.1	40.1-44.6	0.6	0.2	0.16-3.5[#]	12.6-38.5[#]	18.1[a]	(Stenseng, 2001) (Vassilev et al.,2010)
	Rice Husks	61-69	16-17	15-20	38-42	3.0-4.8	0.4-0.6	36-54	n.a.	0.1-0.2	0.1	2.2	15.4[a]	(Varhegyi et al., 2011) (BioBank, 2013)
	RDF[3]	60-84	2-16	8-32	42-72	5-1	0.8-2.4	3-36	0.1-3.9	0.1-0.6	0.1-0.2	0-0.1	14.0	(Tokheim, 1999) (Kobyashi et al., 2005)
	TDF[4]	54-66	23-30	7-23	64-81	5.6-7.2	0.3-0.5	2-6	0.2-2	1.4-1.6	~0	~0	31-32.8	(Larsen, 2007) (Weston, 1992) (Chinyama and Lockwood, 2007)
	MBM[5]	65-72	7.2-9.7	18-28	42-46	5.8-6.4	7.5-11	15-38	0.4-0.6	0.4-1.0	0.31	0.1	16.2-19.9	(Aho and Ferrer, 2005) (Ayllon et al., 2006) (Kaantee et al., 2004)
	PE[6]	100	~ 0	~ 0	86	14	~ 0	~ 0	~ 0	~ 0	~ 0	~ 0	40.2-44.2	(Panagiotou and Levendis, 1994) (Wang et al., 2004)
	PVC[7]	91	9	1	36	5	~ 0	~ 0	57	~ 0	~ 0	~ 0	19.2	
	Sewage sludge	48-64	0-6	17-50	28-39	3.8-4.1	3.8-4.3	29-36	0.1-0.8	~1	0.2	0.6	14.0-19.1	(Nielsen, 2012) (BioBank, 2013)

3.2 Combustion of Alternative Fuels

Many cement plants utilize alternative fuels in the calciner and the main burner, and these two units have been subject to modifications in order to optimize the combustion of such alternative fuels. Despite these modifications, the usage of relatively small particles is required in the calciner and in the kiln burner to ensure a sufficient fuel combustion and the desired flame profile. A consequence of firing large alternative fuels particles in the calciner and main burner is that the combustion may not be complete and subsequently partially or unburned solid fuels may drop into the material bed. In addition, coarse alternative fuels are sometimes fired directly into the material inlet end of the rotary kiln, because this solution requires minimal shredding of the fuel. However, there are several challenges associated with the combustion of fuels in direct physical contact with the cement raw materials, which may lead to modifications of the process conditions, stability, and clinker quality.

Firstly, it is necessary to evaluate the reaction path encountered when the different solid fuels are converted during devolatilization and char combustion, as illustrated in Figure 3-1. This topic has been discussed in details by Larsen (2007) and Nielsen (2012). The conversion pathway of a fuel is important to know and be aware of in the cement industry, because it will influence the total conversion time. The size of the char particle and the time required to complete the char oxidation is determined by the pathway that the fuel follows. For example, the char particle following pathway I or F gets smaller and will convert faster than char particle following pathway H1 and H2.

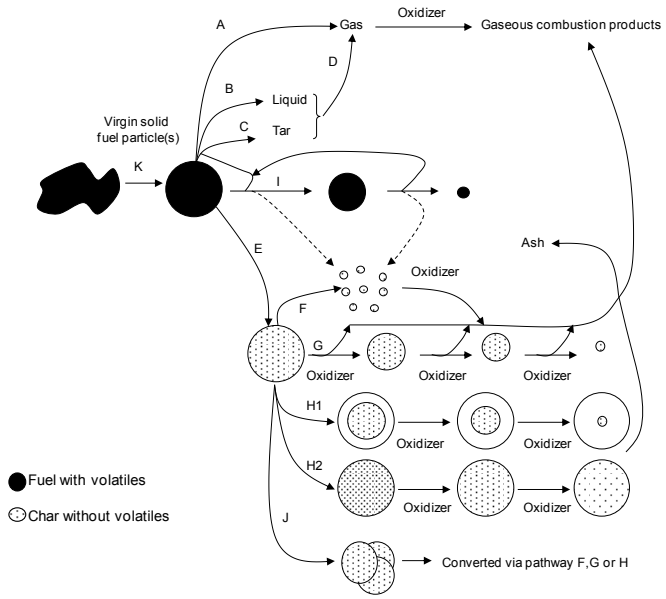

Figure 3-1: Main reaction pathways involved in the combustion process of a solid fuel particle (Larsen, 2007).

Consequently, if the solid fuels do not reach full conversion in the calciner or in the flame of the main burner, the fuel particles may end up in the bed material and affect the process stability. The solid fuels can end up in the bed material in the rotary kiln in four different ways depending on whether the fuels are fired in the calciner, main burner or directly into the material inlet of the kiln (Nielsen, 2012). The four scenarios are illustrated in Figure 3-2 and outlined briefly below:

1. Large solid fuels particles with a considerable weight, which are fired in the calciner and cannot be carried upwards with the gas flow, may drop through the riser duct, and into the rotary kiln.
2. Large solid fuels particles fired through the kiln burners may not be completely combusted in the flame of the main burner, and fall into the bed material.
3. Small and unconverted solid fuel particles, which are light enough to be carried upwards with the gas flow through the calciner and transported into the cyclones, can fall into the kiln inlet with the calcined raw meal.
4. Coarse solid fuels may be fired directly into the rotary kiln material inlet end.

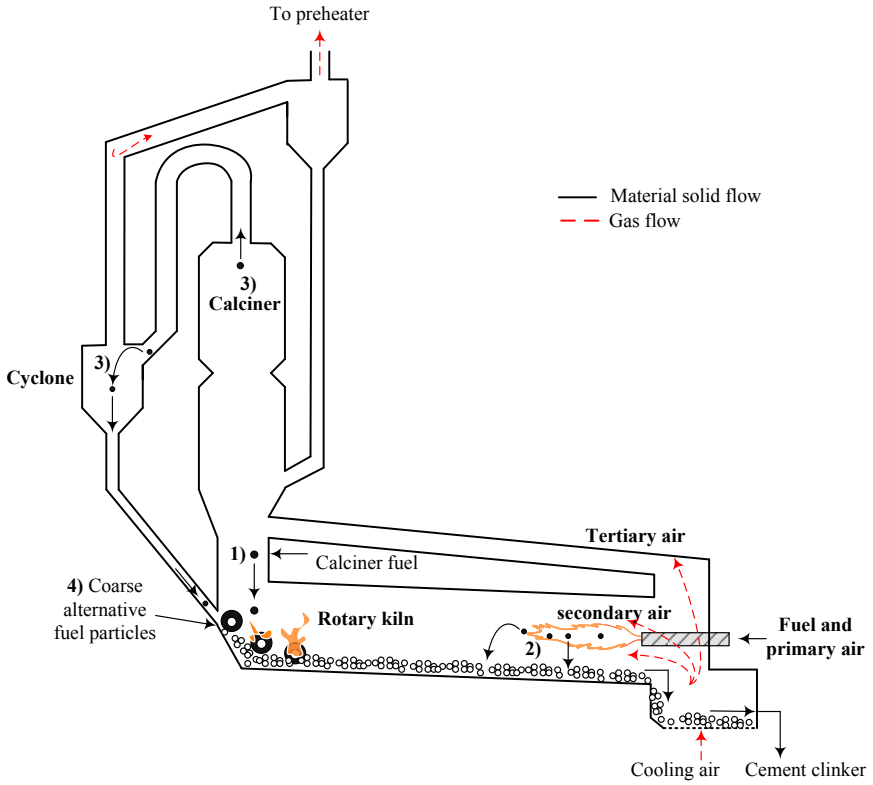

Figure 3-2: Illustrative scheme of the four scenarios, whereby solid fuels can drop into the bed material in the rotary kiln, modified from (Nielsen, 2012). The numbers from 1 to 4 refer to the scenarios described above.

When solid fuel particles are partly or fully combusted in the material inlet of the rotary kiln, three situations can occur: [1)] The particles can be fully covered by raw materials, [2)] the particles can be partly covered by raw materials, or [3)] the particles can be on top of the raw material bed. The position of the fuel particle controls the heating mechanism, the mass transfer of oxygen, and the mass transfer of devolatilization and combustion products. The three situations are illustrated in Figure 3-3, where the mechanisms of the heat transfer and mass transfer of oxygen are also stated. Due to the rotation of the kiln, both the cement raw materials and the solid fuel particles are constantly in motion and the particle will therefore not experience just one situation during its combustion, but a combination of the three situations.

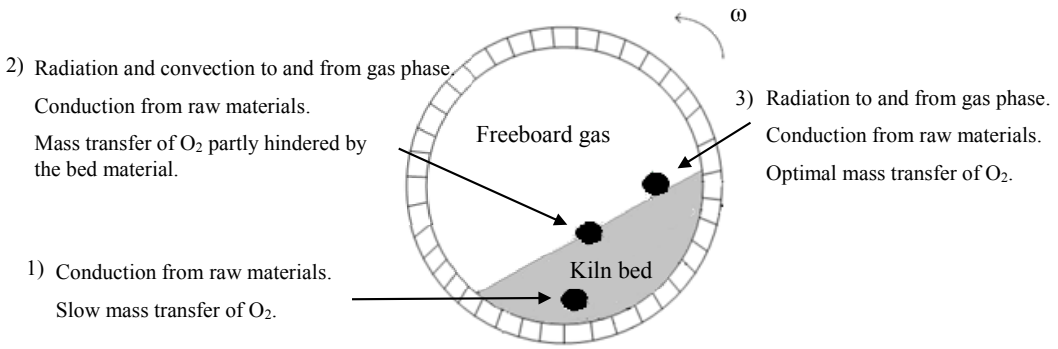

Figure 3-3: Graphical scheme of the three situations with corresponding heat transfer and mass transfer mechanisms that a fuel particle can experience, modified from (Nielsen, 2012).

During the combustion of the fuel particles, volatile gases are released and further combusted in contact with the gas in the freeboard. The gases may be reducing agents, such as CO, H_2, and light hydrocarbons, causing local reducing conditions in the kiln bed material. If no oxygen is available around the fuel particle, the solid fuels will experience pyrolysis and the gases released will not be combusted until they reach the freeboard. The induced reductive conditions in the material inlet of the rotary kiln may affect the product quality by modification of the clinker chemistry and the process stability of the kiln system by an increase in the internal circulation of sulfur, chlorine, and alkali metal species. The circulation of sulfur, which will be further discussed in Chapter 4, is especially important. This thesis will primarily focus on the effects of the combustion of alternative fuels fired in the calciner and directly into the rotary kiln inlet end on the process operation. The effects of firing alternative fuels in the main burner have been investigated previously (Nørskov, 2012). The effect of alternative fuels on the clinker product (quality and chemistry) is outside the scope of this thesis.

In order to provide further insight into the effects and consequences of the combustion of alternative fuels on the kiln bed material, it is necessary to understand how different alternative fuels are converted in the laboratory and industrial scale during combustion. It is also important to be aware of the different compounds

released during devolatilization of different fuels, because these gaseous compounds play a main role in the reductive decomposition of sulfates, as described in section 3.2.2.

3.2.1 Combustion Studies of Alternative Fuels

An extensive parameter laboratory scale study using a high temperature rotary drum with conditions similar to the industrial rotary kiln material inlet has previously been conducted (Nielsen, 2012). The study investigated the combustion of tire rubber, polypropylene, petcoke and pine wood. In the experiments, *real* cement raw material was not used because of its sticky characteristics during heating, and inert sand was therefore used. The effects of fuel mass, particle shape and size were investigated, showing that the external surface area and the particle thickness are more important parameters for the conversion, time of devolatilization and char oxidation than the mass of the fuel sample.

For polypropylene (which doesn't have fixed carbon) and the devolatilization period of the other fuels, the temperature was the major rate influencing parameter. The conversion time decreased as the temperature increased from 700 to 1000 ^{o}C.

The rotational speed was observed to have an effect on the conversion for the char oxidation of tire, wood, and petcoke, as the conversion time increased when the rotational speed was increased in the interval 20 rpm to 6 rpm. There was also a change in bed behavior which affected the mixing process. Experiments with different raw material particle sizes, with average size from 18 to 600 µm, showed that the char oxidation time was dependent on the particle size. The time to complete the char oxidation was longer for the fine raw materials than for the medium and coarse raw materials. This can be explained by the fact that the fine sand follows a slumping bed motion where the mixing is less efficient, which means that the fuel particles are in poor contact with oxygen from the freeboard gas. The char oxidation was found to vary with oxygen concentration in the freeboard gas, which is reasonable because char oxidation is dependent on diffusion of oxygen to the char surface.

Several industrial studies using alternative fuels have been reported in literature (Zabaniotou and Theofilou, 2008; Li and Zhang, 2011). Zabaniotou and Theofilou (2008) studied the usage of 7.5 wt. % wet sewage sludge (60-70 % moisture content) in a cement plant on Cyprus in which the sewage sludge was mixed with conventional solid petcoke. Subsequently, it was fed for drying and grinding in the coal mill. This procedure reduced the moisture content of the fuel to 1 %. In this way, no fuel costs were required for drying. The approach of mixing an alternative fuel and a fossil fuel have been applied in several studies (Mackes and Lightburn, 2003; Kara et al., 2011) and have been found not to affect the clinker quality and the process stability.

The study of Mackes and Lightburn (2003) used wood chips in a US based cement plant and reported that no operation problems were encountered when wood chips were pulverized and burned in combination with petcoke (ratio of 15 % wood and 85 % petcoke) through the burners in the calciner. Another industrial study burning alternative fuel (RDF based on 66 wt. % textile, 17 wt. % paper and 17 wt. % plastic) in the main burner was performed by Kara et al. (2011). The fuel mixture was added to the main fuel (petcoke) in ratios of 0, 8, 12, and 15 %, and it was observed that the clinker produced was acceptable. However, RDF caused low flame temperature and high humidity content inside the kiln and these conditions were reflected by a decrease in NO_x emissions with increasing amount of RDF (Kara et al., 2011).

3.2.2 Volatile Gases from Fuels

The identification of the gases released from different alternative fuels during devolatilization in an oxygen-lean environment or during pyrolysis (absence of oxygen, e.g. when the particle is buried in the bed material) is important to know because amongst these gases may be reducing agents, which can promote the sulfur release from the raw materials.

Several studies in the literature have analyzed and quantified the volatile composition of fuels (Di Blasi et al., 1999; Wang et al., 2003; Kyari et al., 2005; Ouiminga et al., 2009; Wu et al., 2009; Fu et al., 2011). It is possible to identify the volatiles of different fuels at different conditions (pyrolysis, combustion). However, the measurements produced by different studies are not directly comparable due to the differences in the experimental configurations (heat transfer mechanism from the heating system to the specimen), sample characteristics (size, shape, moisture content) and the focus of the investigation. Table 3-3 compares the main volatiles compounds of various alternative fuels, which may be used in the cement industry. The thermal treatment, the reactor type, and the temperature range of the study are also indicated. These investigations are further explained in the following subsections. The nitrogenous species analyzed in the studies have been neglected because they are not an active part of the sulfur chemistry.

Table 3-3: Main volatile compounds for a variety of alternative fuels. Note: [1] Ordered by decreasing order of contribution.

Fuel	Thermal treatment	Main volatiles compounds[1]	Temp. [ºC]	Reactor type	Reference
Millet straws	Pyrolysis	$CO > CO_2 > CH_4$	800 - 1000	Tubular kiln	(Ouiminga et al., 2009)
Biomass (rice straw, corncob, corn straw)	Pyrolysis	$CO > C_xH_y > CO_2 > H_2$	700 - 900	Macro-thermal gravimetric analysis	(Wu et al., 2009)
Agricultural residues (maize stalks, rice straw, cotton straw, rice husk)	Pyrolysis	$CO > CO_2 > CH_4$	600 - 1000	Thermal gravimetric analysis	(Fu et al., 2011)
Wood chips	Pyrolysis	$CO_2 > CO > CH_4$	377-727	Bench-scale plant	(Di Blasi et al.,1999)
Rubber tires	Pyrolysis	$CO_2 > H_2 > CH_4 > CO > C_2H_6$	500	Fixed bed reactor	(Kyari et al., 2005)
Rubber tire granulates	Pyrolysis	$C_xH_y > CH_4 > CO_x$	550, 900	Horizontal electrically heated oven	(Fernandez et al., 2012)
fibers		$CO_x > C_xH_y > CH_4$			
Polyethylene	Pyrolysis	$C_2H_4 > CH_4 > C_6H_6$	800 - 1000	Tubular kiln	(Ouiminga et al., 2009).
Polyethylene	Combustion with air	$CO_2 > CO > C_2H_4 > CH_4 > C_2H_2$	500- 1000	Two stage laminar flow reactor	(Wang et al., 2003).
Polystyrene		$CO_2 > CO > CH_4 > C_2H_2 > C_2H_4$			
Poly-vinyl chloride		$CO_2 > CO > CH_4 > C_2H_4 > C_2H_2$			

3.2.2.1 Biomass

Ouimiga et al. (2009) characterized carbonaceous species from the pyrolysis of millet stalks in a tubular kiln. The kiln was pre-heated to the desired temperature of degradation (between 800 and 1000 ºC) before introducing the fuel. The gaseous compounds from millet stalks were mainly CO and CO_2 for carbonaceous species. The CO formation increased significantly with increasing temperature. The formation of carbon dioxide increased especially from 950 to 1000 ºC and the formation of CH_4 remained constant from 900 to 1000 ºC. The total amount of volatile carbon also increased from 40 % of the total mass at 800 ºC to 53.4 % at 1000 ºC (Ouiminga et al., 2009).

The study of isothermal pyrolysis of biomass (rice straw, pelletized corncob, and pelletized corn straw) at 700, 800, and 900 °C by macro-thermal gravimetric analysis was carried out by Wu et al. (2009). The biomass pyrolysis gas yield increased with increasing temperature, i.e. for pelletized corncob, from 67.2 to 93.2 % at 700 and 900 °C, respectively. About 30 % by volume of total volatile gas was light hydrocarbons, such as CH_4, C_2H_6, and C_2H_4. The CO_2 content decreased with increasing temperature, while the H_2 content increased as the temperature rose, for example from pelletized corn straw pyrolysis almost no H_2 was obtained at 700 °C and

increased to 6.5 % at 900 °C. The light hydrocarbons content decreased from 700 to 900 °C, because the hydrocarbons decomposed into more simple molecules such as CO, CO_2, and H_2.

Maize stalks, rice straw, cotton straw, and rice husk were pyrolized in order to study the effect of the temperature on gas composition and char structure (Fu et al., 2011). The experiments were performed using a fixed bed reactor at different temperatures ranging from 600 to 1000 °C. The main gases produced were CO, CO_2, CH_4, ethane (C_2H_6), and ethylene (C_2H_4). Methane was the most abundant hydrocarbon. The CO and CH_4 content in the product gases increased significantly with increasing temperature from 600 to 1000 °C, i.e. for maize stalk from 45.4 to 59.7 vol. % for CO and from 15.0 and 19.7 vol. % for CH_4. The CO_2 concentration exhibited the opposite trend. The maximum release rate of CO_2, CO, and CH_4 increased significantly with temperature and the time to reach the maximum release rate became shorter. Ethane and ethylene were minor gas products and the concentration of H_2 was below the detection limit of the gas analyzer.

The pyrolysis of wood chips has been studied extensively (Di Blasi et al., 1999; Di Blasi et al., 2001; Di Blasi and Branca, 2001; Di Blasi, 2008). The product distribution and the gas composition was studied on a bench scale in the temperature range of 377-727 °C (Di Blasi et al., 1999). At all temperatures, the pyrolysis gas consisted mainly of CO_2 (the largest contribution), CO, CH_4, and lower amounts of H_2 and C2 hydrocarbons. At temperatures below 800 °C, the production of H_2 was negligible. It was also observed that the CO yield increased with increasing temperature, and the CO fraction decreased with increasing particle size (Jand and Foscolo, 2005).

3.2.2.2 Tires

The pyrolysis gas obtained by different rubber tires consisted mainly of CO_2, CH_4, H_2, C_2H_6, and C_2H_4, but propane, propene, butane, butane, butadiene, and CO have also been found. Overall, the results suggest that the yields of oil, gas, and char from the pyrolysis of tires are not significantly influenced by the type and origin of the tire. However, there are noticeable differences in the composition of the derived gases and oils (Kyari et al., 2005).

Fernandez et al. (2012) studied the pyrolysis of tire rubber at 550 and 900 °C using rubber tire granules and tire fibers obtained as a waste during grinding and shredding of scrap tires. The amount of CH_4 increased with increasing pyrolysis temperature, especially in the case of the rubber granules from 9.9 % of the composition of the gas at 550 °C to 24.1 % at 900 °C. The amount of C3 (propane and propene) did not vary with the temperature. The behavior of C2 (ethane and ethane) was different for the two types of wastes; it increased with temperature in the case of the tire granules and did not show any great variation in the case of the fibers. Sulfuric acid was also detected from tire granulate, because it originated from the decomposition of sulfurous compounds. Hydrogen sulfide did not vary with the pyrolysis temperature, indicating that the vulcanized structure of the rubber had already decomposed at 550 °C. The C4 components of the gas (butane, butane, and

isobutylene) originate from the depolymerization of styrene-butadiene rubber and the diminution with temperature is attributed to the occurrence of reactions which lead to an increase in the amount of lighter hydrocarbons and H_2. For example, for tire granulate the C4 components contributed 38.1 % of the composition of the gas at 550 °C and decreased to 24.8 % at 900 °C, and for tires fibers the amount of C4 decreased from 28 % at 550 °C and 25.6 % at 900 °C.

3.2.2.3 Plastics

Pyrolysis gases from polyethylene (PE) plastic bags have been characterized by Ouiminga et al. (2009). More than 50 % of the volatile carbon was predominantly expressed in the form of light (C_2H_4 and CH_4) and heavy (C_6H_6) hydrocarbons. The CO and CO_2 concentrations were 10 times lower than the concentration of hydrocarbons. The percentage of carbon converted to CO, CO_2, and CH_4 increased with increasing pyrolysis temperature, i.e. at 800 and 1000 °C the percentage of carbon in the form of CO, CO_2, and CH_4 was 0.3, 0, and 13 % and 2, 3, and 23 %, respectively.

The emissions of pollutants from batch combustion of polystyrene (PS), PE, and poly-vinyl chloride (PVC) from 500 to 1000 °C were studied by Wang et al. (2003). The emissions of light hydrocarbon from the combustion consisted mainly of CH_4, C_2H_6, C_2H_4, acetylene, propane, propylene, and butane. In the case of PE, CH_4, C_2H_6, C_2H_4, acetylene, and propylene were identified at all temperatures and C_2H_4 (ethylene) was the most abundant light hydrocarbon specie. In addition, propane was identified at 600 °C, and butane at 800 °C. The maximum CO_2 yield for PS and PE was around 1500 mg CO_2/g sample at 600 ºC, and the CO_2 yield decreased with increasing temperature from 700 to 1000 ºC. The highest CO emission with 150 mg CO/g sample was produced by PE, followed by PS with 80 mg CO/g sample, and in the case of PVC, the yield of CO peaked at 800 ºC with 50 mg CO/g sample. The yields of CO did not change drastically with increasing temperature (Wang et al., 2003).

Pyrolysis studies of plastics and tires have been focusing on the emissions of poly-aromatic hydrocarbons (PHAs) which are considered harmful to the environment. Therefore, the main pyrolized gases have not been quantified (Font et al., 2004; Aracil et al., 2005; Kwon and Castaldi, 2012).

3.3 Technologies for Alternative Fuels Combustion

New types of combustion equipments have been developed in order to avoid operational process challenges when alternative fuels are used in the traditional firing points of cement plants and for optimizing the combustion of alternative fuels. The technologies for alternative fuel combustion can be divided into external reactors which are typically placed next to the calciner, kiln burners, and new kiln designs as emerging technologies.

3.3.1 External reactors

Different types of external reactors for treatment of alternative fuels have been developed and are used at some cement plants. The common concept is to use the high heating value gas in the calciner and incorporate solid residues into the cement chemistry.

3.3.1.1 Combustion Chambers

A combustion chamber, which is an external reactor attached to the calciner or preheater, is a design for combustion of large fuel particles. Many different designs have been developed (Gaser and Tadular, 2009; FLSmidth A/S, 2011; KHD Humboldt Wedag, 2012a; Tyssenkrup Industrial solutions, 2014a) and the combustion chambers operate typically with an excess of air, using the air generated in the clinker cooler and extracted from the tertiary air duct. Two types of large combustion chambers, where lumpy alternative fuels can be fired and the fuel residence time can be varied, will be further described in this section.

The HOTDISC from FLSmidth A/S is a combustion chamber designed for combustion of large and lumpy solid alternative fuels. Figure 3-4 and Figure 3-5 show a cross-sectional view of the HOTDISC and its typical position in an ILC-system. In the HOTDISC chamber, alternative fuels are introduced into a slowly rotating disc, where the fuels burn under oxidizing conditions when meeting the hot tertiary air. The fuel residence time is typically 20-40 min and can be optimized by adjusting the rotational speed of the disc. Raw meal from the lower cyclone stages of the preheater is added in order to control the temperatures inside the HOTDISC (FLSmidth A/S, 2011).

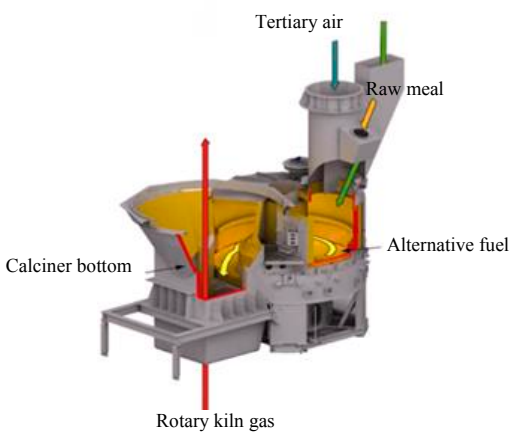

Figure 3-4: Cross-sectional view of the HOTDISC combustion device (FLSmidth A/S, 2011).

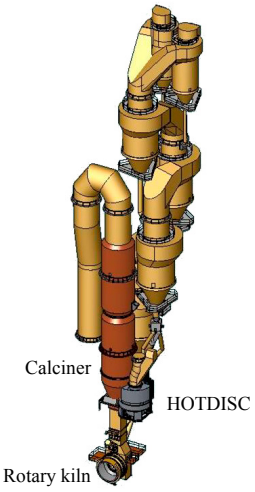

Figure 3-5: Typical position of the HOTDISC installed in preheater of an ILC-system (FLSmidth A/S, 2011).

The step combustor from Tyssenkrup Polysius (Tyssenkrup Industrial solutions, 2014a) is a combustion chamber specifically developed for high feed rates of low calorific and large-sized alternative fuels. Figure 3-6 shows the different parts and the principle of the step combustor. The fuel is fed into the inlet by special screw conveyors and by the conveying pressure of the screws, the fuel is lifted to the first stage, where the material is heated due to the hot tertiary air flowing over the material. The fuel transport through the different steps is realized with pulse jets. As function of the alternative fuel quality, the transport and discharge rates in the step combustor can be separately controlled and retention time extended up to 15 minutes (Menzel et al., 2009).

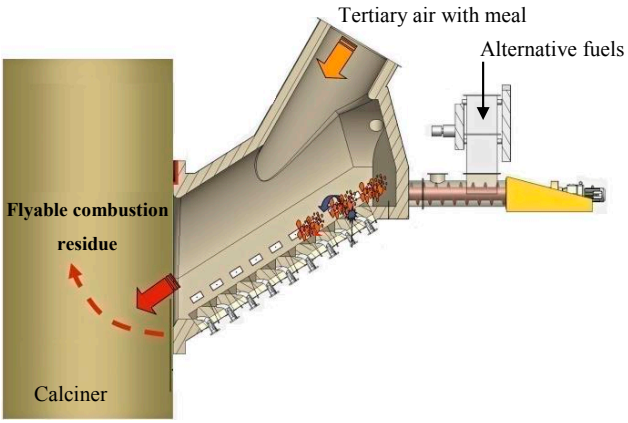

Figure 3-6: Principle of the step combustor (Tyssenkrup Industrial solutions, 2014a).

3.3.1.2 Gasifiers

Fluidized bed gasifiers for alternative fuels are also used in the cement industry (Schmidthals, 2003). In the gasifiers, the fuel is pyrolized under low-oxygen conditions and the lean gas produced is subsequently fed to the calciner as fuel, while the solid residues (char and ashes) are used as raw materials for cement production. The gasifiers can handle a wide variety of waste, regardless of their calorific values, i.e. paper and plastic waste (Wirthwein et al., 2002), whole tires (Saito et al., 1987), and sewage sludge (Kawasaki Heavy industries, 2013).

The world's largest gasification furnace is the Conch Kawasaki Kiln (Kawasaki Heavy industries, 2013), which is able to process 300 tons of waste per day.

3.3.2 Kiln burners

New kiln burners have been designed specially to combust alternative fuels and have been developed by many manufactures (FLSmidth A/S, 2008; Pillard Feuerungen GmbH, 2004; KHD Humboldt Wedag, 2012b; ThyssenKrupp industrial solutions, 2014b; Kaufmann, 2014). The new designs involve a compromise between

high substitution rates of alternative fuels and low NO_x emissions (Hass et al., 1999). A detailed review of rotary kiln burner design configurations for alternative fuels co-firing may be found elsewhere (Emberger and Hoenig, 2011).

Oxygen enrichment in the rotary kiln is a new technology, which has been demonstrated on a commercial scale to increase the alternative fuel utilization, decrease emissions, and improve the kiln performance and productivity (Arslan et al., 2013; Leger and Friday, 2001). However, economic considerations have prevented this technology from becoming a generally accepted practice (Leger and Friday, 2001).

3.3.3 Emerging technologies

3.3.3.1 Pyrorotor

The Pyrorotor is an invention from KHD Humboldt Wedag, which has not currently been installed in any cement plant yet (Streit, 2004). It consists of a rotary kiln that is flanged in between the ILC-system and the tertiary air duct, as illustrated in Figure 3-7. The large alternative fuels particles can be introduced, together with raw meal to control the temperature, in the upper end of the Pyrorotor and are converted by their downward movement caused by the rotation.

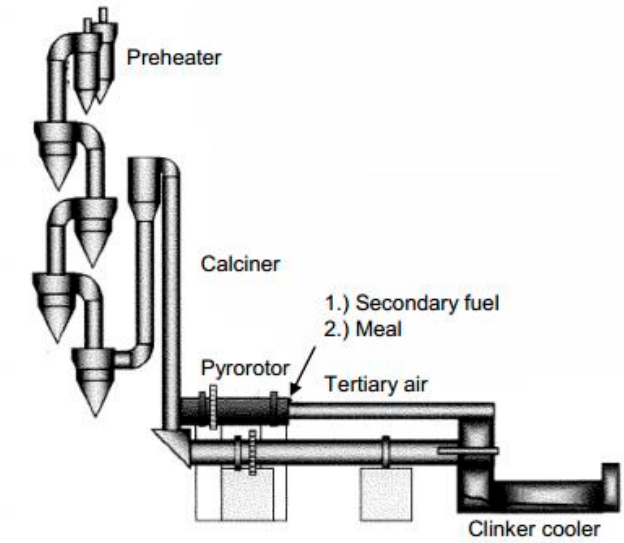

Figure 3-7: Pyrorotor for large fuel particles in cement production (Streit, 2004).

3.3.3.2 New Kiln Concept

The New Kiln Concept is an invention from FLSmidth A/S, which is patented (Jensen et al., 2010) but not commercialized. The equipment consists of a cement kiln that allows separate introduction of the calcined raw material and the fuels, as illustrated in Figure 3-8. Both the calcined raw meal and the fuels are heated by hot gases coming from the kiln burner. The fuel introduced in the cold inlet of the rotary kiln will be converted before the calcined raw meal is introduced. Thereby, the contact with the calcined raw materials and the local reducing zones will be minimized. The gases formed during the combustion of the fuel introduced in the kiln may be utilized for additional process stages, such as the calciner. The ashes from the fuel may be utilized in the forming of cement clinker or extracted with the cement clinker (Jensen et al., 2010).

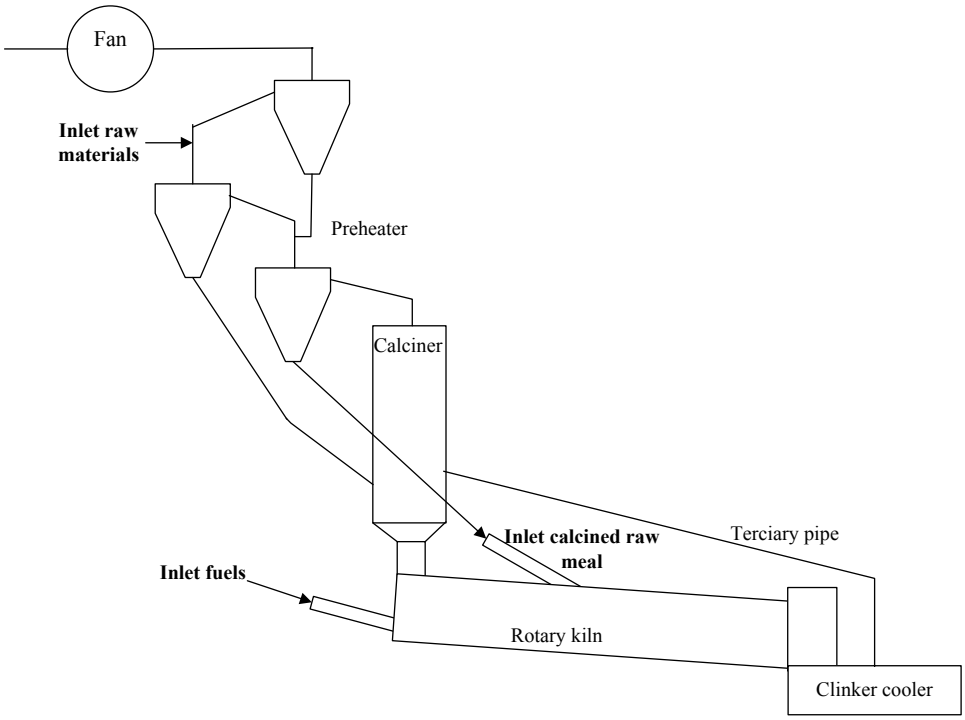

Figure 3-8: Scheme of the New Kiln Concept (Jensen et al., 2010).

3.4 Conclusions

The usage of alternative fuels is increasing continuously due to environmental concerns and the increase of conventional fuel prices. The physical and chemical characteristics of alternative fuels are different from the ones of fossil fuels, examples include higher content of volatiles, moisture and ash, lower heating value and particle size. The introduction of alternative fuels has led to modifications of the traditional firing points and

creation of new combustion equipments specialized for firing alternative fuels, such as external reactors, especially designed kiln burners, and new layouts of kiln systems, in order to optimize the combustion. However, large particles are often fired in the calciner, kiln burner and also directly into the material inlet end of the rotary kiln because this solution requires a minimum of investments. Subsequently, partially or unburned solid fuels end up in the bed material and cause local reducing conditions. The induced reductive conditions in the material inlet of the rotary kiln may affect the process stability of the kiln system due to an increase in the internal circulation of volatiles elements.

Combustion studies of alternative fuels have been reviewed in order to understand the consequences of combusting alternative fuels in cement plants. The main gases released under pyrolysis conditions from biomass and agricultural waste, have been identified as CO, CO_2, CH_4, and light hydrocarbons from tire rubber and plastics. The amount of CO released from biomass and plastics increased with increasing temperature from 800 to 1000 ^oC, and the same trend for CH_4 was observed with biomass and tires. For biomass, the yield of gas and the amount of H_2 released increased with increasing temperature and the fraction of CO decreased with increasing particle size. For tire rubber, sulfur species, such as H_2S and H_2SO_4, were also released due to its sulfur content from vulzanizers. Thereby, the amount of reducing agents increases as well as the gas yield with increasing pyrolysis temperature and these gaseous compounds play an important role in the reductive decomposition of sulfates.

3.5 References

Aho, M., and Ferrer, E.; Importance of coal ash composition in protecting the boiler against chlorine deposition during combustion of chlorine-rich biomass. Fuel, 84, 201-212, 2005.

AFPM (Americal Fuel and Petrochemical Manufactures); Petroleum coke overview, 2012. Available at http://www.afpm.org/policy-position-petroleum-coke/ Accessed 28/08/2014.

Aracil, I., Font, R., and Conesa, J. A.; Semivolatile and volatile compounds from the pyrolysis and combustion of polyvinyl chloride. Journal of Analytical and Applied Pyrolysis, 74, 465-478, 2005.

Arslan, E., Cirucci, J., Farmer, L., Listemann, M. and Shah, J.; Breathing life into fuel use. Air products technology, International Cement Review, 2013.

Ayllon, M., Aznar, M., Sanchez, J. L., Gea, G., and Arauzo, J.; Influence of temperature and heating rate on the fixed bed pyrolysis of meat and bone meal. Chemical Engineering Journal, 121, 85-96, 2006.

Babcock & Wilcox Co.; Steam, its generation and use. 2007. EBook #22657. Available at http://www.gutenberg.org/files/22657/22657-h/22657-h.htm.

BioBank; Biomass database from IEA bioenergy task 32. BIOS bioneregiesysteme GmbH, Graz, Austria. 2013. Available at http://ieabcc.nl/database/biomass.php.

Chinyama, M. P. M., and Lockwood, F. C.; Devolatilisation behaviour of shredded tyre chips in combusting environment. Journal of the Energy Institute, 80, 162-167, 2007.

Di Blasi, C.; Modeling of chemical and physical processes of wood and biomass pyrolysis. Progress in Energy and Combustion Science, 34, 47-90, 2008.

Di Blasi, C., and Branca, C.; Kinetics of primary product formation from wood pyrolysis. Industrial & Engineering Chemistry Research, 40, 5547-56, 2001.

Di Blasi, C., Branca, C., Santoro, A., and Hernandez, E. G.; Pyrolytic behavior and products of some wood varieties. Combustion and Flame, 124, 165-77, 2001.

Di Blasi, C., Signorelli, G., Di Russo, C., and Rea, G.; Product distribution from pyrolysis of wood and agricultural residues. Industrial & Engineering Chemistry Research, 38, 2216-24, 1999.

Directive 2010/75/EU. The Industrial Emissions Directive. Available at hhtp://www.europa.eu.

Emberger, E. and Hoenig, V.; Rotary kiln burner technology for alternative fuel co-firing. Cement International, 9, 5, 84-60, 2011.

European IPPC; Best available techniques (BAT) reference document for the production of cement, lime and magnesium oxide- European Integrated Pollution Prevention and Control Bureau. 2013.

Fernandez, A. M., Barriocanal, C., and Alvarez, R.; Pyrolysis of a waste from the grinding of scrap tyres. Journal of Hazardous Materials, 203-204, 236-243, 2012.

FLSmidth A/S; The next generation Duoflex burner is here. Highlights FLSmidth November, 2008, Available at: www. flsmidth.com.

FLSmidth A/S; HOTDISC combustion device, Brochure, 2011. Available at: www.flsmidth.com.

Font, R., Aracil, I., Fullana, A., and Conesa, J. A.; Semivolatile and volatile compounds in combustion of polyethylene. Chemosphere, 57, 615-627, 2004.

Fu, P., Yi, W., Bai, X., Li, Z., Hu, S., and Xiang, J.; Effect of temperature on gas composition and char structural features of pyrolyzed agricultural residues. Bioresource Technology, 102, 8211-8219, 2011.

Gaser, U., and Tadular, E. L.; Method and device for use of alternative fuels in clinker and cement production. United States. Patent US20090283015. Filed 2009.

Greco, R., and Enfil, G.; Combustion of unusual fuels. World Cement, 37, 33-38, 2006.

Hass, J., Agostini, a., Martens, C., Carrea, E. and van de Kamp, W. L.; The combustion of pulverized coal and alternative fuels in cement kilns. Results on the CEMFLAME-3 experiments. International Flame Research Foundation (IFRF), IFRF doc no F97/y/4, 1999.

Hassan, E. M., Steele, P. H., and Ingram, L.; Characterization of fast pyrolysis bio-oils produced from pretreated pine wood. Applied Biochemistry and Biotechnology, 154, 3-13, 2009.

Jand, N., and Foscolo, P. U.; Decomposition of wood particles in fluidized beds. Industrial & Engineering Chemistry Research, 44, 2005.

Jensen, L., Christensen, N., and Larsen, M.; Rotary kilns for alternative fuels. Denmark. Patent WO 20210/032149, filed 2010.

Kaantee, U., Zevenhoven, R., Backman, R., and Hupa, M.; Cement manufacturing using alternative fuels and the advantages of process modelling. Fuel Processing Technology, 85, 293-301, 2004.

Kara, M., Gunay, E., Tabak, Y., Durgut, U., Yildiz, S., and Enc, V.; Development of refuse derived fuel for cement factories in Turkey. Combustion Science and Technology, 183, 203-19, 2011.

Karstensen, K. H.; Formation, release and control of dioxins in cement kilns. Chemosphere, 70, 543-560, 2008.

Kaufmann, M.; Experience in burning alternative fuels in kiln burners-A TEC GRECO. Presentation at 8th Global Cemfuels Conference and Exhibition, Vienna, Austria, 2014.

Kawasaki Heavy industries; CKK at Work in China. Scope -Kawasaki Heavy industries quarterly newsletter. No. 96, July, 2013. Available at https://www.khi.co.jp.

KHD Humboldt Wedag; Burning Tehcnology: Pyroclon ® calciner, KHD combustion chamber. Brochure, 2012a. Available at www.khd.com.

KHD Humboldt Wedag; High pressure jet burners for multi-fuel scenarios- the PYROSTREAMTM. Brochure, 2012b. Available at www.khd.com.

Kobyashi, N., Itaya, Y., Piao, G., Mori, S., Kondo, M., Hamai, M., and Yamaguchi, M.; The behavior of flue gas from RDF combustion in a fluidized bed. Powder Technology, 151, 87-95, 2005.

Kwon, E. E., and Castaldi, M. J.; Mechanistic understanding of polycyclic aromatic hydrocarbons (PAHs) from the thermal degradation of tires under various oxygen concentration atmospheres. Environmental Science & Technology, 46, 12921-6, 2012.

Kyari, M., Cunliffe, A., and Williams, P.T.; Characterization of oils, gases, and char in relation to the pyrolysis of different brands of scrap automotive tires. Energy & Fuels, 19, 1165-73, 2005.

Larsen, M. B.; Alternative fuels in cement production. Ph.D. thesis, Technical University of Denmark, Department of Chemical and Biochemical Engineering, 2007. ISBN: 978-87-91435-49-8.

Lee, V. K. C., Kwok, K. C. M., Cheung, W. H., and McKay, G.; Operation of a municipal solid waste co-combustion pilot plant. Asia-Pacific Journal of Chemical Engineering, 2, 631-639, 2007.

Leger, C.B. and Friday, J.G.; Oxygen enrichment for cement kiln firing. IEEE/IAS 2001 Cement Industry Technical Conference, 3271-277, 2001.

Lemarchand, D.; Burning issues. International Cement Review, February, 65-67, 2000.

Li, F., and Zhang, W.; Combustion of sewage sludge as alternative fuel for cement industry. Journal of Wuhan University of Technology-Materials Science Edition, 26, 556-560, 2011.

Mackes, K. H., and Lightburn, C. R.; Evaluating the use of green wood chips processed from small-diameter trees as an alternate fuel for making cement. Forest Products Journal, 53, 42-47, 2003.

Menzel, K., Mass, U. and Lampe, Karl; Technologies for alternative fuel enhancement in clinker production lines. IEEE-IAS 2009 Cement Industry Conference, 188-196, 2009.

Milenkova, K. S., Borrego, A. G., Alvarez, D., Xiberta, J., and Menendez, R.; Devolatilisation behaviour of petroleum coke under pulverised fuel combustion conditions. Fuel, 82, 1883-91, 2003.

Mokrzycki, E., and Uliasz-Bochenczyk, A.; Alternative fuels for the cement industry. Applied Energy, 74, 95-100, 2003.

Murray, A., and Price, L. Use of alternative fuels in cement manufacture: Analysis of fuel characteristics and feasibility for use in the Chinese cement sector. USA Ernest Orlando Lawrence Berkeley National Laboratory, 2008.

Nielsen, A. R.; Combustion of large solid fuels in cement rotary kilns. Ph.D. thesis, Technical University of Denmark, Department of Chemical and Biochemical Engineering, 2012. ISBN: 978-87-92481-66-5.

Nørskov, L. K.; Combustion of solid alternative fuels in cements kiln burners. Ph.D. thesis, Technical University of Denmark, Department of Chemical and Biochemical Engineering, 2012. ISBN: 978-87-92481-98-6.

Ouiminga, S. K., Rogaume, T., Sougoti, M., Commandre, J. M., and Koulidiati, J.; Experimental characterization of gaseous species emitted by the fast pyrolysis of biomass and polyethylene. Journal of Analytical and Applied Pyrolysis, 86, 260-268, 2009.

Panagiotou, T., and Levendis, Y.; A study on the combustion characteristics of PVC, poly(styrene), poly(ethylene), and poly(propylene) particles under high heating rates. Combustion and Flame, 99, 53-74, 1994.

Pillard Feuerungen GmbH; Progressive burning. Burner Technology, February, 2004.

Pizant, J., and Gauthier, J. C.; Burning alternative fuels in rotary kilns. World Cement, 9, 64-74, 1997.

Prisciandaro, M., Mazziotti, G., and Veglio, F.; Effect of burning supplementary waste fuels on the pollutant emissions by cement plants: A statistical analysis of process data. Resources Conservation and Recycling, 39, 161-84, 2003.

Realff, M. J., Lemieux, P., Lucero, S., Mulholland, J., and Smith, P. B.; Characterization of transient puff emissions from the burning of carpet waste charges in a rotary kiln combustor. 2005 IEEE Cement Industry Technical Conference Record, 212-228, 2005.

Saito, I., Sakae, K., Origi, T. and Ueda, Y.; Effective use of waste tyres by gasification in cement plant, World Cement, 18, 264-259, 1987.

Schmidthals, H.; The pre-combustion chamber for secondary fuels - development status of a new technology. IEEE-IAS/PCA 2003 Cement Industry Technical Conference, Conference Record, 207-218, 2003.

Schürmann, H.; KHD's combustion chamber, rotary kiln burner and services for alternative fuels use in the cement industry- KHD Humboldt Wedag, 8th Global Cemfuels Conference and Exhibition, Vienna, Austria, 2014.

Singer, J. G.; Combustion Fossil Power: A reference book on Fuel burning and Steam Generation, Fourth Edition, Combustion engineering Inc. 1993. ISBN: 0-9605974-0-9.

Stenseng, M.; Pyrolysis and combustion of biomass. Ph.D. thesis, Technical University of Denmark, Department of Chemical and Biochemical Engineering, 2001. ISBN: 87-90142-65-9.

Streit, N.; A modular Calciner Concept- The Right Solution for any Kind of Fuel; Presented at the ECRA Seminar: Experience with Precalciners, Kilns, Bernburg, Novemeber, 2004.

ThyssenKrup industrial solutions; Special PREPOL calcining systems for different requirement profiles, 2014a. Available at http://www.thyssenkrupp-industrial-solutions.com/.

ThyssenKrup industrial solutions; POLFAME® clinkering zone burner, Brochure, 2014b. Available at http://www.thyssenkrupp-industrial-solutions.com/.

Tokheim, L.; Alternative fuels. 2012. Available at
http://www.hit.no/nor/HiT/Forskning/Forskningsaktiviteter/Technology-and-Engineering/Alternative-Fuels. Accessed in 18/3/2013.

Tokheim, L.; The impact of staged combustion on the operation of a precalciner cement kiln. Ph.D. thesis, Institute of Environmental Technology, Norway, 1999.

Trezza, M. A., and Scian, A. N.; Scrap tire ashes in Portland cement production. Materials Research-Ibero-American Journal of Materials, 12, 489-94, 2009.

Tsubouchi, N., Ohtsuka, S., Nakazato, Y., and Ohtsuka, Y.; Formation of hydrogen chloride during temperature-programmed pyrolysis of coals with different ranks. Energy & Fuels, 19, 554-560, 2005.

US Department of Energy; Hydrogen and fuel cells program: Lower and higher heating values of hydrogen and fuels. 2012. Available at http://hydrogen.pnl.gov/.

Varhegyi, G., Bobaly, B., Jakab, E., and Chen, H.; Thermogravimetric study of biomass pyrolysis kinetics. A distributed activation energy model with prediction tests. Energy & Fuels, 25, 24-32, 2011.

Vassilev, S. V., Baxter, D., Andersen, L. K., Vassileva,C. G.; An overview of the chemical composition of biomass, Fuel, 89, 913-933, 2010.

VDZ (Verein Deutscher Zementwerke); Activity report 2009-2012. 2012. Available at www.vdz.de/.

Wang, Z., Richter, H., Howard, J. B., Jordan, J., Carlson, J., and Levendis, Y.; Laboratory investigation of the products of the incomplete combustion of waste plastics and techniques for their minimization. ndustrial & Engineering Chemistry Research, 43, 2873-2886, 2004.

Wang, Z. L., Wang, J., Richter, H., Howard, J. B., Carlson, J., and Levendis, Y. A.; Comparative study on polycyclic aromatic hydrocarbons, light hydrocarbons, carbon monoxide, and particulate emissions from the combustion of polyethylene, polystyrene, and poly(vinyl chloride). Energy & Fuels, 17, 999-1013, 2003.

Weston, K. C.; Energy conversion. Ws Pub Co., 1992. ISBN: 978-0534938611. Available at http://www.personal.utulsa.edu/~kenneth-weston/.

Wirthwein, R., Scharf, K. F., Scur, P., and Drebelhoff, S.; Operating experience gained with a fluidized-bed gasifier using waste materials for lean gas making. ZKG International, 55, 61-69, 2002.

Wu, W., Chen, Y., Hu, L., and Luo, Y.; Isothermal pyrolysis of biomass by macro-TG. Power and Energy Engineering Conference, 2009. APPEEC 2009. Asia-Pacific, 2009.

Wurst, F., and Prey, T.; Dioxin emissions when using alternative fuels in the cement industry. ZKG International, 56, 74-77, 2003.

Zabaniotou, A., and Theofilou, C.; Green energy at cement kiln in Cyprus-use of sewage sludge as a conventional fuel substitute. Renewable and Sustainable Energy Reviews, 12, 531-541, 2008.

Zevenhoven, R., and Kilpinen, P. Chapter 3: Sulphur. In Control of pollutants in flue gases and fuel gases. Helsinki University of Technology, Finland, 2004. Online book Available at http://users.abo.fi/rzevenho/gasbook.html.

4. Circulation of Inorganic Elements in the Kiln System

This chapter provides an insight into the inorganic chemistry in the cement kiln system. Sulfur, chlorine, sodium, and potassium are considered in this chapter, since these elements are strongly related to operational problems experienced in the kiln. The main focus is on sulfur, in section 4.4 and in further chapters, because this element is most strongly affected by combustion of solid fuels in direct contact with the bed material.

The chapter initially outlines a description of the circulation of each of the volatile elements and the transformations of the different species containing these elements at different locations in the cement plant. The consequences and process challenges related to the combustion of alternative fuels are further described in section 4.2, with a special focus to the modification of the sulfur circulation, since this element is mostly affected by combustion conditions. Finally, thermodynamic equilibrium calculations are applied to map theoretically the inorganic chemistry in the kiln system under different atmospheres.

4.1 Circulation of Volatiles Elements

The circulating or volatile elements are minor components introduced in the kiln system through the raw meal and the fuels. The volatile elements evaporate when exposed to high temperature in the burning zone and then subsequently condense on the incoming raw meal or on plant surfaces in the cooler parts of the kiln system. By repetitive evaporation and condensation, these elements circulate at different temperatures and locations of a cement plant. When they are present in high concentrations, they often cause difficulties in kiln operation due to material build-up and ring formation, which will be further described in section 4.2.

Table 4-1 lists the range of the concentrations of Na_2O, K_2O, SO_3, and Cl found in different raw materials used in the cement industry. Sodium, potassium, and sulfur concentrations are usually expressed as oxides due to the elements analysis method. The concentrations of these elements found in fuels were presented in Table 3-2 in Chapter 3.

Table 4-1: Concentrations of Na, K, Cl, and S in the different raw materials.

Concentration [wt. %]	Raw materials			Reference
	Limestone, marl, chalk	Sand	Clay, shale	
Na_2O	0-0-1.5	0.0-1.0	0.1-1.5	(Jawed and Skalny, 1977; Sturz et al., 1998; Bhatty et al., 2011; European IPPC, 2013)
K_2O	0.0-3.5	0.2-3.0	0.4-5.0	
Cl	0.0-0.6	Traces	0.0-1.0	(European IPPC, 2013; Bhatty et al., 2011)
SO_3	0.0-0.7	0.0-0.5	0.21	(Jawed and Skalny, 1977; European IPPC, 2013)

4.1.1 Reaction Affinity between Volatile Elements

The circulating elements have a strong affinity for other elements, and form chemical species like chlorides and sulfates. The following order of affinity has been observed (Bhatty et al., 2011; Hewlett, 1998; Chinyama, 2011):

1. The chlorine reacts primary with the alkalis, forming KCl and/or NaCl, typically in gas phase. The residual chlorine combines with calcium, forming $CaCl_2$ (s/l). However, it is seldom that the input of chlorine is higher than the input of alkalis.
2. The excess alkali reacts with sulfur, forming K_2SO_4 and/or Na_2SO_4 in solid or gas phase. The residual alkalis combine with CO_2, forming K_2CO_3 and Na_2CO_3 (Glasser, 2011), or with moisture, thereby forming NaOH and KOH in gas phase. The alkalis can also be embedded in clinker minerals.
3. The excess of sulfur present as SO_3 and/or SO_2 in the gas will react with CaO (s), forming $CaSO_4$ (s).

The quantification of the circulation is determined by the volatility, which indicates the portion that is volatilized in the kiln and therefore not leaves the kiln with the clinker. The volatility is described using evaporation factors for each compound varying from 1 to 0, where 1 means that all volatile compounds are evaporated, and 0 that none is evaporated and therefore all leaves with the clinker.

4.1.2 Circulation of Sulfur

The sulfur circulation is the most complex. An illustration of the sulfur containing species and their transformation at different locations in a cement plant is shown Figure 4-1.

Sulfur can be introduced to cement rotary kilns by either cement raw materials and/or by the fuels. Biomass fuels, such as wood waste and straw, contain between 5 to 10 times lower amounts of sulfur, as when compared to fossil fuels. Sulfur can also be found in waste derived fuels, e.g. in car tires as a vulcanizer.

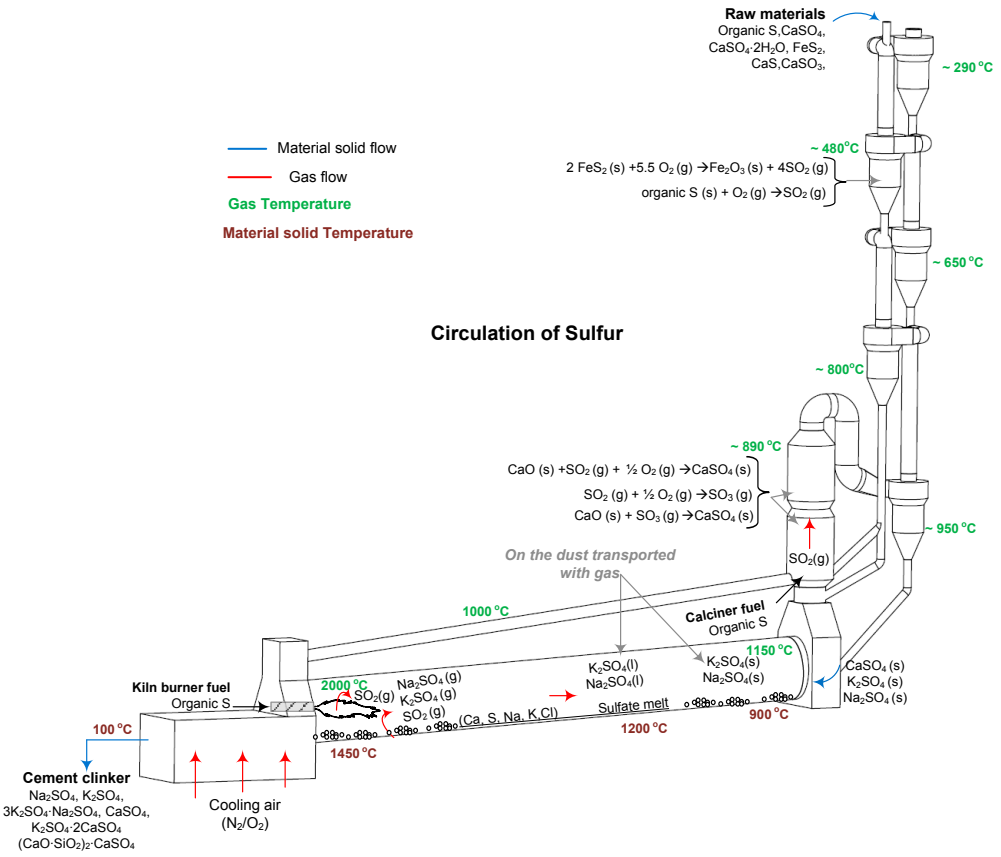

Figure 4-1: Circulation of the sulfur compounds in the kiln system.

In the preheater system, the organic sulfur and the pyrite from the raw meal are oxidized, thereby releasing SO_2 upon heating in an oxidizing environment. The oxidation of sulfur species (pyrite and organic sulfur impurities) occurs between 300 and 600 °C, which corresponds to the temperature in the first or second cyclone in a preheater tower (Klotz, 1997). The decomposition of pyrite has been reviewed by Hu et al. (2006a), who found that in an atmosphere containing oxygen, pyrite can decompose by direct oxidation (reaction (4-1)) or by thermal decomposition of pyrite to pyrrhotite and sulfur, followed by subsequent oxidation to SO_2 (reaction (4-2)). Iron sulfates may also be formed as minor products during the oxidation of pyrite in a gas rich in SO_2 at temperatures lower than 600-650 °C (Hu et al., 2006a).

$$2FeS_2(s) + 5.5O_2 \rightarrow Fe_2O_3(s) + 4SO_2(g) \quad (4\text{-}1)$$

$$2FeS_2(s) \rightarrow 2FeS_x(s) + 2(1-0{,}5x)S_2(g) \xrightarrow{O_2(g)} Fe_2O_3(s) + 4SO_2(g) \quad (4\text{-}2)$$

The gases leaving the preheater tower are used for drying the raw materials in the raw meal mill and a portion of the SO_2 will be captured, and thereby the SO_2 emissions will be lowered. Of the sulfur entering with the raw meal in the form of pyrites, it is often assumed that 30-50 % will leave the preheater tower as SO_2 (Nielsen and Jepsen, 1990; Bech and Gundtoft, 1998; Salmento and Shenk, 2004), but SO_2 emission from stack will account for 15-30 % of the sulfur entering with the raw materials in the form of non-sulfates (Nielsen and Jepsen, 1990). However, incorrect estimations of SO_2 emissions can be led because the amount SO_2 leaving the preheater tower can range from 10 to 65 % (Salmento and Shenk, 2004).

The SO_2 coming from the rotary kiln or from the calciner fuel is let to the calciner, where the good gas-solid mixing and the temperature favor capture of the sulfur, which is nearly 100 % (Salmento and Shenk, 2004). The sulfation of CaO with SO_2 has been recognized as a complex, high-temperature, short-time heterogeneous process, limited by gas-phase and solid-phase diffusion, with simultaneous physical transformation of the solid. The sulfation process can follow a number of routes, and in the literature, there is a lack of agreement on the mechanism. Two possible routes of sulfation have been discussed by Moss (1970), who examined the sulfation mechanisms, if proceeded via formation of $CaSO_3$ or via the conversion of SO_2 to SO_3 and this directly reacts with CaO to form $CaSO_4$. The relevant chemical reactions are:

$$CaO(s) + SO_2(g) \rightarrow CaSO_3(s) \quad (4\text{-}3)$$

$$CaSO_3(s) + \tfrac{1}{2}O_2(g) \rightarrow CaSO_4(s) \quad (4\text{-}4)$$

or

$$SO_2(g) + \tfrac{1}{2}O_2(g) \rightarrow SO_3(g) \quad (4\text{-}5)$$

$$CaO(s) + SO_3(g) \rightarrow CaSO_4(s) \quad (4\text{-}6)$$

It was suggested that the reaction proceeds via the formation of $CaSO_3$ (i.e. reaction (4-3) and (4-4)), at temperatures lower than 850 ^oC, where $CaSO_3$ is thermally stable. While reactions (4-5) and (4-6) dominate at temperatures above 850 ^oC (Moss, 1970) and the formation of SO_3 increases with decreasing temperature favored below 1000 ^oC by gas phase equilibrium, see Figure A-1 in Appendix A. The second route has been supported by many authors (Burdett, 1980; Dam-Johansen and Østergaard, 1991; Hansen et al., 1993; Hu et al., 2006b), although it has been suggested that both mechanisms might take place (Lin, 1988). Hu et al. (2006b) discussed the influence of the reaction conditions, such as SO_2, O_2, CO_2, and H_2O gas concentrations, limestone properties, reaction mechanism and modeling of the direct sulfation reaction via the second route. Kinetic studies have shown that the rate of reaction of CaO with SO_2/O_2 mixture is similar to that of the direct reaction with SO_3 (Allen and Hayhurst, 1996; Qin, 1995). No literature has been found to measure the precise SO_3 concentration because calibration gases for SO_3 analyzers are not available in the market. Both routes may take place simultaneously, however this topic is out of the scope of this review.

Calcium sulfate, $CaSO_4$, is incorporated in the hot meal entering the rotary kiln where it is gradually heated. Sulfates combined with calcium and alkalis forma liquid phase, so-called sulfate melt, at around 1200 ºC (Choi and Glasser, 1988). In the transient zone of the kiln, two immiscible liquids may occur at equilibrium: one is an oxide melt, containing Al_2O_3, Fe_2O_3 and SiO_2, and the other is a sulfate melt, in which Al_2O_3, Fe_2O_3 and SiO_2 are nearly insoluble (Bhattly et al., 2011; Glasser, 2011). The sulfur liquid phase contributes to ion mobility and promotes combination in the clinkering process as fluxing agents allowing a significant increase in the rate of reaction of the calcium silicates. In an absolutely homogenous mixture, no liquid phases are formed below 1338 ºC (Lea and Parker, 1935; de la Torre et al., 2007), where an eutectic in CaO-Al_2O_3-Fe_2O_3-SiO_2 system exists. Nevertheless, local inhomogeneities in the raw meal mixture cause a shift of the eutectic toward lower temperatures (de la Torre et al., 2007). Further explanation on the clinker phases and liquid phase formation has been reviewed by Telschow et al. (2014).

In the burning zone, where the bed material reaches its maximum temperature of 1450 ºC, evaporation of sulfur takes place forming SO_2, K_2SO_4, and/or Na_2SO_4 in the gas phase. The alkali sulfates in the gas phase are transported with the hot gases and the dust, along the rotary kiln. Alkali sulfates condense on dust particles, entrained by the kiln gases. The condensation product obtained between 700 and 800 °C is a melt, but at lower temperatures, condensation may result in a solid. Dust particles are incorporated in the solid stream in the calciner, and alkali sulfates enter then with the hot meal into the rotary kiln and are partly incorporated in the sulfate melt, thereby improving the chemical reactivity of the material in the kiln and lowering the viscosity of the melt, which can facilitate some of the clinker reactions (Choi and Glasser, 1988).

Thus, an internal sulfur cycle is established in the rotary kiln and the calciner, as illustrated in Figure 4-2; a Sankey diagram, in which the width of the lines, are proportional to mass flow. This is a schematic representation made by Nielsen and Jepsen (1990), using data from 12 preheater kiln systems in the US. The SO_2 coming from the kiln is absorbed by the raw meal in the calciner, and reincorporated in the solid stream that is introduced in the rotary kiln. Therefore, there is a significant circulation around the inlet of the rotary kiln and the calciner, considering both the incoming material and the outgoing kiln gases. The molar flow of sulfates in the kiln inlet is approx. three times the molar flow in the outlet (clinker).

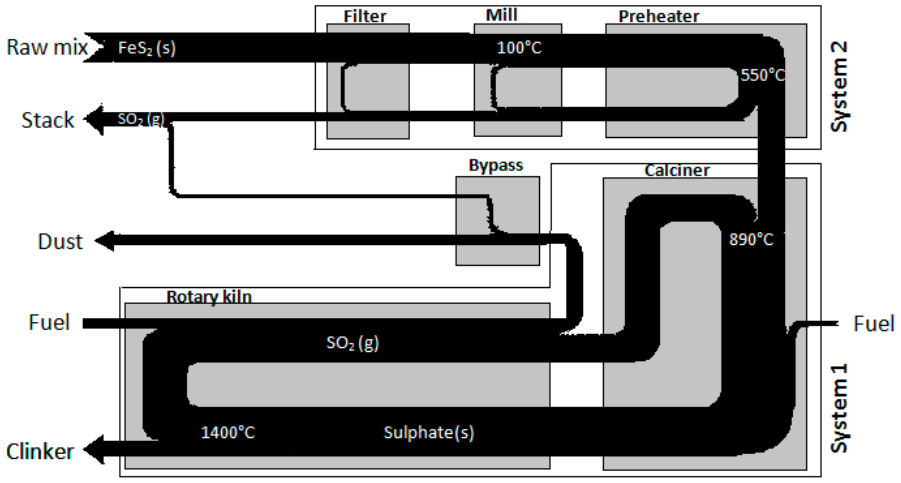

Figure 4-2: Sankey diagram of the sulfur circulation in a cement plant operating by the dry method. Raw meal and fuel are sulfur contributors and the sulfur leaves as emissions, in the dust or embedded in the clinker. The thickness of the lines indicates relative flow rates (Nielsen and Jepsen, 1990)

The fraction of sulfur released as SO_2 depends on the sulfur to alkali ratio in the rotary kiln (Mortensen et al., 1998), which is defined in equation 4.1, and expresses the proportion of sulfur that can be bound with alkalis.

$$\frac{SO_3}{Alk} = \frac{\frac{w_{SO_3,\,LOI\,free}}{M_{SO_3}}}{\frac{w_{K_2O,\,LOI\,free}}{M_{K_2O}} + \alpha \cdot \frac{w_{Na_2O,\,LOI\,free}}{M_{Na_2O}}} \qquad [4.1]$$

where M_i is the molar mass of the component *i*, α is the fraction of Na_2O that reacts with SO_3, and $w_{i,\,LOI\,free}$ is the total input concentrations of the specie *i*, being SO_3, K_2O and Na_2O (representing sulfur, potassium and sodium, respectively) in wt. % loss on ignition free base. The loss on ignition (LOI) indicates how complete the calcination processing is. By practical experience, α has the value of 0.5 because there is substantial excess of K_2O over Na_2O (Bhatty, 1995) and analyses of different clinker compositions have revealed that nearly the entire amount of potassium and half the amount of sodium forms sulfate (Jawed and Skalny, 1977; Hansen, 2003). The optimum SO_3/Alk is close to 1, for a low sulfur evaporation (Newkirk, 1951; Plang-ngern and Rattanussorn, 2003; Whitehopleman, 2011; Rahman and Krapkat, 2012) because there will be enough alkali metals for formation of alkali sulfates, rather than formation of free SO_2 (Mortensen et al., 1998). If SO_3/Alk is lower than 1, the sulfur is bound but there is an excess of alkali, which lead to alkali circulation forming KOH and NaOH in gas phase (Bhatty et al., 2011; Cemnet, 2012). If the ratio is higher than 1, there will be an amount of sulfur in the kiln material which will not be covered by alkalis. The excess of sulfur in the raw

materials to form $CaSO_4$ is termed excess SO_3, usually expressed as g excess SO_3/100 kg clinker, and may be calculated by the equation 4.2 (Fortsch and Smidth, 2004).

$$\text{Excess } SO_3 = w_{SO_3,\,LOI\,free} - \frac{M_{SO_3}}{M_{K_2O}} \cdot w_{K_2O,\,LOI\,free} - \alpha \cdot \frac{M_{SO_3}}{M_{Na_2O}} \cdot w_{Na_2O,\,LOI\,free} \qquad [4.2]$$

The limit on excess sulfur is given to be in the range of 250-600 g/100 kg clinker (Fortsch and Smidth, 2004; Cemnet, 2004). The lower limit is for low burnability raw meal, and the upper limit is for high burnability raw meal. The burnability is a measurement of how easy/difficult the clinker phases are formed. The excess sulfur will form $CaSO_4$, which is least thermally stable sulfate and will be contributing to a higher evaporation factor.

The sulfur volatility depends on the SO_3/Alk ratio and also on the operating conditions of the kiln, i.e.:

- Oxygen content of the kiln atmosphere. Deficiency of oxygen or local reducing kiln atmosphere increases the volatility of sulfur, because low oxygen level shifts reaction (4-7).

  $$CaSO_4(s) \rightleftarrows CaO(s) + SO_2(g) + \frac{1}{2}O_2(g) \qquad (4\text{-}7)$$

  The variation of the oxygen content in the kiln inlet has shown to modify the SO_2 concentration measured in the bypass gas, which is extracted from the kiln inlet. The relationship between SO_2 bypass emissions and O_2 concentration in the kiln inlet of the rotary kiln is shown in Figure 4-3. At higher O_2 concentrations, the SO_2 evaporation gets suppressed, and there will be no SO_2 emission in the bypass stack representing the SO_2 concentration in the material inlet of the rotary kiln. However, when the oxygen level in the kiln material inlet gets below around 2 vol. %, the sulfur evaporation increases steeply, and the bypass emissions can increase significantly (Steuch and Johansen, 1990). At lower oxygen concentrations, reduced sulfur species such as H_2S, COS in presence of carbon, and $SOCl_2$ in presence of Cl may also be formed, however, these species are not measured in cement plants.

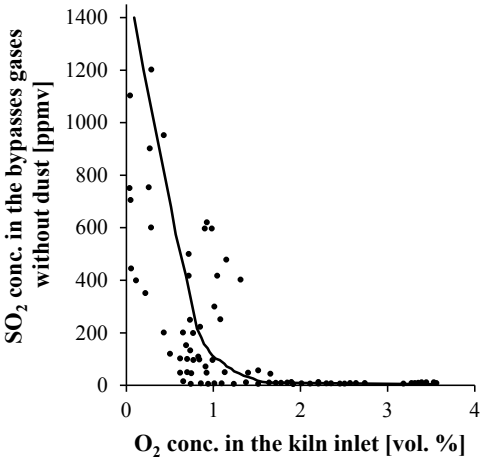

Figure 4-3: Relationship between SO_2 bypass emissions and O_2 concentration in the inlet of the rotary kiln, adapted from (Steuch and Johansen, 1990).

- Temperature in the burning zone. The volatility of the sulfur species is increasing as a function of temperature. Thermal decomposition is avoided by lowering the burning zone temperature. This may be achieved by making the raw meal more chemically reactive (burnability), which means finer grinding of the raw meal or adjusting the chemical composition of the raw meal. If the raw meal has a low burnability, it needs higher temperatures in order to get a low free lime in the clinker. Therefore, raw materials with low burnability or high temperatures overheating the clinker have a high impact on sulfur volatility (Hewlett, 1998; Smith, 2012).

The sulfur volatility can also be modified by carbon from fuels in the bed material, which will be further explained in section 4.3.2 and 4.3.3. Under stable operational conditions, and if there is enough alkali available to combine with the sulfur input, the volatility of the sulfur can vary from 0.35 to 0.6 (Bhatty et al., 2011).

During nodulization, the sulfate melt can be trapped in the inner core of the clinker nodules (Christensens and Johansen, 1979). The sulfate melt reaching the cooler will subsequently crystalize in the clinker. The composition of the sulfate melt at the end of the burning zone will determine the mixture of compounds that will solidify according to the tertiary diagram of $CaSO_4$-K_2SO_4-Na_2SO_4, illustrated in Figure 4-4. It can be seen that there are three primary precipitation areas, corresponding to $CaSO_4$, $K_2SO_4{\cdot}2CaSO_4$ (calcium langbeinite) and $(K,Na,Ca)SO_4$ (aphthitalite). If the composition of the melt is located in one of precipitation areas, the species of that area will precipitate first.

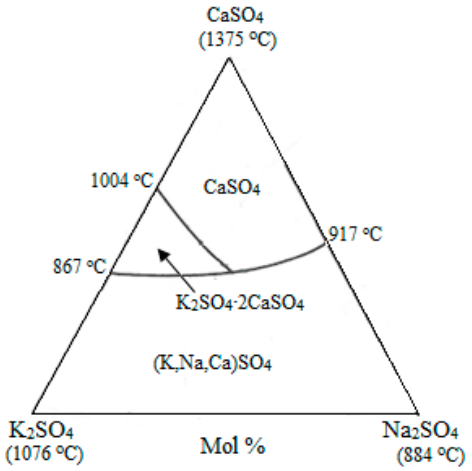

Figure 4-4: Tertiary phase diagram for $CaSO_4$, K_2SO_4 and Na_2SO_4, modified from (Rowe et al., 1972)

Sulfur in the Portland cement clinker is mainly found as Na_2SO_4, K_2SO_4, $CaSO_4$, $(K_x,Na_y)SO_4$ (aphthitalite), $K_2SO_4{\cdot}2CaSO_4$ (calcium langbeinite), and as substituents in the major clinker phases, mainly alite and belite with little in the ferrite (Twomey et al., 2004; Pollitt and Brown, 1969). For most common Portland cement, the upper acceptable limit of sulfur expressed as SO_3 in clinker, in order to assure good quality is 1.6 wt. % (Farag and Kamel, 1994; Cemnet, 2013) . More than half of the sulfur originating from raw materials and fuel appears in the clinker, the rest is lost in the flue gas and in the kiln dust (Jawed and Skalny, 1977).

Larger amounts of sulfur, higher than 2.6 wt. % SO_3 in clinker (Uda et al., 1998), start to negatively influence on the clinker mineral formation, via the inhibition of alite formation, and promoting the stabilization of belite and free lime, which needs to be lower than 1.5 wt. % CaO in clinker. One measure to prevent this phenomenon is to add calcium fluoride (CaF_2) to the raw meal, as a mineralizer. This allows lowering the burning temperature, and consequently the formation of alite is accelerated and the burnability is improved. However, concentrations higher than 0.25 wt. % CaF_2 in clinker are negatively affecting the cement properties such as retarded setting, reduced early strength and increased late strength (Klemm et al., 1979; Ghosh, 1991; Bhatty, 1995; Bhatty et al., 2011).

4.1.3 Circulation of Chlorine

The chlorine circulation and the locations of the formation of different chlorine species in a cement plant are illustrated in Figure 4-5.

The chlorine, as chlorides, is frequently found in limestone and clays, predominantly as NaCl. The raw material meal usually contains relatively small amounts of Cl, mostly less than 0.01 wt. % LOI free (Bhattly, 1995) and

the maximum chlorine concentration allowed in the raw meal is 0.03 wt. % LOI free for ILC-system without a bypass, because higher concentrations will cause heavy build-up problems in the kiln (Norbom, 1973).

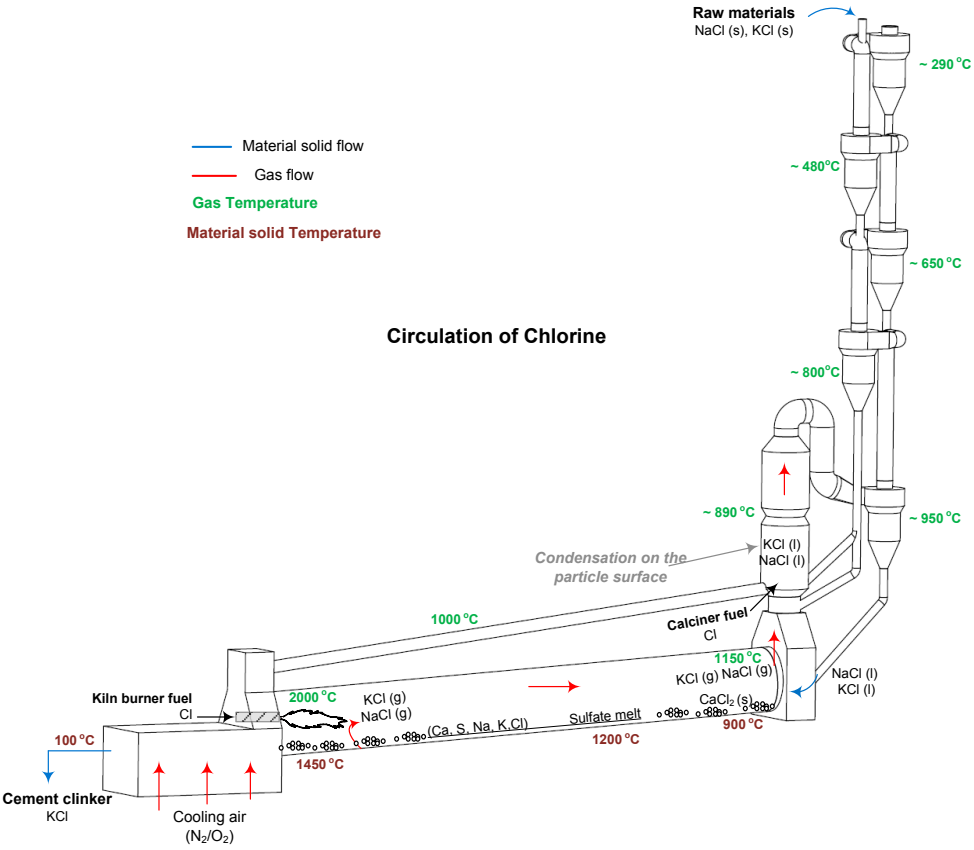

Figure 4-5: Circulation of the chlorine compounds in the kiln system.

Chlorine can be liberated during combustion of fuels, and the chlorine input from fuels can vary significantly, depending on the type of fuel. The Cl-content in fossil fuels, such as coal and petcoke, is rather low, but it can be significant for alternative fuels, such as RDF, see Table 3-2. The possible paths and release mechanisms of Cl during pyrolysis and combustion of biomass are explained elsewhere (Johansen et al., 2013). HCl gas is produced when fuels containing organically bound chlorine or inorganic chloride salts are burned (Partanen, 2004). Organically associated Cl can also be released in the gas phase as CH_3Cl (Sahel et al., 2014). In the calciner, and along lower preheater stages, the HCl will be absorbed by free lime according to reaction (4-8) (Partanen, 2004), however the absorption of HCl by limestone is strongly dependent on the humidity of the flue gas. The absorption of HCl by limestone has been extensively studied by Partanen et al. (2005a, 2005b, 2005c).

$$CaO(s) + 2HCl(g) \rightleftarrows H_2O(g) + CaCl_2(s/l) \quad (4\text{-}8)$$

In the burning zone, there is no reactive free CaO suspended in the flame, and HCl from kiln fuel will therefore go directly to the preheater and be converted to $CaCl_2$ there.

In the calciner and the lower cyclone stages, at a temperature between 800-850 °C, the chlorine species from the raw materials can melt, and the condensation of chlorine species from the kiln gases also occur. Therefore, the chlorine species are present in the liquid phase. The inverse reaction of (4-8), can also occur in presence of moisture.

In the burning zone, KCl and NaCl as chlorine compounds evaporate from the sulfate melt. The chlorine has an evaporation factor range of 0.900 to 0.996, and will evaporate nearly 100 % (Bhattly, 1995; Jøns and Østergaard, 2001; Jøns et al., 2008). The boiling temperatures of KCl and NaCl are approximately 1400 °C at 1 atm. The circulation is determined by the phase equilibrium between liquid and gaseous KCl.

Figure 4-6 shows a Sankey diagram for chlorine circulation showing how the gaseous, liquid, and solid chloride flows. The Sankey diagram was made based on data from a Finnish cement plant, and the diagram is only valid for low chlorine circulation (Jøns, 2013). The chloride has a considerable circulation around the calciner leading to high chlorine concentration. As an approximation, the chlorine mass flow in the kiln inlet is 200 times greater than the discharched mass flow in the outlet.

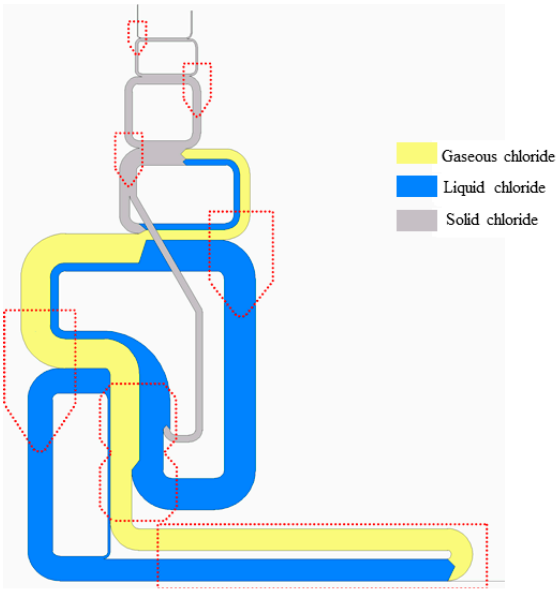

Figure 4-6: Sankey diagram for chlorine circulation in a modern calciner kiln showing the gaseous, liquid and solid chloride flows (Jøns et al., 2008).

High values of the SO_3/Alk ratio are critical in combination with circulation of chlorides, because the sulfidation of alkali chlorides at temperature higher than 900 °C can take place according to the general reaction (4-9), where M can be Na or K. Alkali sulfates can be either solid or gaseous depending on the temperature and whether aerosol formation occurs or not, i.e. dependent on the local concentration and temperature profiles. Reaction (4-10) shows the sulfation of $CaCl_2$ which can also react with SO_2. The combination of HCl and SO_2, in presence of moisture, in the gas phase makes the kiln gas very corrosive and sulfation is enhanced by the presence of chlorides in the middle zone of the kiln (Jøns and Østergaard, 2001). The same gas combination is responsible for deposit build-ups on the riser duct and/or cyclones caused by formation of chloroellestadite (Bhatty et al., 2011), see section 4.2.5.

$$2MCl(g) + ½\ O_2(g) + SO_2(g) + H_2O(g) \rightarrow M_2SO_4(g/l) + 2HCl(g) \quad (4\text{-}9)$$

$$CaCl_2(g) + ½\ O_2(g) + SO_2(g) + H_2O(g) \rightarrow CaSO_4(g/l) + 2HCl(g) \quad (4\text{-}10)$$

Hydrolysis of alkali chlorides in the gas phase contributes to the formation of HCl (g), according to reaction (4-11) especially at temperatures of the burning zone. However, the formation of HCl through this reaction at temperatures below 1000-1150 °C is limited, because the majority of the KCl is in gas phase, and the tendency for KCl (g) to hydrolyze at such temperatures is low (Jøns and Østergård, 2001).

$$KCl(g) + H_2O(g) \rightleftarrows KOH(g) + 2HCl(g) \quad (4\text{-}11)$$

The chlorine can be found in the clinker as $CaCl_2$, and sometimes as KCl, if it is trapped in the inner core of the clinker nodules. Most of the standards for Portland cement restrict the amount of chloride present to 0.1 wt. %, in order to avoid problems of reinforcement corrosion in concrete (Hewlett, 1998; Dalton et al., 2004; Farag and Kamel, 1994) .

4.1.4 Circulation of Alkalis

Circulation of alkalis, which are mainly introduced from the raw materials, is represented in Figure 4-7. It is well known, that potassium species are usually more volatile than the sodium species (Bhatty, 1995), see Figure 4-8. The intensity of the alkali cycle depends upon the nature of the alkali metals in the raw material, on operating practices, and on type of kiln (Bucchi, 1981). The limiting content of Na_2O and K_2O is generally expressed as Na_2O equivalent, which is defined by equation 4.3.

$$w_{Na_2O,\,equiv} = w_{Na_2O,\,LOI\,free} + \frac{M_{Na_2O}}{M_{K_2O}} \cdot w_{SO_3,\,LOI\,free} \quad [4.3]$$

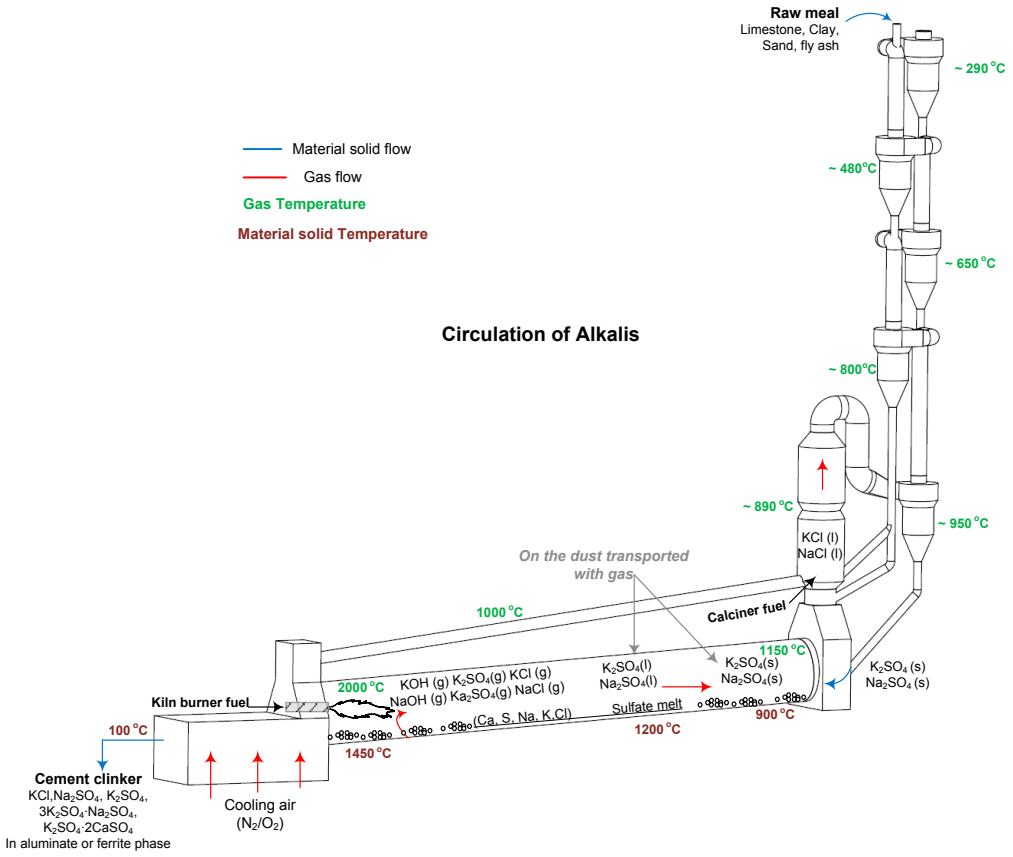

Figure 4-7: Circulation of the alkali compounds in the kiln system.

The source of alkali is most commonly clay or shale, but they can also be present in some limestone, sand, and frequently in various types of alternative raw materials such as fly ashes. The average alkali concentrations are 0.17 wt. % Na_2O and 0.57 wt. % K_2O for the raw materials (Bhatty, 1995). In most cases the alkali input by fossil fuels and/or by alternative fuels is rather small or negligible, except for cases with high alkali content in the ash, i.e. bituminous coal (Vassilev and Vassileva, 2009).

In the preheater tower, the alkalis partly dissociate into the gas phase, and recombine with other elements according to the affinity order, described in section 4.1.1. If the alkalis are not balanced by sulfates, they will remain very volatile and accumulate in the circulation between the kiln and the preheater. The extent of alkali volatilization varies with raw materials, and is higher for clays than for feldspars. About 50 wt. % of alkalis present in the raw feed are volatilized in the kiln, between 800 and 1000 °C (Jawed and Skalny, 1977).

The acceptable range of Na_2O and K_2O concentration in the kiln riser, varies from 3 to 5 wt. % LOI free (Bhatty et al., 2011). Excess alkalis have a potential to form alkali carbonates in the cyclones. Furthermore, too high alkali content without sulfur coverage can also cause build-ups in the kiln riser, or blockages in the tertiary air pipe, as mentioned in the circulation of sulfur (section 4.1.2).

The alkali sulfates form part of the sulfate melt and remains trapped in the nodules as a liquid through the burning process. Clinker nodules more porous tends to contain high alkali sulfates (Harrison, 2009). Studies on the distributions of alkalis in the clinker have confirmed that finer nodules contain lower alkali levels than courser nodules due to the higher surface available for alkali volatilization (Harrison, 2009; Masaki et al., 2002; Samet and Sarkar, 1997). In the burning zone, the alkalis can evaporate as NaCl, KCl, NaOH, KOH, K_2SO_4, and/or Na_2SO_4, as shown in Figure 4-7. Presence of H_2O (g) in the kiln atmosphere promotes the formation of alkali hydroxides, which are more volatile than the corresponding sulfates, according to reaction (4-12). A similar reaction also takes place for sodium.

$$H_2O\,(g) + 2K_2SO_4(g) \rightarrow 4KOH\,(g) + 2SO_2(g) + O_2(g) \qquad (4\text{-}12)$$

The rest of the alkalis not being in the gas phase recombines directly in the bed material with Cl or S, or are integrated into the lattice of the clinker minerals, such as belite and aluminate.

Alkali sulfates condense on dust particles at the exit gas temperature of the rotary kiln. Furthermore, raw meal is added in the riser duct in order to favor the alkali sulfate condensation, otherwise, the alkali sulfates would condensate on the walls of the riser duct, creating deposits. In this way, alkali sulfates in gas phase from the kiln are incorporated in the raw meal after the calciner (Jensen, 2014). Too high alkali content without sulfur coverage can also cause build-ups in the riser or blockages in the tertiary air duct.

The composition of the condensate is not be pure alkali sulfate but may include CO_2 from the gas stream and the clinker meal. Thus, the chemistry of the melt is an alkali sulfate and alkali carbonate melt, containing small amounts of alkali hydroxide. The presence of carbonate dissolved in the molten sulfate phase explains the presence of CO_2 in the clinker analyses (Bhatty et al., 2011).

In the presence of chlorides and sulfates, the volatilization behavior of both Na and K is modified greatly (depending on how Na and K are combined) as shown by the vapor pressure-kiln temperature relationship in Figure 4-8. In the presence of sulfur, alkalis preferentially form sulfates, if present in amounts higher than the required stoichiometric balance (Bhatty et al., 2011).

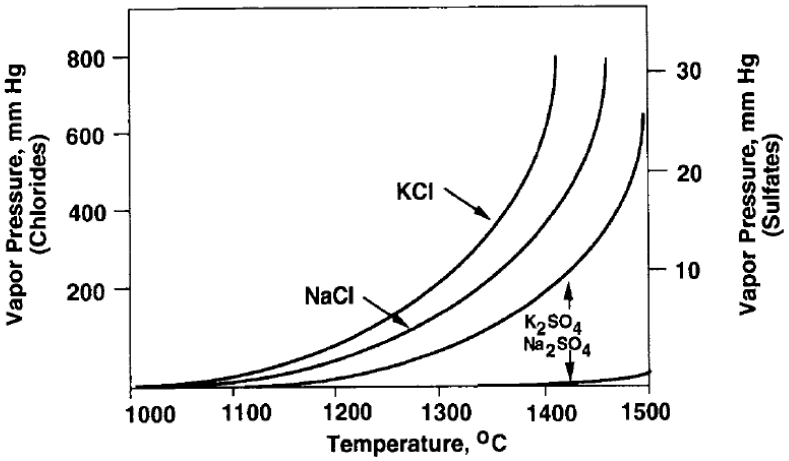

Figure 4-8: Vapor pressure of Na and K chlorides and sulfates (Bhatty, 1995).

Some of the Na_2O and K_2O are incorporated into aluminate, ferrite and belite and the residual alkalis will remain as sulfates. Introduction of alkalis into clinker minerals modifies their crystal structure, which may decrease the hydraulic reactivity of the cement (Jawed and Skalny, 1977). Alkali compounds in the clinker can be divided into three main groups: [1)] alkali sulfates, [2)] alkali aluminates and alumino ferrites, and [3)] alkali silicates. In some cases, alkali may also occur in the form of carbonates (Jawed and Skalny, 1977).

High levels of total alkali in the final cement often lead to higher pH, and better early strength development, but lower later strengths. Soluble alkalis, which are not bound with sulfur, may cause flash set (rapid and early loss of cement workability during water addition), due to activation of the calcium aluminates, and will also cause a significant loss of 28 days strength (Midgley, 1984). Alkalis potentially can give rise to cracking and expansion in concretes, due to their deleterious alkali-silica reaction with reactive aggregates. In this situation, the alkalis react with moisture, and produce a gel which expands (Hewlett, 1998; British ecological survey, 2005). Furthermore, high concentration of alkalis in concrete has harmful effects on most mechanical properties of concrete, such as compressive, splitting, direct tensile, and flexure strengths (Smaoui et al., 2005).

4.2 Consequences of High Volatile Circulation

4.2.1 Deposit Build-up Formation

The consequences of high internal circulation of elements are formation of build-up and blockages. The gaseous species condense in the cooler zones, and the condensation products are often chemically aggressive and with low melting temperature range. Therefore, the liquid is present in the preheater tower, the presence of which, reduces the flowability of raw meal, and causes the particles to stick to the walls (Smith, 2012). This may subsequently cause build-up on cyclone walls and riser ducts. Formation of build-ups may reduce the kiln

production, and cause higher heat consumption, and kiln or plant stops, which are expensive. Table 4-2 lists the common intermediate compounds found in build-ups and kiln rings and their typical location.

Table 4-2: Common intermediate compounds found in build-ups and kiln rings (Saint-Jean et al., 2005, Nievoll et al., 2009).

Name	Formula	Location typically found
Spurrite	$(2CaO \cdot SiO_2)_2 \cdot CaCO_3$	Lower cyclones
Ellestadite	$Ca_{10}(SiO_4)_3(SO_4)_3Z_2$ for Z= OH, F, or Cl	Riser duct
Sulfospurrite	$(2CaO \cdot SiO_2)_2 \cdot CaSO_4$	Kiln rings
Anhydrite	$CaSO_4$	Cyclones and riser duct

In the literature, chemical analysis of the build-up samples from different cement kiln preheaters have shown that the main constituents are SO_2, K_2O, CaO and Cl^- and that their proportions may vary significantly, depending on their location (Recio Dominguez et al., 2010). The dominant phases in most of the samples were $CaSO_4$ or a mixture of $CaSO_4$, and $CaCO_3$. Smaller amounts of other phases, such as ellestadite solid solution ($Ca_{10}(SiO_4)_3(SO_3)Z_2$, where Z can be OH, F, or Cl), more frequently chlorellestadite, $Ca_{10}(SiO_4)_3(SO_3)Cl_2$, and spurrite have also been reported. Microstructural examination showed that the growth of the rings was due to successive deposition of particles and condensation of gases. The study stated that the main cause of the deposit formation was the presence of a glassy phase, $K_{1-x}Na_xCl$ (Recio Dominguez et al., 2010).

The presence of spurrite and KCl were found to be the reasons for the build-up stability in the lower part of the preheater (Kurdowski and Sobon, 1999). The investigation suggested a KCl crystallization model based on a vapor-liquid-solid (VLS) mechanism, which is illustrated in Figure 4-9. The first step is the condensation of volatile elements on the grains of limestone; then agglomerates are formed in the presence of a liquid phase, and stick to the walls of the gas ducts, causing further increase in thickness of the solid material layer. Then, in the accretion formed, good conditions are created for KCl crystallization according to the VLS mechanism, i.e. KCl vapor pressure of and a temperature close to the melting point (Kurdowski and Sobon, 1999).

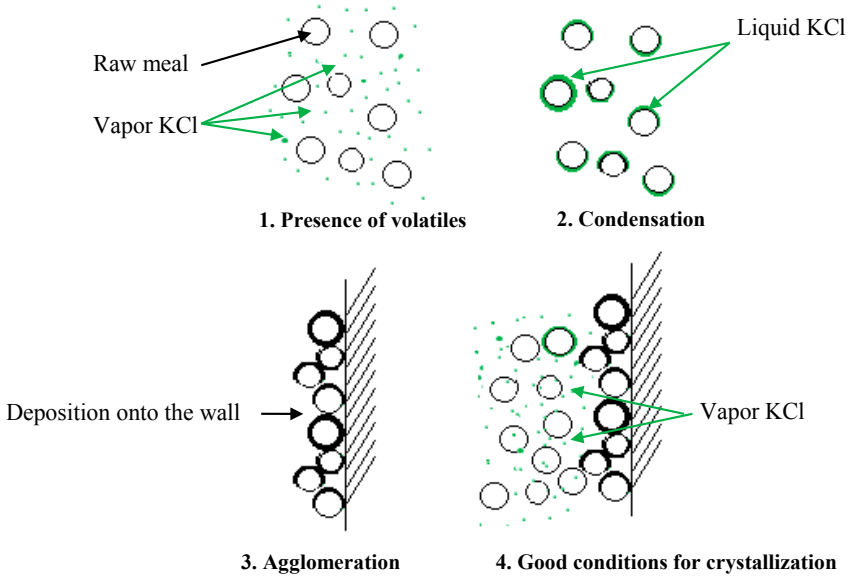

Figure 4-9: Model of KCl crystallization, adapted from (Kurdowski and Sobon, 1999).

The composition of the build-ups has been further investigated by Saint-Jean et al. (2005), using X-ray fluorescence (XRF), scanning electron microscopy (SEM), and chloride potentiometric titration. Based on the analyses, it was found that the corrosion scale contained water-insoluble as well as water-soluble chlorine. Build-ups on the walls of cyclones, and the riser duct, contained substantial amounts of chlorine in water-insoluble form, identified as chlorellestadite instead of the more common water-soluble KCl and NaCl. The chlorellestadite formation might lead to the clogging of pipes, which results in a decreased clinker output, and necessitate cleaning. Based on thermodynamic calculations, Saint-Jean et al. (2005) proposed that the chlorellestadite was formed due to the presence of gaseous HCl, and the reaction (4-8) which becomes more favored, as the temperature decreases. Consequently, the presence of chlorellestadite indicates formation of HCl in the hot atmosphere (Saint-Jean et al., 2005).

$$CaO(s) + 2HCl(g) \rightarrow H_2O(g) + CaCl_2(\mathrm{s}/l) \qquad (4\text{-}8)$$

The degree of contact between the gas and lime-containing dust in the kiln may influence the HCl formation (Saint-Jean et al., 2005). It was proposed two reactions, (4-13) and (4-14), which can take place in the cooler parts of the kiln depending on the extent of contact of the gases with lime-containing dust (Saint-Jean, 2003).

Insufficient dust contact:

$$SO_2(g) + 2KCl(g) + H_2O(g) + \frac{1}{2}O_2(g) \rightleftharpoons K_2SO_4(l) + 2HCl(g) \quad (4\text{-}13)$$

Sufficient dust contact:

$$SO_2(g) + 2KCl(g) + CaO(s) + \frac{1}{2}O_2(g) \rightleftharpoons CaSO_4(s) + 2KCl(g) \quad (4\text{-}14)$$

According to the insufficient dust contact reaction, the poor contact between the hot kiln gases and lime-containing dust in the kiln causes formation of gaseous HCl from KCl and SO_2, and subsequently, HCl in contact with the hot meal in the preheater unit can form chlorellestadite (Saint Jean, 2003). Figure 4-10 and Figure 4-11 illustrate the global equilibrium analyses simulating the reactions with sufficient and insufficient contact with lime-containing dust, respectively. The system was modeled as an enclosed box of variable volume with a fixed pressure of 1 atm and considered two phases: pure solid (chlorides and sulfates) and an ideal gas (N_2, CO_2, O_2, and H_2O). A third phase, which consisted on CaO (s) representing the dust, was only included for the case of the sufficient contact with lime containing dust (Figure 4-10).

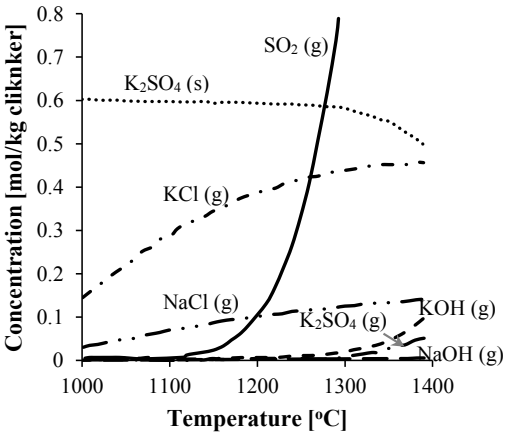

Figure 4-10: Thermodynamic calculations simulating the reactions with sufficient contact with lime-containing dust, modified from (Saint Jean, 2005).

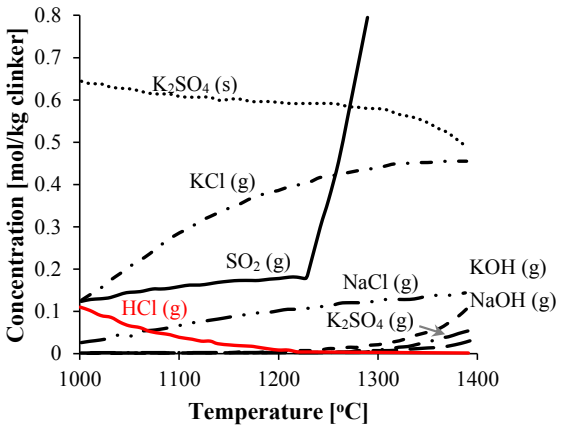

Figure 4-11: Thermodynamic calculations simulating the reactions with insufficient contact with lime-containing dust, modified from (Saint Jean, 2005).

Analyzing the results with decreasing temperature (from 1400 to 1000 ºC), at high temperature there is SO_2 (g) due to the thermal decomposition in the burning zone for both cases. For the case of sufficient contact with dust, the SO_2 concentration decreases to zero below 1200 ºC because it is captured by the lime-containing dust. In addition, no HCl in the gas phase is observed. On the contrary, for the case of insufficient contact with dust, not all the SO_2 in gas phase is not absorbed by CaO when decreasing temperature and below 1200 ºC, formation of alkali sulfates and HCl (g) occurs. Figure 4-11, for the case of insufficient contact with dust, shows that SO_2

and HCl in the gas phase will be observed in the kiln inlet. Jean et al. (2005) concluded that the HCl (g) concentration can be reduced by means of better gas-solid contact in the kiln.

Sulfur and chlorine concentrations in the hot meal can be used to evaluate the risk of build-up formation in the calciner, according to Figure 4-12 (Enders, 2011). The diagram is based on industrial experience, and is divided in 3 zones: low, medium and strong build-up tendency. The build-up tendency is linked to the required cleaning or removal of the build-ups. Therefore, it is recommended to operate a cement plant in the low and medium build-up tendency zones.

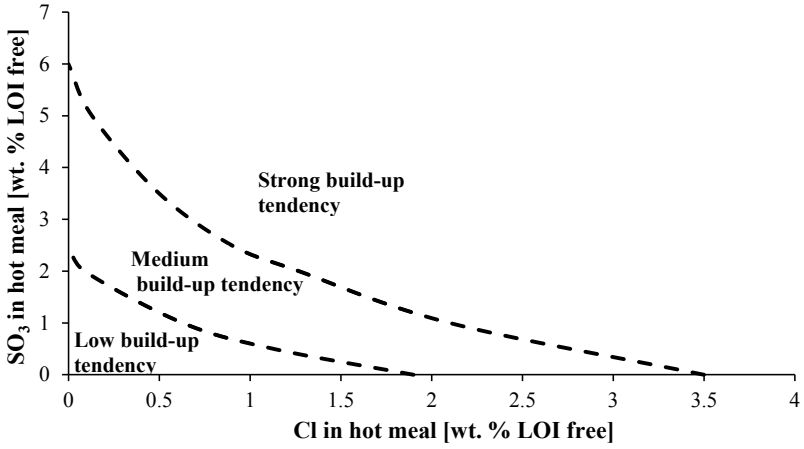

Figure 4-12: Evaluation diagram of build-ups tendency as a function of SO_3 and Cl content in hot meal, modified from (Enders, 2011).

According to Figure 4-12, the hot meal content of SO_3 should be maintained below 6 wt. %, and the Cl content below 3.5 wt. %, in order to avoid strong coating tendency.

It is generally accepted, and in agreement with Table 4-2, that the formation of build-ups in the lower cyclones may be associated with an increase in chlorine evaporation, and the build-ups in the riser duct with an increase in sulfur evaporation.

4.2.2 Coating and Ring Formation in Rotary Kilns

Blockages in the kiln system are normally referred to as either coating or ring formation (Peray and Waddell, 1972), consisting of a mass of clinker or dust that adheres to the wall of the kiln, and solidifies state. They are easily formed, when an excess of sulfur over alkalis exists in the kiln atmosphere.

There are different types of kiln rings and their difference is based on their composition and location in the kiln. Figure 4-13 illustrates a rotary kiln with five typical complications, which are:

1. Nose rings or ash rings
2. Clinker coating
3. Trumpet coating or sinter ring
4. Clinker rings
5. Transition zone rings

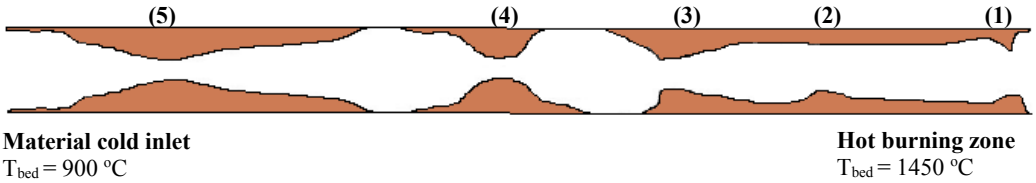

Figure 4-13: Illustration of the five typical coating complications in a cement rotary kiln.

The nose ring, which is marked by point 1 in Figure 4-13, is formed in the hot burning zone, where the clinker leaves. It can be formed very fast, and sometimes needs daily removal. These formations are caused by crystallization of clinker liquid, or free alkali sulfates in the clinker. The liquid available at the kiln nose permits adherence of the dust particles, and therefore the building of the nose ring continues. Microscopic evaluations of clinker produced during the presence of a nose ring, indicate the presence of slow cooling. Slowly cooled clinker causes the alite to revert back to belite and free lime (Hamilton, 1997).The build-up in the clinker cooler back wall, referred as snowman build-up, is illustrated in Figure 4-14, and is caused by the same problem that promotes the nose ring, which is a slow cooling of the clinker.

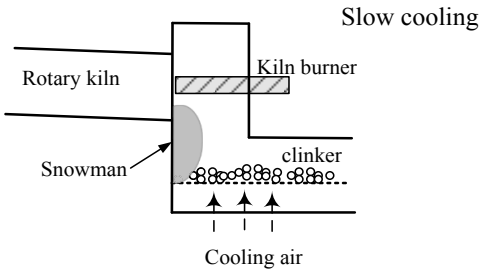

Figure 4-14: Illustration of the snowman build-up on the clinker cooler back wall, adapted from (Hamilton, 1997).

Point 2 in Figure 4-13 shows the clinker coating, which normally has the same chemistry and mineralogy as the clinker bed, since it is made up of the clinker. It is desired to operate the kiln with coating formation in order to protect the lining from thermal shocks, abrasion by the kiln bed and chemical infiltration by the gases, and prolong the lifetime of the kiln (Clark, 2011). The thickness of the coating is under normal conditions determined by the heat transfer through the lining which means that when the surface temperature of the lining reaches the melting point of the clinker liquid, it stops growing in thickness. Thus, an equilibrium exists at

these conditions. Figure 4-15 shows the influence of the temperature on the coating in the rotary kiln. In scenario A, the rotary kiln has a thick coating layer that may continue to grow in thickness until the equilibrium temperature is reached. Scenario C shows a kiln with a hot flame, and the coating layer is seen to become liquefied and drop off the refractory lining. If the thickness of the coating layer becomes too low, it will decrease the refractory lifetime. The surface temperature is the most important factor in the formation of a coating, since the flame shape governs the surface temperature at all points in the burning zone. For that reason, the flame has a considerable effect on the coating formation (Peray and Waddell 1972). The amount and the properties of the liquid phase will also affect the ability to form the coating (Clark, 2011).

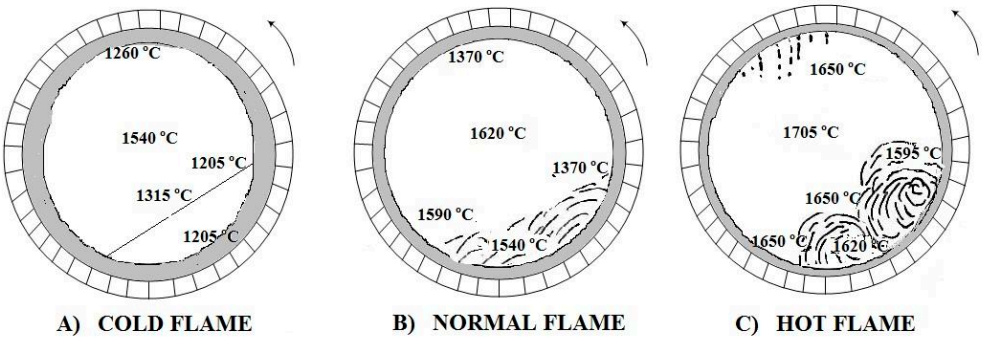

Figure 4-15: Influence of temperature on coating in rotary kiln, modified from (Peray and Waddell, 1972) .

Point 3 of Figure 4-13 marks the position in the rotary kiln, where the burning zone starts. The coating composition is similar to the clinker, because this coating is established where the liquid phase begins to form but the melt comes into contact with a cooler surface and solidifies, thereby binding clinker particles together (Hewlett 1998). Changes in operational temperature can lead to coating formation at one location, which will later come off, when the temperature is changed. Repetitive shedding of coatings and formation of too much coating may lead to ring formations (Peray and Waddell, 1972).

Changes in operation temperatures can lead to coating formation at one temperature, which will later come off, when the temperature is changed. Frequent falling out of coatings and the formation of too much coating can lead to ring formations (Peray and Waddell, 1972) .

Point 4 of Figure 4-13 shows the clinker rings that form inside the kiln. Clinker rings are characterized by their relatively high content of alite and aluminate. They are typically caused by recirculation of clinker dust in the combustion product gases from the main burner. These rings can be avoided by eliminating the dust recirculation from the cooler or by adjustment of the main burner to produce a short and dense flame (Clark, 2011).

The rings in the kiln inlet zone, called transition zone rings, are showed by point 5 of Figure 4-13. These rings do not contain aluminate, and only very little alite (Palmer, 1990). The composition of transition zone rings is often quite complex, and they are associated with operating conditions, such as high concentrations of alkali chlorides in the kiln gas, or reducing condition in the material kiln bed.

Reducing conditions, raw meals with difficult burnability, flame shape, and burner position are known to increase the amount of sulfur in the kiln atmosphere, thereby favoring ring formation (Nievoll et al., 2009). Sulfospurrite appears to be the mineral phase responsible for ring formation in the cement preheater kilns (Nievoll et al., 2009). Sulfospurrite crystals have been found on the surface of the refractory lining, and subsequent rapid growth of the ring, in a SO_3 rich kiln atmosphere, is probably enhanced by the liquid double sulfate $2CaSO_4 \cdot K_2SO_4$ (Ca-langbeinite). The analyzed samples showed an internal variability, which reflected the variations in composition and temperature of the kiln gases (Recio Dominguez et al., 2010). The same study tested different refractory materials against ring formation, and concluded that SiO^{2-} impregnated alumina bricks impeded sulfospurrite crystallization by stabilizing belite very efficiently.

Kiln rings in a preheater kiln system are not as frequent as in previous kiln systems due to the improvements in manufacturing technology, operation control, and raw materials and clinker homogeneity (Herfort et al., 2010). These improvements have also resulted in significant improvements in product performance. The operation process parameters experience nowadays less variation, this can be illustrated for example in Figure 4-16, showing the variation of lime saturation factor (LSF) for three different rotary kilns. The LSF is the ratio of CaO to the other three main oxides, and controls the ratio of alite to belite in the clinker. The clinker produced in batches in bottle kilns in the nineteen century were very heterogeneous as the raw materials. The oldest kiln from 1890, presents a big variation of the LSF percentage in short periods of time, and this large variability was causing operational problems, because the clinker was produced in batches in bottle kilns were very heterogeneous as well as the raw materials. The introduction of rotary kilns facilitated the blending and uniformity of the raw materials. In the long kiln, where calcination was taking place inside the rotary kiln, the process parameters showed still significant variation, but the variability has been significantly reduced for the actual preheater kilns, which show the improvement on operational control. For that reason, kiln rings are rarely formed in the actual preheater kiln systems.

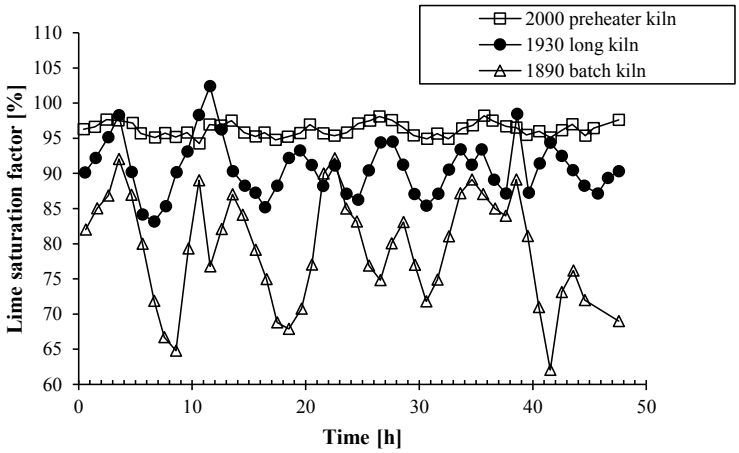

Figure 4-16: Variability in the lime saturation factor of hourly spot clinker samples of different cement rotary kilns (Herfort et al., 2010)

4.2.3 Shell Corrosion and Refractory Deterioration

The combined presence of SO_2 and HCl makes the kiln gas very corrosive (Jøns and Østergaard, 2001). Consequently, the presence of reducing atmospheres coupled with a high sulfur level in the kiln system, may lead to refractory deterioration and corrosion of rotary kiln shells and calciner shells, which subsequently result in high maintenance costs.

Jøns and Østergaard (2001) studied kiln shell corrosion in 12 suspension calciner kilns and found that the corrosion was restricted to a short zone, located from the start of the kiln coating, to 10-20 m in the direction of the kiln inlet. Severe corrosion occurred when the kiln gas contained high levels of both sulfur and chlorine. The corrosion products were found to be brittle, and porous, with chlorides and alkali metals present in different amounts and homogenously distributed. However, it was not possible to link the composition of the corrosion product to the position where the sample was taken.

The corrosion reactions on kiln shell are proposed to be chain reactions (Lai, 1990; Jøns and Østergård, 2001). First, the release of HCl in gas phase takes place by reactions (4-11) and (4-15), occurring in the kiln, where thermally unstable alkali chlorides are transformed to more stable alkali sulfates. Hydrochloric acid can penetrate through the refractory and due to the decrease in temperature, chlorine formation proceeds via reaction (4-16). According to Jøns and Østergård (2001), a temperature gradient, which is established by the lining and the porous deposit, will be formed between the kiln atmosphere and the kiln shell. The elemental chlorine can chemically interact with the metal shell by chlorination of iron, reaction (4-17). Subsequently, the oxidation of $FeCl_2$, the hydrolysis of $FeCl_3$, and sulfidation of iron continue by reactions (4-18), (4-19), and (4-20), respectively.

$$KCl(g) + H_2O(g) \rightarrow KOH(g) + 2HCl(g) \quad \text{for T > 900 °C} \quad (4\text{-}11)$$

$$2KCl(g) + SO_2(g) + ½\ O_2(g) + H_2O(g) \rightarrow K_2SO_4(g) + 2HCl(g) \quad (4\text{-}15)$$

$$2HCl(g) + ½\ O_2(g) \rightarrow Cl_2(g) + H_2O\ (g/l) \quad \text{for T< 400 °C} \quad (4\text{-}16)$$

$$Cl_2(g) + Fe\ (s) \rightarrow FeCl_2(s) \quad (4\text{-}17)$$

$$12\ FeCl_2(s) + O_2(g) \rightarrow 8\,FeS_3(g/l) + 2Fe_2O_3(s) \quad (4\text{-}18)$$

$$FeCl_3(s) + 3H_2O\ (g/l) \rightarrow 3HCl(g) + Fe(OH)_3(s/l) \quad (4\text{-}19)$$

$$4Fe(s) + SO_2(g) \rightarrow FeS_2(s) + Fe_3O_4(s) \quad (4\text{-}20)$$

The chlorine gas is believed to be the main promoter of corrosion since it increases the porosity of the corrosion layer, thus decreasing the diffusion resistance, and thereby making the kiln more vulnerable to further attacks (Jøns and Østergård, 2001). A schematic representation of the shell corrosion is presented in Figure 4-17, where it can be observed the different compounds that may be formed in the shell plate causing corrosion. Two types of corrosion are observed: [1)] corrosion during kiln operation resulting in scaling of the kiln shell, which is the oxidation of the metallic iron by dry gases (containing S and/or Cl) at elevated temperatures, also known as high temperature corrosion; and [2)] rusting during kiln shut downs caused by condensation or absorption of moisture.

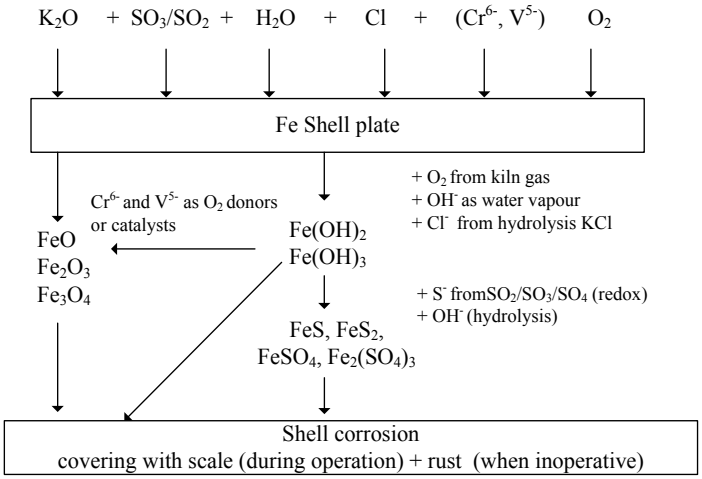

Figure 4-17: Schematic mechanism of shell corrosion, modified from (Kötter and Bartha, 1987).

Experiences from different plants have revealed that as long as chlorine is not present, the corrosion rate stays at an acceptable level, i.e. 1/3 mm per year (Karlsson, 2013). The corrosion rate is calculated for the thinnest

part of the kiln shell, which limits the lifetime of the kiln shell. Assuming a thickness of 25 mm for the thin part, this kiln shell can be worn down by corrosion to 12 mm before the stresses become too high, and the process of thinning down takes 30 to 40 years (Holtemann, 1995).

The calciner corrosion is believed to be caused by the increased sulfur circulation, which penetrates into the refractory material. Sulfur compounds may react with humidity and subsequently H_2SO_4 may condense on the inner steel shell (Jensen, 2012). Figure 4-18 illustrates schematically the mechanism of corrosion due to the infiltration of corrosive gases, such as SO_2 and HCl, through the pore structure of the refractory lining or through joints penetrating the outside steel shell (Lechtenberg and Diller 2012).

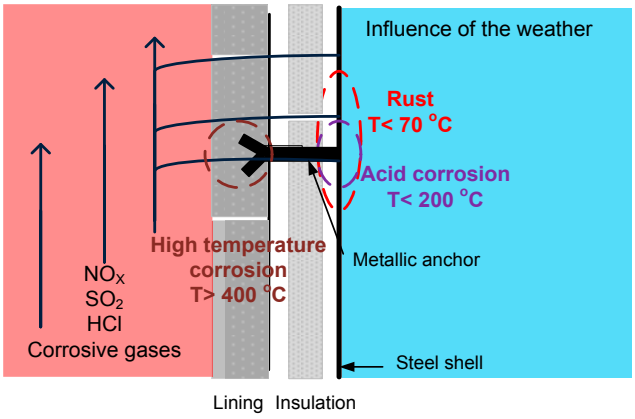

Figure 4-18: Scheme of the mechanism of corrosion, modified from (Lechtenberg and Diller 2012).

Refractory can fail due to chemical attack because brick reaction with clinker melt and alkali salts can occur. The intensity of the chemical attack increases with temperature, time and proximity to the burning zone. The disposal of alternative fuels in cement kilns has intensified chemical attack to the lining in all kiln zones, including the preheater and cooler (Szczerba, 2009; Vadász et al., 2009).

4.3 Circulation of Volatile Elements due to Combustion of Alternative Fuels

Alternative fuels have different characteristics compared to fossil fuels. Their utilization in the cement manufacturing may therefore have several effects on the process stability, such as reducing conditions, poor heat distribution, unstable pre-calciner operation, blockages in the preheater cyclones, build-ups in the kiln riser ducts, higher SO_2, NO_x and CO emissions and dusty kilns (Nielsen, 2012). Furthermore, the type of fuel used may introduce specific material components or increase the concentration of specific elements, which can interfere with the chemistry/quality of the cement, refractory life, gas and material flow or potential emissions to the atmosphere, and thereby affect the operation of the system.

In the following section, the introduction or increase of elements in the cement chemistry coming from alternative fuels is explained, but it is not described in details because the topic is outside of the scope of the project.

4.3.1 Introduction or Increase of Elements in the Cement Chemistry

The main elements introduced with alternative fuels are: Na, K, S, Cl, Zn, P, Fe, Si found as SiO_2, and carbon in cases of incomplete combustion. Furthermore, heavy metals such as As, Cd, Cr, Pb, Hg, Cu, Ni, and Sn may be incorporated as traces. The presence of heavy metals in the clinker does not affect the quality when the amount is under a threshold limit. Trace elements exceeding the threshold limit may affect the clinker, e.g. Cu affects the alite formation, while Zn will affect aluminate (Gineys et al., 2011). However, heavy metals are one of the major hazards in the flue gas from alternative fuels, due to environmental implications. Mercury and Cd are examples of heavy metals, which tend to be highly volatile at burning zone temperatures (Conesa et al., 2008).

Alternative fuels that contain Fe (e.g. TDF, up to 25 wt. % for truck tires (Nielsen, 2012)) or silica (e.g. ash from rice husks, which contain 70-90 % silica (Chinyama, 2011)) contribute to the main oxides of the clinker, and their required content in the raw materials should therefore be reduced.

The clinker quality may also be negatively affected, if the clinker is exposed to reducing conditions induced by the alternative fuel if combusted in direct contact with the material bed in the rotary kiln. The main problem is the reduction of Fe_2O_3 to FeO, which takes place at temperature higher than 450 °C, or to elemental Fe, which occurs under strongly reducing conditions. FeO, which has Fe in the oxidation state +II, catalyzes the decomposition of alite and reduces the ferrite content. This leads to modifications of the Portland cement properties, and potential color change. This phenomenon is known as brown clinker (Klauss, 2000). The clinker quality may also be negatively affected by the addition of metal oxide residues (Trezza and Scian, 2000) and waste material ashes (Karagiannis et al., 2008; Pipilikaki et al., 2005; Trezza and Scian, 2005; Trezza and Scian, 2009) to the clinker during the clinkering process through combustion of alternative fuels if the raw meal mixtures is not adjusted accordingly.

4.3.2 Local Reducing Conditions

The kiln atmosphere is oxidizing in order to produce a good quality cement clinker and ensure a proper combustion of the fuel (Hewlett, 1998). However, when there is fuel spillage from the calciner and/or main burner, and/or fuel are fired into the rotary kiln material inlet end, it can consume oxygen locally and thereby cause local reducing conditions that may have a negative effect on the clinker quality and the process stability. Only the effects on the process stability are considered in this thesis. It should be emphasized that reducing conditions in the material kiln bed do not necessarily mean reducing conditions in the gas phase and vice versa.

The process stability is mainly affected by the increase in sulfur release from the raw meal to the gas phase. The sulfur release in the kiln inlet comes mainly from the decomposition of $CaSO_4$ by the reducing agents released by the fuels, so-called reductive decomposition of $CaSO_4$, which will be further discussed in Chapters 5 and 6. The partial or unburned alternative fuels increase the content of solid carbon, especially CO (g) and can react as follows.

$$CaSO_4(s)+C(s)\rightarrow CaO(s)+SO_2(g)+CO(g) \quad (4\text{-}21)$$

$$CaSO_4(s)+CO(g)\rightarrow CaO(s)+SO_2(g)+CO_2(g) \quad (4\text{-}22)$$

Similar reactions apply for the alkali sulfates. However, these compounds are thermally more stable than $CaSO_4$. The alkali sulfates may decompose and release both sulfur and alkali metals to the gas phase when fuels fired by the kiln burner fall into the material kiln bed, which is one of the scenarios illustrated in Figure 3-2.

Reducing conditions promote SO_2 release and tend to increase the intensity of the sulfur cycle in the kiln system. Therefore, the reducing conditions may alter the material circulation considerably and cause operational problems.

4.3.3 Increase of Circulation Phenomena in the Kiln System

Sulfur and chlorine circulation may often be increased due to the utilization of alternative fuels. High concentrations of these compounds often cause difficulties in kiln operation with build-ups, mainly in the preheater and the kiln inlet section. The intensity of the cycles varies between different systems, and there are also considerable variations within one single kiln system, depending on the operating conditions.

4.3.3.1 Sulfur Circulation

Incomplete combustion of fuels, when they are burned in direct contact with the bed material, can cause an increase of sulfur circulation because reducing agents, which promote the reductive decomposition of $CaSO_4$, are formed during the combustion in an oxygen-lean environment. Normally, the increase of sulfur circulation is associated to alternative fuels due to their physical and chemical properties differences with fossil fuels (particle size, moisture content, and others mentioned in Chapter 3) and their place of firing. While fossil fuels do not theoretically give rise to sulfur circulation because they are finely grinded, which causes full combustion in the calciner or in the main burner. However, an increase of sulfur circulation when petcoke char was combusted in contact with the kiln inlet material bed, has been experienced.

In an industrial cement plant, which was burning pellets of dried sewage sludge through the main burner, the sulfur evaporation has a decreasing linear tendency with the O_2 concentration in the gas phase at the kiln

material inlet, see Figure 4-19. Increasing the oxygen content at the kiln material inlet minimizes the sulfur evaporation. The increase of oxygen concentration is believed to reduce the occurrence of local reducing condition in the clinker be where unburned sewage sludge were dropped from the flame (Nørskov, 2012).

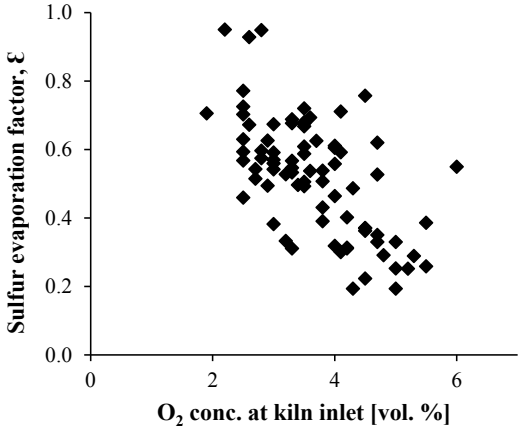

Figure 4-19: Sulfur evaporation factor as function of O_2 exhaust gas concentration measured at the kiln material inlet during firing 0.5-2 tons per hour dried sewage sludge in the kiln burner (Nørskov, 2012).

In the calciner, the fuel and the raw meal is in direct contact, but the SO_2 release is not taking place there. It has been suggested that partly calcined hot meal is less problematic than completely calcined hot meal with regards to sulfur release, since the endothermic calcinations reaction will absorb heat developed from the fuels and thereby prevent temperature increment that leads to sulfur release. However, there is a lack of understanding and experimental results in this area.

4.3.3.2 Chlorine Circulation

Alternative fuels, RDF in particular, may introduce up to 4 wt. % chlorine. The growing use of alternative fuels is increasing the input of chlorine. Some of the waste plastics, such as PVC, sewage sludge, meat and bone meal, and chlorinated hydrocarbons may increase the amount of chlorine introduced into the system significantly. The circulation of chlorine is determined by the phase equilibrium between liquid and gaseous KCl. The evaporation generally occurs in the burning zone of the kiln and the re-condensation in the riser pipes and lower cyclones, where Cl can combine with alkalis and sulfates and form mixtures with a low melting point. The degree of volatile recycling within the system will increase with increasing amounts of alkali chlorides. Too high Cl is influencing the economy of clinker production by causing kiln stoppages, corrosion, and uneven clinker quality.

Under unfavorable circumstances, some of the chlorine, which is normally present in the kiln atmosphere in the form of NaCl and KCl, can be replaced by HCl. The hydrochloric acid can cause corrosion of the steel

walls of the rotary kiln (Saint-Jean et al., 2005). A bypass can be a very effective way of removing chlorides from the kiln system. Approximately 90 % of chlorine can be removed by extracting 5 % of kiln exhaust gas, but no more than 15 % of alkalis or sulfur can be removed (Sutou et al., 1999).

The effects of chloride are strongly influenced by the sulfur load in the kiln (Jøns et al., 2008). A model of the chlorine circulation in the kiln and how this is influenced by the S load based on simple thermodynamic considerations was developed by Jøns et al. (2008). The findings were supported by statistical treatment of data collected from more than 50 modern kiln systems. It was concluded that the higher the sulfate content in clinker, the lower the evaporation factor for chlorine.

4.4 Thermodynamic Calculations

For a better understanding of the inorganic chemistry in the rotary kiln, thermodynamic equilibrium calculations were performed using the commercially available software FactSage 6.2 (Bale et al., 2009). This program uses the principle of minimization of the total Gibbs free energy to calculate the equilibrium composition of a chemical system with known composition, temperature and pressure. The principle of the Gibbs energy minimization is described in Appendix A.

4.4.1 System considering inorganic chemistry with clinker chemistry

A system model including the inorganic chemistry with the clinker chemistry is first considered. Two groups of compounds are differentiated in the bed material: Group 1) containing the elements (Ca, Si, Al, Fe) present in the clinker compounds and Group 2) the volatile elements described in section 4.1. The two groups of solid compounds interact between each other and also with the gas phase. The system examines the equilibrium between the gas species and the solid species in the bed material and also the equilibrium between the solid compounds of the bed. This equilibrium is schematically illustrated in Figure 4-20.

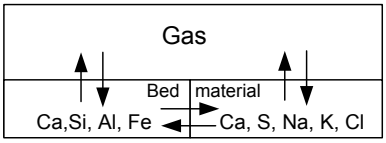

Figure 4-20: Schematic view of the gas and bed material in equilibrium.

4.4.1.1 Assumptions and Limitations

The equilibrium model is based on the composition of hot meal and the flue gas leaving the rotary kiln. The hot meal composition in weight percentage and in mol/kg clinker, from Nielsen (2012), is shown in Table 4-3. Nielsen (2012) specified that the defined hot meal contains a relatively high amount of Cl and S, relative to the guidelines for a stable kiln operation. Mn_2O_3, TiO_2, SrO, MgO and P_2O_5, are specified but they are

neglected in the calculations because these elements are not interacting with sulfur and chlorine due to their small concentration range. The loss on ignition, which is the weight fraction lost by heating the sample to 975 °C, is not considered either in the calculations because it is expected not to have any influence in the inorganic chemistry.

The composition of the hot meal is traditionally expressed as oxides (Table 4-3), however, the oxides are not the compounds present in the hot meal. Therefore, based on the molar amount of S, K, Na, Si, Al, Fe, Cl and Ca, the compound concentrations, such as Na_2SO_4, K_2SO_4, $CaSO_4$, KCl, Ca_2SiO_4 (belite)[1], SiO_2, Al_2O_3, Fe_2O_3, and CaO, in the hot meal can be calculated and used as input for the thermodynamic calculations. The aforementioned compounds with their corresponding concentrations are listed in Table 4-4.

Table 4-3: Typical composition of hot meal used in the equilibrium calculations (Nielsen, 2012).

Hot meal composition	Concentration	
	[wt. %]	[mol/kg clinker]
SiO_2	18.00	3.000
Al_2O_3	4.76	0.467
Fe_2O_3	2.30	0.144
CaO	56.80	10.128
K_2O	2.50	0.266
Na_2O	0.20	0.032
SO_3	6.12	0.765
Cl	1.17	0.330
Mn_2O_3	0.05	No included
TiO_2	0.25	No included
SrO	0.09	No included
MgO	1.86	No included
P_2O_5	0.07	No included
LOI, 975 °C	5.77	No included
Total	99.94	-

Table 4-4: Specific concentration of Na_2SO_4, K_2SO_4, $CaSO_4$, KCl, Ca_2SiO_4, SiO_2, Al_2O_3, Fe_2O_3, and CaO in the hot meal.

Hot meal compounds	Concentration [mol/kg clinker]
Na_2SO_4	0.032
K_2SO_4	0.101
$CaSO_4$	0.632
KCl	0.330
Ca_2SiO_4	1.000
SiO_2	2.000
Al_2O_3	0.467
Fe_2O_3	0.144
CaO	7.497

The flue gas in the kiln is characterized to be oxidizing. The composition and concentration of the gas used for the thermodynamic calculation of the full system is specified in Table 4-5. The values represent typical values found in the kiln inlet of a cement rotary kiln. All the compounds are inserted in the calculations as mol/kg clinker.

[1] The formation of belite starts at temperatures above 700 °C, so it is assumed that part of the silica content is contributed by belite.

Table 4-5: Flue gas composition in oxidizing conditions.

Gas composition in oxidizing conditions	Concentration	
	[vol. %]	[mol/kg clinker]
CO_2	25.00	5.580
O_2	5.00	1.116
H_2O	5.00	1.116
SO_2	0.05	0.011
N_2	64.95	14.49
Total	100.00	-

The following considerations have been taken for the model:

- A closed co-current system is considered.
- The calculations have been performed assuming one kg calcined raw material and 0.5 Nm^3 flue gas for each kg clinker produced.
- The temperature of the calculations is in the range between 900 ºC and 1500 ºC in a step size of 10 ºC and the pressure is 1 atm.
- Ideal gas phase species, solid phase species, and liquid phase species and their physical and chemical properties are included from the software database (Bale et al., 2009). The list of species included in the calculations is specified in Appendix B.

The equilibrium model has the following limitations:

- The model does not consider mass transfer and kinetic limitations. The residence time of the material in the industrial rotary kiln may be too short for the species to transform, decompose or react with each other. Therefore, the predicted formation of species may deviate from reality.
- The model considers pure species and the interaction between the compounds are neglected; just the interactions between the elements of the input compounds are taken into account.
- The data of the software might be not fully reliable at higher range of the temperatures studied, because the C_p data for some of the species listed in Appendix B were out of the temperature ranged.
- The model cannot take into account the uncertainties in the thermodynamic properties.

4.4.1.2 Results and Considerations

Figure 4-21 shows the thermodynamic results of the complex system considering the gas compounds, the main clinker compounds, and compounds containing sulfur, alkali, and chlorine. The concentrations of CO_2 and N_2 in the gas phase are higher than the rest of the species and in order not to shift the magnitude of the y-axis, these species are not presented in the graph.

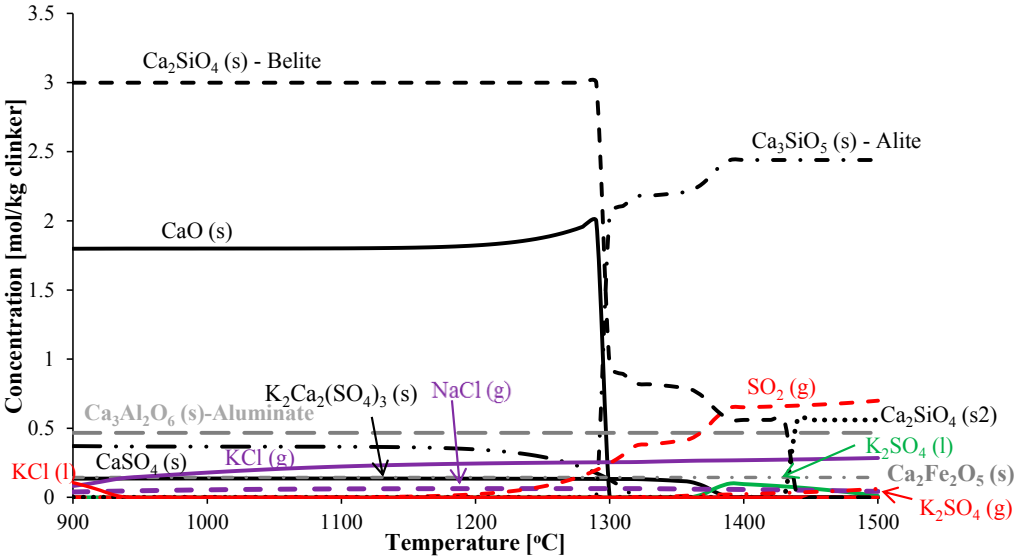

Figure 4-21: Thermodynamic results of the system model including the inorganic chemistry with the clinker chemistry.

The abundant solid compounds from 900 to 1300 ºC are CaO and dicalcium silicate (belite). At 1300 ºC belite starts to not be thermally stable until 1450 ºC, where another solid structure of belite is stable. From 1300 to 1500 ºC, tricalcium silicate (alite) is the most abundant silicate. The equilibrium concentration of CaO at 1300 ºC decreases because calcium is combined with belite to form alite.

In Figure 4-21, Al and Fe are combined as $Ca_3Al_2O_6$ (aluminate) and $Ca_2Fe_2O_5$, respectively. Their equilibrium concentrations do not vary with temperature. However, ferrite ($Ca_4Al_2Fe_2O_{10}$), which is one of the clinker minerals, has not been predicted in this calculation. This may be due to the formation of solid aluminate and ferrite from the liquid phase takes place during the cooling, as mentioned in Chapter 2.

The volatile elements are present in the system in minor equilibrium concentrations. Sulfur is found as $CaSO_4$ and $K_2Ca_2(SO_4)_3$ at the rotary kiln inlet. Calcium sulfate is the abundant sulfate, which is stable until 1200 ºC, where after it starts to decompose until 1320 ºC where $CaSO_4$ is no longer stable. Calcium langbeinite, $K_2Ca_2(SO_4)_3$, is a double sulfate containing potassium and calcium and is more thermally stable than calcium sulfate. Calcium langbeinite is stable until 1380 ºC. At higher temperatures, from 1380 to 1500 ºC, the stable sulfate is K_2SO_4 in liquid phase and gas phase. SO_2 in gas phase is released from 1200 ºC, when calcium sulfate starts to be less stable. Calcium langbeinite also contributes to higher equilibrium concentration of SO_2 when it is no longer thermally stable. The chlorine compounds in gas phase in the system are KCl, which is the most abundant chloride, and NaCl in the whole range of temperatures studied. From 900 to 930 ºC, KCl also appears to be stable in liquid phase.

The results of this complex system do not represent the chemistry of the rotary kiln explained in section 4.1, especially at temperatures higher than 1200 ^{o}C. These calculations are assuming perfect mixing between the compounds and local fluctuations are not considered. The equilibrium conditions where local fluctuations take place inside of the rotary kiln, such as nodulization, can be very different from the simulated conditions, which have transport and kinetics limitations. The local fluctuations can also influence the interaction between the volatile compounds and the main clinker phases, for example it has been reported that K and Na can be incorporated in the clinker minerals (Jawed and Skalny, 1977) and this phenomena has not appeared in the thermodynamic simulations.

Due to the complexity of the system and because the focus of the investigation is on the volatile elements, which are in minor concentrations than the clinker elements, the system is simplified to study thermodynamically the effect of the inorganic chemistry consisting of S, K, Na, and Cl.

4.4.2 System considering inorganic chemistry

The system model is simplified by only considering the inorganic chemistry and is based on the same composition of hot meal presented in Table 4-3 and the flue gas presented in Table 4-5.

In this section, SiO_2, Al_2O_3, and Fe_2O_3 composition is not included. The model does not consider the main clinker chemistry and the interaction with the volatiles species. Therefore, all the volatiles species will be in gas phase in the hot end of the kiln, while in the industrial rotary kiln some of these volatiles will be part of and leave with clinker nodules. So, this model severely overestimates the evaporation of the gas species.

In the next sections, the simplified system model splits apart the different compounds (sulfates and chlorides) in order to study their effect. First, the sulfates are investigated in oxidizing and reducing conditions and then, the effect of chlorides is introduced in the system.

4.4.2.1 Sulfates in Oxidizing Conditions

Based on moles of potassium, sodium, sulfur, and calcium, as elements, in the given composition of the hot meal, the concentration of Na_2SO_4, K_2SO_4, $CaSO_4$, and CaO in moles/kg clinker is specified in Table 4-6. It can be seen that the predominant sulfate is $CaSO_4$ with a higher concentration than the alkali sulfates.

Table 4-6: Specific concentration of Na_2SO_4, K_2SO_4, $CaSO_4$, and CaO in the hot meal.

Hot meal compounds	Concentration [mol/kg clinker]
Na_2SO_4	0.032
K_2SO_4	0.266
$CaSO_4$	0.467
CaO	9.622

The thermodynamics results are shown in Figure 4-22. Abundant species such as are CaO, CO_2, and O_2 are not shown in the graph because the presence of these species would shift the magnitude of the y-axis and make impossible to see the behavior of alkali and sulfate containing species.

Calcium langbeinite, $K_2Ca_2(SO_4)_3$, is the most abundant solid sulfate and appears to be thermally stable until 1250 °C and starts to until 1370 C. In solid phase, a double sulfate of potassium and sodium and K_2SO_4 are also stable in small concentrations, the first one from 900 to 930 °C and the second from 930 to 1060 °C. $CaSO_4$ does not appear in this results; this may be because the input concentration is quite similar to the K_2SO_4 input concentration, therefore they are combined as calcium lagnbenite. This does not happens when the input concentration of $CaSO_4$ is larger than the input concentration of K2SO4 (see section 4.4.2.3).

In In liquid phase, sodium sulfate appears to be the thermally stable compounds until 1350 °C and potassium sulfate from 1060 to 1500 °C with a maximum concentration at 1380° C. The SO_2 in the gas phase is mostly produced from the decomposition of the solid sulfates and the concentration also increases above 1370 °C due to the decomposition of alkali sulfates. In the gas phase at temperatures above 1300 °C, there are also in small quantities of K_2SO_4 and the alkali hydroxides due to the presence of water vapor.

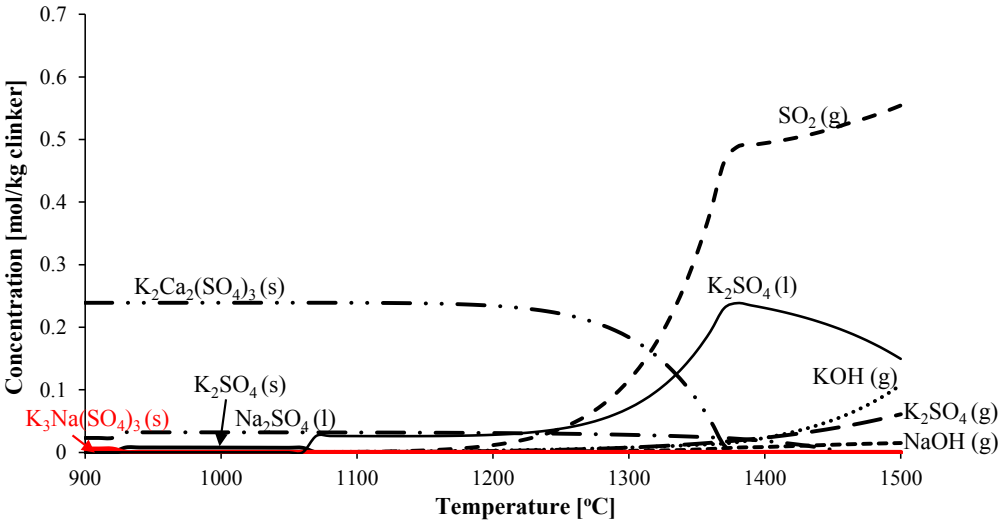

Figure 4-22: Thermodynamic results for the alkali and sulfate species in the temperature of the rotary kiln in oxidizing conditions.

The behaviors of the solid phases are different as observed in the system considering the inorganic and clinker chemistry, where $CaSO_4$ and $K_2Ca_2(SO_4)_3$ appeared to be stable but not $K_3Na(SO_4)_3$ and K_2SO_4 in Figure 4-21. In liquid phase, Na_2SO_4 was not predicted in the complex system while in Figure 4-22 is stable in a wide range of temperatures. Furthermore, K_2SO_4 in liquid phase appeared to be stable above 1300 °C while in the thermodynamic calculations considering only the volatile species is stable from 1060 °C. The gas species

above 1400 °C are in good agreement with the observation of the system considering the inorganic and clinker chemistry (Figure 4-21).

4.4.2.2 Sulfates in Reducing Conditions

When fuel particles are burned in direct contact with the bed material, the volatiles gases released can react with the hot meal. Therefore, two scenarios will be simulated to calculate the behavior of the hot meal using the flue gas composition in reducing conditions which is shown in Table 4-7.

Table 4-7: Flue gas compositions for two different reducing conditions.

Gas composition reducing cond. 1	**Concentration**		**Gas composition reducing cond. 2**	**Concentration**	
	[vol. %]	**[mol/kg clinker]**		**[vol. %]**	**[mol/kg clinker]**
CO_2	25.00	5.580	CO_2	25.00	5.580
CO	0.10	0.020	**CH_4**	0.10	0.020
H_2O	5.00	1.116	H_2O	5.00	1.116
SO_2	0.05	0.011	SO_2	0.05	0.011
N_2	69.85	15.590	N_2	69.85	15.590
Total	100	-	Total	100	-

The thermodynamics results using the flue gas composition for reducing conditions 1, containing 0.1 vol. % CO, are illustrated in Figure 4-23. The calcium langbeinite equilibrium concentration is lower than in Figure 4-22. Potassium sulfate appears at approx. 1070 °C in liquid phase with maximum equilibrium concentration at 1330 °C (at lower temperature than in Figure 4-22) and from 1380 °C in gas phase. The SO_2 release starts at 900 °C, seems stable until 1100 °C, and increases significantly with temperature from 1200 to 1330 °C, which is produced by the decomposition of the double calcium potassium sulfate, and after by the liquid potassium sulfate. From 1350 until 1500 °C, alkali hydroxides are thermodynamically stable in the gas phase.

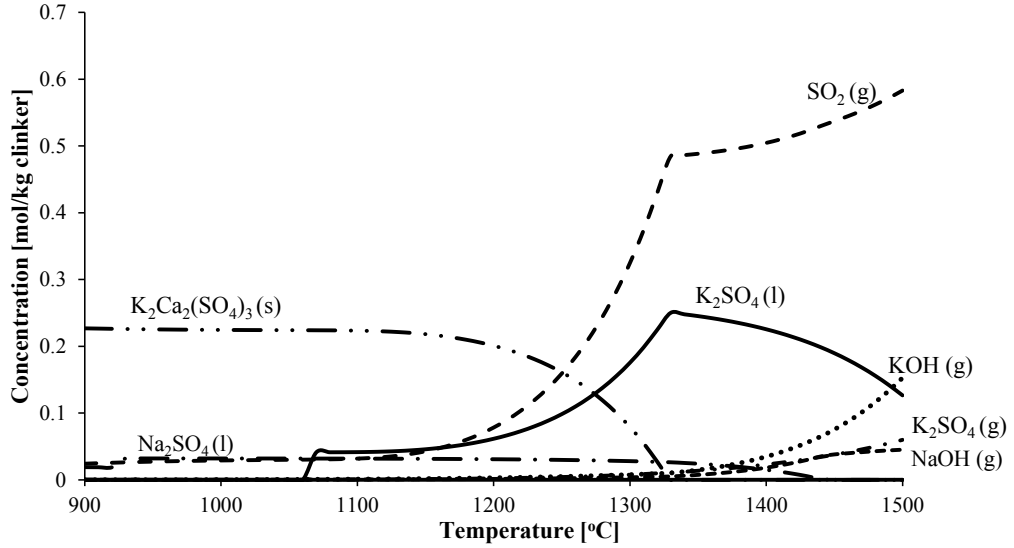

Figure 4-23: Thermodynamic results for the alkali and sulfate species in the temperature of the rotary kiln in reduction conditions 1.

Figure 4-24 shows the thermodynamics results using the flue gas composition for reducing conditions 2, containing 0.1 vol. % CH_4. The results obtained are very similar to the reducing conditions 1. It can be noticed that the SO_2 equilibrium concentration is higher and the calcium potassium sulfate concentration in the kiln inlet of the rotary kiln are lower than for the reducing conditions 1.

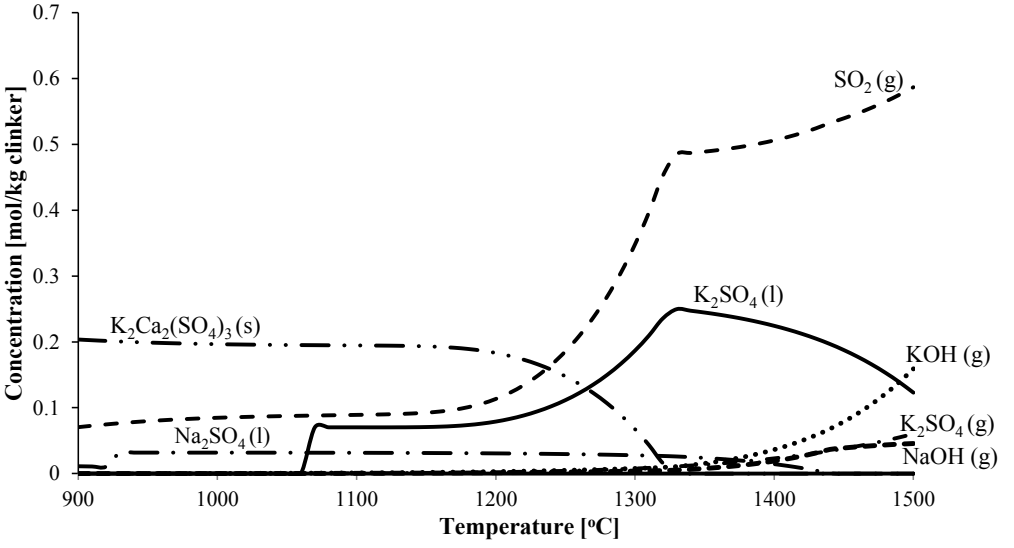

Figure 4-24: Thermodynamic results for the alkali and sulfate species in the temperature of the rotary kiln in reduction conditions 2.

In both scenarios, the SO_2 and $K_2Ca(SO_4)_3$ are mainly affected by the reducing atmosphere from 900 to 1200 °C, in the temperature range of the kiln inlet. At the burning zone temperatures 1400-1500 °C, the equilibrium concentrations of the gas species are not affected.

4.4.2.3 Effect of Chlorine Addition

The effect of the chlorine species is investigated in this section. Based on moles of potassium, sodium, sulfur, chlorine, and calcium of the hot meal composition in Table 4-3, the concentration of NaCl, KCl, Na_2SO_4, K_2SO_4, $CaSO_4$, and CaO in moles/kg clinker is specified in Table 4-8. The flue gas composition in oxidizing conditions is used.

Table 4-8: Specific concentration of NaCl, KCl, Na_2SO_4, K_2SO_4, $CaSO_4$, and CaO in the hot meal.

Hot meal compounds	Concentration [mol/kg clinker]
NaCl	0.065
KCl	0.265
K_2SO_4	0.133
Na_2SO_4	0.000
$CaSO_4$	0.632
CaO	9.496

The thermodynamic results with the effect of chlorine are shown in Figure 4-25. The behaviors of the sulfates and chlorides are quite similar to the observed behavior in the system considering inorganic chemistry with clinker chemistry. KCl is mainly thermodynamic stable in the gas phase, liquid phase between 900 to 930 °C, and a dimer of KCl in the gas phase is also thermally stable in the material kiln inlet. This was also observed in the thermodynamic results of the complex system. $CaSO_4$ and the double calcium potassium sulfate are found to be thermodynamically stable until 1200 and 1350 °C, respectively. The SO_2 is mainly caused by the decomposition of $CaSO_4$ and after of $K_2Ca_2(SO_4)_3$. There are no sulfates in liquid phase as observed in Figure 4-22, Figure 4-23 and Figure 4-24. At temperatures corresponding to the burning zone, from 1350 °C, potassium sulfate and alkali hydroxides in gas phase appear stable and this has also been observed in the previous graphs.

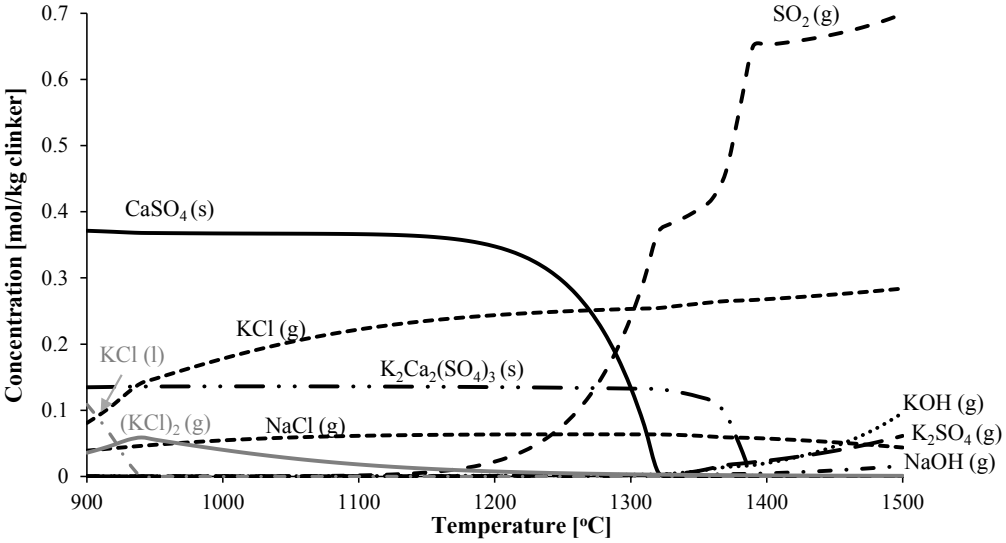

Figure 4-25: Thermodynamic results for the alkali, chloride and sulfate species in the temperature of the rotary kiln for the calcined raw material in oxidizing conditions.

Through the thermodynamic software, the presence of sodium species, such as NaOH and Na_2SO_4 in gas phase has been observed. However, the concentrations are in the order of 10^{-2} mol/kg clinker, or lower, and can therefore not be noticed in Figure 4-25.

4.4.2.4 Effect of Higher Concentration of Alkali than Sulfur

The effect of higher concentration of alkali than sulfur is investigated in this section. A hypothetical composition of the hot meal is specified in Table 4-9. This composition would also contain Mn_2O_3, TiO_2, SrO, MgO and P_2O_5 but are not considered in the calculations and therefore not specified. It needs to be noticed that this composition may not be realistic, because it is not desired to have excess of alkali content in the clinker due to its negative effect on the cement mechanical properties. This hot meal is exposed to the flue gas in oxidizing conditions.

Table 4-9: Hypothetical composition of hot meal used in the equilibrium calculations in section 4.4.2.4, when the concentration of alkali is higher than the sulfur concentration. This composition would also contain Mn_2O_3, TiO_2, SrO, MgO and P_2O_5 but are not considered in the calculations and therefore not specified.

Hot meal composition	Concentration	
	[wt. %]	[mol/kg clinker]
SiO_2	18.00	3.000
Al_2O_3	4.76	0.467
Fe_2O_3	2.30	0.144
CaO	56.80	10.128
K_2O	2.25	0.240
Na_2O	1.67	0.269
SO_3	3.4	0.425
Cl	1.17	0.330

Based on moles of K, Na, S, and Ca from the hypothetical composition of hot meal, the Na_2SO_4, K_2SO_4, $CaSO_4$, and CaO concentrations in mol/kg clinker are specified in Table 4-10.

Table 4-10: Specific concentration of Na_2SO_4, K_2SO_4, $CaSO_4$, and CaO in the hot meal.

Hot meal compounds	Concentration [mol/kg clinker]
Na_2SO_4	0.269
K_2SO_4	0.240
$CaSO_4$	0.000
CaO	10.128

The results of the thermodynamic calculation for this system are shown in Figure 4-26. It should be noticed that the y-axis scale of this figure is different from the previous graphs in this section. The SO_2 in equilibrium concentration is much lower than in the previous calculations. Calcium sulfate is not present in the system, instead calcium sulfate is bound with alkali as calcium langbeinite, $K_2Ca_2(SO_4)_3$, which is stable until 1300 °C. Double alkali sulfate, $K_3Na(SO_4)_2$ is stable at the inlet of the rotary kiln. Sodium and potassium sulfate are mainly thermodynamic stable in liquid phase, from 900 to 1200 °C and thereafter their equilibrium concentrations decrease. In the burning zone, potassium hydroxide is the main alkali gas species, followed by potassium sulfate and sodium hydroxide, which are stable in low concentrations.

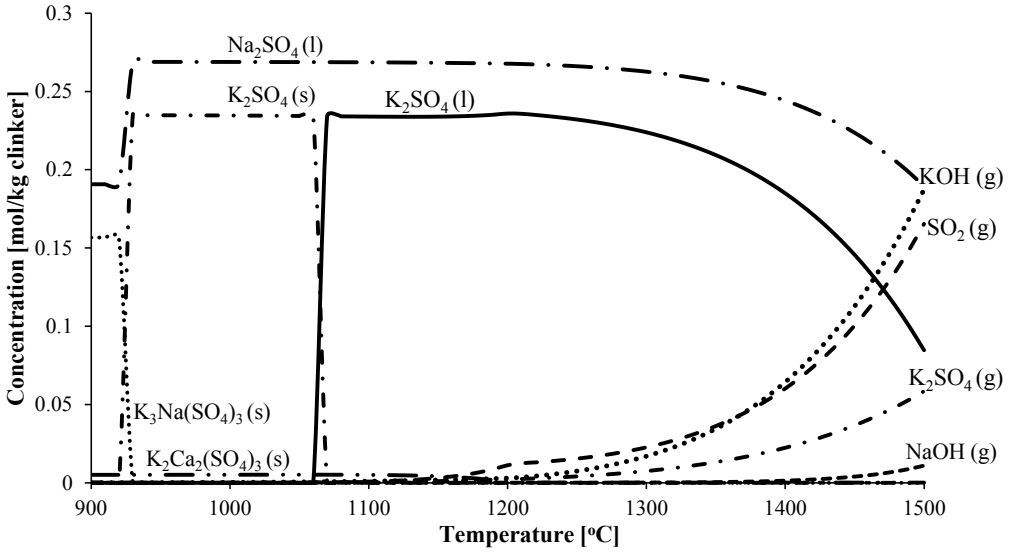

Figure 4-26: Thermodynamic results for the alkali and sulfate species when the content of alkalis is higher than sulfur in the temperature of the rotary kiln.

The inorganic chemistry is significantly changed when higher alkali concentrations than sulfur are present in the system. Even though an acceptable clinker quality might be obtained, the liquid phases may disturb the operation process by, for example, rings in the kiln. The SO_2 concentration in the gas phase is lower than in previous cases, but there is a higher concentrations of alkali species in the gas phase, which may cause operational problems. For that reason, a balance between sulfur and alkalis is needed in order to avoid high amounts of volatiles species.

4.4.3 Concluding Remarks about Thermodynamic Equilibrium Calculations

Comparing the thermodynamics results and the behavior of the circulation of volatiles explained in section 4.1, it can be seen that the behavior of the system including sulfates and chlorides (Figure 4-25) is in a good agreement with the reaction affinity between the volatiles elements (section 4.1.1) and with the description of stability of the sulfates in the kiln inlet of the rotary kiln. However, the thermodynamic calculations do not simulate the behavior of the sulfate species in the transition and hot zone of the kiln. The sulfate melt is not predicted in the calculations and the concentrations in the gas species are overestimated because these species are not retained in the solid phase (clinker). The deviations may be due to the model limitations about perfect mixing, mass transfer and kinetics.

Under reducing atmospheres, the thermodynamics results showed that the stability of sulfates in the inlet of the rotary kiln is strongly affected by the gas atmosphere and become more sensitive. The reducing gas also

affects to the stability of SO_2, which starts to be stable already at 900 °C. Therefore, the reducing conditions in the kiln inlet will be the focus of this thesis in the following chapters.

The volatility of the chlorine is not affected by the gas atmosphere, but is very sensitive to the temperature. Higher levels of alkali compared sulfur reduces the sulfur release in gas phase, but increases the liquid formation in the kiln and the alkali species in the gas phase. This might lead to unacceptable clinker quality and an increase of volatile compounds in the gas phase which could probably cause an increase of blockages when these species condense in cooler part of the kiln system.

4.5 Conclusions

Volatiles elements, such S, Cl, K, and Na, form a high degree of internal circulation in the rotary kiln, calciner and preheater, by repetitive evaporation and condensation at different temperatures. The volatilization of sulfur depends on the alkali-sulfur ratio, and on the operating conditions, while the volatilization of Cl depends only on the burning zone temperature. The high internal circulation of S and Cl may cause formation of build-ups in the lower cyclones and the riser pipe. In order to avoid this tendency, the hot meal content of SO_3 should be maintained below 6 wt. %, and the Cl content below 2 wt. %.

The process stability of the kiln system can be affected by introduction or an increase of the elements involved in the cement chemistry, reducing conditions, increase in the circulation phenomena in the kiln system, build-ups formation and shell corrosion.

The sulfur and chlorine circulation may increase when alternative fuels are combusted. Sulfur circulation is provoked by the reducing agents released during the combustion of alternative fuels.

Coatings from different cement plants have been characterized analytically. Spurrite and KCl have been found to be responsible for the tendency of build-ups and the crystallization of KCl has been postulated to take place by a vapor-liquid-solid mechanism. The risk of formation of buildups can be evaluated by the sulfur and chlorine content in the raw meal.

The high concentrations of SO_2 and HCl in presence of moisture makes the kiln gas very corrosive atmosphere and can lead to corrosion of rotary kiln shells and calciner shells.

The thermodynamic calculations have further investigated the inorganic chemistry of sulfur, chlorine, and alkali compounds. In a system containing sulfur, chlorine and alkalis, the stability of the sulfate species in the kiln inlet is in good agreement with the real behavior observed in the cement plants. The reducing agents in the gas phase affect significantly the stability of $CaSO_4$ and SO_2 in the kiln inlet, which decreases for $CaSO_4$ and increases for SO_2 already at temperatures between 900 to 1100 ºC. Thereby the focus of the following chapters will be on the effect of reducing conditions on calcium sulfate in the kiln inlet.

4.6 References

Allen, D., and Hayhurst, A. N.; Kinetics of the reaction between gaseous sulfur trioxide and solid calcium oxide. Journal of the Chemical Society-Faraday Transactions, 92, 1239-42, 1996.

Bale, C. W., et al.; FactSage thermochemical software and databases - recent developments. Calphad-Computer Coupling of Phase Diagrams and Thermochemistry, 33, 295-311, 2009.

Bech, C., and Gundtoft, L.; Study of NO_x, SO_x, and CO mechanisms based on actual plant data. IEEE/PCA Cement Industry Technical Conference: XI Conference Record, 141-154, 1998.

Bhatty, J. I.; Role of minor elements in cement manufacture and use. Research and Development Bulletin RD109T. Portland Cement Association, USA. 1995. ISBN: 0-89312-131-2.

Bhatty, J. I., Miller, F. M., and Kosmathka, S. K.; Innovations in Portland cement manufacturing. Illinois, USA. 2011. ISBN: 978-0893122713.

British ecological survey; Mineral profile. Cement raw materials. 2005. Available at www.britishecologicalsociety.org/.

Bucchi, R.; Feature on the role of minor compounds in cement clinker - part l. World Cement Technology, 210-231, 1981.

Burdett, N. A.; The mechanism of the sulphation of limestone during fluidised bed desulphurisation. Institute of Energy, London, Fluidized Combustion: Systems and Applications, p. V1-1–V1-7, 1980.

Cemnet; Technical cement forum: Maximum SO_3 permissible, 2013. Available at http://www.cemnet.com/Forum/thread/108042/re-re-maximum-so3-permissible.html Accessed in 26/4/2013.

Cemnet; Technical cement forum: Effect of reducing raw meal SO_3 in clinker alkali, 2012. Available at http://cemnet.com/Forum/thread/109139/effect-of-reducing-raw-meal-so3-in clinker-alkalis.htlm Accessed in 26/4/2013.

Cemnet; Technical cement forum: Akl/ SO_3 ratio, 2004. Available at http://www.cemnet.com/Forum/thread/108410/re-alk-so3-ratio.html. Accessed in 26/4/2013.

Chinyama, M. P. M.; Alternative fuels in cement manufacturing. InTech, 2011. ISBN: 978-953-307-372-9. Available at http://www.intechopen.com/

Christensens, N. H., and Johansen, V.; Role of liquid phase and mineralizers. Conference Cement Production and Use, USA, 1979.

Choi, G. S., and Glasser, F. P.; The sulfur cycle in cement kilns - vapor-pressures and solid-phase stability of the sulfate phases. Cement and Concrete Research, 18, 367-74, 1988.

Clark, M.; Coating, Rings and balls. International Cement Review, October, 60-63, 2011.

Conesa, J. A., Galvez, A., Mateos, F., Martin-Gullon, I., and Font, R.; Organic and inorganic pollutants from cement kiln stack feeding alternative fuels. Journal of Hazardous Materials, 158, 585-92, 2008.

Dalton, J. L., Gardner, K. H., Seager, T. P., Weimer, M. L., Spear, J. C. M., and Magee, B. J.; Properties of Portland cement made from contaminated sediments. Resources Conservation and Recycling, 41, 227-41, 2004.

Dam-Johansen, K., and Østergaard, K.; High-temperature reaction between sulfur dioxide and limestone - IV. A discussion of chemical reaction mechanisms and kinetics. Chemical Engineering Science, 46, 855-9, 1991.

de la Torre, A. G., Morsli, K., Zahir, M., and Aranda, M. A. G.; In situ synchrotron powder diffraction study of active belite clinkers. Journal of Applied Crystallography, 40, 999-1007, 2007.

Enders, M.; Reactions of alkalis, chlorine and sulfur during clinker production. Cement International, 9, 38-53, 2011.

European IPPC; Best available techniques (BAT) reference document for the production of cement, lime and magnesium oxide- European Integrated Pollution Prevention and Control Bureau. 2013.

Farag, L. M., and Kamel, H. M.; Effect of high intakes of chlorine, sulfur and alkalis on cement kiln operation. Zement-Kalk-Gips, 47, 586-90, 1994.

Fortsch, D. S., and Smidth, F. L.; The effects of excess sulfur on clinker properties. IEEE-IAS/PCA 2004 Cement Industry Technical Conference, Conference Record, 103-9, 2004.

Ghosh, S. N.; Cement and concrete science and technology. Vol 1, part 1. New Delhi. 1991. ISBN: 978-81-81479-85-3.

Gineys, N., Aouad, G., Sorrentino, F., and Damidot, D.; Incorporation of trace elements in Portland cement clinker: Thresholds limits for Cu, Ni, Sn or Zn. Cement and Concrete Research, 41, 1177-84, 2011.

Glasser, F. P.; Advances in cement clinkering. In *Innovations in Portland cement manufacturing*. J. I. Bhatty, F. M. Miller and S. K. Kosmathka. Portland Cement Association (PCA), Illinois, USA. 2011.

Hamilton, F. C.; Rings and build-ups in cement kilns. International Cement Review. December, 54-62, 1997.

Hansen, J.P.; SO_2 Emissions from Cement Production. Ph.D. thesis, Technical University of Denmark, Department of Chemical and Biochemical Engineering, 2003. ISBN: 87-90142-96-9.

Harrison, A.; Alkalis in cement. International Cement Review, 80-82, 2009.

Herfort, D., Moir, G. K., Johansen, V., Sorrentino, F., and Arceo, H. Bolio; The chemistry of Portland cement clinker. Advances in Cement Research, 22, 187-94, 2010.

Hewlett, P. C.; Lea's chemistry of cement and concrete. Fourth edition. New York. 1998. ISBN: 978-0-7506-6256-7.

Holtemann, J.; Korrosion indvendigt i ovnrør. Internal FLSmidth memo (in Danish). 1995.

Hu, G., Dam-Johansen, K., Wedel, S. and Hansen, J.P.; Decomposition and oxidation of pyrite. Progress in Energy and Combustion Science, 32, 3, 295-314, 2006a.

Hu, G., Dam-Johansen, K., Wedel, S. and Hansen, J.P.; Review of the direct sulfation reaction of limestone. Progress in Energy and Combustion Science, 32, 386-407, 2006b.

Jawed, I., and Skalny, J.; Alkalies in cement - review 1. Forms of alkalis and their effect on clinker formation. Cement and Concrete Research, 7, 719-29, 1977.

Jensen, L.K.; Personal communication about high temperature splits in the calciners, August 27, 2014.

Johansen, J. M., Aho, M., Paakkinen, K., Taipale, R., Egsgaard, H., Jakobsen, J. G., Frandsen, F. J., and Glarborg, P.; Release of K, Cl, and S during combustion and co-combustion with wood of high-chlorine biomass in bench and pilot scale fuel beds. Proceedings of the Combustion Institute, 34, 2363-72, 2013.

Jøns, E.; Managing volatile components in kiln and preheater, IPSC lecture nr: 05-02. The International Cement Production Seminar. FLSmidth Institute, Valby, Denmark, 2013.

Jøns, E., and Østergaard, M. J.; Kiln shell corrosion. IEEE-IAS/PCA Cement Industry Technical Conference, Vancouver, British Columbia, Canada, 343-359, 2001.

Jøns, E., Hundebol, S., and Clausen, K.; New reasons for installing a chloride by-pass. Interaction between chloride and sulphur. IEEE Cement Industry Technical Conference Record, 178-92, 2008.

Karagiannis, J., Ftikos, C., and Nikojopouios, P.; The use of wastes as alternative fuels in cement production. Waste Management and the Environment, 109, 105-14, 2008.

Karlsson, A., Personal communication about an acceptable level corrosion rate in kiln shell, November 22, 2013.

Klauss, J.; Burning cement clinker under reducing conditions in a rotary kiln. ZKG International, 53, 132-144, 2000.

Klemm, W. A., Jawed, I., and Holub, K. J.; Effects of calcium-fluoride mineralization on silicates and melt formation in Portland-cement clinker. Cement and Concrete Research, 9, 489-96, 1979.

Klotz, B.; New developments in precalciners and preheaters. 1997 IEEE Cement Industry Technical Conference Record XXXVIII, 255-280, 1997.

Kötter, E. and Bartha, P.; Investigations into the problem of kiln shell corrosion (in German). ZKG, 40, 157-161, 1987.

Kurdowski, W., and Sobon, M.; Mineral composition of build-up in cement kiln preheater. Journal of Thermal Analysis and Calorimetry, 55, 1021-9, 1999.

Lai, G. Y.; High Temperature Corrosion of Engineering Alloys. ASM International, 1990. ISBN: 978-0871704115.

Lea, F. M., and Parker, T. W.; Investigations on a portion of quaternary system $CaO\text{-}A1_2O_3\text{-}SiO_2\text{-}Fe_2O_3$ - the quaternary system $CaO\text{-}2CaO{\cdot}SiO_2\text{-}5CaO\ 3A1_2O_3\text{-}4CaO\ A1_2O_3\ Fe_2O_3$. Philosophical Transactions of the Royal Society of London Series A-Mathematical and Physical Sciences, 234, 1-U6, 1935.

Lechtenberg, D., and Diller, H.; Alternative fuels and raw materials handbook for the cement and lime industry. MVW Lechtenberg & Partner, Düsseldorf, Germany. 2012. ISBN: 978-3-7640-0550-4.

Lin, W.; Interactions between SO_2 and NO_x emissions in fluidized bed combustion of coal. Ph.D. Thesis, Technical University of Delft, Netherlands. 1988. ISBN: 90-9006861-9.

Midgley, H. G.; Measurement of high-alumina cement - calcium carbonate reactions using DTA. Clays Minerals, 19, 857-864, 1984.

Mortensen, A. H., Hintsteiner, E. A., and Rosholm, P.; Converting two kiln lines to 100% high sulphur petroleum coke firing. ZKG International, 51, 84, 1998.

Moss, G.; The fluidized desulphation gasifier. Proceedings of the Second International Conference on Fluidized Bed, II-6, 1-7, 1970.

Newkirk, T. F.; Effect of SO_3 on the alkali compounds of Portland cement clinker. Journal of Research of the National Bureau of Standards, Research paper 2261, 1951.

Nielsen, A. R.; Combustion of large solid fuels in cement rotary kilns. Ph.D. thesis, Technical University of Denmark, Department of Chemical and Biochemical Engineering, 2012. ISBN: 978-87-92481-66-5.

Nielsen, P. B., and Jepsen, O. L.; An overview of the formation of SO_x and NO_x in various pyroprocessing systems. IEEE Cement Industry Technical Conference XXXII, 255-76, 1990.

Nievoll, J., Jörg, S., Dösinger, K., and Corpus, J.; Studying ring formation. World Cement, 78-83, 2009.

Norbom, H.R.; Application of Suspension Preheater Kilns versus Other Kilns in North America, Proceedings of the IEEE, Cement Industry Technical Conference, Miami, USA, 1973.

Nørskov, L. K.; Combustion of solid alternative fuels in cements kiln burners. Ph.D. thesis, Technical University of Denmark, Department of Chemical and Biochemical Engineering, 2012. ISBN: 978-87-92481-98-6.

Palmer, G.; Ring formations in cement kilns. World Cement, 538-543, December 1990.

Partanen, J.; Chemistry of HCl and Limestone in Fluidized Bed combustion. Ph.D. thesis, Åbo Akademi, Faculty of Chemical Engineering, Finland, 2004. ISNB: 952-12-1287-X.

Partanen, J., Backman, P., Backman, R., and Hupa, M.; Absorption of HCl by limestone in hot flue gases. Part I: The effects of temperature, gas atmosphere and absorbent quality. Fuel, 84, 1664-73, 2005a.

Partanen, J., Backman, P., Backman, R., and Hupa, M.; Absorption of HCl by limestone in hot flue gases. Part II: Importance of calcium hydroxychloride. Fuel, 84, 1674-84, 2005b.

Partanen, J., Backman, P., Backman, R., and Hupa, M.; Absorption of HCl by limestone in hot flue gases. Part III: Simultaneous absorption with SO_2. Fuel, 84, 1685-94, 2005c.

Peray, K. E., and Waddell, J. J.; The rotary cement kiln. Chemical Publishing Co., New York. 1972. ISBN: 978-08-20603-67-4.

Pipilikaki, P., Katsioti, M., Papageorgiou, D., Fragoulis, D., and Chaniotakis, E.; Use of tire derived fuel in clinker burning. Cement & Concrete Composites, 27, 843-7, 2005.

Plang-ngern, S., and Rattanussorn, M.; The effect of sulfur to alkali ratio on clinker properties. The Siam Research and Development Co., Ltd, Bangsue, Bangkok, Thailand, 2003.

Pollitt, H. W. W., and Brown, A. W.; The distribution of alkalis in Portland cement clinker. Proceedings of the 5th International Symposium on the Chemistry of Cement, 1, 322-333, 1969.

Qin, Z.; Thermogravimetric studies of the reaction of CaO with SO_2. Journal of Thermal Analysis, 45, 211-9, 1995.

Rahman, H., and Krapkat, T.; Discussion about "*Ideally the value alkali to sulphate ratio should be as close to 1 as possible, i.e. the alkali and sulphate should be in molar balance*" in Cement Industry Expert group in www.linkedin.com, 2012. Accessed in 10/3/2013.

Recio Dominguez, I., Gomez-Millan, J., Alvarez, M., De Aza, S., Contreras, L., and De Aza, A. H.; Build-up formation and corrosion of monolithic refractories in cement kiln preheaters. Journal of the European Ceramic Society, 30, 1879-85, 2010.

Rowe, J. J., Morey, G. W., and Zen, C. S.; The quinary reciprocal salt system Na, K, Mg, Ca/Cl, $SO4^-$-A review of the literature with new data. Geololical Survey Professional Paper. (U.S.), No 741, 1-37, 1972.

Saint-Jean, S. J.; Crystallographic studies of chlorellestadite, an intermediate compound in the production of Portland cement. Licentiate thesis, Material Chemistry, Lund Institute of Technology, Lund, Sweden, 2003. ISBN: 91-628-5731-2.

Saint-Jean, S. J., Jøns, E., Lundgaard, N., and Hansen, S.; Chlorellestadite in the preheater system of cement kilns as an indicator of HCl formation. Cement and Concrete Research, 35, 431-7, 2005.

Saleh, S.B., Flensborg, J. P., Shoulaifar,T. K., Sarossy, Z., Hansen, B. B., Egsgaard, H., DeMartini, N., Jensen, P. A., Glarborg, P., and Dam-Johansen, K.; Release of chlorine and sulfur during biomass torrefaction and pyrolysis. Energy & Fuels, 28, 3738-46, 2014.

Salmento, J. S., and Shenk, R. E.; Accurately predicting cement plant emissions. IEEE-IAS/PCA 2004 Cement Industry Technical Conference, 333-43, 2004.

Samet, B., and Sarkar, S. L.; Influence of kiln atmosphere on development of clinker phases and distribution of alkalis. World Cement Research and Development, 77-82, 1997.

Smaoui, N., Berube, M. A., Fournier, B., Bissonnette, B., and Durand, B.; Effects of alkali addition on the mechanical properties and durability of concrete. Cement and Concrete Research, 35, 203-12, 2005.

Smith, L.; Volatile matter, IPSC lecture nr: 05-02. The International Cement Production Seminar. FLSmidth Institute, Valby, Denmark, 2012.

Steuch, H. E., and Johansen, V.; Sulfur dioxide emission from cement kilns. Rock Product International Seminar, USA, December, 1990.

Sturz, A., Itoh, M., and Smith, S.; Mineralogy and chemical composition of clay minerals, tag hydrothermal mound. Proceedings of the Ocean Drilling Program, Scientific Results, Vol. 158, 1998.

Sutou, K., Harada, H., and Ueno, N.; Chlorine bypass system for stable kiln operation and the recycling of waste. IEEE/PCA Cement Industry Technical Conference, Virginia, 179-193, 1999.

Szczerba, J.; Changes in basic bricks from preheater cement kilns using secondary fuels. Industrial Ceramics, 29, 19, 2009.

Telschow, S., Frandsen, F. J., Theisen, K., and Dam-Johansen, K.; Cement formation: A success story in a black box: High temperature phase formation of Portland cement clinker. Industrial & Engineering Chemistry Research, 51, 10983-11004, 2012.

Trezza, M. A., and Scian, A. N.; Scrap tire ashes in Portland cement production. Materials Research-Ibero-American Journal of Materials, 12, 489-494, 2009.

Trezza, M. A., and Scian, A. N.; Waste fuels: Their effect on Portland cement clinker. Cement and Concrete Research, 35, 438-444, 2005.

Trezza, M. A., and Scian, A. N.; Burning wastes as an industrial resource - their effect on Portland cement clinker. Cement and Concrete Research, 30, 137-144, 2000.

Twomey, C., Birkinshaw, C., and Breen, S.; The identity of the sulfur-containing phases present in cement clinker manufactured using a high sulfur petroleum coke fuel. Journal of Chemical Technology and Biotechnology, 79, 486-490, 2004.

Uda, S., Asakura, E., and Nagashima, M.; Influence of SO3 on the phase relationship in the system CaO-SiO_2-Al_2O_3-Fe_2O_3. Journal of the American Ceramic Society, 81, 725-729, 1998.

Vadász, P., Kamoda, I., and Strigác, J.; Influence of alternative fuels on the corrosion of basic refractory lining. Interceram, 58, 130-135, 2009.

Vassilev, S. V., and Vassileva, C. G.; A new approach for the combined chemical and mineral classification of the inorganic matter in coal. 1. Chemical and mineral classification systems. Fuel, 88, 235-245, 2009.

Whitehopleman; Sulphur-to-alkali ratio- Home cement industry expertise. 2011. Available at http://whitehopleman.com/node/300. Accessed in 26/4/2013.

5. Sulfur Release during Combustion of Alternative Fuels Particles

This chapter seeks to extend the knowledge of the sulfur release from hot meal during combustion of solid alternative fuel particles in the kiln inlet of a rotary kiln.

Section 5.1 covers the literature study about the sulfur release during combustion of solid fuels, which will be the starting point for the experimental investigations. The experimental part, section 5.2, describes the pilot scale equipment used for simulating the process conditions at the material inlet end of industrial rotary kilns. The solid fuels used for the experiments, tire derived fuels and wood, and their preparation are also introduced in the experimental section. Section 5.3 presents a parametric study of the effect on the release of sulfur; parameters such as particle size of different fuel types, fuel conversion degree, sulfur load in the bed and moisture content of the fuel are modified.

5.1 Literature Study on Sulfur Release in the Kiln System

5.1.1 Phase Diagrams for $CaSO_4$-CaO-CaS system

The high temperature reactions of SO_2 absorption and release under fluidized bed and entrained flow conditions have been studied extensively (Dam-Johansen and Østergaard, 1991a; Dam-Johansen and Østergaard, 1991b; Hansen et al., 1993; Lyngfelt and Eckner, 1993; Barletta et al., 2002). However, these investigations cannot be used directly to describe the conditions at the kiln inlet, because the Ca/S molar ratio studied under fluidized bed conditions were typically in the rage of 1:1 to 4:1, which differs from the conditions in cement rotary kilns where Ca/S molar ratio is typically higher than 10:1 (Hewlett, 1998). The descriptions of the mechanism for sulfur release and capture will be discussed further in Chapter 6.

In Hansen's investigations, it was proposed that in a system consisting of $CaSO_4$, CaO, CaS, SO_2, CO, and CO_2, sulfur is captured as $CaSO_4$ under oxidizing conditions, and as CaS under reducing conditions, i.e. in the presence of CO (Hansen et al., 1993). Any transformation of $CaSO_4$ to CaS and vice versa appears to proceed via CaO, as illustrated in Figure 5-1. Equilibrium phase diagrams for this system show that the transformation cycle depends on the partial pressures of SO_2, CO and CO_2 and the temperature (Hansen et al., 1993), as illustrated in Figure 5-2.

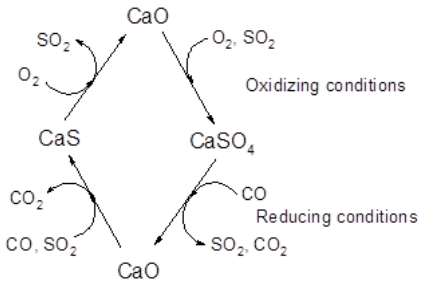

Figure 5-1: Transformation cycle of limestone exposed to alternating oxidizing and reducing conditions (Hansen et al., 1993).

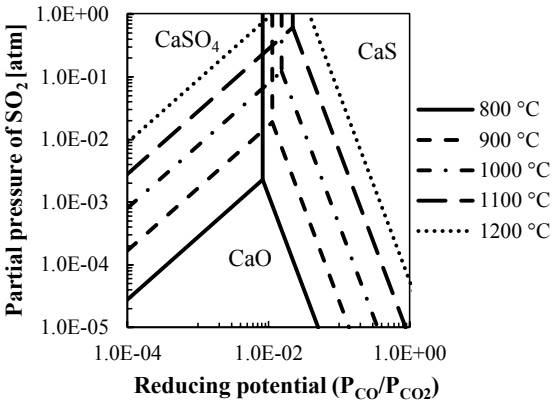

Figure 5-2: Phase diagram for the SO_2-CaO-$CaSO_4$-CaS-CO-CO_2 system at 800, 900, 1000, 1100 and 1200 °C (thermodynamic data from Barin, 1995) .

Figure 5-2 shows three regions, corresponding to the stability of $CaSO_4$, CaO and CaS. Moving from left to right in this figure indicates a shift from oxidizing to reducing conditions. It is seen that $CaSO_4$ is stable under oxidizing conditions, whereas CaS is stable at higher reducing potentials. An increase in temperature rapidly shifts the phase limits upwards, where the stability regions of $CaSO_4$ and CaS decreases and the stability region of CaO increases. For low SO_2 partial pressures, the transition from $CaSO_4$ to CaS passes through CaO and this transition is favored by increasing temperature. However, this contradicts Figure 5-1 and the mechanism of sulfur release and capture proposed by Hansen et al. (1993).

Similar phase diagrams for the equilibrium system consisting of $CaSO_4$, CaO, CaS, SO_2, H_2, and H_2O are shown in Figure 5-3 and Figure 5-4. The H_2O partial pressures are 0.6 and 0.2 atm, respectively. The effect of temperature on the stability regions is similar to the observed effect on the $CaSO_4$, CaO, CaS, SO_2, CO, and CO_2 system. Increasing the H_2O partial pressure (the moisture content in the system), the stability region for $CaSO_4$ is increased and therefore favoring the oxidizing conditions.

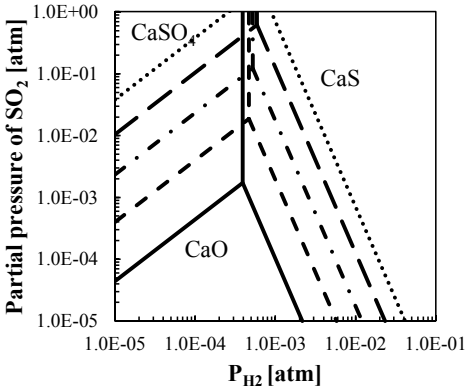

Figure 5-3: Phase diagram for the SO_2-CaO-$CaSO_4$-CaS-H_2-H_2O system at 800, 900, 1000, 1100 and 1200 °C. Total pressure 1 atm and 6 vol. % H_2O giving P_{H2O}=0.06 atm (thermodynamic data from Barin, 1995).

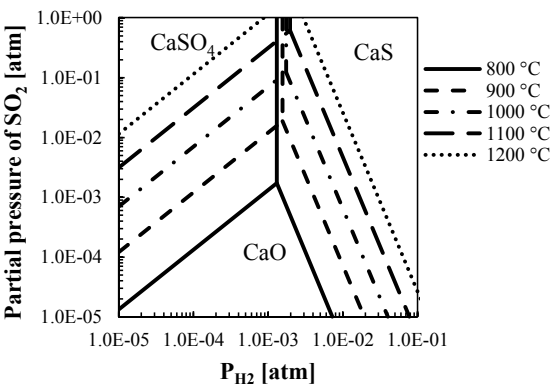

Figure 5-4: Phase diagram for the SO_2-CaO-$CaSO_4$-CaS- H_2-H_2O system at 800, 900, 1000, 1100 and 1200 °C. Total pressure 1 atm and 20 vol. % H_2O giving P_{H2O}=0.2 atm (thermodynamic data from Barin, 1995).

Phase diagram for the system containing $CaSO_4$, CaO, CaS, and SO_2 as function of the partial pressure of O_2 in the temperature range 800 to 1200 °C is illustrated Figure 5-5. The phase diagram shows that the $CaSO_4$ stability decreases with decreasing partial pressure of oxygen, passing to CaS or CaO, depending on the partial pressure of SO_2 and the temperature (Hansen et al., 1993).

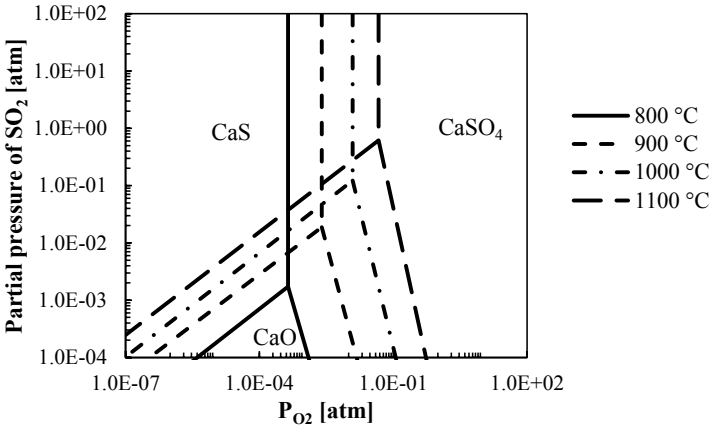

Figure 5-5: Phase diagram for the $CaSO_4$-CaO-CaS- SO_2-O_2 system at 800, 900, 1000 and 1100 °C. Pressure 1 atm (thermodynamic data from Barin, 1995).

5.1.2 Sulfur Release during Combustion of Solid Fuels

Sulfur release from the cement raw materials during combustion of solid fuels has been studied scarcely. Nielsen (2012) studied sulfur release from model raw materials consisting of a mixture of $CaSO_4$ and quartz sand in a rotary drum in the temperature range between 700 to 1000 °C. The alternative fuels used were

polypropylene, petcoke, wood, saw dust, tire, and sewage sludge. Table 5-1 specifies the fuel analysis, where a.r. denotes as received, and the lower heating values, and Table 5-2, their shape and dimensions. The effects of energy input, fuel type, temperature, and bulk oxygen concentration were studied.

Table 5-1: Fuel analyses and lower heating values (LHV) for solid fuels used in the experiments of used in Figure 5-6, Figure 5-7, and Figure 5-8.

Fuel	Proximate analysis [wt. %]			Ultimate analysis [wt. %]				LHV
	VM	FC	Ash	C	H	N	S	[MJ/kg]
Tire rubber	64.6	32.6	2.8	87.4	7.1	0.3	1.2	36.9
Pine wood	75.3	24.5	0.2	38.9	5.2	0.1	-	16.2
Poly propylene	97.5	0.0	2.5	83.0	14.0	0.0	-	44.5
Petcoke	13.4	85.1	1.5	87.3	3.7	1.5	4.7	34.0

Table 5-2: Approximate shapes and dimensions of the fuels used in Figure 5-6, Figure 5-7, and Figure 5-8 (Nielsen, 2012). Length (L) and diameter (ø).

Fuel	Shape	Dimensions
Tire rubber granulate	Irregular	ø ≈ 2 mm
Tire rubber cylinders	Cylindrical	L = 12 mm, ø= 9 mm
Pine wood cubes	Rectangular	30x15x10 mm
Pine wood saw dust	Needles	L= 1 mm
Poly propylene flakes	Rectangular	20x10x1 mm
Petcoke	Spherical	ø≈ 1 mm
Sewage sludge granulate	Spherical	ø ≈ 0.5 mm

The sulfur release was corrected by subtracting the sulfur release coming from the fuel sulfur content and from the thermal decomposition of the calcium sulfate. Figure 5-6 shows the total sulfur release as a function of the energy input from different fuels at 900 °C. Increasing energy input led to a higher degree of reducing conditions near the raw materials bed and more sulfur was therefore released. Figure 5-7 shows the results of the sulfur release from raw materials in the temperature range 700 to 1000 °C for different fuels with different dimensions, specified in Table 5-2. The uncertainties of the results have been added in both graphs. The relative uncertainty of the experimental data in Figure 5-6 is greater when using high energy input, i.e. for the experiments using 15 kJ, the relative uncertainty varies between 10 to 19 %, and 27 to 42 % using 50 kJ.

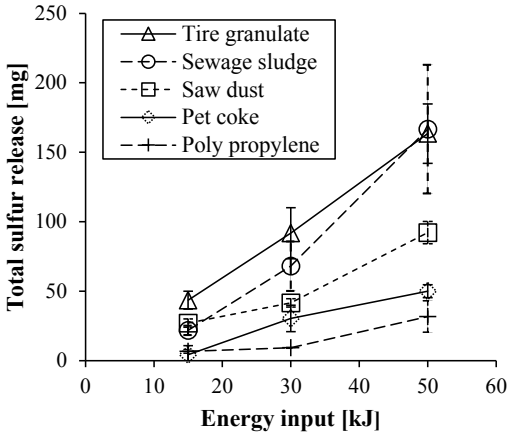

Figure 5-6: Effect of energy input from different fuels on total sulfur release. Conditions: 900 °C, 10 vol. % O_2, 5 % fill, 5 wt. % $CaSO_4$, 100 NL/min, 6 rpm. Modified from (Nielsen et al., 2011).

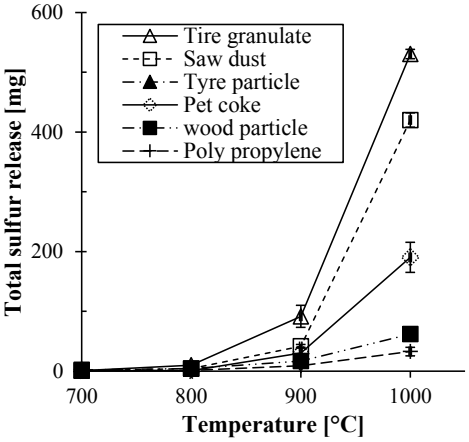

Figure 5-7: Effect of temperature and particle size on total sulfur release. Conditions: 5 % fill degree, 5 wt. % $CaSO_4$, 10 vol. % O_2, 100 NL/min, 6 rpm. Energy input in each experiment: 30 kJ. Modified from (Nielsen et al., 2011).

The fuel particle size had an insignificant influence on sulfur release at 700 and 800 °C, where there were almost no sulfur release for any fuels. The influence of particle size became more evident at 900 and 1000 °C for the different fuels. Comparing the tire rubber and wood particles, the tire granulate and saw dust gave rise to higher sulfur release while the sulfur release was much less for the tire and wood particles. The sulfur releases from the tire granulate and the saw dust in Figure 5-7, was estimated by extrapolation since the SO_2 concentration exceeded the range of the analyzer. The relative uncertainty of the results at different temperatures is normally higher at 700 °C and lower at 1000 °C, but does not follow any trend and varies from 3 to 83 %.

The effect of oxygen concentration on sulfur release is shown in Figure 5-8. The total sulfur release increased with decreasing oxygen concentration. This is in a good agreement with the phase diagram of Figure 5-5, because $CaSO_4$ is more stable at higher O_2 concentrations and will need stronger reducing conditions to be transformed to CaS and/or CaO. The relative uncertainties are greatest at 5 and 10 vol. % O_2, which are around 20 % for tire granulate and polypropylene, and 72 and 51 %, for petcoke and wood at 10 vol. % O_2, respectively. This may be due to incomplete combustion, creating significant amount of soot, and how the particles were mixed with the bed, which could have been very different from experiment to experiment. At higher O_2 content, the relative uncertainties are 10 % or below.

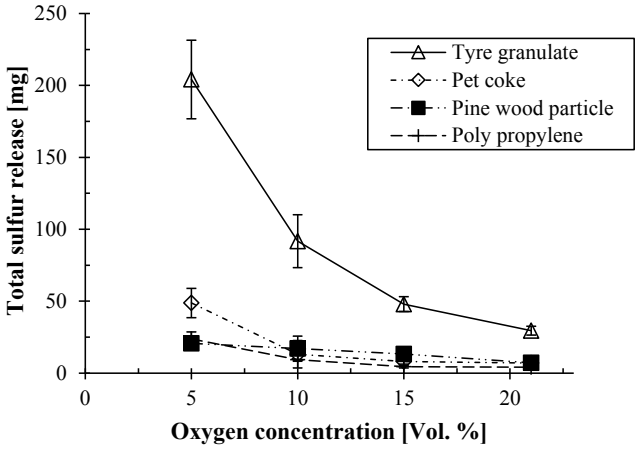

Figure 5-8: Effect of oxygen concentration on total sulfur for different fuels. Conditions: 5 % fill degree, 5 wt. % $CaSO_4$, 900 °C, 100 NL/min, 6 rpm. Energy input in each experiment: 30 kJ. Modified from (Nielsen et al., 2011).

5.1.2.1 Pre-experimental Considerations

In previous experiments, it has been observed that the fuel particle size is of high importance for the sulfur release, but it is not clear why. Further experiments with different particle sizes will be done in order to clarify whether this is due to fuel composition, the conversion pathway, or the number of particles.

Furthermore, the effect of fuel devolatilization degree would represent the sulfur release of partly unburned alternative fuel and give an idea of the sulfur release from calcined raw meal when partly unburned solid alternative fuels from the calciner fuel fall into the kiln inlet directly or after being carried upwards with the gas flow in the calciner and transported into the bottom stage cyclone to the kiln inlet. It is well known that the reducing gases such as CO, H_2, and CH_4, which can be released from the fuel particle, cause reductive decomposition of $CaSO_4$ (Swift and Wheelock, 1975; Wheelock and Boylan, 1960; Oh and Wheelock, 1990; Nielsen, 2012) but the effect of the fuel char or partly converted fuel has been not investigated in the literature.

In all the experiments performed by Nielsen (2012), the alternative fuel was dried. In reality, most of the alternative fuels contain a high degree of moisture, which could affect the sulfur release, and this will also be investigated in section 5.3.

Nielsen (2012) did not use cement raw materials based on clay and limestone because it adhered to the rotary drum inner walls and formed nodules during the experiments. In addition, the raw meal did not roll in the drum but moved in a slumping motion. It has been noticed that the uncertainties of Nielsen's experiments are large. The used quartz sand had a particle size range between 0.4 to 1 mm with average size of 0.6 mm (Nielsen, 2012). The actual particle size distribution of the quartz sand is shown in Figure 5-9. Pre-experiments were

done to improve the repeatability. Differences in the distribution of the quartz particles in the experimental setup prior to and after an experimental serie was noticed. Prior to experiments the particles were homogenously distributed in the setup whereas after experiments the smaller particles were placed on the sides of the reactor and the bigger particles in the middle.

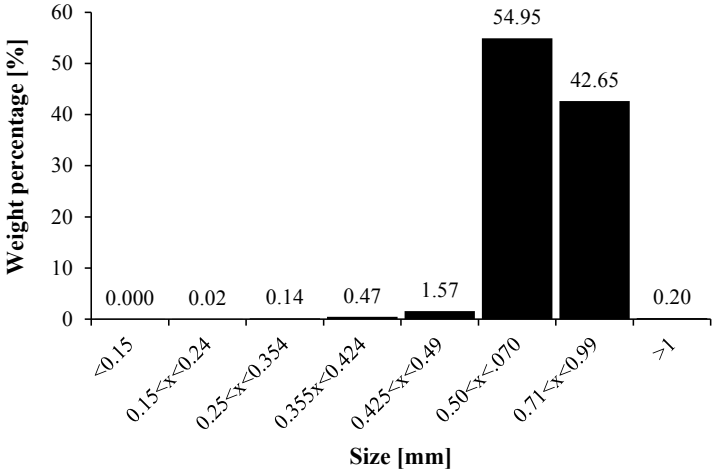

Figure 5-9: Particle size distribution for the quartz sand.

The particle size distribution of the quartz sand clearly affected the calcium sulfate added in the mixture because it was moving in the axial direction, which means that the sulfur content was not homogeneous along the bed. Therefore, it was decided to narrow the particle size distribution of the quartz sand, which improved the experimental repeatability significantly from 16-28 % to 1-5 % in relative uncertainty. Quart sand with a particle size range from 0.4 to 0.8 mm are used in the experiments of this thesis.

5.2 Experimental

The aim of the experimental section is to investigate the effect of particle size of different fuels, degree of fuel devolatilization, sulfur content in the bed, and moisture content on release of sulfur from cement raw materials.

5.2.1 Experimental Set-up

The experiments are performed in a high temperature rotary drum (Nielsen, 2012). This equipment is able to simulate the process conditions at the material inlet end of an industrial rotary kiln. The rotary drum is electrically heated by a furnace. Gas can be introduced into the chamber furnace through a hole in the roof in order to have a controlled atmosphere. The gas is transported into the rotating drum by an externally placed gas pump that pumps the gas through the rotating drum and the steel tube where after the gas exiting the reactor

is cooled and analyzed. The exit concentrations of SO_2, CO, CO_2, and O_2 in the gas are analyzed and logged during the fuel combustion. The chamber furnace door is equipped with a window for visual inspection, two holes for thermocouples, and a centrally placed water cooled tube for introduction of solid fuel. The solid fuels are placed in a sample container which can be pushed into the hot rotary drum or pulled out to the water cooled tube. Figure 5-10 shows a side and top view of the high temperature rotary drum and its dimensions in mm.

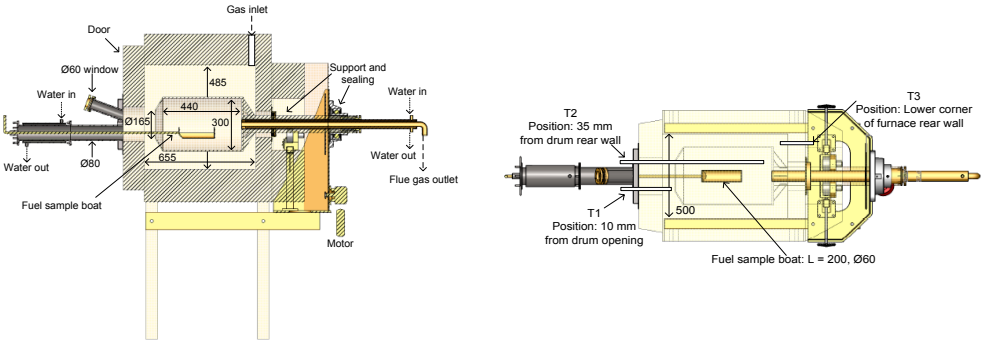

Figure 5-10: High temperature rotary drum. Left: Side view. Right: Top view (Nielsen, 2012). Note: T1, T2 and T3 refer thermocouples, L refers to length and ø to diameter in mm.

Figure 5-11 shows the piping and instrumentation diagram of the high temperature rotary drum. The nitrogen and air can be sent into the furnace but can also be bypassed during calibration of flow meter controllers and leakage tests. The gas temperature is measured at three different positions in the rotary drum reactor: at the rear wall in the chamber furnace (T1), which is regulated by a Programmable Logic Controller (PLC), at the center of the rotary drum (T2) and at the door just in front of the rotary drum (T3). The rotation of the rotary drum is regulated by a speed controller (S1), which controls the motor (M1).

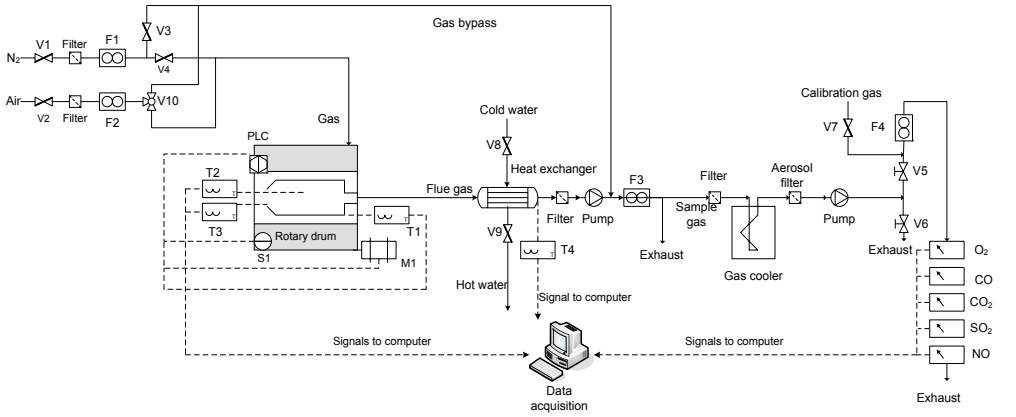

Figure 5-11: P&I diagram of the high temperature rotary drum (Nielsen, 2012).

A pump transports the flue gas out of the rotary drum reactor. Before passing the pump, the flue gas is cooled in a heat exchanger and soot particles are captured in a filter. After having passed the pump, the flue gas is either sent directly to the stack, or to the gas analyzers for measurement of O_2, CO, CO_2, SO_2, and NO. The fraction of the flue gas which is sent to the analyzers will pass additional two filters, a gas cooler for condensation of water and a sample gas pump before reaching the gas analyzers. IR analyzers are used for CO and CO_2, an UV analyzer is used for NO and SO_2, and a paramagnetic analyzer is used for O_2.

The operational limits of the experimental set-up are described in Table 5-3.

Table 5-3: Key specifications for high temperature drum experimental setup (Nielsen, 2012).

Parameter	Specification
Operating temperature	≤ 1000 °C
Rotational speed	0-20 rpm
Gas flow	≤ 500 NL/min
Oxygen concentration	2-21 vol. %
Load capacity	≤ 6 L
Fill degree	≤ 17 %

5.2.2 Experimental Method

As stated in the pre-experimental considerations, a model mixture of raw materials is used in the experiments of this project. The mixture is based on inert quartz sand with a particle size ranging from 0.5 to 0.71 mm, and $CaSO_4$, as source of sulfur.

The synthetic mixture is placed in the rotary drum in the desired volumetric filling degree, typically 5 %. The furnace door is closed and the reactor heated to the desired temperature. The drum is rotating with 6 rotations per minute, which keeps the raw materials in a rolling motion with an angle of repose of approximately 30-40°. A constant flow of 100 NL/min of gas with the desired O_2 concentration in N_2 is sent through the rotary drum.

At a desired temperature, controlled by T2, and oxygen concentration monitored by the gas analyzer, the fuel sample is placed in the sample boat, which is then positioned in the water cooled tube. The water cooled tube is closed in the end, in order to obtain a controlled atmosphere inside the rotary drum reactor. When the temperature measured by T2 and oxygen concentration are stable inside the reactor, the fuel sample boat is pushed into the rotary drum, turned 180° and pulled out in the water cooled tube again. Thereby, the fuel sample will drop on the synthetic bed material and immediately be heated and start combustion.

The filters in the experimental set-up are changed regularly in order to avoid significant pressure drop over the system because this creates an unstable gas flow, which will affect the repeatability of the individual experiments.

The release of sulfur during the experiments is quantified by integration of the gas concentration of SO_2 over the relevant time interval, which mathematically is expressed by equation 5.1. The SO_2 release during thermal decomposition of $CaSO_4$ (when no experiments are conducted) must be subtracted from the actual measurements in order to quantify only the release caused by the fuel combustion.

$$n_{S\,release} = \int_0^t y_{SO_2}\,dt \cdot 10^{-6} \cdot \frac{P \cdot Q}{R \cdot T} \qquad [5.1]$$

where y_{SO2} is the SO_2 concentration in ppm, R the gas ideal constant (8.314 $m^3 \cdot Pa/mol \cdot K$), P the atmospheric pressure in Pa, T the temperature in K, and Q the volumetric gas flow in m^3/s.

Assuming that the fuel conversion is proportional to the carbon conversion, the degree of fuel conversion, X, can be calculated by integration of the concentrations profiles of CO_2 and CO (y_{CO2} and y_{CO}), as described by equation 5.2.

$$X(t) = \frac{\int_0^t y_{CO} + y_{CO_2}\,dt}{\int_0^\infty y_{CO} + y_{CO_2}\,dt} \qquad [5.2]$$

5.2.3 Fuel Samples

Pine wood and tire rubber cylinders are used as fuels. Their proximate and ultimate analyses as received and the lower heating values are shown in Table 5-4.

Table 5-4: Pine wood and tire rubber proximate and ultimate analyses and their lower heating values (LHV). Notes: [1] Volatile matter, [2] Fixed carbon.

Fuel	Moisture [wt. %]	Proximate analysis [wt. %]			Ultimate analysis [wt. %]				LHV [MJ/kg]
		VM[1]	FC[2]	Ash	C	H	N	S	
Pine Wood	11.4	76.8	11.3	0.5	44.7	5.54	0.04	-	15.97
Tire rubber	-	64.4	32.6	2.8	87.4	7.1	0.3	1.2	36.9

Three types of particle size of pine wood and tire rubber are chosen in order to investigate the effect of particle size. The cylinder dimensions of pine wood and tire rubber are specified in Table 5-5. It was not possible to use identical dimensions of wood and tire cylinders due to the high energy input of tire.

Table 5-5: Cylinders dimensions of pine wood and tire rubber. Length (L) and diameter (ø).Note:* Granulate.

Fuel	Particle size [mm]		
Pine wood	ø19 , L= 25	ø=13 , L=25	ø=8 , L=25
Tire rubber	ø13, L=12	ø=9 , L=12	ø≈ 2*

5.2.4 Wood Char Preparation

The wood char is made by introducing the wood cylinders into a horizontal tube reactor under a nitrogen atmosphere for 20 minutes at a specific temperature. The horizontal tube reactor is an Entech two-zone electrically heated furnace consisting of a ceramic pipe, which is heated by three electrical heaters, and water cooled flanges at both ends. The length of the ceramic pipe is 1150 mm and the inner and outer diameters are 50 and 60 mm, respectively. The reactor has also a gas panel, which allows using the desired gas and flow. The outlet gas can be filtrated and analyzed or send it directly to ventilation. Figure 5-12 shows a schematic view of the different parts of the horizontal tube reactor.

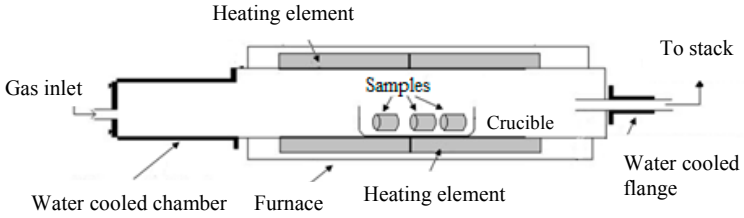

Figure 5-12: Sketch of the horizontal tube reactor.

The wood cylinders are placed in a porcelain crucible with dimensions of HxWxL=17x35x90 cm. The porcelain crucible is placed in the water cooled chamber, which makes it possible to remove and insert the wood cylinder while the oven is hot and while maintaining the gas composition. For all the wood char preparation, a minimum time of 5 minutes after sealing of the oven is kept to ensure that no oxygen is inside the system after the pipe has been open. The sealing is done with a stainless steel plate which contains an opening for the gas inlet. The crucible is pushed into the center of the ceramic tube using a metal stick. After 20 minutes, the crucible is pushed fast to the water cooled chamber with a metal tube from the back end in order to minimize the entrance of oxygen into the reactor. In the water cooled chamber the crucible and the samples are cooled down in nitrogen during 10 minutes.

Wood char is produced at temperatures of 300, 500, 700 and 900 °C with a constant N_2 flow of 5 NL/min in all the experiments. The used nitrogen has a purity of 99.999 %. The mass before and after the pyrolysis of each cylinder are measured. It should be noticed that the cylinders shrink during pyrolysis. Table 5-6 shows the average dimensions of the wood cylinders after the pyrolysis at different temperatures. The degree of devolatilization for the three different wood cylinders and the average at different temperatures are also specified in Table 5-6.

Table 5-6: Average dimensions and degree of devolatilization for the wood cylinders after the 20 min of pyrolysis at different temperatures. Length (L) and diameter (ø). Note: [A]Average, [B]Degree of devolatilization above 100 %, which means that the particle does not contain volatiles and have experience char degradation.

T [°C]	Particle size after pyrolysis [mm]			Degree of devolatilization [%]			
	ø 8, L= 25	**ø 13, L= 25**	**ø 19, L= 25**	**ø 8, L= 25**	**ø 13, L= 25**	**ø 19, L=25**	**Avg[A]**
300	ø 7, L= 24	ø 11-12, L=24	ø 17-18, L= 24	25.68 ± 2.4	26.33 ± 4.3	21.67 ± 3.7	24.5
500	ø 5-6, L= 21	ø 8-9, L= 21	ø 12-14, L= 22	98.57 ± 2.0	99.79 ± 0.4	101.55 ± 0.6	99.9
700	ø 4-5,L= 20	ø 8-9, L= 20	ø 12-10, L= 21	107.5 ± 0.6	108.2 ±1.1	109.19 ± 0.3	107.9[B]
900	ø 4-6, L= 20	ø 9, L=20	ø 10-12, L= 20	110.8 ± 0.8	110.6 ±0.9	110.3 ± 0.02	110.6[B]

The degree of devolatilization is calculated on basis of the content of volatiles before and after pyrolysis. The analysis of the volatiles content of the non-pyrolized wood was determined at 900 °C during 7 minutes (FLSmidth A/S, 2007). It can be seen that the degrees of devolatilization for the wood particles at 700 and 900 °C are above 100 %, which naturally does not have physical meaning. These numbers occur because the release of volatiles has been completed and decomposition of the char residue starts to occur due to the increased pyrolysis temperature (Koufopanos et al., 1989; Di Blasi, 2009). The degrees of devolatilization of the three different diameters at the same temperature differ slightly due to the internal heat transfer limitations where internal temperature gradients in the fuel particle occur during heating. The boundary between internal and external heat transfer limitations is defined by the Biot number (Bi), which depends on the thermal conductivity and particle size of the fuel. For the particle sizes used, the internal heating rate is more important than the external heating rate (Bi > 0.2).

5.3 Results and Discussion

5.3.1 General Observations

Figure 5-13 and Figure 5-14 show an example of the flue gas concentrations (O_2, CO, CO_2 and SO_2) from a typical experiment with combustion of a single wood cylinder with a diameter of 19 mm performed at 900 °C and 5 vol. % O_2, and a bed material of 5 % fill degree with 2 wt. % $CaSO_4$. When the devolatilization starts, the oxygen concentrations drops to approximately 2 vol. % and the CO and CO_2 concentrations increases. The

SO_2 concentration increases rapidly from 0 to almost 300 ppm and gradually decreases towards 0 ppm again while the CO_2 concentration also decreases.

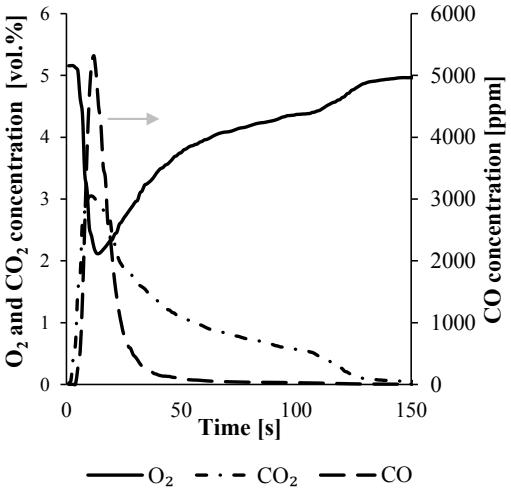

Figure 5-13: O_2, CO, and CO_2 concentrations in the flue gas during the combustion of due to combustion of one ø 19 mm pine wood cylinder. 900 °C, 5 % fill degree, 2 wt. % $CaSO_4$, 5 vol. % O_2, 100 NL/min, 6 rpm.

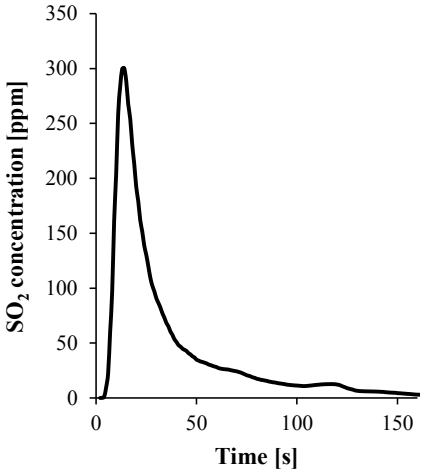

Figure 5-14: SO_2 concentration in the flue gas which is release from the raw materials due to combustion of one ø 19 mm pine wood cylinder. Experimental conditions: 900 °C, 5 % fill degree, 2 wt. % $CaSO_4$, 5 vol. % O_2, 100 NL/min, 6 rpm.

The normalized carbon conversion curve for the wood cylinder of 19 mm diameter is shown in Figure 5-15 from which the devolatilization and char oxidation times can be determined as indicated. The devolatilization period ends when the slope of the conversion curve decreases significantly, indicating the start of the slower char oxidation period. The char oxidation is assumed to be finished when the CO_2 concentration reaches the same value as the CO_2 concentration in 5 vol. % O_2 in the mixture nitrogen and air, which is 0.03 vol. % CO_2. This assumption is in good agreement with the visual observations during the experiment where red-glowing char particles can be observed in the bed until the CO_2 concentration reaches values below 0.03 vol. % CO_2.

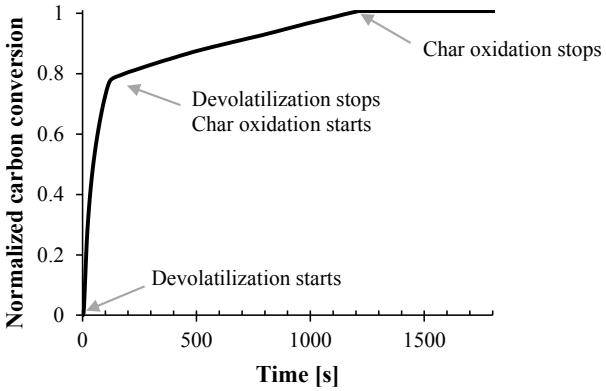

Figure 5-15: Normalized carbon conversion for ø 19 mm pine wood cylinder. Experimental conditions: 900 °C, 5 % fill degree, 2 wt. % $CaSO_4$, 100 NL/min, 5 vol. % O_2 in N_2, 6 rpm.

5.3.2 Effect of Particle Size of Different Fuel Types

The influence of particle size on sulfur release from the synthetic raw materials at conditions corresponding to the kiln inlet is illustrated in Figure 5-16 and in Figure 5-17, respectively for tire rubber and pine wood. The experiments are performed in a quartz sand bed of 5 % fill degree with 2 wt. % $CaSO_4$ at 900 °C and oxygen concentrations of 5 and 10 vol. % in N_2. All experiments use an identical energy input of 55 kJ in order to compare the effect of particle size. This means the mass of the wood cylinders and the mass of tire rubber are kept constant, therefore 5 cylinders of 8 mm diameter, 2 cylinders of 13 mm diameter and 1 cylinder of 19 mm are used, while for the tire rubber, a single cylinder of 13 mm diameter, and two cylinders of 9 mm diameter are used. It was not possible to use identical dimensions of wood and tire cylinders due to the high energy input of tire.

When combusting tire particles, sulfur is emitted due to the chemical composition of the particles. The sulfur emission originating from the tire particles is quantified by measuring the SO_2 release in a bed consisting of quartz sand without $CaSO_4$, and the displayed figure shows the corrected SO_2 release from the simulated raw materials after subtraction of the SO_2 release from the fuels.

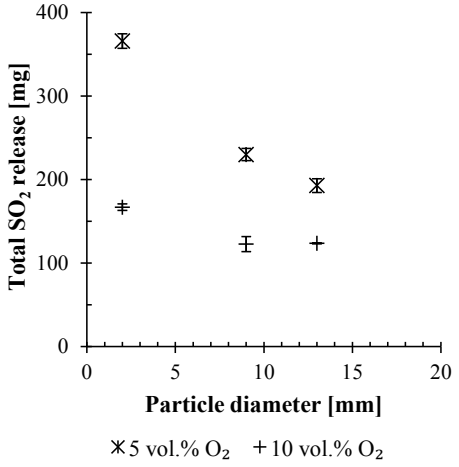

Figure 5-16: Effect of particle diameter of tire rubber cylinders (ø 9 mm and ø 13 mm) and granulate (~ø 2 mm) on corrected sulfur release from the raw materials due to combustion. Energy input of 55 kJ in each experiment. Experimental conditions: 900 °C, 5 % fill degree, 2 wt. % $CaSO_4$, 100 NL/min, 6 rpm.

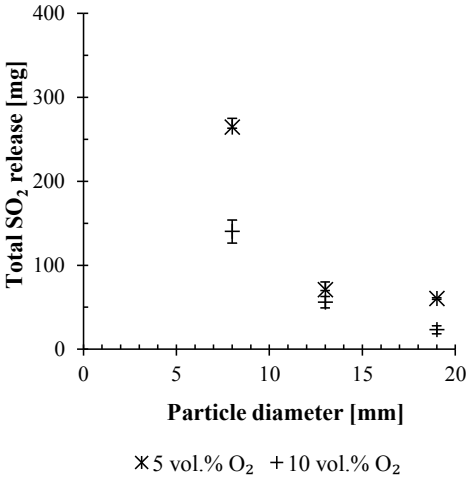

Figure 5-17: Effect of particle diameter of pine wood cylinders on sulfur release from the raw materials due to combustion. Energy input of 55 kJ in each experiment. Experimental conditions: 900 °C, 5 % fill degree, 2 wt. % $CaSO_4$, 100 NL/min, 6 rpm.

For all particles sizes and both fuels, the SO_2 release decreases with increasing oxygen concentration. This effect is also observed by Nielsen (2012) but current results have a better repeatability, an average relative uncertainty of 22 versus 3 %. The high concentration of oxygen in the freeboard atmosphere may react with the reducing agent and thereby lower the concentration of the reducing agent, which react with $CaSO_4$. Another possibility is that the oxygen may influence the reductive decomposition reactions.

The total SO_2 release increases with decreasing particle size of tire rubber and pine wood, as shown in Figure 5-16 and Figure 5-17, respectively. This is also reflected in the magnitude of SO_2 concentration peak measured in the analyzers, which is higher for the smallest particles than for the larger particle dimensions. For example, the SO_2 concentration peak reaches a maximum of 1413 ppm for the ø 8 mm pine wood particles while 213 and 198 ppm SO_2 are measured for wood particles of 13 and 19 mm diameter, under the same conditions, as illustrated in Figure 5-18.

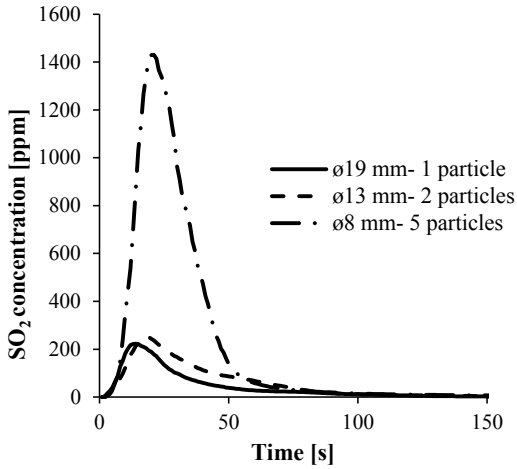

Figure 5-18: SO_2 concentrations from the raw materials due to combustion of the different dimensions of pine wood cylinders. Energy input of 55 kJ in each experiment. Experimental conditions: 900 °C, 5 % fill degree, 5 vol. % O_2 in N_2. 2 wt. % $CaSO_4$, 100 NL/min, 6 rpm.

Figure 5-16 shows that tire rubber tends to release more sulfur than pine wood, even though identical energy input is used in the experiments. It is known that the tire rubber follows the conversion pathway I in Figure 3-1 (Larsen, 2007) and experience cracking. It is therefore possible that the tire particle cracks into smaller particles, whereby the tire particle would be in contact with larger surface area of the bed and therefore cause more sulfur release than wood particles, which follows the conversion pathway G in Figure 3-1, in which the char experiences a decrease of particle size.

Thee wood particles were observed to be situated on the top of the bed surface during devolatilization due to the flame front surrounding the fuels particle, which seems to avoid the coverage of the particle under the bed. The particles kept their shape during the devolatilization process and during char oxidation the particle got fragmented due to the mechanical action of the bed. A sketch of the observation is illustrated schematically in Figure 5-19.

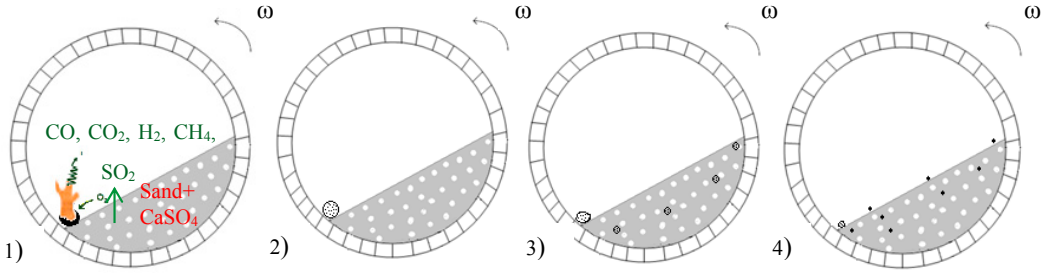

Figure 5-19: Sketch of the conversion a wood particle in the high temperature rotary drum.

The tire rubber particles were also observed to be on top of the bed surface, keeping the particle shape under devolatilization (scenario 1) and char oxidation with some fragmentation (scenario 2, 3 and 4). It was however difficult to visualize the fragmentation due to the angle of visibility from the window. During char combustion, the tire fragmented into several smaller char particles. This is in good agreement with the observations of Nielsen (2012) and Hansens (2011), who observed that tire rubber swells during devolatilization and after gets fragmented.

The carbon conversion for the different dimensions of tire rubber and pine wood are presented in Figure 5-20 and Figure 5-21, respectively. The carbon conversion is much faster for tire rubber than for pine wood and the devolatilization period is not as clear as for pine wood, which may be due to fragmentation. The total conversion time is shorter for the small particles than for the bigger particles for a fixed energy input. This is related to the internal heating up, because the smallest particles are heated faster and releases the volatiles gases faster and with higher concentrations. Consequently, stronger local reducing conditions are formed.

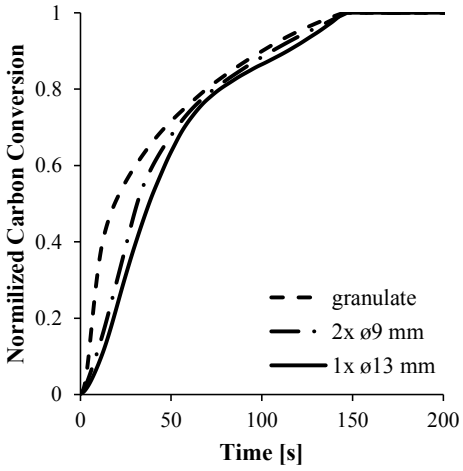

Figure 5-20: Normalized carbon conversion curves for the tire rubber particles. Experimental conditions: 900 °C, 5 % fill degree, 2 wt. % $CaSO_4$, 100 NL/min, 10 vol. % O_2 in N_2, 6 rpm.

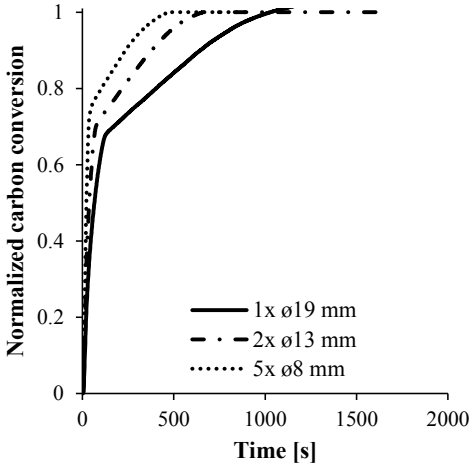

Figure 5-21: Normalized carbon conversion curves for the pine wood particles. Experimental conditions: 900 °C, 5 % fill degree, 2 wt. % $CaSO_4$, 100 NL/min, 10 vol. % O_2 in N_2, 6 rpm.

5.3.3 Effect of Degree of Devolatilization of Wood Particles

The pine wood cylinders are pyrolized at different temperatures in order to obtain wood char with different degree of volatiles, as explained in section 5.2.4. All the experiments are performed with the same initial

energy input, 55 kJ, from the virgin wood, which is the non-pyrolized wood, in order to enable a direct comparison.

The normalized carbon conversion curves versus time for the different particle sizes are shown from Figure 5-22 to Figure 5-25 for wood char made at 300, 500, 700 and 900 °C, respectively. These curves can be compared to the carbon conversion for the virgin wood at the same conditions, which was presented in Figure 5-21.

For the virgin wood and the wood chars made at different temperatures, the time required for the complete combustion is decreasing in the sequence of one cylinder of 19 mm diameter > 2 cylinders of 13 mm diameter > 5 cylinders of 8 mm diameter. This is the consequence of smaller particles being heated up faster than larger particles due to the internal heat transfer limitations.

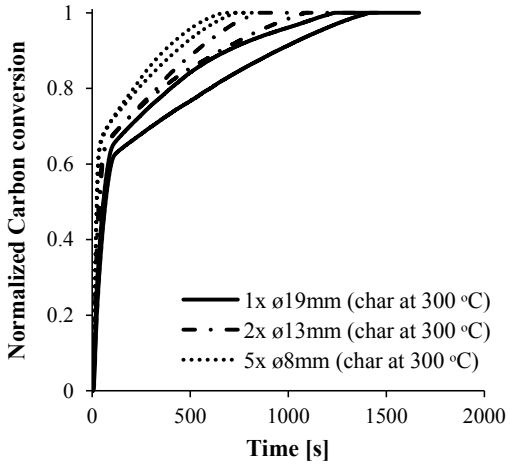

Figure 5-22: Normalized carbon conversion curves for different wood char particles (with the same initial mass) made at 300 °C. Experimental conditions: 900 °C, 5 % fill degree, 2 wt. % $CaSO_4$, 100 NL/min, 10 vol. % O_2 in N_2, 6 rpm.

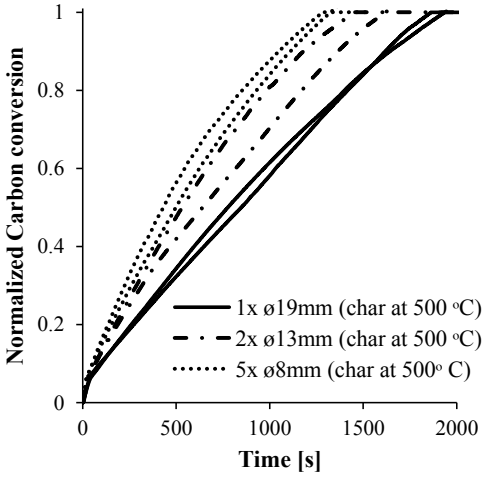

Figure 5-23: Normalized carbon conversion for different wood char particles (with the same initial mass) made at 500 °C. Experimental conditions: 900 °C, 5 % fill degree, 2 wt. % $CaSO_4$, 100 NL/min, 10 vol. % O_2 in N_2, 6 rpm.

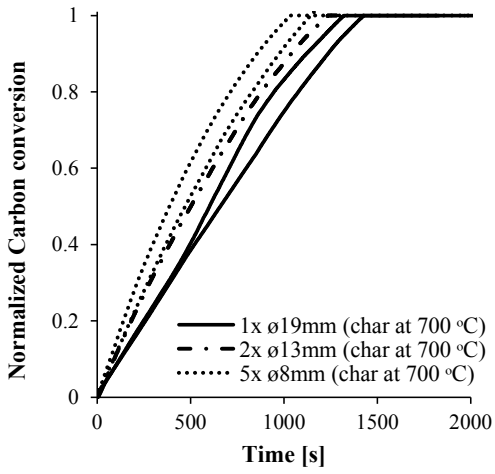

Figure 5-24: Normalized carbon conversion for different wood char particles (with the same initial mass) made at 700 °C. Experimental conditions: 900 °C, 5 % fill degree, 2 wt. % $CaSO_4$, 100 NL/min, 10 vol. % O_2 in N_2, 6 rpm.

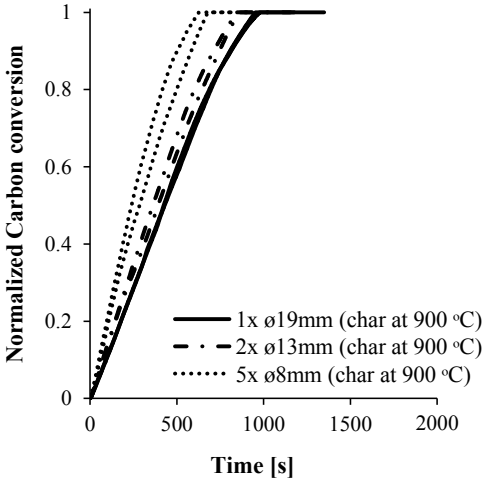

Figure 5-25: Normalized carbon conversion curves for different wood char particles (with the same initial mass) made at 900 °C. Experimental conditions: 900 °C, 5 % fill degree, 2 wt. % $CaSO_4$, 100 NL/min, 10 vol. % O_2 in N_2, 6 rpm.

The devolatilization period is observed for the virgin wood, and wood chars made at 300 and 500 °C, according to the definition given in the general observations. The average time for complete devolatilization and the char oxidation for virgin wood and the different wood chars of 19, 13, and 8 mm diameters are summarized with the corresponding uncertainties in Figure 5-26 and Figure 5-27, respectively. It should be noted that the virgin wood is considered as being pretreated at 25 °C.

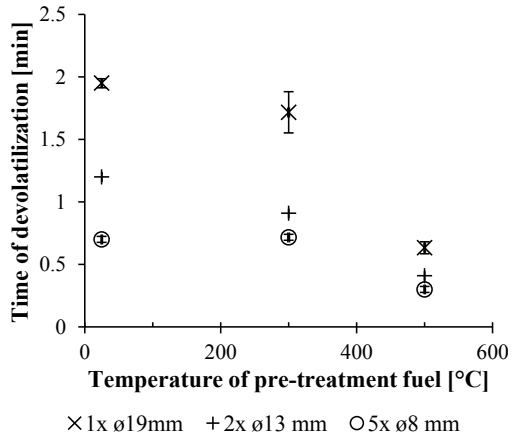

Figure 5-26: Effect of pre-treatment temperature on the average time of devolatilization for the different wood particle sizes. Experimental conditions: 900 °C, 5 % fill degree, 2 wt. % $CaSO_4$, 100 NL/min, 6 rpm, 10 vol. % O_2 in N_2.

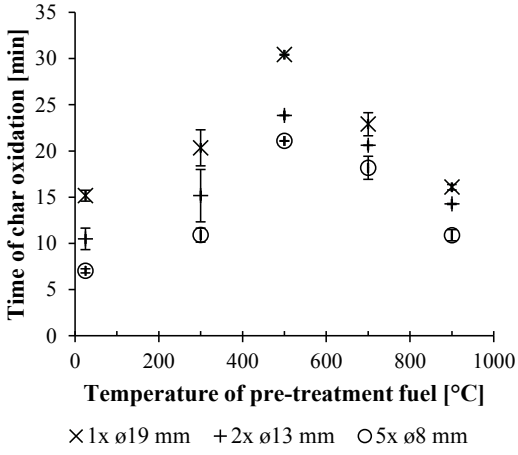

Figure 5-27: Effect of pre-treatment temperature on the average time of char oxidation for the different wood particle sizes. Experimental conditions: 900 °C, 5 % fill degree, 2 wt. % $CaSO_4$, 100 NL/min, 6 rpm, 10 vol. % O_2 in N_2.

The devolatilization period is shortened when the temperature of pre-treatment is increased, which can be explained in terms of the reduced content of volatiles. While the required time to complete char oxidation increases with increasing the temperature of pre-treatment until 500 °C and decreasing from 500 to 900 °C. The same tendency is also seen in the total conversion time for wood char made at 700 and 900 °C, which are shorter than for 500 °C. Monitoring the mass loss of the fuel particle after pyrolysis shows that the char residue decreases for the wood chars made at 700 and 900 °C in comparison with wood char made at 500 °C. The decreased time of char oxidation for these wood chars may be due to their reactivity, which depends on the porosity and the chemical structure (Di Blasi, 2009; Laurendeau, 1978). However, the reactivity has not been further studied because it is considered outside of the scope of this project.

The SO_2 concentration for the 5 cylinders of 8 mm diameter virgin wood and wood char made at 300, 500 and 700 °C experiments is plotted in Figure 5-28. The combustion of wood char made at 700 °C leads to SO_2 concentration of 1-2 ppm, which is insignificant compared to the release of virgin wood and wood char at lower temperatures and the uncertainties related to the thermal decomposition of $CaSO_4$ and the gas analyzers.

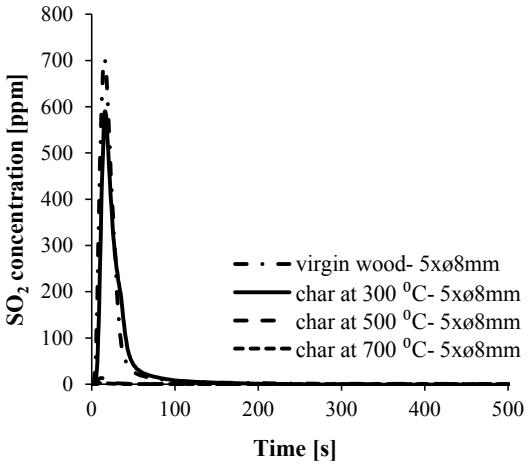

Figure 5-28: Corrected SO_2 concentration for 5 cylinders of ø 8 mm of virgin wood and char wood made at 300, 500 and 700 °C. Experimental conditions: 900 °C, 5 % fill degree, 2 wt. % $CaSO_4$, 100 NL/min, 10 vol. % O_2 in N_2, 6 rpm. Note: SO_2 concentration from the char at 700 °C cannot be observed.

Hence, SO_2 release is only observed in the cases where devolatilization takes place. During the time of char oxidation there is almost no sulfur release, although the particle releases CO due to the conversion of the char and the combustion is diffusion limited. It may be that the CO from the char oxidization is released in low concentrations, which do not provoke significant sulfur release. Moreover, the oxygen concentration during this period is higher than during devolatilization and the CO may thus be converted faster to CO_2.

Figure 5-29 shows the total SO_2 release from the raw materials as a function of the particle size of the combusted virgin wood and wood char made at 300 and 500 °C. The results show that the sulfur release decreases with decreasing degree of conversion. However, it is not possible neither to identify nor quantify which volatile gases that are released in each case because the CO is oxidized in the freeboard atmosphere and the analyzers do not give the possibility to detect other reducing agents.

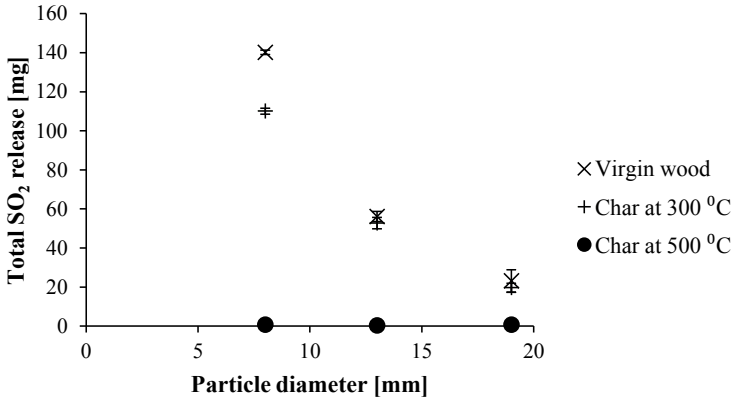

Figure 5-29: Sulfur release from the raw materials due to combustion of the combustion of different particle size wood and wood char at 300 and 500 °C. Experimental conditions: 900 °C, 5 % fill degree, 2 wt. % $CaSO_4$, 100 NL/min, 10 vol. % O_2 in N_2, 6 rpm.

The total SO_2 release increases, as previously discussed, with decreasing particle size of virgin wood and wood char made at 300 °C. There is a big difference in the SO_2 release for wood char made at 300 and 500 °C due to the degree of fuel conversion at the different temperatures. The total sulfur release for the wood char made at 500 °C is below 1 mg and had almost the same value for the different fuel particle sizes. This is due to the high degree of conversion, whereby few volatile gases are released. It should be remarked that the actual energy input used in the experiments is not constant due to the different content of volatiles.

5.3.4 Effect of Sulfur Concentration in the Bed Material

The effect of sulfur concentration in the bed material is investigated using two different concentration of $CaSO_4$ and three different particle diameters of pine wood, all with an energy input of 55 kJ. The experiments are performed at 950 °C using a bed material of 5 % filling degree with 5 wt. % and 2 wt. % $CaSO_4$.

Figure 5-30 shows the sulfur release from the raw materials during combustion of pine wood cylinders of 8, 13 and 19 mm diameter in beds containing 5 and 2 wt. % $CaSO_4$ and a gas atmosphere with 5 vol. % O_2. Figure 5-31 shows the sulfur release for the same conditions for a gas atmosphere with 10 vol. % O_2.

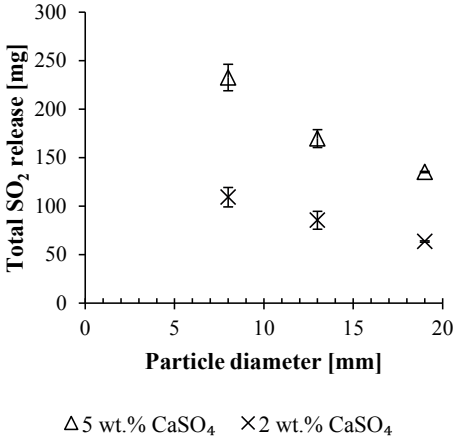

Figure 5-30: Sulfur release from the raw materials due to combustion of pine wood cylinders on a bed containing 5 and 2 wt. % of $CaSO_4$. Experimental conditions: 950 °C, 5 % fill degree, 100 NL/min, 6 rpm, 5 vol. % O_2 in N_2.

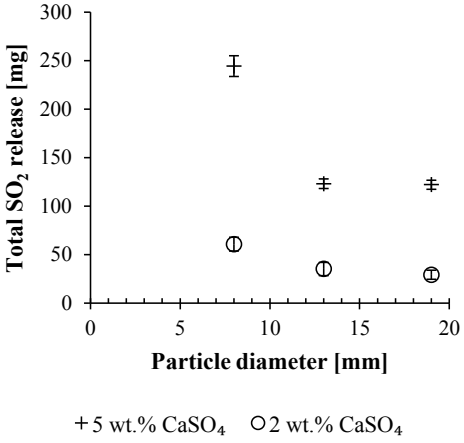

Figure 5-31: Sulfur release from the raw materials due to combustion of pine wood cylinders on a bed containing 5 and 2 wt. % of $CaSO_4$. Experimental conditions: 950 °C, 5 % fill degree, 100 NL/min, 6 rpm, 10 vol. % O_2 in N_2.

The graphs show that the sulfur release increases with increasing sulfur content in the bed. This may be because the volatiles gases are more likely to get in contact with more $CaSO_4$ in the bed and therefore more SO_2 is released. The SO_2 release decreases with increasing oxygen content for 2 wt. % $CaSO_4$ in the bed because the reducing conditions become less prominent at higher concentrations of O_2, but this tendency is less clear for 5 wt. % $CaSO_4$.

5.3.5 Effect of Moisture Content

The effect of moisture content of the wood is studied using wood cylinders of 8 mm diameter with different moisture content. The 30 and 60 wt. % water content is obtained by submerging the wood cylinders in water for different periods. The water content is determined by weighing the wood particles prior and after submersion in water.

Figure 5-32 shows the carbon conversion curves for the dried wood cylinder and wet cylinders with 30 and 60 wt. % of water content. Figure 5-33 shows the sulfur release from the raw materials during the combustion at 900 °C and 10 vol. % O_2 of a dry wood cylinder and humidified wood cylinders with 30 and 60 wt. % water content.

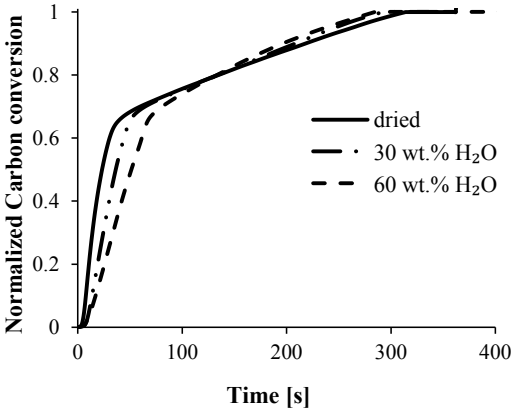

Figure 5-32: Normalized carbon conversion for a single ø 8 mm wood cylinder dried and with 30 and 60 wt. % water contents. Experimental conditions: 900 °C, 5 % fill degree, 2 wt. % $CaSO_4$, 100 NL/min, 6 rpm, 10 vol. % O_2.

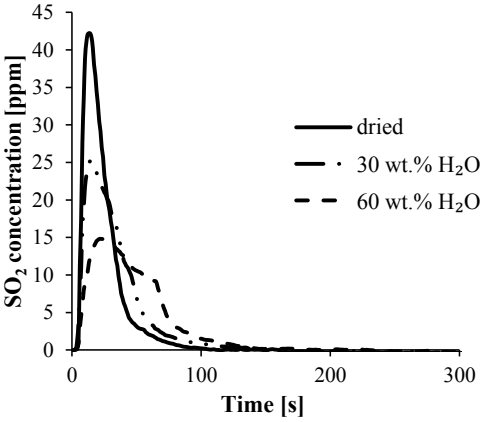

Figure 5-33: SO_2 release from the raw materials due to combustion of single ø 8 mm wood cylinder dried and with 30 and 60 wt. % water contents. Experimental conditions: 900 °C, 5 % fill, 2 wt. % $CaSO_4$, 100 NL/min, 6 rpm, 10 vol. % O_2.

When the moisture content of the wood particles increases, more water must be evaporated and therefore the devolatilization rate decreases. This has also been observed using non-spherical pine wood containing 0, 22 and 40 wt. % moisture in fluidized bed experiments (de Diego et al., 2002). Even though the devolatilization period is prolonged with increasing water content, the full conversion ends at a similar time.

The magnitude of the SO_2 peaks in Figure 5-33 are influenced by the water content. The dry wood cylinder has the highest SO_2 peak, while the SO_2 peaks for the cylinders with a water content of 30 and 60 wt. % have lower values and are wider than the one obtained for the dry wood. The tendency observed is that increasing water content lowers the SO_2 concentration level. This may be due to a delayed devolatilization and the reduced rate of conversion because the volatiles are released at lower concentrations for longer periods, giving rise to lower SO_2 release for a longer time period.

Table 5-7 summarizes the total SO_2 release calculated by equation 5.1 for each case.

Table 5-7: Total SO_2 release from the combustion experiments of the single ø 8 mm wood cylinder dried and with 30 and 60 wt. % water content.

	Dried wood	**Wood with 30 wt. % H_2O**	**Wood with 60 wt. % H_2O**
Total SO_2 release [mg]	5.77	3.68	3.41

The total SO_2 release differs between the dry wood cylinder and the wet wood cylinders, but the total sulfur release is quite similar for cylinders containing 30 and 60 wt. % water. The release takes more time when the water content is increased from 30 to 60 %, but total amount release is almost the same.

5.3.6 Discussion

The importance of particle size of the fuel has been investigated using pine wood and tire rubber. The results showed that smaller particle sizes gives more SO_2 release due to the faster internal heating up while larger particles present more pronounced internal temperature gradients, resulting in a slower heating up. The release and concentration of volatile gases is related to the heating up of the particle. Therefore, higher concentrations of volatiles are released during a shorter period for smaller particles, giving higher concentrations of SO_2 release and total SO_2 release. Larger particles will release the volatile gases during longer periods, giving lower SO_2 concentrations and total SO_2 release. Furthermore, the conversion pathway that a fuel type follows and the fragmentation also influence the SO_2 release.

The oxygen content in the freeboard atmosphere influences the sulfur release from the bed material. The phase diagram of the sulfur species with oxygen shows that the stability of $CaSO_4$ increases with higher oxygen partial pressure. It may be possible that oxygen influences the reductive decomposition reactions or that the excess oxygen from the freeboard atmosphere oxidizes the reducing agents released from the fuel particle. This influence needs further investigation, which will be conducted in the next chapter.

The effect of particle size on SO_2 release is also observed when wood char made at different temperatures are used. SO_2 release is only observed for the wood chars containing volatiles and not during char oxidation. This is contradictory to the general experience if coal or petcoke combustion in the calciner is incomplete and is admitted to the industrial kiln inlet causing a dramatically increase of sulfur circulation (Nielsen and Jepsen, 1990). Additional experiments using few grams of granulate wood char (approx. 1 mm diameter) made at 900 ^oC in the rotary drum provoked a significant SO_2 release from the raw materials and the particles following the rolling mode of the material. This shows that the SO_2 release is not associated just to devolatilization and is depending on the concentration of the gas released. The CO released during char combustion using wood char made at 700 and 900 ^oC in the experiments where the degree of devolatilization were investigated, may have not been high enough to provoke SO_2 release. Furthermore, the experiments using char wood did not have an actual constant thermal input, only the initial energy input before pyrolysis was constant. Hence, less fuel was introduced when the devolatilization degree was increased. However, in the next chapter this will be further investigated by introduction of the same total amount of gas with different concentrations and time of exposure.

Different phenomena occur simultaneously during the experiments, such as mixing of the fuel with the bed material, heating up of a particle and release of volatiles gases, char combustion, reaction of the reducing agents with $CaSO_4$, and release of SO_2. It is not possible to control all of these processes and the current equipment cannot identify and/or quantify the reducing agents released from fuel particles during devolatilization and/or char oxidation. For that reason, the effect of the concentration of different reducing agent in the high temperature rotary drum will be investigated in Chapter 6.

The effect of the fuel moisture content affects the concentration of the reducing agents by delaying heating up of the particle and by means of dilution by the moisture vapor. The phenomenon may be explained by understanding the effect of the concentration of the reducing agent and this will be further investigated in Chapter 6, however, without addition of H_2O (g).

5.4 Conclusions

A literature study of sulfur release during combustion of alternative fuel particles showed that reducing gases from the fuel devolatilization cause reductive decomposition of $CaSO_4$ and indicated that fuel particle size is of high importance for the degree of sulfur release.

The sulfur release from raw materials during combustion of tire rubber and pine wood in this chapter was studied using three different particle sizes and the identical energy inputs. The sulfur release from the raw materials increased with decreasing particle size. Tire rubber released more sulfur than pine wood. This may be explained by the conversion pathway of fuel and the mixing of the fuel and raw materials.

The effect of wood cylinders with different degree of volatiles showed that the sulfur release mainly took place during devolatilization, corresponding to the cases with virgin wood and wood chars made at 300 and 500 °C, which contained volatiles. The sulfur release decreased with decreasing degree of conversion.

The sulfur release obtained during the combustion of pine wood increased when the sulfur load in the bed material was increased from 2 to 5 wt. % $CaSO_4$.

In all the experimental series the SO_2 release decreases with increasing oxygen concentration due to less prominent reducing conditions at higher O_2 concentrations.

The effect of water content was investigated with single wood cylinders with a diameter of 8 mm. The results showed the SO_2 peak reaches lower values and the release occurs in a longer time period with increasing water content in a sample, the total amount of sulfur released is however similar for the wet wood cylinder and is less than the dry wood.

5.5 References

Barin, I.; Thermochemical data of pure substances. Third Edition. VCH, Germany. 1995. ISBN: 3-527-28745-0.

Barletta, D., Marzocchella, A., and Salatino, P.; Modelling the SO_2–limestone reaction under periodically changing oxidizing/reducing conditions: The influence of cycle time on reaction rate. Chemical Engineering Science, 57, 631-41, 2002.

Dam-Johansen, K., and Østergaard, K.; High-temperature reaction between sulfur dioxide and limestone - II. An improved experimental basis for a mathematical model. Chemical Engineering Science, 46, 839-45, 1991a.

Dam-Johansen, K., and Østergaard, K.; High-temperature reaction between sulfur dioxide and limestone - IV. A discussion of chemical reaction mechanisms and kinetics. Chemical Engineering Science, 46, 855-9, 1991b.

de Diego, L. F., Garcia-Labiano, F., Abad, A., Gayan, P., and Adanez, J.; Coupled drying and devolatilisation of non-spherical wet pine wood particles in fluidised beds. Journal of Analytical and Applied Pyrolysis, 65, 173-84, 2002.

Di Blasi, C.; Combustion and gasification rates of lignocellulosic chars. Progress in Energy and Combustion Science, 35, 121-40, 2009.

FLSmidth A/S, Determination of volatile matter content, Internal report. 2007.

Hansen, P. F. B., Johansen, K. Dam, and Østergaard, K.; High-temperature reaction between sulfur dioxide and limestone. V. the effect of periodically changing oxidizing and reducing conditions. Chemical Engineering Science, 48, 1325-41, 1993.

Hansens, T.B.; Combustion characterization of alternative fuels. Master thesis (in Danish). Technical University of Denmark, Department of Chemical and Biochemical Engineering, 2001.

Hewlett, P. C.; Lea's chemistry of cement and concrete. Fourth edition. New York, 1998. ISBN: 978-0-7506-6256-7.

Koufopanos, C. A., Maschio, G., and Lucchesi, A.; Kinetic modeling of the pyrolysis of biomass and biomass components. Canadian Journal of Chemical Engineering, 67, 75-84, 1989.

Larsen, M. B.; Alternative fuels in cement production. Ph.D. thesis, Technical University of Denmark, Department of Chemical and Biochemical Engineering, 2007. ISBN: 978-87-91435-49-8.

Laurendeau, N. M.; Heterogeneous kinetics of coal char gasification and combustion. Progress in Energy and Combustion Science, 4, 221-70, 1978.

Lyngfelt, A., and Eckner, B.; Model of sulfur capture in fluidized-bed boilers under conditions changing between oxidizing and reducing. Chemical Engineering Science, 48, 1131-41, 1993.

Nielsen, A. R.; Combustion of large solid fuels in cement rotary kilns. Ph.D. thesis, Technical University of Denmark, Department of Chemical and Biochemical Engineering, 2012. ISBN: 978-87-92481-66-5.

Nielsen, A. R., Larsen, M. B., Glarborg, P., and Dam-Johansen, K.; Sulfur release from cement raw materials during solid fuel combustion. Energy & Fuels, 25, 3917-24, 2011.

Nielsen, P. B. and Jepsen, O. L.; An overview of the formation of SO_x and NO_x in various pyroporcessing systems. IEEE cement industrial Technical Conference, 1990.

Oh, J. S., and Wheelock, T. D.; Reductive decomposition of calcium-sulfate with carbon-monoxide - reaction-mechanism. Industrial & Engineering Chemistry Research, 29, 544-50, 1990.

Swift, W. M., and Wheelock, T. D.; Decomposition of calcium sulfate in a two-zone reactor. Industrial & Engineering Chemistry Process Design and Development, 14, 323-7, 1975.

Wheelock, T. D., and Boylan, D. R.; Reductive decomposition of gypsum by carbon monoxide. Industrial & Engineering Chemistry Research, 52, 215-8, 1960.

6. Effect of Different Pyrolysis Gases on Sulfur Release

As mentioned in previous chapters, the main reducing agents (CO, CH_4, and H_2) released from fuel particles under local reducing conditions react with $CaSO_4$, releasing SO_2. This chapter investigates the effect of the single pyrolized gases and their mixtures on sulfur release under the conditions at the inlet of the rotary kiln.

The chapter covers a literature study about the reductive decomposition of $CaSO_4$ by the main reducing agents released by the fuels. The experimental part describes the modification of the high temperature rotary drum, which allows introduction of reducing agents through a steel tube under the bed material. The experimental results using single reducing agents and binary mixtures are presented in section 6.3.

6.1 Literature Study of the $CaSO_4$ Reductive Decomposition

The fundamentals of the $CaSO_4$ reductive decomposition in a wide range of conditions have been studied in relation to chemical-looping combustion, which is a combustion technology for controlling the greenhouse gas emission. Normally, these studies consider $CaSO_4$ as an oxygen carrier and use two reactors; the first reactor, to reduce $CaSO_4$ to CaS by a reducing gas, and the second to oxidize CaS by O_2 to $CaSO_4$. However, side reactions, which reduce $CaSO_4$ to CaO, exist.

Investigations about sulfur release and capture by limestone at high temperature under fluidized bed (Dam-Johansen and Østergaard, 1991; Hansen et al., 1993) have also suggested the mechanism for sulfur release (reductive decomposition of $CaSO_4$ on limestone) and capture.

6.1.1 Carbon Monoxide

The reductive decomposition of $CaSO_4$ by CO has been investigated by many authors (Diaz-Bossio et al., 1985; Kuusik et al., 1985; Oh and Wheelock, 1990; Okumura et al., 2003; Tian and Guo, 2009; Xiao and Song, 2011; Zheng et al., 2011) and can be described by reactions (6-1) and (6-2).

$$CaSO_4(s) + CO(g) \rightarrow CaO(s) + SO_2(g) + CO_2(g) \qquad \Delta H_{298}° = 220.0 \text{ kJ/mol} \qquad (6\text{-}1)$$

$$CaSO_4(s) + 4CO(g) \rightarrow CaS(s) + 4CO_2(g) \qquad \Delta H_{298}° = -171 \text{ kJ/mol} \qquad (6\text{-}2)$$

Different studies (Kuusik et al., 1985; Oh and Wheelock, 1990; Xiao and Song, 2011) have stated that reaction 6-1 is thermodynamically favored at a high reaction temperatures and a low reductive potential of the gas phase, as represented by the ratio of the partial pressures P_{CO}/P_{CO2}. When the CO concentration increases, the yield of CaO decreases because the formation of CaS (reaction (6-2)) becomes predominant within the temperature of 800-1000 °C (Xiao and Song, 2011). Increasing reaction temperature inhibits the exothermic reaction, reaction (6-2), while greatly promoting the endothermic reaction, reaction (6-1) (Tian and Guo, 2009).

The chemical stability of $CaSO_4$/CaS/CaO species is dependent on three factors: temperature, SO_2 partial pressure and reductive potential of the gas phase (Shen et al., 2008). The reactivity of the reduction reaction of $CaSO_4$ by CO has been studied varying these three factors, using isothermal gas (Oh and Wheelock, 1990; Talukdar et al., 1996; Shen et al., 2008) and non-isothermal methods (Tian et al., 2008; Tian and Guo, 2009), and introducing pure CO or in combination with CO_2, which makes more difficult to compare the results. The majority of the investigations has been carried out in a thermogravimetric analyzer (TGA) or in a fluidized reactor, which is a challenge for the quantitative measurement of the products.

The formation of CaS and CaO with reaction time cannot be clearly distinguished from the overlapped TGA curves due to the simultaneous formation of the two solid compounds. A solution was to connect a FTIR to identify the solid products to the TGA (Shen et al., 2008; Zheng et al., 2011). Using 10 vol. % CO in N_2 at the temperature range between 850-1050 °C, the reaction rate of $CaSO_4$ reduction was found to increase remarkably with increasing temperature. At 900 °C, no CaO or $CaSO_4$ were found, only CaS was the reduction product and there was no SO_2 in the flue gas (Shen et al., 2008; Zheng et al., 2011). From 950 °C, no $CaSO_4$ was found and a small amount of CaO was found. Increasing the reaction temperature, more CaO in the residue product was found. This indicated that the reduction of $CaSO_4$ with CO predominately occurs via reaction (6-2) in conjunction with reaction (6-1) in the temperature range from 950-1050 °C (Shen et al., 2008) and sulfur emission from the parallel reactions rose (Zheng et al., 2011) .

The decomposition of $CaSO_4$ using a non-isothermal method was studied by Tian and Guo (2009) using five different heating rates (5 to 20 °C/min from 20 to 1200 °C). It was observed that the CaO mole fraction in the products increased with increasing heating rate, which greatly promoted reaction (6-1) and also the side reaction (6-3) (Tian and Guo, 2009).

$$CaS(s)+3CaSO_4(s)\rightarrow 4CaO(s)+4SO_2(g) \qquad \Delta H_{298}^{\circ}= 1047.9 \text{ kJ/mol} \qquad (6\text{-}3)$$

Reductive decomposition of $CaSO_4$ by CO, in presence of CO_2 has also been studied by Oh and Weelock (1990) and Okumura et al. (2003), varying CO concentration, CO/CO_2 ratio and the temperature. It was found that the proportion of CaO in the products increased as the CO/CO_2 ratio decreased (Oh and Wheelock, 1990; Okumura et al., 2003). The SO_2 concentration profile was largely dependent on the reaction temperature and CO and CO_2 concentrations. It was suggested that higher CO_2 concentration may suppress reaction (6-2) more than reaction (6-1) from the viewpoint of stoichiometry because the CO_2 concentration has more influence on reaction (6-2). Consequently, reaction (6-1), which forms CaO and SO_2, proceeds more favorably than reaction (6-2) (Okumura et al., 2003). In agreement, several authors (Wheelock and Boylan, 1960; Kuusik et al., 1985; Hayhurst and Tucker, 1992) mentioned that an increase in the reaction temperature and the addition of either CO_2 or O_2 into the system, would promote the decomposition of $CaSO_4$ to CaO, while an increase of CO

concentration promotes the production of CaS. In presence of oxygen, CaS is rapidly oxidized to CaO (Hansen, 1991).

In addition, the presence of O_2 showed to inhibit the decomposition of $CaSO_4$ as well as the conversion and the reaction rate, depending on the O_2 molar percentage (Tian et al., 2008). The stability of $CaSO_4$ decreases with increasing temperatures and CO content in the gas phase (Tian and Guo, 2009). This is in a good agreement with the phase diagram shown in Figure 5-2. The performance of a cycle test alternating reducing and oxidizing condition at 950 °C in a fluidized bed reactor (Song et al., 2008) discovered the formation of large amounts of SO_2 and H_2S during the reduction process.

The reaction mechanisms of the reductive decomposition of $CaSO_4$ proposed, based on experimental studies, by Robbins (1966), which has not been available, however it is described by Swift et al. (1976), Oh and Wheelock (1990), and Hansen (1991) with good agreement. First, CO forms an unstable intermediate at the $CaSO_4$ surface, according to reaction (6-4) and desorbs rapidly by the reaction (6-5). The final step in the formation of CaO involves desorption of SO_2 (reaction 6-6)).

$$CaSO_4 + CO \rightleftarrows CaO \cdot SO_2 \cdot CO_2 \tag{6-4}$$

$$CaO \cdot SO_2 \cdot CO_2 \rightleftarrows CaO \cdot SO_2 + CO_2 \tag{6-5}$$

$$CaO \cdot SO_2 \rightleftarrows CaO + SO_2 \tag{6-6}$$

A similar mechanism for CaO formation was suggested by Pechkovskii and Ketvo (1961), elaborated by Swift et al. (1976). The reactions from (6-4) to (6-6) are similar to reactions (6-7) and (6-8) with $CaO \cdot SO_2$ written as $CaSO_3$, and based on experimental investigations $CaSO_3$ has been suggested as an important intermediate (Oh and Wheelock, 1990), however its existence is not favored thermodynamically (Hayhurst and Tucker, 1992).

$$CaSO_4 + CO \rightleftarrows CaSO_3 + CO_2 \tag{6-7}$$

$$CaSO_3 \rightleftarrows CaO + SO_2 \tag{6-8}$$

It has been suggested that the formation of CaS from $CaSO_4$ proceeds via CaO as intermediate and nothing indicated that CaS is an intermediate when $CaSO_4$ is converted to CaO (Oh and Wheelock, 1990; Hansen, 1991). However, Oh and Wheelock (1990) do not exclude that some $CaSO_4$ may be converted directly to CaS. The mechanism of CaS formation (suggested by Robbins in 1966) proceeds by reaction (6-9), where adsorbed SO_2 on CaO is reduced to elemental sulfur, and the sulfur can then be further reduced to CaS by reaction (6-10) (Swift et al., 1976). Pechkovskii and Ketvo (1961) also proposed a mechanism for CaS formation involving S_2, however the reactions were mechanistically unrealistic (Swift et al., 1976).

$$CaO \cdot SO_2 + 2CO \rightleftarrows CaO \cdot S + 2CO_2 \quad (6\text{-}9)$$

$$CaO \cdot S + CO \rightleftarrows CaS + CO_2 \quad (6\text{-}10)$$

6.1.2 Hydrogen

The reductive decomposition of $CaSO_4$ with H_2 has not been studied extensively. The kinetic investigation of Kim and Sohn (2002) identified reactions (6-11), (6-12) and (6-13) in the temperature range 700-800 °C. Reactions (6-12) and (6-13) are favored at low reducing concentrations, while reaction (6-11) is favored at high concentration of reducing gas (P_{H2}/P_{H2O} between 10^3 and 10^2) within the temperature 600-950 °C (Xiao and Song, 2011; Kim and Sohn, 2002; Shen et al., 2008).

$$CaSO_4(s) + 4H_2(g) \rightarrow CaS(s) + 4H_2O\,(g) \quad \Delta H_{298}° = -64 \text{ kJ/mol} \quad (6\text{-}11)$$

$$CaSO_4(s) + H_2(g) \rightarrow CaO(s) + SO_2(g) + H_2O\,(g) \quad \Delta H_{298}° = 260.4 \text{ kJ/mol} \quad (6\text{-}12)$$

$$CaSO_4(s) + 4H_2(g) \rightarrow CaO\,(s) + H_2S(g) + 3H_2O\,(g) \quad \Delta H_{298}° = 53.0 \text{ kJ/mol} \quad (6\text{-}13)$$

The reduction of $CaSO_4$ by 5 vol. % H_2 and 95 vol. % N_2 in the temperature range 870- 970 °C was investigated by Shen et al. (2008). It was observed that the rate of reduction of $CaSO_4$ by H_2 increases remarkably with increasing temperature.

The reductive decomposition of calcium sulfate using CO and H_2 in a thermogravimetric analyzer (TGA) has been studied by Diaz-Bossio et al. (1985), who found that the direct reductive products of $CaSO_4$ were pure CaO from 900 to 1180 °C and that the reaction was first order with respect to the concentration both of hydrogen and carbon monoxide. In the temperature range 700-800 °C, the reaction between $CaSO_4$ and H_2 was found also to be a first order respect to the H_2 concentration (Kim and Sohn, 2002). However, several studies (Diaz-Bossio et al., 1985; Hansen et al., 1993) state that the rate of reductive decomposition is higher for H_2 than for CO.

The equilibrium phase diagrams of $CaSO_4$, CaO and CaS influenced by H_2 and H_2O, presented in Chapter 5, showed that the partial pressure of H_2O was influencing the stability zones of $CaSO_4$, CaO and CaS. However, studies of the reductive decomposition of $CaSO_4$ with H_2 introducing H_2O vapor has not been reported in literature.

6.1.3 Methane

The reactivity of methane with calcium sulfate has been studied scarcely (Song et al., 2008; Song et al., 2009). The reactivity of $CaSO_4$ as oxygen carrier using CH_4 was investigated by Song et al. (2009) where the experiments consisted of six cycles of alternating reducing and oxidizing conditions, in a fixed bed at 950 °C

for the reducing period and 850 °C for the oxidizing period. The majority of inlet methane reacted with the $CaSO_4$, forming CO_2 and H_2O according to reaction (6-14). Slight amounts of SO_2 were also observed during the reducing period and the formation was stated to be mainly due to the solid-solid reaction (6-3). A side reaction during the reduction period was also a possibility according to reaction (6-15). The contact between CaS and $CaSO_4$ was enhanced and consequently SO_2 release increased during the initial cycles. H_2S was not observed, which indicated that reaction (6-16) did not take place. XRD analysis revealed that CaS was the main reduction product, and small amounts of CaO were also formed in the cyclic test.

$$CaSO_4(s) + CH_4(g) \rightarrow CaS(s) + CO_2(g) + 2H_2O(g) \qquad \Delta H_{298}° = 159.6 \text{ kJ/mol} \qquad (6\text{-}14)$$

$$4CaSO_4(s) + CH_4(g) \rightarrow 4CaO(s) + CO_2(g) + 4SO_2(g) + 2H_2O(g) \qquad \Delta H_{298}° = 1220.8 \text{ kJ/mol} \qquad (6\text{-}15)$$

$$CaSO_4(s) + CH_4(g) \rightarrow CaO(s) + CO_2(g) + H_2S(g) + 3H_2O(g) \qquad (6\text{-}16)$$

The effects of reaction temperature, gas flow rate, sample mass, and particle size on reduction reactions were investigated. The conversion of CH_4 increases with high temperature, smaller gas flow rate, larger sample mass and smaller particle size (Song et al., 2008).

6.1.4 Alternating Oxidizing and Reducing conditions

In a laboratory scale horizontal tube reactor the release of SO_2 from a synthetic cement calcined raw material containing $CaSO_4$ as sulfur source was quantified as a function of gas atmosphere, alternating oxidizing and reducing conditions with CO, H_2 and CH_4 in the temperature range from 900 to 1100 °C (Nielsen, 2012). The alternating oxidizing and reducing conditions were applied in intervals of 2 minutes and were repeated over 20 minutes. Figure 6-1 shows the results of sulfur release under the alternating oxidizing and reducing conditions using different reducing agents.

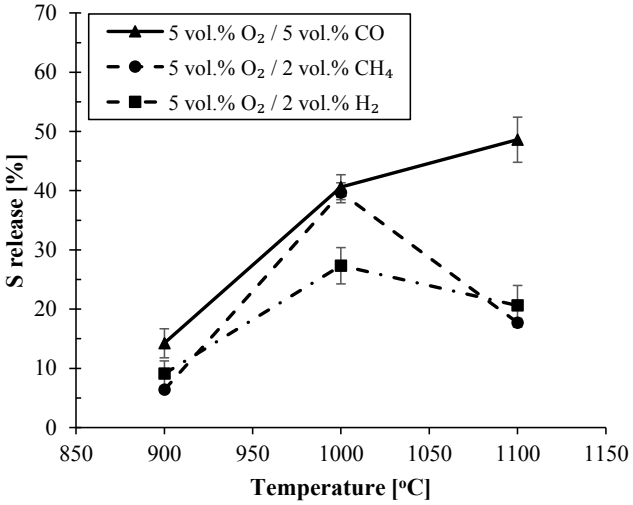

Figure 6-1: Effect of reducing agents on sulfur release from calcined raw material under alternating oxidizing and reducing conditions. Sulfur release evaluated after 20 minutes of reaction time, modified from (Nielsen, 2012).

The results with CO showed an increase in sulfur release with increasing temperature. The sulfur release due to reaction with H_2 or CH_4 increased from 900 to 1000 °C but decreased at 1100 °C. However, the experiments suffered from mass transfer limitations between the solid material and gas, and the gas analysis system failed to detect H_2S, which most probably was formed under the reducing conditions with H_2 and CH_4. Sulfur mass balances for the experiments were not checked and therefore the effect of the reducing agent on sulfur release was not quantified. A direct comparison between these results and Hansen's finding, without reductive decomposition (Hansen, 1991), is not possible due to the different conditions of the experiments.

6.1.5 Pre-experimental Considerations

From chemical-looping combustion studies of the reductive decomposition of $CaSO_4$, it can be concluded that depending on the temperature and the reducing agent concentration the reduction of $CaSO_4$ can proceed forming CaO, or CaS, or a mixture of both products. However, it is difficult to link these studies with the conditions of the rotary kiln because the reducing gases in the kiln will be in contact with the bed material, producing local reducing conditions but the flue gas will not experience the reducing conditions because it is rich in oxygen. For that reason, it is experimentally desired to introduce the reductive gases under a rolling bed material and have an oxidizing atmosphere in the freeboard. In this manner, the H_2S or other reduced sulfur species will be oxidized to SO_2. In the current facilities and also in the cement plants, there are no analyzers to measure H_2S or other reduced sulfur species in the flue gas if these are not oxidized. Furthermore, without an oxidizing atmosphere the reduced sulfur species may react with SO_2 which give a wrong measured concentration.

Moreover, it was observed during the experiments in Chapter 5 that the fuel particles were on top of the bed during devolatilization. The worst scenario for the sulfur release is when the reducing gases are in contact with the whole bed material. In the high temperature rotary drum it is not possible to force a fuel particle to be converted under the bed. This is another reason for introducing the gases through a steel tube under the bed material.

The reductive decomposition of $CaSO_4$ with a mixture of two reducing gases have not been investigated previously. So, the main reducing gases released from fuel particles will be first studied individually and then mixtures of them will be used.

6.2 Experimental

The high temperature rotary drum setup has already been presented in section 5.2.1. The setup has been slightly modified for the purpose of the new experiments. The modification consists of removing a thermocouple from the door and through the vacant hole a steel tube in L-shape is inserted in order to introduce reducing agents at the bottom of the material bed. Figure 6-2 shows a schematic 3D view of the modification of the setup. The steel tube is an alloy 600 (75 Ni/16 Cr) which can resist high temperatures. It is bent in an L-shape and the tip is fixed at a distance of 0.5 cm from the bottom of the rotary drum.

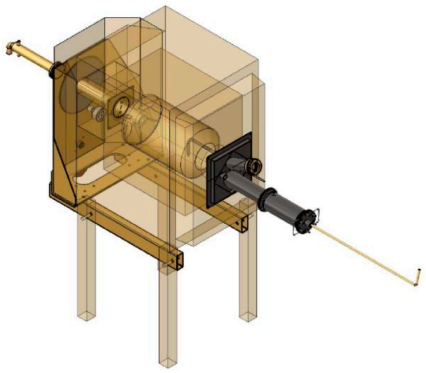

Figure 6-2: Schematic 3D view of the modified high temperature rotary drum.

Figure 6-3 illustrates the piping and instrumentation diagram of the modified setup. The tube is connected to a flow line which mixes the nitrogen and two reducing agents. The flowmeters used for the nitrogen and the reducing agents have the capacity of 2 NL/min and 1 NL/min, respectively, and the mixture flow has been set to 1 NL/min, which does not fluidize the bed material. The tube has an internal radius of 1.7 mm, giving a cross-section of $9.08 \cdot 10^{-6}$ m^2. Thereby, the velocity of the gas introduced under the bed material is 7.22 m/s at 900 ^oC.

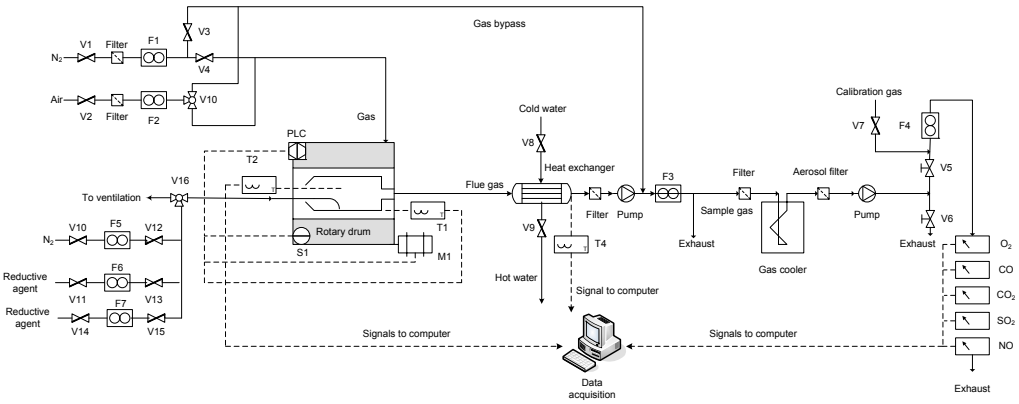

Figure 6-3: P&I diagram of the modified high temperature rotary drum setup.

The synthetic mixture of coarse quartz sand and 2 wt. % calcium sulfate is used for a 5 % volumetric filling degree, which corresponds to a bed high of 3 cm. Therefore, the release of the reducing agent takes place 2.5 cm from the top of the bed.

The CO, CH_4 and H_2 are supplied by pressurized 50 L gas bottles with a purity of 99.97 % CO, 99.5 % CH_4 and 50 mol. % H_2 in N_2, respectively. The reducing agents are mixed with nitrogen in order to vary their concentration from 5 vol. % to 40 vol. % and the nitrogen had a purity of 99.999 %.

The procedure followed during these experiments is first to set the flow of N_2 and the flow of the reducing agent sending the mixture to ventilation. When the flow is stable and well mixed, the 3 way valve V16 is turned and the mixture is sent to the high temperature rotary drum and the timer is started for controlling the time of introduction of the reducing agent. When the desired time is reached, the flowmeter of the reducing agent is set to zero and the valve of the reducing agent and the nitrogen are closed. A new experiment is started when the SO_2 and CO_2 concentrations had reached their initial values. Each measurement is repeated 2-3 times to ensure repeatability.

6.3 Results and Discussion

The effect of the single reducing agents on sulfur release is first investigated by varying the concentration introduced, the oxygen content of the freeboard atmosphere and the temperature. It must be emphasized that the SO_2 concentrations plotted in the following graphs do not take into account the thermal decomposition of $CaSO_4$, i.e. the SO_2 originating from thermal decomposition is set as the baseline. In addition, to resemble a mixture of volatile release from fuels the effect of binary mixtures amongst CO, CH_4 and H_2 on SO_2 release is investigated.

6.3.1 Carbon Monoxide

6.3.1.1 Effect of the Oxygen Content

The effect of different concentrations of carbon monoxide, from 5 to 20 vol. % CO, on SO_2 release is investigated at 900 ºC and at two different oxygen concentrations, 5 and 10 vol. % O_2. The duration of the period where CO is introduced under the bed material for each concentration is 4 or 5 min in order to reach a steady-state and have a constant SO_2 concentration. An example of the constant SO_2 concentration is illustrated in Figure C-1 in Appendix C. The averages of the constant SO_2 concentrations and the standard deviations of results obtained are presented in Figure 6-4. Lower concentrations than 5 vol. % CO, for example 2 vol. % CO, are tested at 5 vol. % O_2, releasing less than 1 ppm SO_2, which is insignificant compared to the release of 10 ppm SO_2 when 5 vol. % CO is introduced under the bed.

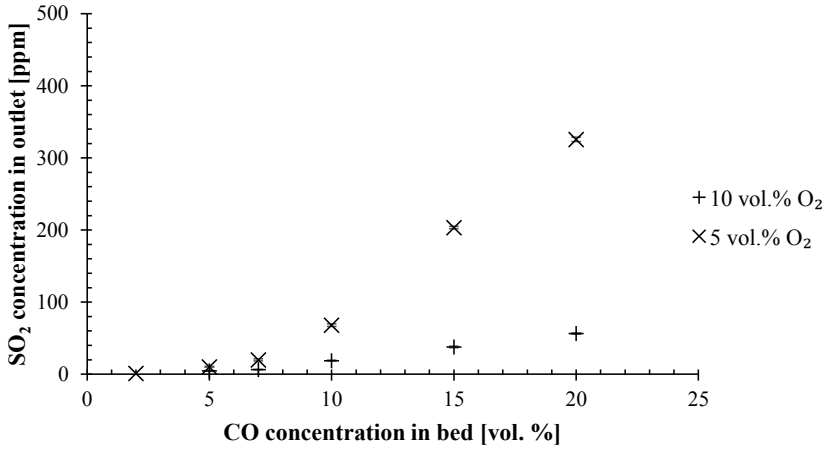

Figure 6-4: Effect of different CO concentrations introduced under the bed material on SO_2 concentration with 5 and 10 vol. % O_2 in the freeboard gas. Experimental conditions: flow tube 1NL/min, 900 °C, 5 % fill degree, 2 wt. % $CaSO_4$, 100 NL/min, 6 rpm.

The SO_2 release at 5 vol. % O_2 is not proportional to the CO concentration introduced. For example, using 10 vol. % CO the release of SO_2 is around 70 ppm, while using 15 vol. % CO the SO_2 concentration is 200 ppm, which is more than the double. Comparing the results at 10 vol. % O_2, SO_2 is released below 100 ppm up to 20 vol. % CO, while at 5 vol. % O_2 the SO_2 release is above 300 ppm SO_2 for 20 vol. % CO. Therefore, it can be seen the sulfur release is reduced when the oxygen content is increased. The corresponding CO_2 concentrations measured for each experiment are plotted in Figure C-2 in Appendix C.

The carbon mass balance of the experiments performed using CO as reducing agent is checked considering the molar mass flow rate of CO introduced and CO_2 measured by the gas analyzer. The results for the experiments performed at 900 ºC with 5 vol. % and 10 vol. % O_2 and at 1000 ºC are shown in Appendix C (Table C-1,

Table C-2, and Table C-3). In the calculations, the CO_2 in the atmospheric air (base line) has been removed from the total CO_2 measured in the outlet. The deviations are within 0.2 and 8 %.

6.3.1.2 Effect of the Temperature

The effect of the temperature on sulfur release using CO is also investigated. The previous experiments are performed at 5 vol. % O_2 and at 900 and 1000 °C. Figure 6-5 shows the average SO_2 concentrations with their standard deviation obtained by introducing the different CO concentrations. It can be seen that at 1000 °C the SO_2 release is higher for the same CO concentration, for example, 10 vol. % CO yields an average of 66 ppm SO_2 at 900 °C and 148 ppm SO_2 at 1000 °C. The corresponding CO_2 concentrations measured for each experiment are plotted in Figure C-3 in Appendix C.

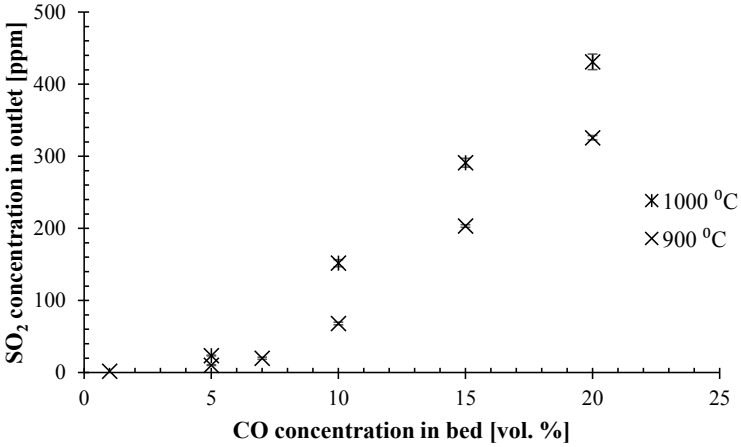

Figure 6-5: Effect of different CO concentrations introduced under the bed material on SO_2 concentration at 900 and 1000 °C. Experimental conditions: flow tube 1 NL/min, 5 % fill degree, 2 wt. % $CaSO_4$, 100 NL/min with 5 vol. % O_2 in the freeboard gas atmosphere, 6 rpm.

Concentrations of 30 vol. % and 40 vol. % CO are also tested at both temperatures. At 900 °C, different SO_2 concentration results were obtained in each repetition, while at 1000 °C the SO_2 release reached concentrations higher than 500 ppm but decreased with time, without reaching a stable concentration and the repeatability of the results were not achieved. The strong reducing conditions may indicate the formation of CaS because after stopping the injection of CO, a SO_2 peak was measured corresponding to CaS oxidation. It was noticed after cooling down the equipment, that the tube outlet was blocked. At these high CO concentrations, CO can react with a steel tube causing carbon deposition, which could be the reason why different SO_2 concentrations were obtained.

6.3.1.3 Effect of the Exposure Time

Since the release of reducing agents from a fuel particle can be very rapid with high concentrations, i.e. during the devolatilization period, or very slow with low concentrations, i.e. during the char oxidation, depending on the volatile and char content, the exposure time of the hot meal to the reducing agents may also vary. Therefore, the time of exposure is investigated by exposing the bed material to the same total amount of CO introduced varying the CO concentration and the injection time.

A total amount of 0.4 L CO is introduced under the bed material using CO concentrations from 5 to 20 vol. % at 900 and 1000 °C. The time required to introduce a total of 0.4 L CO at 5, 7, 10, 15 and 20 vol. % CO is 8 min, 5 min 43 s, 4 min, 2 min 40 s, and 2 min, respectively. Figure 6-6 and Figure 6-7 show the SO_2 concentration profiles for the different CO concentrations at 900 and 1000 °C, respectively. As explained in 6.3.1.2, the SO_2 release increases with increasing temperature for the same applied CO concentration. The results shows that introducing high CO concentrations for a short time gives high concentrations of SO_2 but without reaching a stable level such as in the case of 20 vol. % CO. The corresponding CO_2 concentration profiles to these experiments are plotted in Figure C-4 and Figure C-5 in Appendix C.

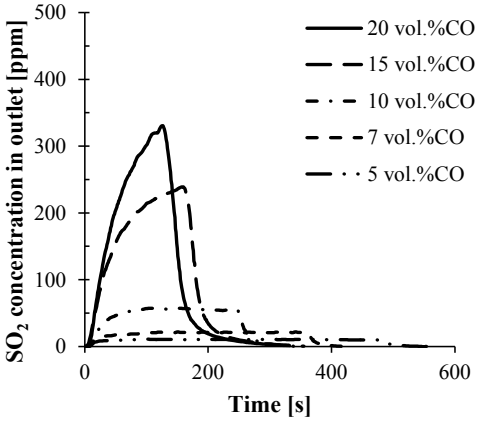

Figure 6-6: SO_2 concentrations when a total of 0.4 L of CO is introduced under the bed material with 5, 7, 10, 15 and 20 vol. % CO at 900 °C. Experimental conditions: flow tube 1 NL/min, 5 % fill degree, 2 wt. % $CaSO_4$, 100 NL/min with 5 vol. % O_2, 6 rpm.

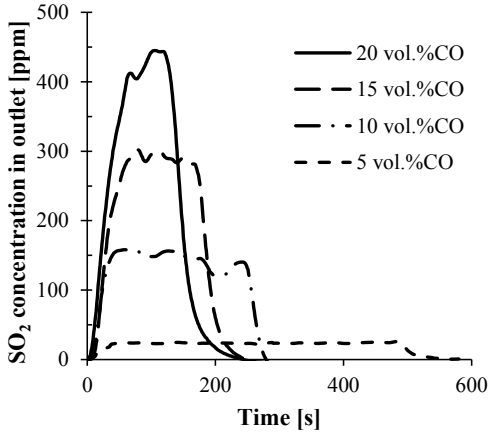

Figure 6-7: SO_2 concentrations when a total of 0.4 L of CO is introduced under the bed material with 5, 10, 15 and 20 vol. % CO at 1000 °C. Experimental conditions: flow tube 1 NL/min, 5 % fill degree, 2 wt. % $CaSO_4$, 100 NL/min with 5 vol. % O_2, 6 rpm.

In order to illustrate the influence of the exposure time, the total sulfur release which corresponds to the total integration of the SO_2 curves is calculated. Figure 6-8 shows the total SO_2 release for the CO concentrations between 5 and 20 vol. % at both temperatures.

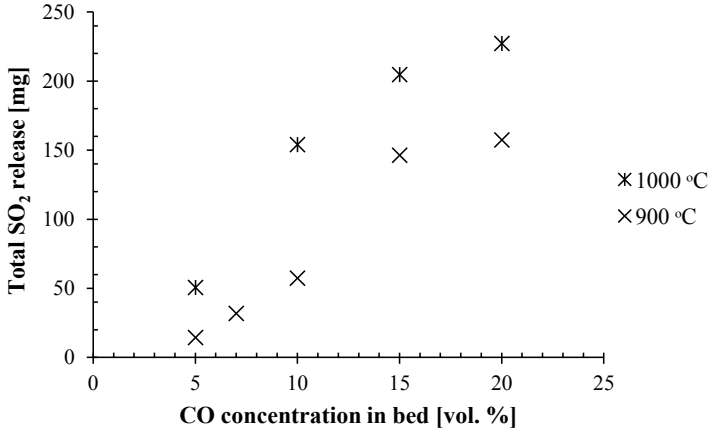

Figure 6-8: Total SO_2 release from the raw material when a total of 0.4 L of CO is introduced under the bed material with different CO concentrations at 900 and 1000 °C. Experimental conditions: flow tube 1 NL/min, 5 % fill degree, 2 wt. % $CaSO_4$, 100 NL/min with 5 vol. % O_2, 6 rpm.

Introducing the same total amount of CO, the total SO_2 release is different for each CO concentration. For a long exposure of low CO concentrations, the total SO_2 release is low compared to the total SO_2 release obtained for a short exposure of high CO concentrations. The total SO_2 release increases with increasing temperature. At 1000 °C, the main increase in the total SO_2 takes place when CO is increased from 5 to 10 vol. %, while at 900 °C, this occurs when CO is increased from 10 to 15 vol. %.

6.3.1.4 Equilibrium Phase Diagrams

The results obtained using CO at 900 °C and 5 vol. % O_2 are further used to evaluate the stable phase by using the equilibrium phase diagrams for the SO_2-CaO-$CaSO_4$-CaS-CO-CO_2 system. Figure 6-9 shows schematically the chemical species of the system. CO is introduced in the bed and forms CO_2 and SO_2 by reaction with $CaSO_4$, the non-reacted CO is further oxidized to CO_2 in the freeboard atmosphere.

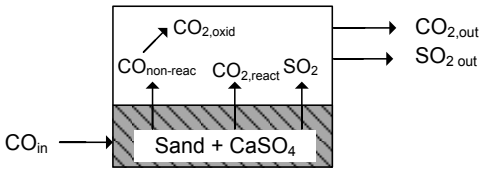

Figure 6-9: Sketch of the chemical species in the system.

In the system, it cannot be distinguished whether the CO_2 is formed by the reaction with $CaSO_4$ or by oxidation of CO. Since there are two competing reactions, the experimental reducing potentials, P_{CO}/P_{CO2}, for the equilibrium phase diagram are calculated by two different cases: [1)] assuming that CO reacts with $CaSO_4$ only according to reaction (6-1), and [2)] CO reacts only according to reaction (6-2).

For the first case, the calculations are done considering only reaction (6-1). The partial pressure of the CO_2 formed by the reaction, $P_{CO2\ react}$, is equal to the partial pressure of the formed, $P_{SO2\ out}$, defined by equation 6.1. The partial pressure of the reacted CO, $P_{CO\ react}$, is the difference between the initial CO partial pressure, $P_{CO,in}$, and the partial pressure of SO_2, as defined by equation 6.2.

$$CaSO_4(s) + CO(g) \rightarrow CaO(s) + SO_2(g) + CO_2(g) \quad (6\text{-}1)$$

$$P_{CO_2\,react} = P_{SO_2\,out} \quad [6.1]$$

$$P_{CO\,react} = P_{CO,in} - P_{SO_2,\mathrm{out}} \quad [6.2]$$

Thereby, the reducing potential at equilibrium is defined by equation 6.3.

$$\frac{P_{CO}}{P_{CO_2}} = \frac{P_{CO,in} - P_{SO_2,\mathrm{out}}}{P_{SO_2,\mathrm{out}}} \quad [6.3]$$

For each concentration of CO introduced, the CO_2 and SO_2 concentration are measured. The reducing potential at equilibrium is calculated for each experiment and the results are shown in Figure 6-10. For all CO concentrations, the stable phase is CaS.

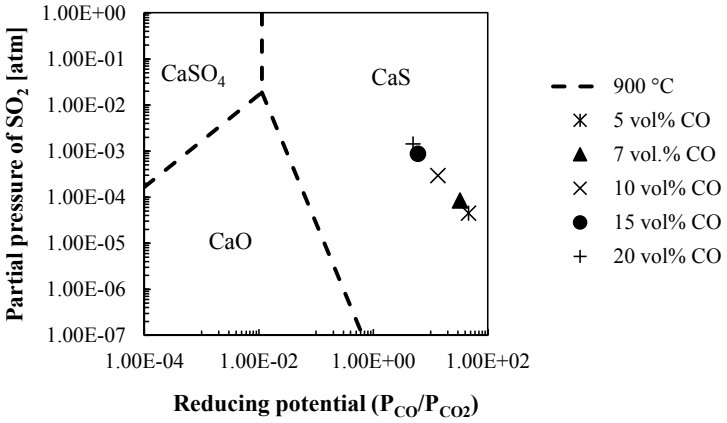

Figure 6-10: Phase diagram for the SO_2-CaO-$CaSO_4$-CaS-CO-CO_2 system at 900 °C and 5 vol. % O_2. Considering assumption 1, the experimental data obtained in the pilot plant setup introducing different CO concentrations under the bed material is used to show the stable phase in each case.

For the second case, the CO is assumed to react only according to reaction (6-2) and CaS is subsequently oxidized by reaction (6-17).

$$CaSO_4(s) + 4CO(g) \rightarrow CaS(s) + 4CO_2(g) \quad (6\text{-}2)$$

$$CaS(s) + \frac{3}{2}O_2(g) \rightarrow CaO(s) + SO_2(g) \quad (6\text{-}17)$$

The stoichiometry of reaction (6-2) shows that 4 moles of CO react to give 1 mol of SO_2. Therefore, the partial pressure of CO_2 and CO from the reaction can be calculated according to equation 6.4 and equation 6.5, respectively.

$$P_{CO_2,\text{react}} = 4 \cdot P_{SO_2,out} \quad [6.4]$$

$$P_{CO\,react} = P_{CO,in} - 4 \cdot P_{SO_2,\text{out}} \quad [6.5]$$

With the new definitions, the reducing potential at equilibrium can be calculated for each experiment and the results are shown in Figure 6-11. The results are in the stable area of CaS for all CO concentrations. Comparing Figure 6-10 and Figure 6-11, the reducing potential is lower for case 2, where it is assumed that CO reacts by reaction (6-2).

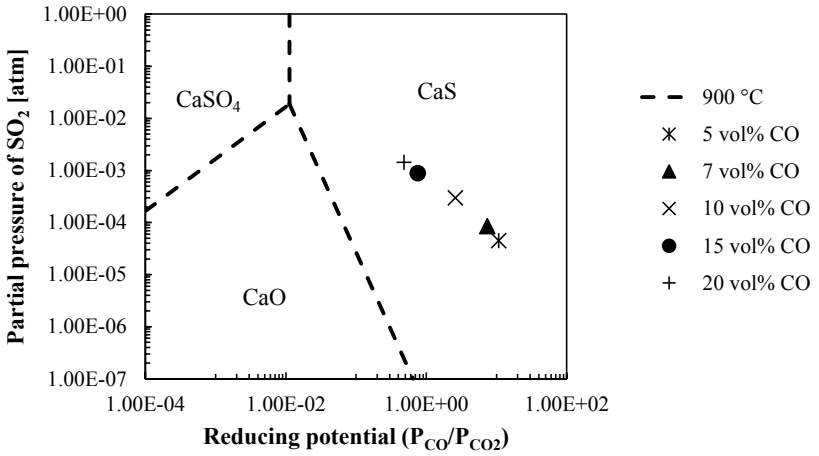

Figure 6-11: Phase diagram for the SO_2-CaO-$CaSO_4$-CaS-CO-CO_2 system at 900 °C and 5 vol. % O_2. Considering assumption 2, the experimental data obtained in the pilot plant setup introducing different CO concentrations under the bed material is used to show the stable phase in each case.

6.3.1.5 Effect of the Rotational Speed

The effect of the rotational speed of the rotary drum, varying from 4 to 20 rpm, has been investigating by injecting 5 vol. % CO at 900 ºC and 5 vol. % O_2. Figure 6-12 shows the SO_2 concentration obtained in each case. It seems that the SO_2 release increases with increasing rotational speed, except for the cases of 4 and 6 rpm, however, the difference are few ppm.

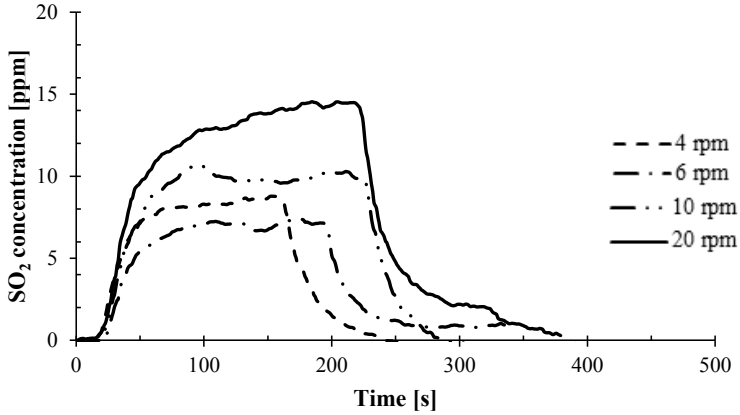

Figure 6-12: Effect of the rotational speed on SO_2 concentration when 5 vol. % CO is introduced under the bed material at 900 °C and at 5 vol. % O_2. Experimental conditions: flow tube 1NL/min, 5 % fill degree, 2 wt. % $CaSO_4$, 100 NL/min.

6.3.1.6 Discussion

The investigation of the influence of CO on SO_2 release has shown that CO concentrations lower than 5 vol. % does not provoke significant SO_2 release, only a few ppm which is insignificant in comparison with the SO_2 concentration from the thermal decomposition of $CaSO_4$. It seems that there is a minimum concentration below which SO_2 release does not occur and it can be suggested that the SO_2 rate of formation could follow the a first order expression, $r_{SO2}= k (C_{CO}- C_{CO,t})$, where $C_{CO,\,t}$ is the threshold CO concentration below which no SO_2 is released. Kinetic studies of the reductive decomposition of $CaSO_4$ with CO, summarized in Appendix D, have been performed at different concentrations and temperature ranges by many authors (Diaz-Bossio et al., 1985; Xiao and Song, 2011; Zheng et al., 2011; Kim and Sohn, 2002; Talukdar et al., 1996), however a threshold CO concentration has not been observed.

The effect of the CO concentration can be related to the effect of gases released from alternative fuels. During char combustion, the CO concentration may be quite low, even below 5 vol. % CO, for a long period, and for that reason SO_2 release is not measured. It could be that this minimum CO concentration is dependent on the sulfur content of the bed material. However, this has not been investigated.

The increase of the oxygen concentration resulted in a decrease in SO_2 concentration. This is in agreement with Tian et al. (2008) who stated that the presence of oxygen in the system inhibited the decomposition of $CaSO_4$ by reducing the reaction rate. In Chapter 5, it was also found that the sulfur release caused by the combustion of pine wood and tire rubber decreased with increasing O_2 content in the gas phase. During devolatilization of the solid fuels, the particles were placed on top of the bed and the gases released will be thus oxidized in the proximity of the particle by oxygen because the gas-gas reaction is faster than a gas-solid reaction. Thereby, some of the gases released will not be in contact with the bed material. This means that

more CO is able to react with $CaSO_4$ in the experiments when the gas is introduced under the bed material. Hence, the oxygen concentration influences the SO_2 release both when the gases are released under the bed material and in the proximity of the bed material. It is possible that the oxygen diffuses into the bed, oxidizing the reducing agent and consequently influences the SO_2 release. The oxygen concentration next to the bed surface or inside the bed has not been measured; however this would help understanding the conditions that the bed material experiences. In addition, the *real* cement raw material in the kiln inlet has a lower porosity and higher fill degree than the quartz sand used in these experiments and this can reduce the diffusion of oxygen from the freeboard to the bed.

The percentage of CO introduced that has reacted to SO_2 for each experiment has been calculated by dividing the SO_2 release by the CO injected in molar basis. This ratio has calculated assuming that the reaction is 1:1, following reaction (6-1), due to simplicity and further comparison with the model in Chapter 7. This ratio may however be smaller because the reaction may also take place according to reaction (6-2). Table 6-1 summaries the SO_2/CO percentage for the different CO concentrations, varying the temperature and the O_2 concentration. A minor fraction of CO has reacted to form SO_2, while most of the CO may diffuse to the freeboard atmosphere or may be oxidized to CO_2. The percentage of CO reacted increases with increasing injected CO concentration, temperature and decreasing oxygen concentration.

Table 6-1: Percentage of SO_2 release relative to CO injected for different CO concentrations varying temperature and O_2 content.

CO conc. [vol. %]	**SO_2/CO ratio [%]**		
	900 ºC, 5 vol. % O_2	900 ºC, 10 vol. % O_2	1000 ºC, 5 vol. % O_2
5	2.02	0.98	4.44
7	2.74	0.93	-
10	6.67	1.90	15.7
15	13.2	2.54	19.5
20	16.1	2.85	22.4

The phase diagram results indicate that CaS is the stable phase for the different CO concentrations used in the present experiment, both when considering reaction (6-1) or reaction (6-2). This is in agreement with the findings of Shen et al. (2008) and Zheng et al. (2011), who found that CaS was the only reduction product at 900 °C, while CaO or $CaSO_4$ were not found. This may indicate that CO preferentially reacts via reaction (6-2) and CaS is fast oxidized to CaO in contact with the oxygen of the freeboard atmosphere releasing SO_2. At higher temperatures, reaction (6-1) may also contribute to the emissions of SO_2. However, in the high temperature rotary drum the composition of the sulfur products in the bed material for each experiment cannot be determined and these products may not be significantly important at the kiln inlet conditions for the cement industry.

$$CaSO_4(s) + CO\,(g) \rightarrow CaO\,(s) + SO_2(g) + CO_2(g) \quad (6\text{-}1)$$

$$CaSO_4(s) + 4\,CO\,(g) \rightarrow CaS\,(s) + 4CO_2(g) \quad (6\text{-}2)$$

The results of the investigation regarding the effect of exposure time support the results of the different degrees of devolatilization from Chapter 5. The volatile gases from a fuel particle are released in high concentrations during a short period, while lower CO concentrations for longer time are released during char oxidation or devolatilization of large particles. Keeping the total amount of CO introduced constant, showed that 20 vol. % CO concentration introduced during 2 minutes (representing devolatilization) released a higher total SO_2 release compared to 5 vol. % CO concentration during 8 minutes (representing char combustion or devolatilization of large fuel particles). Thus, the CO concentration and the time of exposure are of high importance for SO_2 release.

An increase of SO_2 release was observed by varying the rotation speed of the rotary drum. The increase of the speed may improve the net contact time of the gas–solid, in other words, the residence time of the gas in the bed increases. Thereby, the $CaSO_4$ particles may be in more frequent contact with the reducing agent promoting the release of SO_2.

From the observations of the experiments and the literature review, it is suggested that the conversion of $CaSO_4$ can give CaS and CaO under reducing conditions and CaS is oxidized to CaO under oxidizing conditions, as illustrated in Figure 6-13. According to Robbins' reaction mechanism (Swift et al., 1976), the intermediate $CaO{\cdot}SO_2$ is responsible for producing either CaO (by reaction (6-6)) or CaS (by reaction (6-9) and (6-10)). Firstly, CaO may be produced but then $CaO{\cdot}SO_2$ can react with CO in excess forming directly CaS. The stability of this intermediate may be affected by the temperature, since the CaO, CaS or mixtures of both have been identified in different studies (Shen et al., 2008; Zheng et al., 2011). However, the products were not analyzed in the current study.

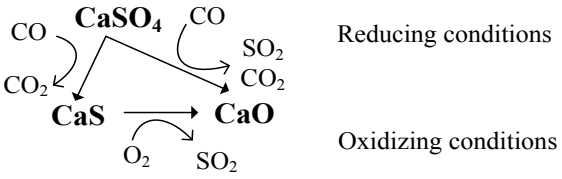

Figure 6-13: Scheme of the conversion paths of $CaSO_4$ under reducing and oxidizing conditions.

6.3.2 Methane

6.3.2.1 Effect of the Oxygen Content

The effect of different concentrations of methane at different oxygen content is investigated. Figure 6-14 shows the SO_2 concentration yielded by the introduction of CH_4 concentrations varying from 5 to 40 vol. % at 5 and 10 vol. % O_2 of the gas atmosphere and 900 °C.

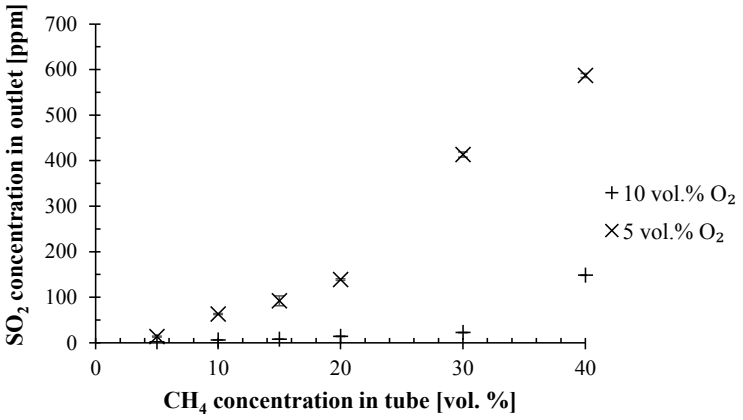

Figure 6-14: Effect of different CH_4 concentrations introduced under the bed material on SO_2 concentration with 5 and 10 vol. % O_2. Experimental conditions: flow tube 1NL/min, 900 °C, 5 % fill degree, 2 wt. % $CaSO_4$, 100 NL/min, 6 rpm.

At 5 vol. % O_2, the results at shows that 5 and 10 vol. % CH_4 yield a SO_2 concentrations below 100 ppm. When using 15 and 20 vol. % CH_4, the SO_2 concentration is between 100 and 200 ppm, and the introduction of 30 and 40 vol. % CH_4 yield a SO_2 concentrations above 400 ppm, which is the highest SO_2 release from the experiments performed with the single reducing agents. When the CH_4 concentration is increased from 20 to 30 vol. %, the measured SO_2 release increases more than the double.

At 10 vol. % O_2, the results show that the SO_2 release is lower than 50 ppm when CH_4 is introduced under the bed material up to a concentration of 30 vol. %. It can be also seen that when 40 vol. % CH_4 is introduced under the bed material, a big increase on the SO_2 concentration is observed but the SO_2 concentration is in a similar level when 30 vol. % CH_4 is introduced at 5 vol. % O_2. The corresponding CO_2 concentrations measured in the flue gas for each experiment are plotted in Figure C-6 of Appendix C.

6.3.2.2 Effect of the Temperature

The results of SO_2 release of the experiments performed at 1000 °C are shown in Figure 6-15. The SO_2 release increases with increasing temperature and is more than doubled when the applied CH_4 is doubled. The measured CO_2 concentration for each experiment is plotted in Figure C-7 of Appendix C.

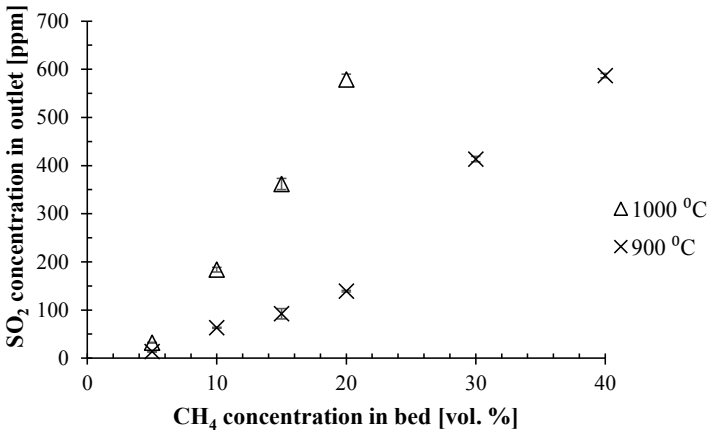

Figure 6-15: Effect of different CH_4 concentrations introduced under the bed material on SO_2 concentration at 900 and 1000 °C. Experimental conditions: flow tube 1 NL/min, 5 % fill degree, 2 wt. % $CaSO_4$, 100 NL/min with 5 vol. % O_2, 6 rpm.

6.3.2.3 Effect of the Exposure Time

The time of exposure is also investigated using CH_4 as a reducing agent. A total of 0.4 L of CH_4 is introduced under the bed material with CH_4 concentrations varying from 5 to 20 vol. %. These experiments are performed with an oxygen content of 5 vol. % and both at 900 and 1000 °C. Figure 6-16 and Figure 6-17 show the SO_2 concentrations obtained with identical total amount of CH_4 is introduced under the bed material by different CH_4 concentrations at 900 and 1000 °C, respectively. The corresponding CO_2 concentrations for each experiment at 900 and 1000 °C, are shown in Figure C-8 and Figure C-9 in Appendix C, respectively.

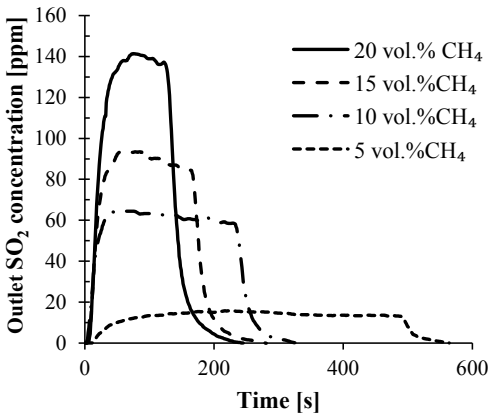

Figure 6-16: SO_2 concentrations when a total of 0.4 L CH_4 is introduced under the bed material with 5, 10, 15 and 20 vol. % CH_4 at 900 °C. Experimental conditions: flow tube 1NL/min, 5 % fill degree, 2 wt. % $CaSO_4$, 100 NL/min with 5 vol. % O_2, 6 rpm.

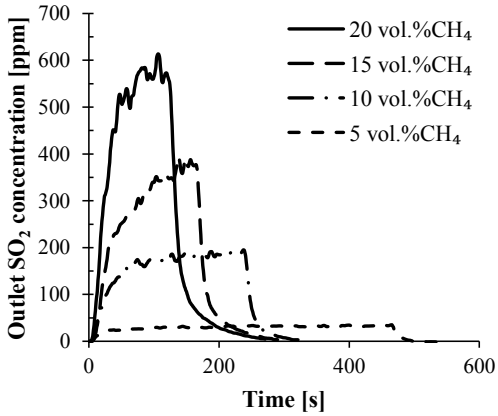

Figure 6-17: SO_2 concentrations when a total of 0.4 L CH_4 is introduced under the bed material with 5, 10, 15 and 20 vol. % CH_4 at 1000 °C. Experimental conditions: flow tube 1NL/min, 5 % fill degree, 2 wt. % $CaSO_4$, 100 NL/min with 5 vol. % O_2, 6 rpm.

Figure 6-18 illustrates the total SO_2 release of the experiments shown in Figure 6-16 and in Figure 6-17 for the different CH_4 concentrations at 900 and 1000 °C. The total SO_2 release increases almost linearly with increasing CH_4 concentration at 1000 °C. On the other hand, at 900 °C the total SO_2 release increases when the CH_4 concentration is increased from 5 to 10 vol. % and for higher concentrations the total SO_2 release remains around the same level.

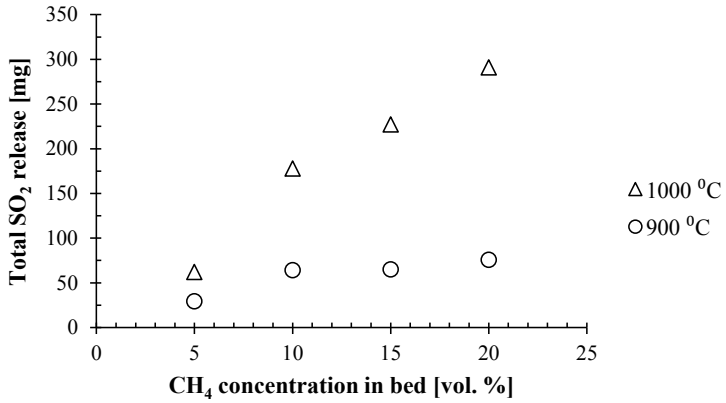

Figure 6-18: Total SO_2 release from the raw material when a total of 0.4 L of CH_4 is introduced under the bed material with different CH_4 concentrations at 900 and 1000 °C. Experimental conditions: flow tube 1 NL/min, 5 % fill degree, 2 wt. % $CaSO_4$, 100 NL/min with 5 vol. % O_2 in the freeboard gas, 6 rpm.

6.3.2.4 Discussion

In the literature, the decomposition of $CaSO_4$ has been studied using pure CH_4. In good agreement with Song et al. (2008), the reaction rate of CH_4 increases with increasing temperature. However, it is not possible to compare the effect of CH_4 concentration and the effect of oxygen content on sulfur release with previous studies. The SO_2 release increases with increasing CH_4 concentration, which is the same trend as with introducing CO. The partial pressure of CH_4 increases when higher concentrations of CH_4 are introduced and this may have a positive effect on the reaction rate of the reactions (6-14) and (6-15).

$$CaSO_4(s) + CH_4(g) \rightarrow CaS\,(s) + CO_2(g) + 2H_2O\,(g) \quad (6\text{-}14)$$

$$4CaSO_4(s) + CH_4(g) \rightarrow 4CaO\,(s) + CO_2(g) + 4SO_2(g) + 2H_2O\,(g) \quad (6\text{-}15)$$

CaS was the main product together with small amounts of CaO when using 100 % CH_4 (Song et al., 2008), but it may be that lower CH_4 concentrations will result in a mixture of CaO and CaS, instead of mainly CaS. The same discussion about concentration and oxygen, when CO was introduced, may also be valid for CH_4 since the same tendencies are observed.

Song et al. (2009) conducted their investigations in a fixed bed reactor and stated that SO_2 formation is mainly due to solid-solid reaction (6-3) due to a good contact between CaS and $CaSO_4$ (Song et al., 2009). However, a solid-solid reaction is normally quite slow and in a fixed bed reactor there is no mixing enhancing the contact. For that reason, it is not viable that the main SO_2 formation is via reaction (6-3). Therefore, the SO_2 formation may be mainly due to the formation and oxidation of CaS in contact with the freeboard atmosphere.

$$CaS(s) + 3CaSO_4(s) \rightarrow 4CaO(s) + 4SO_2(g) \quad (6\text{-}3)$$

Formation of H_2S was not observed by Song et al. (2009), and in the high rotary drum is not possible to analyze this compound. However, the oxidation of H_2S to SO_2 would be favored in the rotary drum due to the presence of oxygen and high temperature, but it is still not possible to determine if reaction (6-16) occurred.

$$CaSO_4(s) + CH_4(g) \rightarrow CaO(s) + CO_2(g) + H_2S(g) + 3H_2O(g) \quad (6\text{-}16)$$

For each experiment of CH_4, the percentage of SO_2 release relative to the CH_4 introduced was calculated in the same way as for CO. The percentage of CH_4 reacted may be even smaller if other reactions take place in parallel. Table 6-2 summaries the SO_2/CH_4 percentage for the different CH_4 concentrations, varying the temperature and the O_2 concentration. The results show that a maximum of almost 30 % of CH_4 reacted to form SO_2. Methane in comparison with CO reacts less to form SO_2. The percentage of CH_4 reacted, which follows the same tendency observed in Table 6-1, increases with increasing injected CH_4 concentration, temperature and decreasing oxygen concentration.

Table 6-2: Percentage of SO_2 release relative to CH_4 injected for different CH_4 concentrations varying temperature and O_2 content.

CH_4 conc. [vol. %]	**SO_2/CH_4 ratio [%]:**		
	900 °C, 5 vol. % O_2	900 °C, 10 vol. % O_2	1000 °C, 5 vol. % O_2
5	2.75	0.43	6.49
10	6.38	0.62	18.6
15	6.21	0.54	24.4
20	7.02	0.71	29.2
30	13.9	0.76	-
40	14.8	3.75	-

6.3.3 Hydrogen

The effect of different concentrations of H_2, from 5 to 40 vol. %, on SO_2 release has been investigated at 900 °C and 5 vol. % O_2, as illustrated in Figure 6-19.

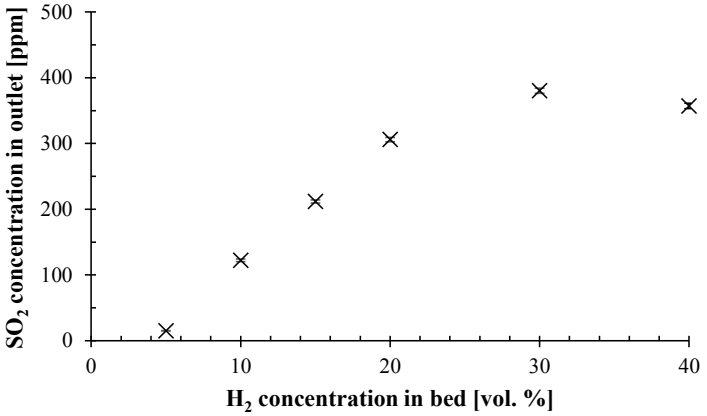

Figure 6-19: Effect of different H_2 concentrations introduced under the bed material on SO_2 concentration. Experimental conditions: flow tube 1 NL/min, 900 °C, 5 % fill degree, 2 wt. % $CaSO_4$, 100 NL/min with 5 vol. % O_2 in the freeboard, 6 rpm.

The results show that SO_2 concentration increases with increasing H_2 concentration, except from 30 to 40 vol. % H_2 where the SO_2 concentration decreases. The SO_2 concentrations measured are higher than the ones obtained using CO with the same concentration of reducing agent.

6.3.3.1 Effect of the Oxygen Content

In a similar experimental series with an oxygen concentration of 10 vol. %, SO_2 release is only observed from 15 vol. % to 30 vol. % H_2, as shown in Figure 6-20. Higher concentrations than of 30 vol. % H_2 are not tested. During the experiments where 5 and 10 vol. % H_2 are introduced under the bed material, no SO_2 is measured and it is observed that the oxygen concentration decreased slightly, meaning that the H_2 is combusted. Comparing Figure 6-19 and Figure 6-20, the SO_2 release has decreased more than half when the oxygen concentration has doubled.

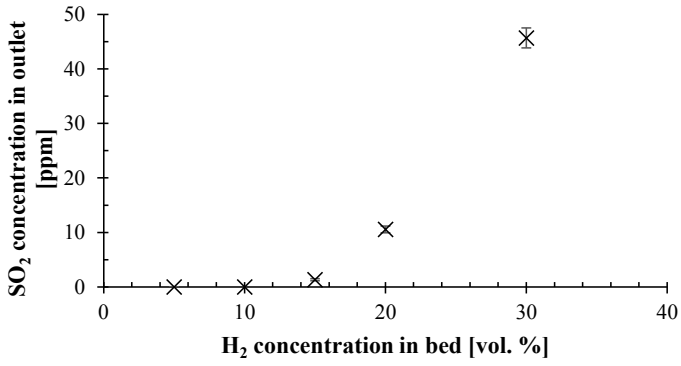

Figure 6-20: Effect of different H_2 concentrations introduced under the bed material on SO_2 concentration with 10 vol. % O_2. Experimental conditions: flow tube 1 NL/min, 900 °C, 5 % fill degree, 2 wt. % $CaSO_4$, 100 NL/min, 6 rpm.

6.3.3.2 Effect of the Temperature

Figure 6-21 compares the SO_2 concentration measured for the different applied H_2 concentration at temperatures of 900 and 1000 °C. The sulfur release decreases with increasing temperature, which is not the same trend as observed when introducing CO and CH_4.

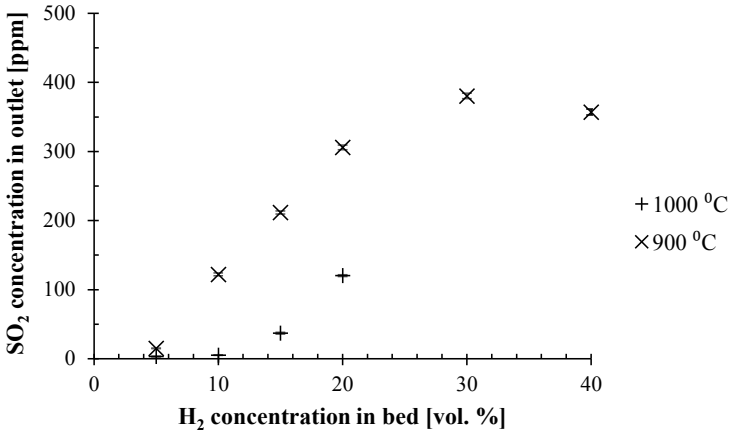

Figure 6-21: Effect of different H_2 concentrations introduced under the bed material on SO_2 concentration at 900 and 1000 °C. Experimental conditions: flow tube 1 NL/min, 5 vol. % O_2, 5 % fill degree, 2 wt. % $CaSO_4$, 100 NL/min, 6 rpm.

In Chapter 3, it is mentioned that the hydrogen content released during pyrolysis of biomass increases as the temperature rises (Wu et al., 2009) but on the other hand less SO_2 is released when increasing temperature, even at high H_2 concentrations.

6.3.3.3 Effect of the Exposure Time

The time of exposure is also investigated using H_2 as a reducing agent. At the same conditions as CO and CH_4, a total of 0.4 L of H_2 is introduced under the bed material with a H_2 concentration varying from 5 to 20 vol. %, at 5 vol. % O_2 and at temperatures of 900 and 1000 °C. The results at 900 and 1000 °C are shown in Figure 6-22 and in Figure 6-23, respectively. The results shows that the SO_2 release at 1000 °C is lower than for at 900 °C for the same applied H_2 concentration, as also showed in Figure 6-21.

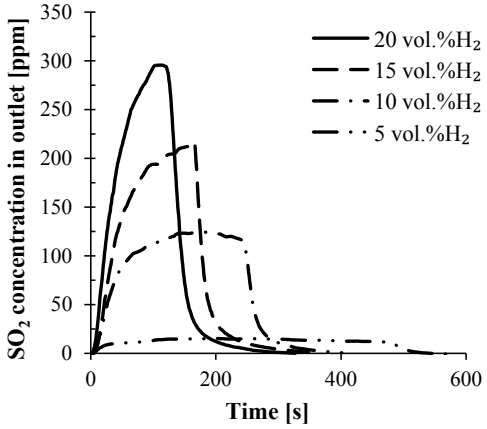

Figure 6-22: SO_2 concentrations when a total of 0.4 L of H_2 is introduced under the bed material with 5, 10, 15 and 20 vol. % H_2 at 900 °C. Experimental conditions: flow tube 1 NL/min, 5 % fill degree, 2 wt. % $CaSO_4$, 100 NL/min with 5 vol. % O_2, 6 rpm.

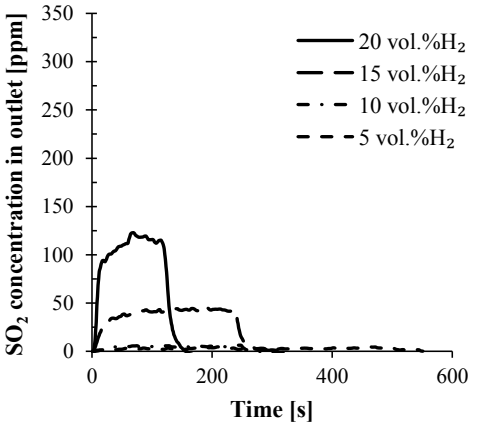

Figure 6-23: SO_2 concentrations when a total of 0.4 L of H_2 is introduced under the bed material with 5, 10, 15 and 20 vol. % H_2 at 1000 °C. Experimental conditions: flow tube 1 NL/min, 5 % fill degree, 2 wt. % $CaSO_4$, 100 NL/min with 5 vol. % O_2, 6 rpm.

Figure 6-24 summarizes the total sulfur release for each H_2 concentration at both temperatures. There is a big increase in the total SO_2 release from 5 to 10 vol. % H_2 at 900 °C and the total SO_2 release is lower for all H_2 concentrations at 1000 °C compared to 900 °C. Short pulses with a high concentration yield higher SO_2 release than long pulses with low concentrations.

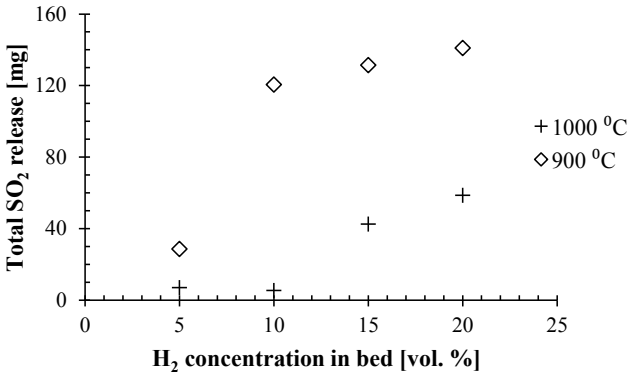

Figure 6-24: Total SO_2 release from the raw material when a total of 0.4 L of H_2 is introduced under the bed material with different H_2 concentrations at 900 °C and 1000 °C. Experimental conditions: flow tube 1 NL/min, 5 % fill degree, 2 wt. % $CaSO_4$, 100 NL/min with 5 vol. % O_2, 6 rpm.

6.3.3.4 Equilibrium Phase Diagrams

The results obtained using H_2 at 900 ºC and 5 vol. % O_2 are used to evaluate the stable phase of the equilibrium phase diagrams for the SO_2-CaO-$CaSO_4$-CaS-H_2-H_2O system. In the same way as for CO, H_2 is introduced in the bed and by reaction with $CaSO_4$ forms H_2O and SO_2.

Since there are competing reactions and it cannot be distinguished which reactions take place, the experimental reducing potentials, P_{H2}/P_{H2O}, for the equilibrium phase diagram are calculated considering two different approached: [1)] assuming that H_2 reacts with $CaSO_4$ only according to reaction (6-11), and [2)] H_2 reacts only according to reaction (6-12).

$$CaSO_4(s) + 4H_2(g) \rightarrow CaS\ (s) + 4H_2O\ (g) \quad (6\text{-}11)$$

$$CaSO_4(s) + H_2(g) \rightarrow CaO\ (s) + SO_2(g) + H_2O\ (g) \quad (6\text{-}12)$$

For the first case, CaS is subsequently oxidized by reaction (6-17).

$$CaS\ (s) + \frac{3}{2}\ O_2\ (g) \rightarrow CaO\ (s) + SO_2(g) \quad (6\text{-}17)$$

The partial pressure of H_2O and H_2 for the reaction (6-11) can be calculated according to equation 6.6 and equation 6.7, respectively. The reducing potential is therefore expressed mathematically by equation 6.8.

$$P_{H_2O,\text{react}} = 4 \cdot P_{SO_2,out} \quad [6.6]$$

$$P_{H_2\ react} = P_{H_2,in} - 4 \cdot P_{SO_2,\text{out}} \quad [6.7]$$

$$\frac{P_{H_2}}{P_{H_2O}} = \frac{P_{H_2,in} - 4 \cdot P_{SO_2,\text{out}}}{4 \cdot P_{SO_2,\text{out}}} \quad [6.8]$$

For the second scenario, the reducing potential is defined by equation 6.9.

$$\frac{P_{H_2}}{P_{H_2O}} = \frac{P_{H_2,in} - P_{SO_2,\text{out}}}{P_{SO_2,\text{out}}} \quad [6.9]$$

The reducing potentials at equilibrium are calculated for each experiment considering either reaction (6-11) or reaction (6-12), respectively. The corresponding results are shown in Figure 6-25 and Figure 6-26, respectively. The experimental points are in the stable area of CaS for all H_2 concentrations, in the same way as the results with CO. Comparing Figure 6-25 and Figure 6-26, the reducing potentials are slightly lower for case 1, when assuming that H_2 reacts with $CaSO_4$ forming CaS.

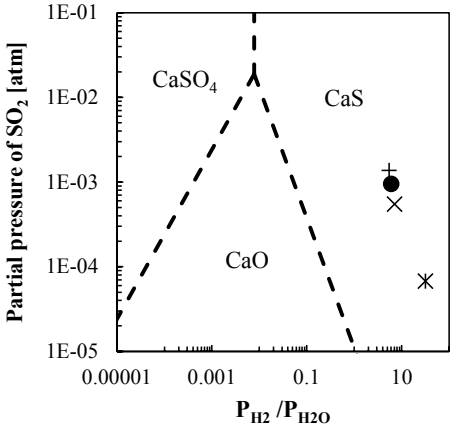

Figure 6-25 Phase diagram for the SO_2-CaO-$CaSO_4$-CaS-H_2-H_2O system at 900 °C and 5 vol. % O_2. Considering case 1, the experimental data obtained in the pilot plant setup introducing different H_2 concentrations under the bed material is used to show the stable phase in each case.

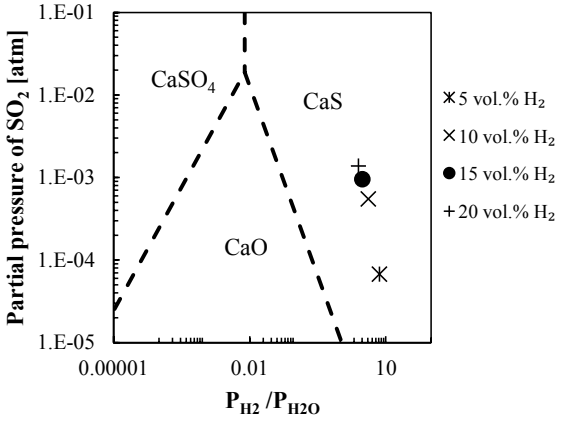

Figure 6-26: Phase diagram for the SO_2-CaO-$CaSO_4$-CaS-H_2-H_2O system at 900 °C and 5 vol. % O_2. Considering case 2, the experimental data obtained in the pilot plant setup introducing different H_2 concentrations under the bed material is used to show the stable phase in each case.

6.3.3.5 Discussion

The results obtained introducing H_2 under the bed showed that the SO_2 release increases with increasing H_2 concentration. In the literature it is mentioned that reaction (6-11) is favored at reducing potentials (P_{H2}/P_{H2O}) between 10^3 and 10^2 within the temperature 600-950 °C, while reactions (6-12) and (6-13) are favored at lower reducing potentials (Xiao and Song, 2011; Kim and Sohn, 2002; Shen et al., 2008). On the other hand, according to the equilibrium phase diagrams, the stable phase under the experimental conditions is CaS, which is formed by reaction (6-11) and the subsequent oxidation releases SO_2.

$$CaSO_4(s) + 4H_2(g) \rightarrow CaS(s) + 4H_2O(g) \quad (6\text{-}11)$$

$$CaSO_4(s) + H_2(g) \rightarrow CaO(s) + SO_2(g) + H_2O(g) \quad (6\text{-}12)$$

$$CaSO_4(s) + 4H_2(g) \rightarrow CaO(s) + H_2S(g) + 3H_2O(g) \quad (6\text{-}13)$$

The formation of H_2S via reaction (6-13) may take place, but cannot be detected by the analyzers and the H_2S may interact with SO_2. However, in an excess of oxygen and at high temperature H_2S will oxidize rapidly to SO_2 (Montoya et al., 2005).

The experiments investigating the effect of the temperature showed that less SO_2 was released at 1000 ºC in comparison with the same experiments performed at 900 ºC. This is contradictory to the observations of Shen et al. (2008), who stated that the rate of reduction of $CaSO_4$ with H_2 increases remarkably with the temperature (Shen et al., 2008). However, this study only investigated the rate of $CaSO_4$ reduction with 5 vol. % H_2 and 95

vol. % N_2 in the temperature range 870- 970 °C in a TGA. Therefore, it could be that at temperatures above 970 °C, the rate of $CaSO_4$ reduction decreases. However, no plausible explanation may be offered based on the present investigations.

The percentage of SO_2 release relative to the H_2 introduced has been calculated as previously described with the other reducing agents. Table 6-3 summaries the SO_2/H_2 percentage for the different H_2 concentrations, varying the temperature and the O_2 concentration. The maximum percentage of H_2 reacted is 15 % at 900 °C and 20 vol. % H_2. In agreement with the graphs, the SO_2 release relative to H_2 injected is below 2 % for the tested H_2 concentrations and decreases when the temperature is increased to 1000 °C.

Table 6-3: Percentage of SO_2 release relative to H_2 injected for different H_2 concentrations varying temperature and O_2 content.

H_2 conc. [vol. %]	**SO_2/H_2 ratio [%]**		
	900 °C, 5 vol. % O_2	900 °C, 10 vol. % O_2	1000 °C, 5 vol. % O_2
5	3.03	0.00	0.67
10	12.34	0.00	0.52
15	14.26	0.09	2.49
20	15.46	0.53	6.08
30	12.8	1.54	-
40	9.02	-	-

6.3.4 Carbon Monoxide, Hydrogen, and Methane Comparison

6.3.4.1 Effect of the Concentrations

In the previous section, the effect of the reducing agents on SO_2 release is discussed individually. Comparing the three reducing gases together, the total SO_2 release when a total of 0.4 L of either CO, H_2 or CH_4 using different concentrations is introduced under the bed material at 900 °C and 5 vol. % O_2 is plotted in Figure 6-27. Using the same concentration of reducing agent during the same time, it can be seen that the total SO_2 release is different. The total SO_2 release is around the same level for 5 vol. % CH_4 and 5 vol. % H_2 and a bit lower for 5 vol. %. CO. Increasing reducing agent concentration to 10 vol. %, the total SO_2 release yielded by CH_4 and CO is similar and much higher for H_2. At higher reducing agent concentrations, the total SO_2 release is higher when using CO and H_2 and is almost double the total SO_2 for CH_4. So, the introduction of high concentrations of CO and H_2 during a short time leads to high SO_2 release in comparison with the introduction of low concentration of reducing agents for a long time for all these reducing agents.

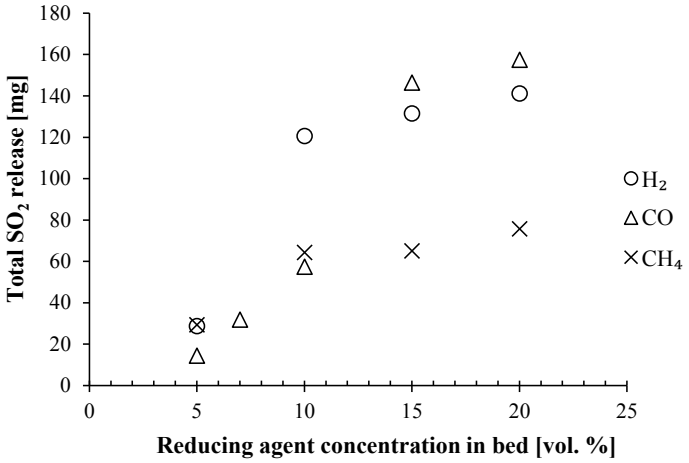

Figure 6-27: Total SO_2 release from the raw material when a total of 0.4 L of reducing agent is introduced under the bed material with different concentrations of CO, H_2 and CH_4 . Experimental conditions: flow tube 1 NL/min, 900 °C, 5 % fill degree, 2 wt. % $CaSO_4$, 100 NL/min with 5 vol. % O_2, 6 rpm.

6.3.4.2 Effect of Heat of Combustion

The reducing agents used are having different heat of combustion. Reactions (6-18), (6-19) and (6-20) show the combustion reaction and the corresponding heat of combustion. It can be seen that 1 mol of CH_4 gives more than the triple energy than combusting 1 mol of CO or H_2. Therefore, it is desired to investigate how sulfur release is affected by the reducing gases when the same heat of combustion is introduced.

$$CH_4(g) + 2\,O_2(g) \rightarrow CO_2(g) + 2H_2O(g) \qquad \Delta H_c = \text{-890 kJ/mol} \qquad (6\text{-}18)$$

$$CO(g) + \tfrac{1}{2}\,O_2(g) \rightarrow CO_2(g) \qquad \Delta H_c = \text{-283 kJ/mol} \qquad (6\text{-}19)$$

$$H_2(g) + \tfrac{1}{2}\,O_2(g) \rightarrow H_2O(g) \qquad \Delta H_c = \text{-286 kJ/mol} \qquad (6\text{-}20)$$

Experiments introducing 20 vol. % CO, 18 vol. % CH_4, and 6 vol. % H_2 under the bed material have been performed supplying the energy 0.039 kJ/s and the SO_2 release from these experiments are shown in Figure 6-28. It can be seen proving the same energy, CO gives most sulfur release, 325 ppm, followed by H_2 where the SO_2 release is 120 ppm and the SO_2 release by the injection of CH_4 is around 15 ppm SO_2.

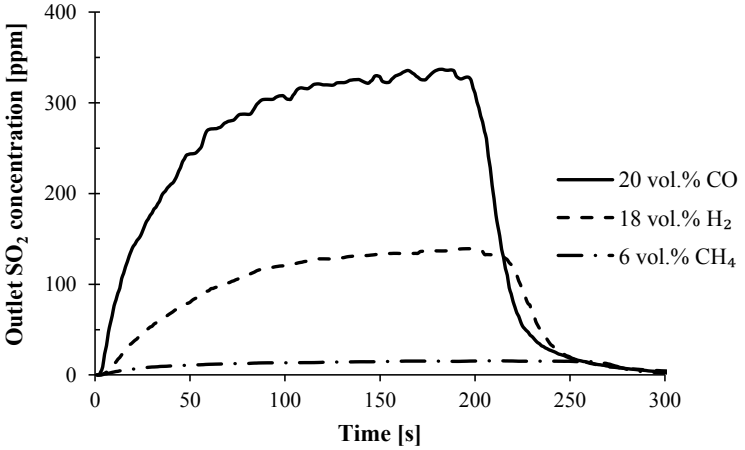

Figure 6-28: SO_2 concentrations when 0.039 kJ/s is provided by CO, H_2 and CH_4 under the bed material. Experimental conditions: flow tube 1NL/min, 5 % fill degree, 900 °C, 2 wt. % $CaSO_4$, 100 NL/min with 5 vol. % O_2, 6 rpm

6.3.5 Binary Mixtures

The volatiles gas released during devolatilization of a solid fuel consist of many different gases and the reducing gases are not released only as a single component. The behavior of binary mixtures of CO, CH_4 and H_2 on sulfur release has been investigated.

The binary mixtures with different concentrations of CO, from 0 to 20 vol. %, combined with H_2 and CH_4 in 80 vol. % N_2 have been investigated at the same conditions as in the previous section. The average steady state SO_2 concentration for the different mixture combinations are shown in Figure 6-29. The SO_2 release increases with decreasing CO content in the mixture CO/H_2 but the concentrations are lower than using only 20 vol. % CO or 20 vol. % H_2. For the CO/CH_4 mixture, the highest and the lowest SO_2 concentration are obtained applying 20 vol. % CO in N_2 and 20 vol. % CH_4 in N_2, respectively. The SO_2 concentration increases with increasing CO concentration in the mixture and with decreasing CH_4 concentration. However, the increase is not significant between the intermediate mixtures.

In Appendix C, the average CO_2 concentration profiles for each experiment for both CO/H_2 and CO/CH_4 mixtures are plotted in Figure C-10. The tendency observed is that the CO_2 concentration increases with increasing injected CO concentration.

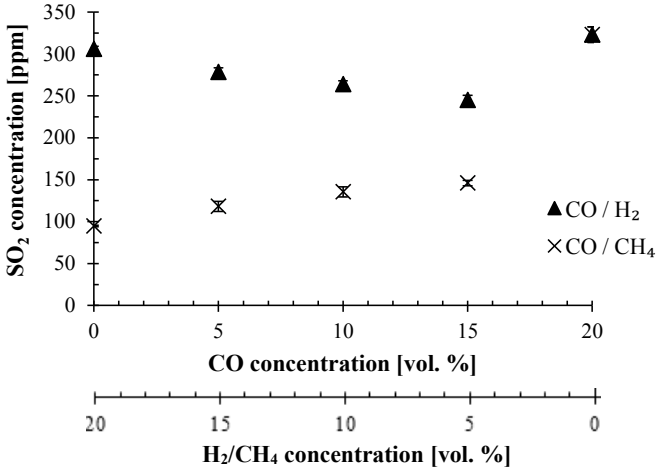

Figure 6-29: SO_2 concentrations when mixtures of CO/H_2 and CO/CH_4 are introduced under the bed material at 900 °C. Experimental conditions: flow tube 1 NL/min, 5 % fill degree, 2 wt. % $CaSO_4$, 100 NL/min with 5 vol. % O_2, 6 rpm.

Binary mixtures of different concentrations of CH_4, from 0 to 20 vol. %, combined with H_2 in 80 vol. % N_2 are also investigated. Figure 6-30 shows the average SO_2 concentrations released for the mixtures containing CH_4. For the CH_4/H_2 mixture, the highest and the lowest SO_2 release concentration are obtained applying 20 vol. % H_2 in N_2 and 20 vol. % CH_4 in N_2, respectively. However, the SO_2 release is similar for the three mixtures containing 15, 10 and 5 vol. % CH_4 and 5, 10 and 15 vol. % H_2, respectively. The differences in the SO_2 levels between the three intermediate mixtures are so small that no clear tendency can be concluded. Therefore, the SO_2 release does not vary significantly with changing the concentration of CH_4/H_2 mixture.

The measured CO_2 concentrations from the binary mixtures containing CH_4 are plotted in Figure C-11 in Appendix C.

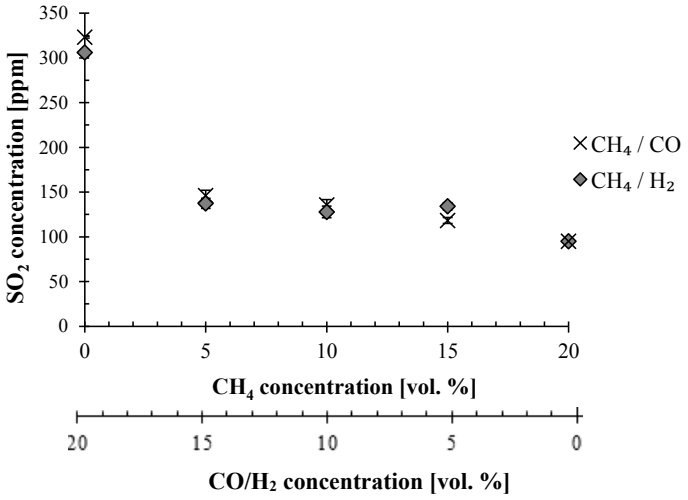

Figure 6-30: SO_2 concentrations when mixtures of CH_4/CO and CH_4/H_2 are introduced under the bed material at 900 °C. Experimental conditions: flow tube 1 NL/min, 5 % fill degree, 2 wt. % $CaSO_4$, 100 NL/min with 5 vol. % O_2, 6 rpm.

From the previous results, SO_2 concentrations from the binary mixtures containing H_2 are plotted in Figure 6-31. The SO_2 release increases with increasing H_2 concentration when it is mixed with CO, while the SO_2 concentration is similar for different mixtures of H_2 and CH_4.

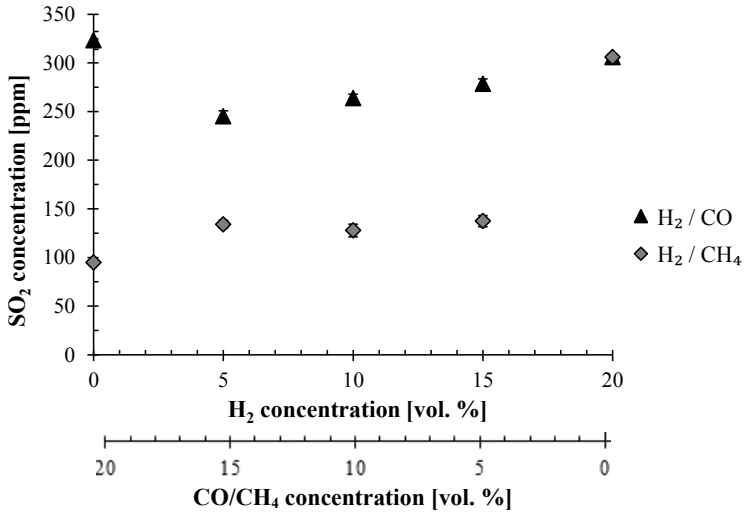

Figure 6-31: SO_2 concentrations when mixtures of H_2/CO and H_2/CH_4 are introduced under the bed material at 900 °C. Experimental conditions: flow tube 1 NL/min, 5 % fill degree, 2 wt. % $CaSO_4$, 100 NL/min with 5 vol. % O_2, 6 rpm.

6.3.6 Thermal Decomposition of $CaSO_4$

During and in between all the experiments, decomposition of $CaSO_4$ is taking place due to the high operational temperature of the rotary drum. Table 6-4 summarizes the intervals of the SO_2 concentration measured in the analyzers when no reducing gas is introduced at different conditions. The thermal decomposition increases with temperature and decreases with increasing oxygen concentration. The most influencing parameter is the temperature followed by the oxygen content. The rotational speed has a very little influence and the variation is only 1 to 3 ppm, which is insignificant compared to the other parameters.

Table 6-4: SO_2 concentration from thermal decomposition changing temperature, O_2 concentration and rotational speed. Note: [A] Experiments performed at 5 vol. % O_2 and 6 rpm, [B] Experiments performed at 900 °C and 6 rpm, [C] Experiments performed at 5 vol. % O_2 and 900 °C.

	Temperature [A] [°C]		**O_2 conc. [B] [vol. %]**		**Rotational speed [C] [rpm]**			
	900	1000	5	10	4	6	10	20
SO_2 conc. [ppm]	50-40	100-130	50-40	20-30	46	45	46	48

The SO_2 concentration from the thermal decomposition has been subtracted in the previous results shown. However, this concentration contributes significant when the sulfur release by reducing agent is low at higher temperatures.

6.4 Conclusions

Investigations and kinetic studies of reductive decomposition of $CaSO_4$ by CO, and to less extent H_2 and CH_4 in relation to chemical-looping combustion have reported that CaO, CaS or mixtures of both products are favored, depending on the temperature and the concentration of the reducing gas. The most influencing parameter to the reaction rate of $CaSO_4$ reduction is the partial pressure of the gaseous reductive agent.

The high temperature rotary drum has been modified in order to introduce reducing gases under the bed material. The effect of different concentrations of CO, H_2, and CH_4 on sulfur release has been experimentally investigated modifying temperature, oxygen content and time of exposure.

Introducing the same total amount with different concentrations has a significant influence. Short pulses with high reducing gas concentrations of reducing as yielded higher concentrations of SO_2 and higher total SO_2 release than long pulses with low reducing gas concentrations.

The experiments using different concentrations of reducing agent, especially CO, indicated that a threshold concentration, below which SO_2 release does not occur, exists.

The SO_2 release increased significantly with increasing temperature, except when H_2 was injected under the bed material. Here the SO_2 release was lower at 1000 ºC than at 900 ºC.

The percentage of reducing agent that reacted was calculated for each experiment. For CO and CH_4, the SO_2/CO increases with increasing injected concentration of CO or CH_4, temperature and decreasing oxygen concentration. The maximum percentage reached was nearly 30 % when 20 vol. % CH_4 was introduced at 1000 ºC and 5 vol. % O_2. For H_2, the SO_2 release relative to H_2 injected is below 2 % for the tested H_2 concentrations and decreases when the temperature is increased from 900 to 1000 ºC.

Comparing the total SO_2 release using the same concentrations for the three reducing agents, the highest total SO_2 release was obtained using CO at higher concentrations that 10 vol. %, followed by H_2, while at low concentrations CH_4 and H_2 seem to give higher total SO_2 release than CO. When the same heat of combustion is introduced, the sulfur release is higher using CO and followed by H_2 and CH_4.

The equilibrium phase diagrams for CO and H_2 were used to evaluate the stable phase using the experimental results and with both reducing agents, CaS was indicated to be the stable phase for the different concentrations.

The experimental results of binary mixtures when CO was present showed that SO_2 increases with increasing CO concentration in the mixture. Similar SO_2 release was obtained for the different mixtures of CH_4 and H_2.

6.5 References

Diaz-Bossio, L. M., Squier, S. E., and Pulsifer, A. H.; Reductive decomposition of calcium sulfate utilizing carbon monoxide and hydrogen. Chemical Engineering Science, 40, 319-24, 1985.

Hansen, P. F. B.; Sulphur Capture in Fluidized Bed Combusters, Ph.D. thesis. Technical University of Denmark. 1991. ISBN: 87-983894-2-4.

Hansen, P. F. B., Johansen, K. Dam, and Østergaard, K.; High-temperature reaction between sulfur dioxide and limestone. V. the effect of periodically changing oxidizing and reducing conditions. Chemical Engineering Science, 48, 1325-41, 1993.

Dam-Johansen, K., and Østergaard, K.; High-temperature reaction between sulfur dioxide and limestone - II. an improved experimental basis for a mathematical model. Chemical Engineering Science, 46, 839-45, 1991.

Kim, B., and Sohn, H. Y.; A novel cyclic reaction system involving CaS and $CaSO_4$ for converting sulfur dioxide to elemental sulfur without generating secondary pollutants. 3. Kinetics of the hydrogen reduction of the calcium sulfate powder to calcium sulfide. Industrial & Engineering Chemistry Research, 41, 3092-6, 2002.

Kuusik, R., Sikkonen, P., and Niinistö, L.; Thermal decomposition of calcium sulfate in carbon monoxide. Journal of Thermal Analysis, 30, 187-193, 1985.

Hayhurst, N. and Tucker, R.F.; The reductive regeneration of sulphated limestone for flue gas desulphurization: X-ray diffraction studies. Journal of the institute of Energy, 65, 166-176, 1992.

Montoya, A., Sendt, K., and Haynes, B.R.; Gas phase interaction of H_2S with O_2: A kinetic and Quantum Chemistry Study of the Potential Energy Surface. Journal of Physical Chemistry A, 109, 1057-1062, 2005.

Nielsen, A. R.; Combustion of large solid fuels in cement rotary kilns. Ph.D. thesis, Technical University of Denmark, Department of Chemical and Biochemical Engineering, 2012. ISBN: 978-87-92481-66-5.

Oh, J. S., and Wheelock, T. D.; Reductive decomposition of calcium-sulfate with carbon-monoxide - reaction-mechanism. Industrial & Engineering Chemistry Research, 29, 544-50, 1990.

Okumura, S., Mihara, N., Kamiya, K., Ozawa, S., Onyango, MS, Kojima, Y., and Matsuda, H.; Recovery of CaO by reductive decomposition of spent gypsum in a CO-CO_2-N_2 atmosphere. Industrial & Engineering Chemistry Research, 42, 6046-52, 2003.

Shen, L., Zheng, M., Xiao, J., and Xiao, R.; A mechanistic investigation of a calcium-based oxygen carrier for chemical looping combustion. Combustion and Flame, 154, 489-506, 2008.

Song, Q., Xiao, R., Deng, Z., Zhang, H., Shen, L., Xiao, J., and Zhang, M.; Chemical-looping combustion of methane with $CaSO_4$ oxygen carrier in a fixed bed reactor. Energy Conversion and Management, 49, 3178-87, 2008.

Song, Q., Xiao, R., Deng, Z., Zhang, M.; Reactivity of a $CaSO_4$-oxygen carrier in chemical –looping combustion of methane in a fixed bed reaction, Korean. Journal of Chemical Engineering. 26, 2, 592-602, 2009.

Swift, W.M., Panec, A.F., Smith, G.W., Vogel, G.J., and Jonke, A. A.; Decomposition of Calcium Sulphate. A Review of Literature. Argonne National Laboratory ANL-76-122. Chemical Engineering Divisions, 1976.

Talukdar, J., Basu, P., and Greenblatt, J. H.; Reduction of calcium sulfate in a coal-fired circulating fluidized bed furnace. Fuel, 75, 1115-23, 1996.

Tian, H., Guo, Q., and Chang, J.; Investigation into decomposition behavior of $CaSO_4$ in chemical-looping combustion. Energy Fuels, 22, 3915-21, 2008.

Tian, H., and Guo, Q.; Investigation into the behavior of reductive decomposition of calcium sulfate by carbon monoxide in chemical-looping combustion. Industrial & Engineering Chemistry Research, 48, 5624-32, 2009.

Wheelock, T.D. and Boyland, D.R.; Reductive decomposition of Gypsum by Carbon monoxide, Industrial and Engineering Chemistry Research, 52, 3, 215-218, 1960.

Wu, W., Chen, Y., Hu, L., and Luo, Y.; Isothermal pyrolysis of biomass by macro-TG. Power and Energy Engineering Conference, 2009. APPEEC 2009. Asia-Pacific, 2009.

Xiao, R., and Song, Q.; Characterization and kinetics of reduction of $CaSO_4$ with carbon monoxide for chemical-looping combustion. Combustion and Flame, 158, 2524-39, 2011.

Zheng, M., Shen, L., Feng, X., and Xiao, J.; Kinetic model for parallel reactions of $CaSO_4$ with CO in chemical-looping combustion. Industrial & Engineering Chemistry Research, 50, 5414-27, 2011.

7. Modeling the Sulfur Release in the Inlet of the Rotary Kiln

The rotary kiln is one of the key components, often referred to as the heart of the cement plant, in the cement industry for converting raw meal to cement clinker. It is the appropriate reactor for manufacturing cement clinker because it has the ability to provide a high temperature environment, appropriate residence time for the clinker reactions and ability to handle solids with a large size distribution. A variety of processes are taking place simultaneously in the rotary kilns, such as particulate mixing, gas-solid and solid phase reactions with intensive heat and mass transfer. The behavior of the rotary kiln is highly nonlinear and very difficult to analyze and control. Measurements are difficult to perform on industrial rotary kilns due to its size and inaccessible design, and theoretical models have been developed for simulating such processes.

This chapter focuses on modeling the sulfur release from the bed material due to combustion of alternative fuels in the inlet of the rotary kiln. First, a review of rotary kilns models for the cement industry is described. In sections 7.2, 7.3, and 7.4, the chosen model approach, the assumptions considered and the model development are explained. The results from the model considering wood as fuel varying different parameters and applying sensitivity analysis are shown and discussed in section 7.5.

7.1 Literature Study on Rotary Kiln Models for the Cement Industry

7.1.1 Review of Rotary Kilns Models

The rotary kiln models based on a reaction engineering approach are typically formulated as a counter-current plug flow reactor with two phases: solid and gas (Levenspiel, 1999). Different dynamic models for the behavior of a cement kiln have been developed and can vary from simple descriptive black box models (Sullivan et al., 1927) and one-dimensional models (Spang, 1972; Witsel et al., 2005; Locher, 2009; Sadighi et al., 2011) to more sophisticated physical three-dimensional models based on computational fluid dynamics, CFD, (Wang et al., 2006; Ma et al., 2006; Ranade and Mujumdar, 2006; Akhtar et al., 2008; Mujumdar and Ranade, 2008; Svedin et al., 2009).

Several modeling studies of the rotary kiln solid can be found in the literature, including models of particle transport and mixing (Ferron and Singh, 1991; Boateng and Barr, 1996a; Boateng, 2008; Mujumdar and Ranade, 2009), clinker reactions (Spang, 1972; Mastorakos et al., 1999; Mujumdar and Ranade, 2009), and heat transfer phenomena, focusing in radiation heat transfer (Barr et al., 1989; Boateng and Barr, 1996b; Dhanjal et al., 2004; Agustini et al., 2008). In one-dimensional models, the changes in the heat transfer and reaction kinetics for different bed heights are neglected, while the CFD models are limited in their ability to model the clinker chemistry, bed motion, and thermodynamics (Kaantee et al., 2004).

In order to overcome modelling limitations, coupled models, consisting of a one-dimensional model for simulation of the reactions in the bed region and a CFD model for the free board region, have been developed in the last decade (Mastorakos et al., 1999; Lu et al., 2004; Küssel et al., 2009). Advanced simulators programs have also been developed (Mujumdar et al., 2007; Stadler et al., 2011). For example, the Rotary Cement Kiln Simulator software is an integrated reaction engineering based mathematical model for clinker formation and was built by combining separate models for preheater, calciner, rotary kiln and cooler previously developed (Mujumdar et al., 2007).

7.1.2 Kiln System Models including Alternative Fuels Usage

The different combustion behavior of alternative fuels has promoted the development of new models for predicting the influence of alternative fuels in kiln system.

The initial rotary kilns models with alternative fuels were developed by the lime industry (Eriksson et al., 1991; Ivarsson and Svedin, 2007; Adams and Svedin, 2008; Svedin et al., 2009) investigating the effect of firing a range of biofuels on the lime kiln performance.

A one-dimensional mathematical model firing full scrap tires dropped into a dry long kiln has been developed (Darabi et al., 2008). The tire combustion model considered that tires were continuously fed into the kiln and absorbed heat through radiation. The different steps of combustion were also taken into account, considering that devolatilization was controlled by external heat transfer and chemical reaction kinetics and char combustion only by oxygen diffusion. This model was incorporated in a CFD cement kiln model, where the calcination process took place in the kiln and reached the calcination temperature in the middle of the kiln. The cement kiln model consisted of different sub-models, such as fluid flow, gas and coal combustion, radiation heat transfer, clinker formation, refractory heat transfer, and NO_x formation. The kiln simulation predicted the gas temperature, velocity and species concentration inside the kiln, the clinker temperature and composition along the kiln, and the refractory and shell temperatures. The simulation without tire combustion showed a high flame temperature, high NO_x emissions, and good quality product. Replacing 20 % of the total kiln heat with tires as fuel resulted in a reduced flame temperature, a 33 % reduction of NO_x emission and good clinker quality. The drop-in location of the tires was a critical factor in mid-kiln tire combustion. The simulation results showed that the drop-in location should be within the calcination zone so that the tire combustion can provide enough energy for the calcination reaction. Further downstream dropping of tires worsened the clinker quality and reduced the kiln efficiency.

The combustion of solid fuels, such as tire rubber and pine wood, fired directly into the material inlet of the industrial rotary kiln was modeled using a reaction engineering approach (Nielsen, 2012). The drying, devolatilization and char oxidations models were combined to estimate conversion times, oxygen consumption, and an approximate gas and bed temperature during fuel conversion. The models may be used

to estimate how far different fuel particles will be transported into the rotary kiln as a function of particle size and key process parameters. The individual models were validated in a pilot scale rotary drum, however validation of the combined models on an industrial plant was not performed due to the extreme environment and poor accessibility.

Rotary kiln flame models for combustion of alternative fuels through the kiln burner have also developed (Svedin et al., 2009; Haas and Weber, 2010; Nørskov, 2012) using different modeling approaches such as well-stirred reactor model (Haas and Weber, 2010) and as a plug flow reactor (Nørskov, 2012). Hass and Weber focused on the impact of firing RDF on the cement production. The axial dispersion of heat and mass transfer was considered to be controlled by the number of continuous stirred tank reactors (CSTR) in series and the effect of fuel calorific value and the adiabatic flame temperature was modeled as a well-stirred reactor model. Therefore, it is reasonable that the well-stirred reactor model provided very simplified predictions of the energy requirements for varying degrees of RDF substitution. The model did not to take into account recirculation and aerodynamics in the kiln and changes in flame heat transfer when substitution fuels occurred. The model calculations showed that with increasing RDF substitution the position of the flame maximum temperature moved downstream and its value decreased. The influence of changing process parameters were evaluated; i.e. decreasing RDF particle size, increasing the preheated combustion air temperature, using oxygen enrichment, and changing the fuel heating value.

A simplified one-dimensional rotary kiln flame model for combustion of alternative fuels, focusing on describing the flame temperature profile and the fuel combustion time was developed (Nørskov, 2012). The fuel conversion was based on heating, moisture evaporation, devolatilization and char oxidation while was in suspension. The fuel was heated by convection and radiation from the gas and hot kiln wall but the clinker bed was not included in the model. The model describing co-fired dried sewage sludge and petcoke was validated against experiments performed in a pilot-scale swirl-flow burner setup. Full-scale validation at an industrial cement kiln was not possible due to the inaccessibility of the combustion processes.

The clinker chemistry and thermodynamics in the rotary kiln and the effect of alternative fuels on full scale cement plant was modeled using the commercial software Aspen Plus® (Kaantee et al., 2004). The goal of this model was to be able to select a suitable alternative fuel, optimize process control and alternative fuel consumption, while maintaining the quality of the clinker product. The model divided the full process into segments and determined the effect of alternative fuels on material flows, emissions, and product quality. The calculations for the alternative fuels (meat and bone meal and sewage sludge) were compared to a reference case, where petcoke was used as primary and secondary fuel. Higher amount of air and higher speed of kiln fans were needed during operation with larger amounts of alternative fuels in order to maintain the product quality.

Other models considering solid waste for other usages of rotary kilns, such as rotary kilns incinerators and iron ore reduction process, have been developed (Silcox and Pershing, 1990; Pershing et al., 1993; Ramakrishnan and Sai, 1999; Yang et al., 2004). However, due to the differences of the design and operational system the models cannot be compared with rotary kilns models for the cement industry.

In conclusion, combustion models for alternative fuels in the kiln have been developed in order to evaluate the effect of fuel characteristics, such particle size, process variables, such oxygen content, and clinker quality. However, a model which is able to predict sulfur release when alternative fuels are in contact with the kiln bed material has not been described in the literature.

7.2 System Description and Modeling approach

The aim of the model is to predict sulfur release caused by volatiles from alternative fuels particles fired in the material kiln inlet. The modeling approach of this system consist of modeling the bed material as continuous stirred tank reactors in series where the alternative fuels particles, the volatile gases, and the bed material are well mixed.

In section 7.1, it has been described that well stirred reactors in series are considered for modeling the heat and mass transfer in kiln flame models. This approach has been chosen because it is a simple and engineering approach to evaluate the progress of reactions based on kinetics. Furthermore, when a continuous stirred tank is considered, the rotational speed is taken into account in the model. A computational fluid dynamics approach was not chosen because the system is more complex to define and it has computational limitations with gas-solid reactions together with the turbulent gas flow (Kuipers and van Swaaij, 1998; Paschedag, 2005). If the focus of the model was the physical behavior of the kiln bed, the CFD approach would have been convenient.

The rotary kiln is divided in slices, where each one will be modeled as a CSTR connected in series, as illustrated in Figure 7-1. The initial and final bed temperature and the residence time for the material to go through the rotary kiln are specified in Figure 7-1. The fuel particles are continuously fired in the kiln inlet of the rotary kiln and transported through the different kiln slices.

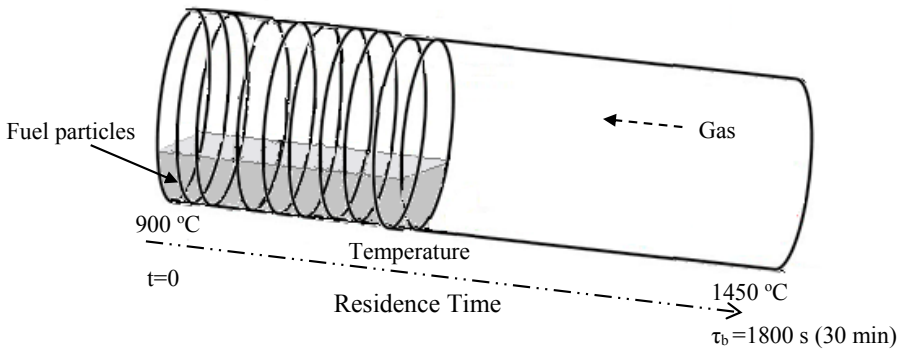

Figure 7-1: Rotary kiln divided in Continuous Stirred Tank Reactors.

The model has three steps, which are graphically summarized in Figure 7-2. First, the particle temperature profile is calculated for a single fuel particle. The heating takes place from ambient temperature to 900 ºC, which is the temperature of the bed material in the kiln inlet. Secondly, the temperature profile is used to determine the mass loss under pyrolysis corresponding to the volatiles release. Finally, the release of volatiles is used as input in the kiln model, which calculates the consumption of the volatiles, and the formation of the SO_2 that will be incorporated in the gas of the freeboard in counter-current.

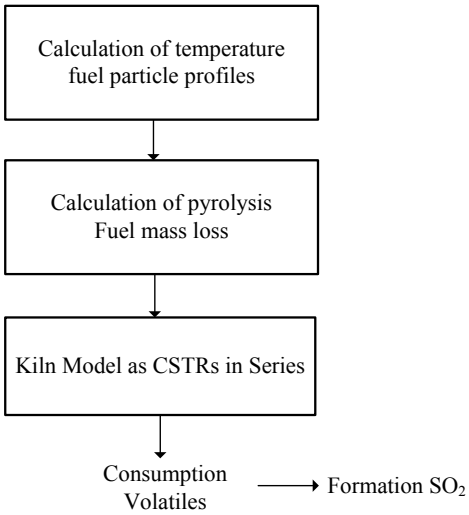

Figure 7-2: Scheme of the modeling steps for predicting sulfur release from the bed rotary kiln material.

7.3 Assumptions

The model of heating up and pyrolysis of a fuel particle have been formulated taking into account the following assumptions:

- The fuel particles are spherical.
- The fuel particles are fired directly into the rotary kiln from the surroundings. This means that they are not experiencing preheating.
- The density, heat capacity, and thermal conductivity of the fuel particle are considered constants.
- The fuel particles are converted under pyrolysis (with no oxygen present) in order to calculate the release rate of volatiles.
- The release of volatiles for a single particle is assumed to be additive for the multiple particles.
- The char combustion of the fuel particles is neglected.
- Energy contribution from the fuel particles to the bed material and to the freeboard gas from heating the particles and fuel combustion is neglected.

The kiln model has been formulated taking into account the following assumptions:

- The fuel particles are evenly distributed in the bed material and the release of the volatiles are perfectly mixed with the bed due to the rotation of the rotary kiln. Therefore, the bed material can be modeled as a well-mixed reactor (CSTR), where all the particles in the bed material experience the same conditions.
- Each CSTR is in a steady state, where the temperature and the concentration are homogenous in the whole bed.
- The bed material consists only of CaO particles, which are identical with the same diameter.
- All the sulfur content is assumed to be $CaSO_4$, which is distributed evenly between all the particles as a shell surrounding the CaO particles.
- The surface area of $CaSO_4$ does not change with the reaction.
- There is no residence time distribution of the particles of bed material in each CSTR. The bed material is considered that moves from one CSTR to another CSTR.
- A degree of coverage of the fuel is defined to describe the fraction of fuel that is covered by the bed, hence how much of the volatiles is released in the bed and may react with $CaSO_4$.
- The reaction of $CaSO_4$ with CO or H_2 follows a 1^{st} order reaction and the kinetic constants have a form of 1^{st} order Arrhenius equation. Since most of the volatile composition is CO, it is assumed that the reaction of $CaSO_4$ with the volatiles also follows a first order reaction and has a form of 1^{st} order Arrhenius equation. It is assumed that for 1 mol of volatiles consumed, 1 mol of SO_2 is formed, as

illustrated in reaction (7-1). The reaction may give a mixture of CaO and CaS as reviewed in Chapter 6, but the oxidation of CaS releasing SO_2 is not considered in the model.

$$CaSO_4(s) + Vol(g) \rightarrow CaO/CaS(s) + SO_2(g) + H_2O/CO_2(g) \quad (7\text{-}1)$$

- The bed temperature increases linearly from the kiln inlet, 900 °C, to the hot end zone, 1450 °C.
- There is no heat exchange between the bed material and the gas phase and through the kiln shell to the surroundings.
- There is no SO_2 in the gas phase coming from the kiln burner or the evaporation of sulfur in the hot end of the rotary kiln.
- The SO_2 formed in the bed is added to the gas phase.
- The SO_2 in the gas phase does not react either with any other gas species or is absorbed by dust.
- The gas flows of the non-reacted volatiles released and the combustion products to the freeboard gas are neglected.

7.4 Mathematical Development

7.4.1 Calculation of the Particle Temperature Profile

The heat up of a large non-isothermal and spherical fuel particle is determined by solving numerically the transient heat transfer differential equation (equation 7.1), because the fuel particles are too large to be considered isothermal.

$$\frac{\partial T(r,t)}{\partial t} = \frac{1}{r^2} \cdot \frac{\partial}{\partial r}\left(r^2 \cdot \frac{k_p}{\rho_p \cdot C_p} \frac{\partial T(r,t)}{\partial r} \right) \quad [7.1]$$

where ρ_p is the density of the fuel particle in kg/m^3, C_p is the fuel particle heat capacity in J/(kg·K), T is the temperature in K, r is the distance from the center in m, and k_p is thermal conductivity of the fuel particle in W/(m·K).

The initial condition for the fuel particle is expressed by equation 7.2.

$$T(t=0,r) = T_{p,0} = 293\,K \quad [7.2]$$

The boundary conditions consist of:

- No heat transfer at the center of the particle, which is mathematically expressed by equation 7.3.

$$\frac{\partial T(t, r=R)}{\partial r} = 0 \quad [7.3]$$

- The temperature at the fuel particle surface is determined by the heat transfer by conduction with the bed material. Mathematically expressed by equation 7.4.

$$k_p \cdot \frac{\partial T(t, r = R)}{\partial r} = h_{cond} \cdot (T - T_{b,0}) \quad [7.4]$$

where $T_{b,0}$ is the initial bed temperature in K, which will be the final temperature of the fuel particle, and h_{cond} is the heat transfer coefficient for conduction in W/(m²·K). There parameters are specified in Table 7-1.

7.4.2 Calculation of Pyrolysis

The fuel used for this model is wood, so the decomposition of wood material under pyrolysis is described for this material. For other fuels, the decomposition mechanism and the kinetic parameters should probably be changed.

The temperature profiles for the wood particle are used to predict the release of volatiles as a result of the ongoing pyrolysis. Di Blasi (2008) describes the decomposition of wood material to be first order regarding the decomposition of wood and formation of volatiles and char. The general one-component equation for the disappearance of a component during the pyrolysis is presented as dimensionless model by equation 7.5 (Di Blasi, 2008) and it is transformed into a model with dimensions (equation 7.6) to describe the measureable release of volatiles.

$$\frac{dX}{dt} = -k_{pyr} \cdot (X - X_\infty) \quad [7.5]$$

Substitution of X and X_∞, defined as $X = 1 - \frac{m_w}{m_{w,0}}$ and $X_\infty = 1 - \frac{m_{w,\infty}}{m_{w,0}}$, yields to equation 7.6.

$$\frac{dm_w}{dt} = -k_{pyr} \cdot (m_w - m_{w,\infty}) \quad [7.6]$$

where X and m_w denote the degree of conversion and the remaining mass of wood at time *t* in kg, X_∞ and $m_{w,\infty}$ are the fraction and the mass which cannot be pyrolized, $m_{w,0}$ is the initial mass in kg, and k_{pyr} is kinetic constant for the pyrolysis, which has a form of 1st order Arrhenius equation. The difference between the initial mass and the mass of the particle at any time is the cumulative amount of volatiles released.

7.4.3 Rotary Kiln Model

The model development of the rotary kiln model as CSTR in series is based on a steady-state mass balance. The general mass balance for the volatiles is presented in words by equation 7.7.

$$Accumulation = In - Out + Generation \quad [7.7]$$

In = Volatiles from the fuel particle + Volatiles from the previous reactor
Out = Volatiles transferred to next reactor + Volatiles diffusion to freeboard
Generation = – Volatiles consumed by the reaction with $CaSO_4$
Accumulation = Zero due to the steady state assumption

Mathematically, equation 7.7 can be expressed in terms of molar flows, as shown in equation 7.8.

$$\frac{d\dot{n}}{dt} = \left(\dot{n}_{in} + \dot{n}_{Vol,fuel}\right) - \left(\dot{n}_{out} + \dot{n}_{diff}\right) - \dot{n}_{reac} \qquad [7.8]$$

where $\dot{n}_{in}$ is the volatiles molar flow from the previous reactor in mol/s, $\dot{n}_{Vol,fuel}$ the molar flow of the volatiles released from the fuel particle in mol/s, $\dot{n}_{out}$ is the volatiles molar flow transferred to the next reactor in mol/s, $\dot{n}_{diff}$ is the molar flow of the volatiles that diffuses to the freeboard in mol/s, and $\dot{n}_{reac}$ is the molar flow of the volatiles consumed by the reaction with $CaSO_4$ in mol/s. By specifying the mol fluxes, the mol balance for a CSTR *i* is expressed by equation 7.9.

$$0 = Q \cdot C_{Vol_{i-1}} + Q \cdot C_{Vol_{fuel}}(t) - Q \cdot C_{Vol_i} - A_{b,top} \cdot k_g \cdot \Delta C_{Vol} - k_{Vol \to SO_2} \cdot A_S \cdot C_{Vol_i} \qquad [7.9]$$

where $C_{Vol,i}$ is the volatile concentration flux in the *i* CSTR in mol/m^3, $C_{Vol,i-1}$ is the volatiles concentration flux coming from the previous CSTR in mol/m^3 (this term will not exist for the first CSTR), $C_{Vol,fuel}$ is the released volatiles concentration from the fuel in mol/m^3, Q is the volumetric flow rate of the volatiles m^3/s, $A_{b,top}$ is the bed area in contact with the freeboard area in m^2, k_g is the volatiles mass transfer coefficient in m/s, ΔC_{vol} is the difference volatile concentration in the bed ($C_{Vol,i}$) and in the freeboard (which is zero), A_S is the total surface area of sulfur in m^2, and $k_{Vol \to SO2}$ is the kinetic constant of the reaction between $CaSO_4$ and the volatiles in m/s.

The mass transfer coefficient, k_g, is found from a Sherwood correlation. For an industrial rotary kiln, this correlation is used (Coulson and Richardson, 1999):

$$Sh = \frac{k_g \cdot L_{b,avg}}{D_{Vol,eff}} = 2 + 0.552 \cdot \mathrm{Re}^{1/2} \cdot Sc^{1/3} \qquad [7.10]$$

where $L_{b,avg}$ is the average depth of the bed in m, $D_{Vol,eff}$ is the effective diffusion coefficient of the volatiles in m/s, Re is the Reynolds number and Sc is the Schmidt number, which are calculated by the density, the viscosity, and the velocity of the volatile released. The parameters for the volatiles are assumed to be equal to the CO parameters, because CO is the main contribution to the volatile gases. The effective diffusion coefficient of CO in atmospheric, $D_{CO,eff}$, is therefore calculated by 7.11.

$$D_{CO,eff} = \frac{\varepsilon}{\tau} \cdot D_{CO} \qquad [7.11]$$

where D_{CO} is diffusion coefficient of CO in atmospheric air in m^2/s, τ is the bed tortuosity, and ε is the bed porosity. Dias et al. (2006) found that the tortuosity, τ, of a mixed bed of granular particles could be described as $\tau = 1/\varepsilon^n$, where n depends on the particle packing but usually are in the range of 0.4-0.5. The diffusion coefficient of CO in atmospheric air is defined by equation 7.12 (Fueller et al., 1966).

$$D_{CO} = \frac{10^{-3} \cdot T^{1.75} \cdot \left(M_{CO}^{-1} + M_{air}^{-1}\right)^{1/2}}{\left[\left(z_{CO}\right)^{\frac{1}{3}} + \left(z_{air}\right)^{\frac{1}{3}}\right]^2} \qquad [7.12]$$

where M_i is the molar mass of compound *i* in g/mol, and z_i is the special atomic diffusion volume of compound *i* (dimensionless), which are 20.1 for air and 18.9 for CO (Fueller et al., 1966).

The kinetic constant for reaction (7-1) is defined by equation 7.13. Since most of the volatile composition is CO and the model validation will be with CO, these parameters will are taken from reaction $CaSO_4$ with CO given by Xiao and Song (2011). These parameters have been chosen because the study of Xiao and Song (2011) was in a temperature range 880-950 ºC with high concentrations of CO but without introducing CO_2 (see Appendix D).

$$k_{Vol \rightarrow SO_2} = A_{Vol \rightarrow SO_2} \cdot \exp\left(-\frac{E_{a,Vol \rightarrow SO_2}}{R \cdot T_b}\right) \qquad [7.13]$$

where $A_{Vol \rightarrow SO2}$ is the pre-exponential factor in m/s, $E_{a,Vol \rightarrow SO2}$ is the activation energy in J/mol, R is the ideal gas constant in J/(mol·K), and T_b is the bed temperature in K.

For each CSTR, the bed temperature is calculated according to equation 7.14.

$$T_b(i) = T_{b,0} + \frac{T_{b,f} - T_{b,0}}{\tau_b} \cdot i \qquad \text{for } i\text{=1 to } N_{CSTR} \qquad [7.14]$$

where $T_{b,f}$ is the final bed temperature in K, *i* is the number of CSTRs which are defined for each second, N_{CSTR} is the total number of CSTR, and τ_b is the bed residence time of the kiln in s.

Since the fuel is converted under pyrolysis, it is assumed that the particle is fully covered by the bed material and therefore the volatiles from the fuel are in contact with the entire bed in the cross-section. In order to include scenarios where the fuel particle is partly covered, the fuel degree of coverage, ϕ, is defined from 0 to 1. When the fuel degree of coverage is 1, it means that the entire amount of volatiles released from the fuel

will be in contact with the bed material, while 0 will mean that the volatiles release takes place on top of the bed without reacting with the sulfur. The fuel degree of coverage affects the concentration of volatiles in contact with the bed material according to equation 7.15, giving the apparent volatile concentration from the fuel, $C^*_{Vol_{fuel}}$.

$$C^*_{Vol_{fuel}}(\mathrm{t}) = C_{Vol_{fuel}}(\mathrm{t}) - C_{Vol_{fuel}}(\mathrm{t}) \cdot (1-\phi) \qquad [7.15]$$

The volatile concentration at steady state for a CSTR *i* is found by rearranging equation 7.9 and is given by equation 7.16.

$$C_{Vol_i} = \frac{Q(t) \cdot \left(C_{Vol_{i-1}} + C^*_{Vol_{fuel}}(t) \right)}{\left(Q(t) + k_{Vol \to SO_2} \cdot A_S + A_{top} \cdot k_g \right)} \qquad \text{for } i\text{=1 to } N_{CSTR} \qquad [7.16]$$

The number of moles of SO_2 formed is calculated by the difference between the inlet and outlet volatile concentrations in each CSTR, according to equation 7.17. The sulfur consumption is monitored along the kiln and compared to the initial moles of sulfur. The calculations are stopped if all the sulfur content in the bed has been released.

$$\dot{n}_{SO_2,i} = \left(\dot{n}_{Vol_{i-1}} + \dot{n}^*_{Vol_{fuel}} \right)_{in} - \left(\dot{n}_{Vol_i} \right)_{out} \qquad \text{for } i\text{=1 to } N_{CSTR} \qquad [7.17]$$

In order to calculate the corresponding SO_2 concentration in the flue gas from the release, the molar flow of flue gas, $\dot{n}_g$ in mol/s, is calculated according to equation 7.18.

$$\dot{n}_g = \frac{\dot{m}_b \cdot n_{g,clikbasis}}{M_g} \qquad [7.18]$$

where $n_{g,clikbasis}$ is the flow of the gas in clinker basis in kg/kg clinker, M_g is the molar mass of the flue gas in kg/mol, and $\dot{m}_b$ is the solid material flow in kg clinker/s, calculated based on the filling degree and bed velocity as shown by equation 7.19.

$$\dot{m}_b = \pi \cdot \left(\frac{\varnothing_k}{2} \right)^2 \cdot F \cdot v_b \cdot \rho_b \qquad [7.19]$$

where $\varnothing_k$ is the diameter of the kiln in m, F is the fill degree, ρ_b is the bed density in kg/m^3, and v_b is the velocity of the bed in m/s, which is calculated dividing the length of the kiln by the bed residence time required to pass through the entire kiln and.

The molar fraction of SO_2 in the flue gas in counter-current, y_{SO2}, is calculated according to equation 7.20 and the SO_2 concentration in ppm is then determinedd by equation 7.21.

$$y_{SO_2,i} = \frac{\dot{n}_{SO_2 i}}{\dot{n}_g + \sum_N^i \dot{n}_{SO_2 i}} \qquad \text{for } i = N_{CSTR},\ N_{CSTR}-1,\ \ldots \text{ to } 1 \qquad [7.20]$$

$$C_{SO_2,i} = \left(\sum_N^i y_{SO_2,i} \right) \cdot 10^6 \qquad \text{for } i = N_{CSTR},\ N_{CSTR}-1,\ \ldots \text{ to } 1 \qquad [7.21]$$

Figure 7-3 schematically illustrates the flows directions and concentrations of volatiles and SO_2, previously described, for a general three CSTR in series.

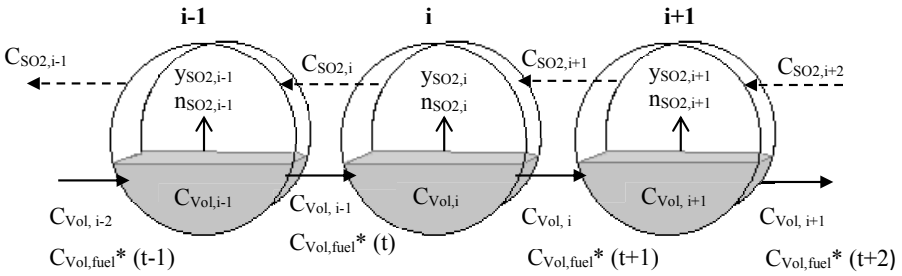

Figure 7-3: Drawing of three CSTR in series with the volatile and SO_2 concentrations at different locations.

The sulfur evaporation factor, ε_s, is defined by the SO_3 concentrations in the hot meal and in the clinker. For the model sulfur evaporation factor in the kiln inlet, this definition can be estimated in molar basis with the total moles of sulfur released and the initial moles of sulfur that the bed material, as expressed in equation 7.22.

$$\varepsilon_S [\%] = \frac{w_{SO_3,\,hot\,meal} - w_{SO_3,\,clinker}}{w_{SO_3,\,hot\,meal}} \overset{in\,molar}{\approx} \frac{n_{0,S} - (n_{0,S} - n_{total\,S\,released})}{n_{0,S}} \cdot 100 \qquad [7.22]$$

7.5 Results

7.5.1 Substitution 10 % Energy with Alternative Fuels fired in the Kiln Inlet

A cement plant with a clinker production of 3500 tons per day is considered. The kiln system is a typical ILC-configuration of a preheater kiln with 5 cyclones and uses 2.993 MJ/kg clinker of which 60 % is fired in the calciner and 40 % in the kiln burner. Ten percent of the energy in the kiln burner, which corresponds to 0.119 MJ/kg clinker, is substituted with fuel fired in the kiln inlet.

The rotary kiln characteristics are 4.35 m of diameter and 51 m of length (FLSMIDTH A/S, 2011) with a fill degree of 10 % and the bed material has a porosity of 0.4. The material residence time is assumed to be 30 minutes, therefore, the corresponding bed velocity along the rotary kiln is 0.025 m/s.

The input parameters for the sub-models: heating up, pyrolysis, and kiln model are specified in Table 7-1. The CO diffusion coefficient and the mass transfer coefficient calculated at 900 ºC are listed in order to show their order of magnitude.

Table 7-1: Input parameters for the, heating up a fuel particle, pyrolysis and kiln models.

	Input parameters			Reference
	Parameter	**Symbol**	**Value**	
Heating up a fuel particle	Wood lower heating value [MJ/kg]	LHV_w	19.7	(Guo et al., 2013)
	Density wood [kg/m^3]	ρ_w	330	(Guo et al., 2013)
	Heat capacity [J/(kg·K)]	$C_{p,w}$	1733	(Guo et al., 2013)
	Thermal conductivity [W/(m·K)]	$k_{s,w}$	0.20	(Guo et al., 2013)
	Initial bed temperature [ºC]	$T_{b,0}$	900	(Hewlett, 1998)
	Heat transfer coefficient for conduction [W/(m^2·K)]	h_{cond}	300	(Linjewile et al., 1993)
	Initial temperature [ºC]	T_o	20	Assumed
Pyrolysis	Pyrolysis pre-exponential factor [s^{-1}]	A_{pyr}	$7.68 \cdot 10^7$	(Reina et al., 1998)
	Pyrolysis activation energy [J/mol]	$E_{a,\,pyr}$	$124.87 \cdot 10^3$	(Reina et al., 1998)
	Wood volatiles content [wt. % wood]	w_{vol}	40	(Nunn et al.,1985)
Kiln Model	Sulfur content [wt. %]	$w_{S,in}$	2	Assumed
	Porosity [-]	α	0.4	Assumed
	Final bed temperature [ºC]	$T_{b,f}$	1450	(Hewlett, 1998)
	Density bed material [kg/m^3]	ρ_b	1650	(Nielsen, 2012)
	Pre-exponential factor [m/s]	$A_{Vol \rightarrow SO2}$	14280	(Xiao and Song, 2011)
	Activation energy [J/mol]	$E_{a,Vol \rightarrow SO2}$	1890	(Xiao and Song, 2011)
	CO diffusion coefficient at 900 ºC [m^2/s]	D_{CO}	$2.15 \cdot 10^{-4}$	Calculated
	Mass transfer coefficient at 900 ºC [m/s]	k_g	$1.69 \cdot 10^{-4}$	Calculated

The fuel used to fire in the kiln inlet is wood. The fuel flow required to cover the energy in the kiln inlet is 0.246 kg/s wood. Different particles are defined and their mass and dimension characteristics as well as the number of particles fired are specified in Table 7-2.

Table 7-2: Mass and dimension characteristics of different fuel particles and number of particles fired per second.

Particle mass [g]	Particle diameter [mm]	Number of particles /s
30	27.9	8
15	22.1	16
10	19.3	25
5	15.4	49
1	9.00	246

The temperature profile and the pyrolysis calculation are performed for a single wood particle. The temperature profiles from the center to the surface of a 30 g and 1 g spherical wood particles are plotted in Figure 7-4 and Figure 7-5 at different times. The heating up of the particle of 30 g is quite slow in the center, after 200 seconds the surface temperature is almost 900 ºC while the center is just 200 ºC. On the contrary, the 1g wood particle reaches almost 900 ºC after 100 seconds.

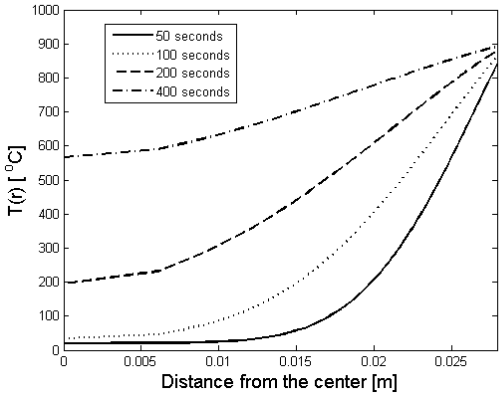

Figure 7-4: Temperature profiles for a single wood particle of 30 g at 50, 100, 200 and 400 seconds.

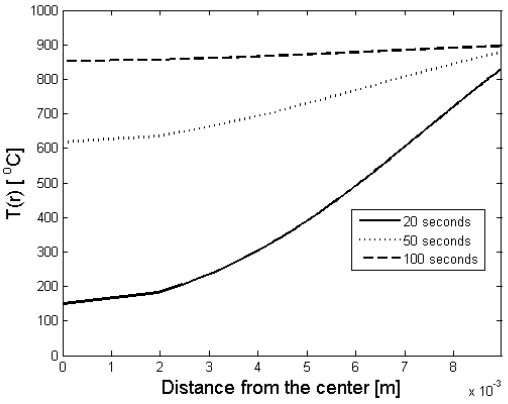

Figure 7-5: Temperature profiles for a single wood particle of 1 g at 20, 50 and 100 seconds.

The degrees of devolatilization for the different wood particles, which is calculated based on the mass decrease due to the volatiles release under pyrolysis, are shown in Figure 7-6. The results show that the degree of devolatilization requires longer time to achieve 100 % with increasing particle mass. Moreover, the rate of volatiles release, illustrated in Figure 7-7, is faster and takes place in shorter time with decreasing particle mass.

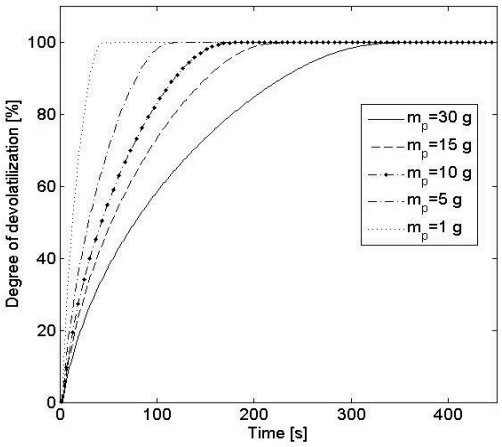

Figure 7-6: Degree of devolatilization for a wood particle of 30, 15, 10, 5, and 1 g.

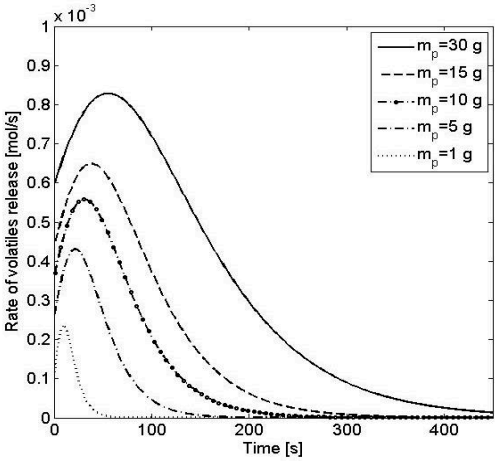

Figure 7-7: Rate of volatiles release for a single wood particle of 30, 15, 10, 5, and 1 g.

The SO_2 release rate is calculated for each wood particle mass and the results are shown in Figure 7-8. For these calculations, the fuel degree of coverage, ϕ, is considered to be 1, which means that all the volatiles released from the fuel are in contact with the bed material, and this is the worst case scenario giving the highest SO_2 release. The SO_2 release rate is higher and last shorter time for smaller particles than larger particles. The integration of the SO_2 release rate gives the total SO_2 release, which is illustrated in Figure 7-9, and determines that more SO_2 is release decreasing particle size. This is in good agreement with the experimental results presented in Chapter 5. The particle size affects mainly the release rate but not so much the total release, because the total release is quite similar while the SO_2 release rate increases with decreasing particle size.

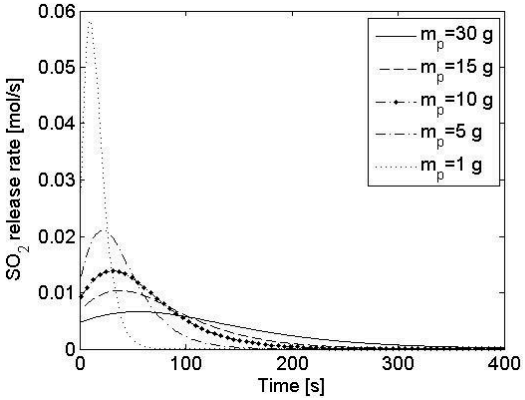

Figure 7-8: SO_2 release rate for 8 wood particles of 30 g, 16 wood particles of 15 g, 25 wood particles of 10 g, 49 wood particles of 5 g, and 246 wood particles of 1 g.

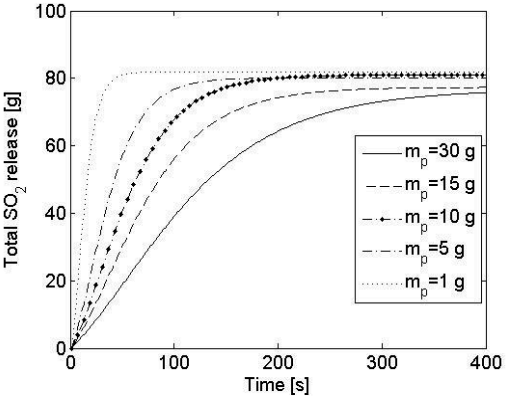

Figure 7-9: Total SO_2 release in g for 8 wood particles of 30 g, 16 wood particles of 15 g, 25 wood particles of 10 g, 49 wood particles of 5 g, and 246 wood particles of 1 g.

The SO_2 concentration accumulated in the gas phase in counter-current is calculated as function of the distance from the kiln inlet and the results are plotted in Figure 7-10. Higher SO_2 concentrations in the kiln inlet are obtained with decreasing the mass of the particle. Furthermore, the SO_2 release takes place closer to the kiln inlet with decreasing the wood mass particle. For example, firing 246 wood particles of 1 g the SO_2 release stops before 2 m from the kiln inlet, while firing 8 wood particles of 30 g the sulfur release stops after 12 meters. The different mass particles giving different sizes influence more the distance in the kiln where SO_2 release takes place than the SO_2 concentration in the kiln inlet.

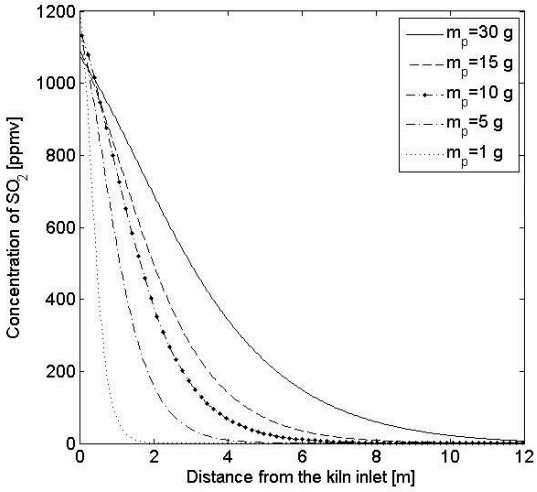

Figure 7-10: SO_2 concentration as function of the distance from the kiln inlet for 8 wood particles of 30 g, 16 wood particles of 15 g, 25 wood particles of 10 g, 49 wood particles of 5 g, and 246 wood particles of 1 g.

Table 7-3 summarizes the time of devolatilization for the different wood particles supplying 10 % of the energy as well as the total SO_2 release, the concentration of SO_2 in the kiln inlet, the sulfur evaporation factor, and the percentage of SO_2 release to CO injected. The time to complete devolatilization increases with increasing particle size, and it is in good agreement with the experimental results of Chapter 5, and the experimental and predicted results of Nielsen (2012). The total SO_2 release and the concentration of SO_2 in the kiln inlet factor increase with decreasing particle mass, and the evaporation factor follows thereby the same tendency. The SO_2 release relative to the CO injected is nearly 100 % indicating that almost all CO reacts with $CaSO_4$ for the different scenarios.

Table 7-3: Summary of the time of devolatilization, total SO_2 release, SO_2 concentration in the kiln inlet, sulfur evaporation factor, and the percentage of SO_2 release to CO injected for the different mass particles with the same energy input.

Particle mass [g]	Particle diameter [mm]	Time of devolatilization [s]	Total SO_2 release [g]	Conc. SO_2 in kiln inlet [ppm]	ε_s [%]	SO_2/CO ratio [%]
30	27.9	340	76.46	1072	3.27	99.9
15	22.1	230	77.34	1087	3.77	99.9
10	19.3	180	80.13	1134	3.93	99.9
5	15.4	120	81.02	1141	3.96	99.9
1	9.00	44.0	81.88	1181	4.10	99.9

7.5.1.1 Effect of the Fuel Degree of Coverage

The effect of the fuel degree of coverage is investigated using 25 wood particles of 10 g corresponding to 10 % energy input. This particle size is chosen because it is an intermediate size and it is reasonable to be used in the industry. Figure 7-11 and Figure 7-12 show the effect of the fuel degree of coverage on the SO_2 release rate and the SO_2 concentration as function of the distance from the kiln inlet, respectively. The SO_2 release rate and the SO_2 concentration decrease with decreasing fuel degree of coverage because less volatiles are in contact with the bed material and consequently less volatiles can react with $CaSO_4$ releasing SO_2.

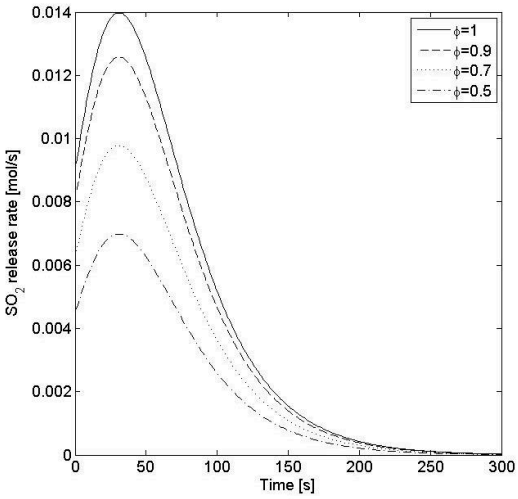

Figure 7-11: Effect of the fuel degree of coverage (ϕ) of 25 wood particles of 10 g each on the SO_2 release rate.

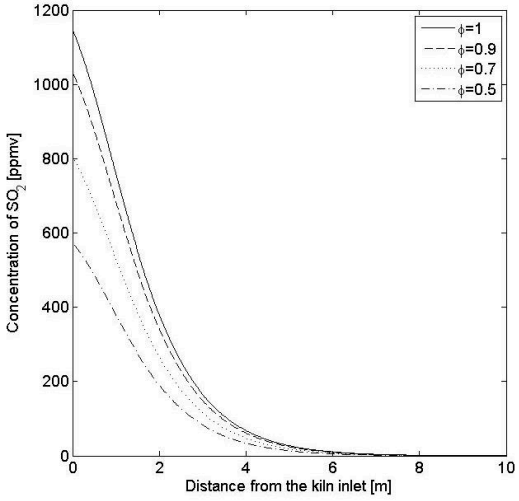

Figure 7-12: Effect of the fuel degree of coverage (ϕ) of 25 wood particles of 10 g each on the SO_2 concentration in the flue gas as function of the distance from the kiln inlet.

The total SO_2 release, the SO_2 concentration in the kiln inlet, the sulfur evaporation factor, and the percentage of SO_2 release to CO injected for the different degree of coverage are specified in Table 7-4.

Table 7-4: Summary of the total SO_2 release, SO_2 concentration in the kiln inlet, sulfur evaporation factor, and the percentage of SO_2 release to CO injected for the different fuel degree of coverage of 25 wood particles of 10 g.

Fuel degree of coverage	Total SO_2 release [g]	Conc. SO_2 in kiln inlet [ppm]	ε_s [%]	SO_2/CO ratio [%]
1	80.13	1134	3.93	99.9
0.9	72.92	1027	3.56	90.0
0.7	56.71	799.2	2.77	70.0
0.5	40.51	570.9	1.98	50.0

The three variables are highest when the fuel particle is fully covered by bed material (ϕ=1), because the contact between the CO concentration and the $CaSO_4$ in the bed material is higher. The sulfur evaporation factor decreases linearly with decreasing the fuel degree of coverage.

The fuel degree of coverage is a parameter, which cannot be directly controlled, because it depends on the mixing between fuel particles with the bed material. Nielsen (2012) investigated experimentally the mixing of large and small particles in rotary kilns and showed that the degree of visibility above the bed depends on the material fill degree, the dimensions and sphericity of the fuel particle, and the fuel density. A probability correlation was derived dependent on the characteristics of the bed, the sphericity and the density of the fuel, and fitting parameters from the conducted experiments at room temperature (Nielsen, 2012). The tendency at room temperature was that large fuel particle were more visible than smaller fuel particles, however, this correlation has not been validated at temperatures relevant for the cement rotary kilns.

7.5.1.2 Effect of the Fill Degree

The fill degree of the kiln bed has been modified in order to investigate its influence on SO_2 release when firing 25 wood particle of 10 g. Figure 7-13 shows the SO_2 release rate, the total SO_2 release, and the concentration of SO_2 when the bed material has a fill degree of 20, 10, and 5 % with the same sulfur concentration, 2 wt. %, in each case. Graph a) shows that the SO_2 release rate is the same for the different fill degrees because nearly 100 % of volatiles gases reacted with the sulfur in the bed, which is in excess. The total SO_2 release, illustrated in graph b), is equal for the different fill degrees. The SO_2 concentration as function of the distance from the kiln inlet, graph c), increases with decreasing fill degree, this is because the material bed flow is decreased and consequently the gas flow also decreases, according to equations 7.16 and 7.17.

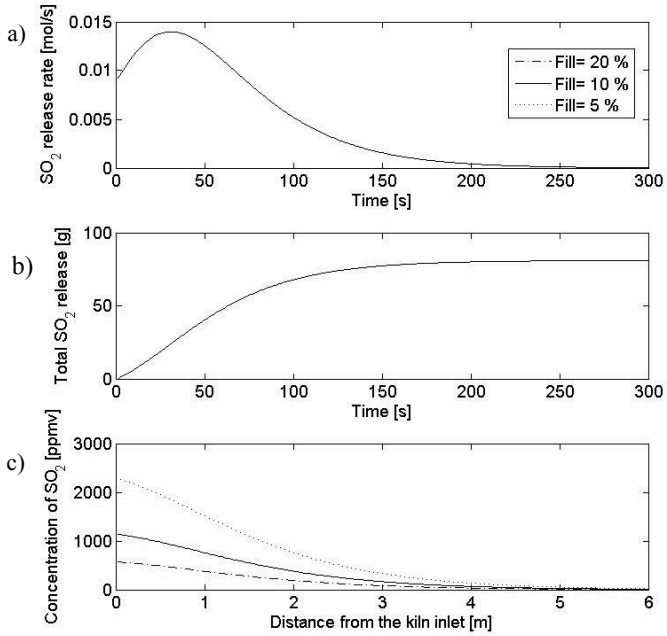

Figure 7-13: Effect of the fill degree on a) the SO_2 release rate, b) total SO_2 release and c) the SO_2 concentration in the flue gas as function of the distance from the kiln inlet when 25 wood particles of 10 g each are fired.

The summary of the SO_2 release, the SO_2 concentration in the kiln inlet, the sulfur evaporation factor, and the percentage of SO_2 release to CO injected for the scenarios varying the bed fill degree containing the same sulfur concentration is shown in Table 7-5. The total SO_2 release is the same for the different bed fill degrees as illustrated in Figure 7-13, because the $CaSO_4$ is reactant in excess for the three cases. This means that the same volatile concentration gives the same SO_2 release, but the concentration in the gas phase is different, because the gas flow depends on the solid material flow, which is a function of the fill degree. The highest SO_2 concentration in the kiln inlet and the sulfur evaporation factor correspond to 5 % fill degree, while the lowest SO_2 concentration in the kiln inlet and sulfur evaporation factor to 20 % fill degree.

Table 7-5: Summary of the SO_2 release, SO_2 concentration in the kiln inlet, sulfur evaporation factor, and the percentage of SO_2 release to CO injected for the scenarios varying the bed fill degree using 25 wood particles of 10 g.

Fill degree [%]	Total SO_2 release [g]	Conc. SO_2 in kiln inlet [ppm]	ε_s [%]	SO_2/CO ratio [%]
5	80.13	2281	7.92	99.9
10	80.13	1134	3.93	99.9
20	80.13	570.9	1.98	99.9

7.5.1.3 Effect of $CaSO_4$ Content in the Bed Material

The effect of sulfur content in the bed material on sulfur release is studied using 25 wood particles of 10 g. Figure 7-14 shows the results of the SO_2 release rate, the total SO_2 release, and the SO_2 concentration in the gas phase, which are not modified by the variation of sulfur content. This can be explained by the reaction of nearly 100 % of the volatiles with $CaSO_4$ in excess. Furthermore, the variation of the surface area of sulfur for each case is insignificant and not influences the output results. However, this is not in good agreement with the experimental finding from Chapter 5 (Figure 5-30 and Figure 5-31).

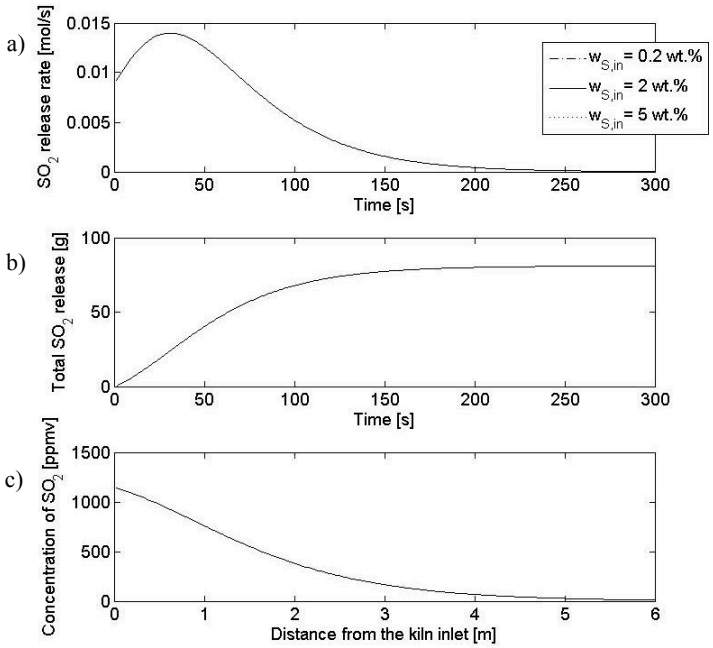

Figure 7-14: Effect of the sulfur input in the bed material on a) the SO_2 release rate, b) total SO_2 release and c) the SO_2 concentration in the flue gas as function of the distance from the kiln inlet when 25 wood particles of 10 g each are fired.

The sulfur evaporation factor is calculated in each case and significantly increases with decreasing sulfur content, as illustrated in Table 7-6. That is because the fraction gets larger if the initial sulfur amount is lower and the same amount of sulfur is released.

Table 7-6: Summary of the total SO_2 release, SO_2 concentration in the kiln inlet, sulfur evaporation factor, and the percentage of SO_2 release to CO injected for different sulfur bed content using 25 wood particles of 10 g.

$CaSO_4$ in bed material [wt. %]	Total SO_2 release [g]	Conc. SO_2 in kiln inlet [ppm]	ε_s [%]	SO_2/CO ratio [%]
0.2	80.13	1134	36.68	99.9
2	80.13	1134	3.93	99.9
5	80.13	1134	1.78	99.9

7.5.2 Effect of Firing Degree in the Kiln Inlet

The firing degree is the rate of energy substituted in the kiln inlet. The effect of the firing degree in the kiln inlet on sulfur release is also investigated when wood particles of 10 g are fired under the bed material with 10 % fill degree and 2 wt. % $CaSO_4$. The modification of the firing degree varies the number of wood particles used in order to satisfy the fuel flow required to cover the energy in the kiln inlet. Figure 7-15 shows the SO_2 release rate, the total SO_2 release, and the SO_2 concentration in the kiln inlet for the scenarios of 5 and 15 % firing degree in the kiln inlet and compared to the 10 %. The numbers of wood particles of 10 g required are 12, 25, and 37 for 5, 10, and 15 % firing degree, respectively. The SO_2 release rate, the total SO_2 release, and the SO_2 concentration increase with increasing substitution energy. This observation is in good agreement with the experimental results of Nielsen (2012) investigating the energy input on sulfur release, which were presented in Figure 5-7.

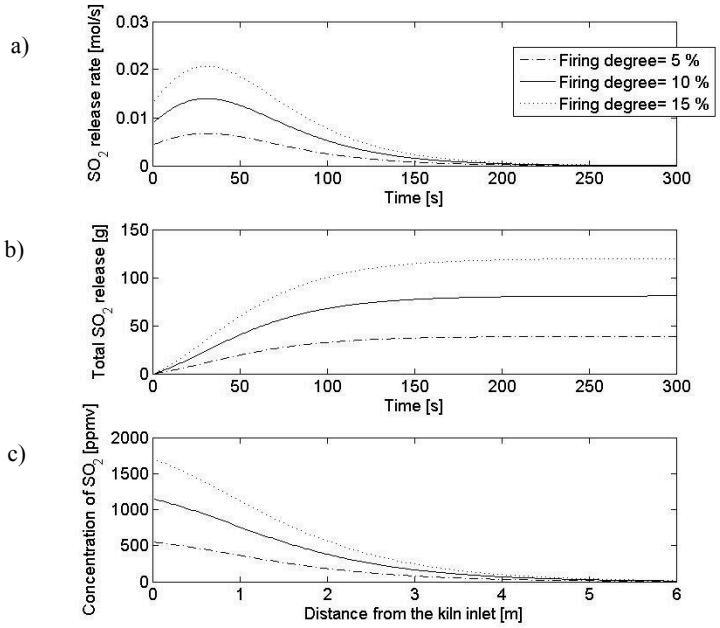

Figure 7-15: Effect of the energy substitution in the kiln inlet using 10 g wood particles on a) the SO_2 release rate, b) total SO_2 release and c) the SO_2 concentration in the flue gas as function of the distance from the kiln inlet.

The corresponding total SO_2 release, SO_2 concentrations in the kiln inlet, sulfur evaporation factors and the percentages of SO_2 release to CO injected in the kiln inlet for the different firing degree scenarios are listed in Table 7-7. The total SO_2 release and the SO_2 concentration in the kiln inlet increase with increasing energy

substitution, because the volatiles gases in contact with the sulfur bed material also increases. Consequently, the sulfur evaporation factor increases.

Table 7-7: Summary of the total SO_2 release, SO_2 concentration in the kiln inlet, sulfur evaporation factor, and the percentage of SO_2 release to CO injected for different firing degree scenarios using wood particles of 10 g.

Firing degree in kiln inlet [%]	Total SO_2 release [g]	Conc. SO_2 in kiln inlet [ppm]	ε_s [%]	SO_2/CO ratio [%]
5	38.89	548.1	1.90	99.9
10	80.13	1134	3.93	99.9
15	119.9	1668	5.86	99.9

7.5.3 Sensitivity analysis

A sensitivity analysis is performed to evaluate the importance of the input variables in the kiln model on the total SO_2 release, the sulfur evaporation factor, and the SO_2 concentration in the kiln inlet. This method only addresses sensitivity relative to the chosen reference case, but parameter interactions are not evaluated. The input parameters for a chosen reference case are specified in Table 7-8 as well as the output results.

Table 7-8: Input parameters and output results for the reference case.

Input parameter	Symbol	Reference value
Mass particle [g]	m_p	10
Sulfur input [wt. %]	$w_{S,in}$	2
Fill degree [%]	F	10
Bed porosity [-]	α	0.4
Degree of coverage [-]	ϕ	0.7
Activation energy [J/mol]	$E_{a,Vol\rightarrow SO2}$	14280
Pre-exponential factor [m/s]	$A_{Vol\rightarrow SO2}$	1890
Firing degree [%]	-	10
Output results		
Total SO_2 release [g]		56.71
Conc. SO_2 kiln inlet [ppm]		799.2
ε_s [%]		2.77

Each input parameter is changed with +/- 25 % while keeping the remaining parameters constant. Table 7-9 summarizes the output results obtained for each case, and their percentage deviation from the output results obtained to the reference case. The results show that the parameters with the largest influence on the three output variables are the firing degree and the fuel degree of coverage. On the contrary, the activation energy and the pre-exponential factor do not influence the output results. The variation of +/- 25 % of the sulfur bed content influences only the evaporation factor, because the variation of the initial bed properties affects the

initial sulfur, but the sulfur released is the same since the volatiles are the limited reactant. The modification of the fill degree does not influence the total SO_2 release, as shown in Figure 7-13, graph b). It can be seen that applying the same variation in an input parameter, the deviation is not the same for the positive and the negative variation, for example, a + 25 % variation on the mass particle deviates more from the reference results than the same negative variation.

Table 7-9: Sensitivity analysis of the kiln model on the total SO_2 release, the sulfur evaporation factor, and the SO_2 concentration in the kiln inlet.

Input parameters		**Change in output variables**			**Deviation [%]**		
	Variation +/- 25 %	Total SO_2 [g]	ε_s [%]	Conc. SO_2 kiln inlet [ppm]	Total SO_2	ε_s	Conc. SO_2 kiln inlet
Mass particle [g]	7.5	56.39	2.76	796.1	-0.56	-0.36	-0.39
	12.5	59.88	2.89	835.8	5.59	4.33	4.58
Sulfur content [wt. %]	1.5	56.71	3.62	799.2	0.00	30.7	0.00
	2.5	56.71	2.26	799.2	0.00	-18.4	0.00
Fill degree [%]	7.5	56.71	3.69	1065	0.00	33.2	33.3
	12.5	56.71	2.22	639.4	0.00	-19.9	-20.0
Degree of coverage [-]	0.525	42.54	2.07	599.5	-25.0	-25.3	-25.0
	0.875	70.89	3.46	998.9	25.0	24.9	25.0
Activation energy [J/mol]	108960	56.71	2.77	799.2	0.00	0.00	0.00
	181600	56.71	2.77	799.2	0.00	0.00	0.00
Pre-exponential factor [m/s]	1417.5	56.71	2.77	799.2	0.00	0.00	0.00
	2362.5	56.71	2.77	799.2	0.00	0.00	0.00
Firing degree [%]	7.5	40.83	1.99	575.5	-28.0	-28.2	-28.0
	12.5	70.33	3.44	699.9	24.0	24.2	-12.4

The actual uncertainty of the parameters may be higher than the +/- 25 % variation depending on the operation control of a cement plant, for instance, the mass particle of fuels can have a wide range if the particle size is not screened, and the fuel degree of coverage will depend also on the mixing of the fuel with the raw materials. Furthermore, the uncertainty of the sulfur content in the bed material may also be higher if there is a significant circulation of sulfur, or it may be affected if the raw materials present significant inhomogeneities.

7.6 Model Evaluation

The rotary kiln model has been adapted to the pilot scale dimensions of the high temperature rotary drum in order to evaluate this model against the experimental data obtained in Chapter 6.

The model development, presented in section 7.4.3, is used with the dimensions for the high temperature rotary drum, which were specified in sections 5.2.1 and 6.2. The main difference between the rotary kiln model for

an industrial case and the one adapted to the high temperature rotary drum is that the bed material consists of quartz sand and $CaSO_4$ and not of CaO surrounded by $CaSO_4$ as in the industrial case. The mean diameter of the used $CaSO_4$ is 6.49 µm with a specific surface area of 3.23 m^2/g. The analysis of the particle size is shown in Appendix E.

The axial length of rotary drum is 44 cm. The experimental results have shown that only a minor amount of $CaSO_4$ reacts, indicating that the reaction takes place in the proximity of the tube where the reducing agent is released. A finite length of the bed for the CSTR system, x, needs therefore to be defined in the model, where the reaction will take place only in this finite volume. Figure 7-16 illustrates the axial length rotary drum and for the CSTR.

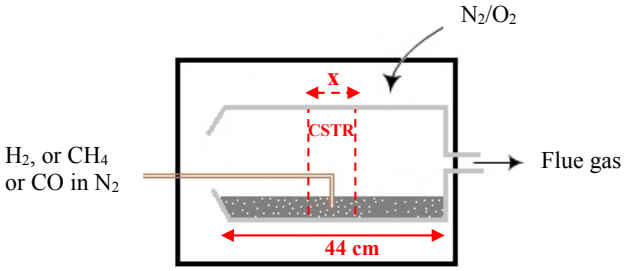

Figure 7-16: Sketch of the rotary drum bed length and the defined bed length of the CSTR for the model validation.

Using 10 vol. % CO, different lengths of the bed material are considered for the CSTR in the model to investigate the effect of this parameter, as shown in Figure 7-17. The variation in the bed length affects the surface area of the $CaSO_4$ involved in the reaction (A_s in equation 7.16), this means that not all $CaSO_4$ present in the bed material is accounted in the CSTR system. Consequently, the surface area needs to be scaled to the proportion of $CaSO_4$ in length of the bed, considering that the $CaSO_4$ is evenly distributed.

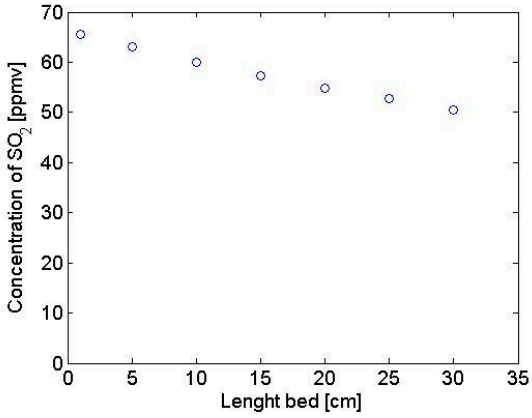

Figure 7-17: SO_2 concentrations using 10 vol. % CO concentration varying the length of the bed considered in the model.

The predicted SO_2 concentration decreases with increasing length of the bed, because the top area where the CO can diffuse out of the bed also increases and more CO can diffuse out. It may not be realistic to assume that the CO may diffuse in the axial direction and react with $CaSO_4$ from a long distance of the injection. Therefore, the bed length of the CSTR is assumed to be 10 cm where the reaction takes place (5 cm in each side of the location of the tube). The surface area is thereby scaled to the proportion of $CaSO_4$ in 10 cm of the bed. The model calculates the steady-state concentration of SO_2 release when the CO is introduced. The modelling results are shown in Figure 7-18 together with the experimental results of SO_2 concentration using different CO concentrations at 5 and 10 vol. % O_2.

It can be seen that the modeling results follow the tendency of the experimental data, however the oxygen content in the freeboard atmosphere is not included in the mathematical model and it is assumed that the CO is well mixed. In the experiments, CO may not be a well-mixed in the bed and may be oxidized by the oxygen, which may diffuse to the bed, occupying the voids and causing a gradient of concentrations inside the bed. Furthermore, the adapted model has the uncertainty of the considered bed porosity and surface area of $CaSO_4$, which may be different in the experiments because agglomeration of particles may also take place.

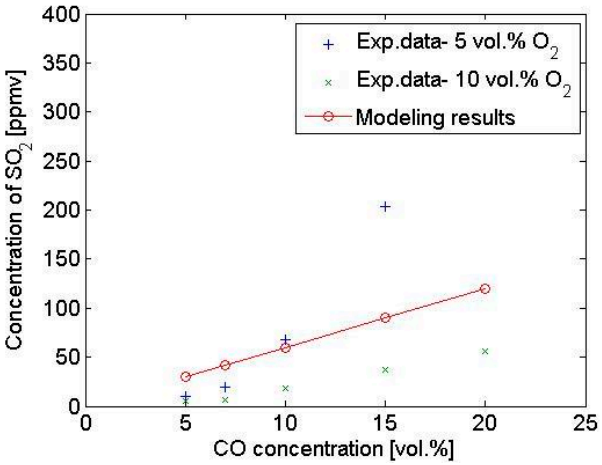

Figure 7-18: Comparison of the experimental results of SO_2 concentration using different CO concentrations at 5 and 10 vol. % O_2 and the modeling results.

The absolute level of the SO_2 concentration cannot be predicted by the model since the bed length and the oxygen concentration are uncertain parameters. It can however be used for qualitative validation, i.e. to evaluate how a relative change in an input parameter affects the sulfur release. The percentage of SO_2 release relative to the CO injected for the experimental data and for the modeling results are presented in Table 7-10 in order to compare how much CO has reacted.

Table 7-10: Percentage of SO_2 release relative to CO injected for different CO concentrations for the experimental and modelling results.

CO conc. [vol. %]	SO_2/CO ratio [%]		
	900 °C, 5 vol. % O_2	900 °C, 10 vol. % O_2	Model
5	2.02	0.98	6.07
7	2.74	0.93	6.07
10	6.67	1.90	6.07
15	13.2	2.54	6.07
20	16.1	2.85	6.07

The results for the model evaluation indicates that only a 6.07 % of CO reacts to form SO_2, while for the rotary kiln model the CO was reacting almost 100 %. This is because in the rotary kiln model the CO that has not reacted is transferred to the next reactor increasing the probability of CO to react. For the evaluation of the adapted model only one CSTR is considered to calculate the steady-state concentration of SO_2 release, because bed material is not moving in the axial direction.

Furthermore, to investigate in which scenario the model can fit the experimental data obtained at 10 vol. % O_2, the fitting of the model results is performed varying the bed length and the degree of coverage. The results are shown in Figure 7-19. In this case, since there is no particle in either the model or the experiments, the degree of coverage influences the amount of CO that is in contact with the material bed. A length of 20 cm which is almost the half of the rotary drum is required. Varying the contact of CO with the material bed, the predicted SO_2 concentration can be fitted at low concentrations of CO with 0.2 degree of coverage and at high CO concentrations with a degree of coverage of 0.5. The model was not able to simulate the experimental data obtained at 5 vol. % O_2.

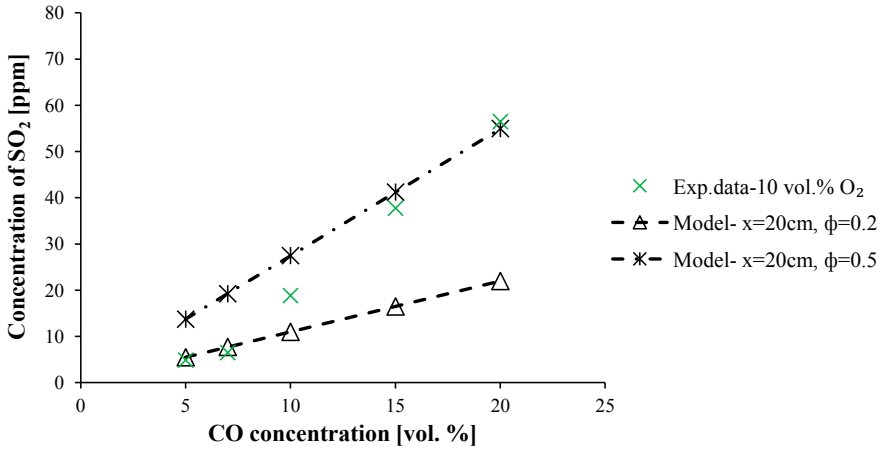

Figure 7-19: Model fitting to the experimental data obtained at 10 vol. % O_2 varying the bed length and the degree of coverage.

In Chapter 6, it is mentioned that the SO_2 rate of formation could follow a first order expression, $r_{SO2}= k (C_{CO}-C_{CO,t})$, where $C_{CO,\,t}$ is the threshold CO concentration which below this concentration no SO_2 is released. However, this is not implemented in the model because the kinetic constants for the reaction are developed for this case and it is believed that this threshold concentration may change depending on the sulfur content of the bed.

The validation of the kiln model is difficult to perform against industrial cement plant data because part of the SO_2 release may get absorbed and the measurement of SO_2 in the kiln inlet has some challenges, as will be explained in Chapter 9.

7.7 Conclusions

Modeling the behavior of rotary kilns is a complicated task involving heat transfer, gas-solid and solid-solid reactions, and particle mixing. In the literature, most of the models for rotary kilns are one-dimensional models for fossil fuels and are based on heat and mass transfer along the length of the kiln. More sophisticated physical three-dimensional models based on computational fluid dynamics have been also developed but are limited in their ability to model the clinker chemistry, bed motion, and thermodynamics. The different behavior between fossil and alternative fuels has encouraged the development of separate models for rotary kilns using alternative fuels.

A mathematical model which is able to predict sulfur release caused by volatiles from wood particles fired in the material kiln inlet has been developed in this chapter. The model is based on the reaction between the volatiles and $CaSO_4$ in the bed material, which is considered as continuous stirred tank reactors in series and therefore assuming well mixing between the volatile gases and the bed material.

SO_2 release was predicted when firing different wood particle mass substituting 10 % of the energy required for production in the kiln inlet. The SO_2 released and consequently the sulfur evaporation factor increased with decreasing particle mass. The effect of the fuel degree of coverage, the bed fill degree, and the bed sulfur content was investigated for 25 wood particles of 10 g. The calculations showed that almost all CO reacts with $CaSO_4$ for the different cases. The total SO_2 release was the same for the different fill degrees, but the SO_2 concentration in the kiln inlet increased with increasing fill degree, because the material bed flow was decreased as well as the gas flow. For the different bed sulfur content, the same total SO_2 release and concentration in the kiln inlet was obtained because the limiting reactant was the volatiles, which was equal for the different cases. The sulfur evaporation factor increased with decreasing sulfur content in the bed and fill degree, while it decreased with increasing the fuel degree of coverage.

The modification of the firing degree was also studied considering wood particles of 10 g. The total SO_2 release and the sulfur evaporation factor increased with increasing firing degree in the kiln inlet. These model

predictions are in a good agreement with the experimental results from Chapter 5, except the effect of bed sulfur input.

A sensitivity analysis have been applied to the kiln model in order to investigate the importance of the input parameters by evaluating the uncertainty in the outputs variables. By modifying one parameter at the time, the firing degree and the fuel degree of coverage were identified as the most influencing factors for the total SO_2 release and the sulfur evaporation factor, while the kinetic parameters did not modify the output results.

The evaluation of the modeling results have been carried out by adapting the model to the high temperature rotary drum and comparing with the experimental results of Chapter 6. The modeling results follow the correct tendency of the experimental data, however, the absolute level of the SO_2 concentration cannot be predicted by the model since the bed length and the oxygen concentration are uncertain parameters. The predictions of the kiln model can be used to evaluate how a relative change in an input parameter affects the sulfur release in a cement plant.

7.8 References

Adams, T. N., and Svedin, K.; Alternative fuel impact on lime reburning kiln performance. TAPPI Press - Engineering, Pulping and Environmental Conference 2008, 4, 2550-2570, 2008.

Agustini, S. S., Queck, A., and Specht, E.; Modeling of the regenerative heat flow of the wall in direct fired rotary kilns. Heat Transfer Engineering, 29, 57-66, 2008.

Akhtar, S. S., Abbas, T., and Lockwood, F. C.; Advanced computational tools for cement plants. 2008 IEEE Cement Industry Technical Conference Record, 154-69, 2008.

Barr, P. V., Brimacombe, J. K., and Watkinson, A. P.; A heat-transfer model for the rotary kiln .2 development of the cross-section model. Metallurgical Transactions B-Process Metallurgy, 20, 403-19, 1989.

Boateng, A. A.; Rotary kilns transport phenomena and transport processes. Elsevier, United States of America. 2008. ISBN: 978-0-7506-7877-3.

Boateng, A. A., and Barr, P. V.; A thermal model for the rotary kiln including heat transfer within the bed. International Journal of Heat and Mass Transfer, 39, 2131, 1996a.

Boateng, A. A., and Barr, P. V.; Modelling of particle mixing and segregation in the transverse plane of a rotary kiln, Chemical Engineering Science, 51, 17, 4167-4181, 1996b.

Coulson, J.M., and Richardson, J.F.; Chemical Engineering, Volume 1: Fluid flow, heat transfer and mass transfer. Sixth edition, Butterworth –Heinemann.1999. ISBN: 0-7506-4444-3.

Darabi, P., Yuan, J., and Salcudean, M.; Numerical studies of mid-kiln tyre combustion. Advances in Cement Research, 20, 121-8, 2008.

Dhanjal, S. K., Barr, P. V., and Watkinson, A. P.; The rotary kiln: An investigation of bed heat transfer in the transverse plane. Metallurgical and Materials Transactions B-Process Metallurgy and Materials Processing Science, 35, 1059-70, 2004.

Di Blasi, C.; Modeling chemical and physical processes of wood and biomass pyrolysis. Progress in Energy and Combustion Science, 34, 1, 47–90, 2008.

Dias, R., Teixeira, J. A., Mota, M., and Yeshin, A.; tortuosity variation in a low density binary particulate bed. Separation and Purification Technology, 51, 180-184, 2006.

Eriksson, J. E., Maripuu, M., and Theiliander, H.; Simulation of the lime mud kiln. AIChE Annual Meeting, Conference Proceedings, 1991.

Ferron, J. R., and Singh, D. K.; Rotary kiln transport processes. AIChE Journal, 37, 747-758, 1991.

FLSMIDTH A/S; Rotary kilns for cement plants. Brochure, 2011. Available at www.flsmidth.com.

Fueller, E. N., Schettler, P. D., and Giddings, C. J.; A new method for prediction of binary gas-phase diffusion coefficients. Industrial and Engineering Chemistry, 58, 19–27, 1966.

Guo, W., Lim, C. J., Bi, X., Sokhansanj, S., and Melin, S.; Determination of effective thermal conductivity and specific heat capacity of wood pellets. Fuel, 103, 347-55, 2013.

Haas, J., and Weber, R.; Co-firing of refuse derived fuels with coals in cement kilns: Combustion conditions for stable sintering. Journal of the Energy Institute, 83, 225-34, 2010.

Hewlett, P. C.; Lea's chemistry of cement and concrete. Fourth edition. New York, 1998. ISBN: 978-0-7506-6256-7.

Ivarsson, C., and Svedin, K.; Study of the lime reburning process with biofuels. International Chemical Recovery Conference, 2007.

Kaantee, U., Zevenhoven, R., Backman, R., and Hupa, M.; Cement manufacturing using alternative fuels and the advantages of process modelling. Fuel Processing Technology, 85, 293-301, 2004.

Kuipers, J. A. M., and van Swaaij, W. P. M.; Computational fluid dynamics applied to chemical reaction engineering. Advances in Chemical Engineering, 24, 227-318, 1998.

Küssel, U., Able, D., Schumacher, M., and Weng, M.; Modeling of rotary kilns and application to limestone calcination. Proceedings 7th Modelica Conference, Como, Italy, 2009.

Levenspiel, O.; Chemical reaction engineering. Third Edition. John Wiley & Sons, 1999. ISBN: 978-0471254249.

Linjewile, T. M., Hull, A. S., and Agarwal, P.K.; Heat transfer to a large mobile particle in a gas fluidized beds of smaller particles. Chemical Engineering Science, 48, 21, 3671-3675, 1993.

Locher, G.; Modelling circulating sulfur, chlorine and alkali systems in the clinker burning process; part 2: Theory and discussion. Cement International, 7, 64-75, 2009.

Lu, J., Huang, L., Hu, Z., and Wang, S.; Simulation of the gas-solid two-phase flow, coal combustion and raw meal calcination in a pre-calciner. ZKG International, 57, 55-63, 2004.

Ma, A. C., Zhou, J. M., Ou, J. P., and Li, W. X.; CFD prediction of physical field for multi-air channel pulverized coal burner in rotary kiln. Journal of Central South University of Technology, 13, 75-9, 2006.

Mastorakos, E., Massias, A., Tsakiroglou, C. D., Goussis, D. A., Burganos, V. N., and Payatakes, A. C.; CFD predictions for cement kilns including flame modelling, heat transfer and clinker chemistry. Applied Mathematical Modelling, 23, 55-76, 1999.

Mujumdar, K. S., and Ranade, V.; Modeling of rotary cement kiln- reaction engineering and CFD. VDM erlag Dr. Müller, USA. 2009. ISBN: 978-3-639-11219-1.

Mujumdar, K. S., Ganesh, K. V., Kulkarni, S. B., and Ranade, V. V.; Rotary cement kiln simulator (RoCKS): Integrated modeling of pre-heater, calciner, kiln and clinker cooler RID A-5627-2009. Chemical Engineering Science, 62, 2590-607, 2007.

Mujumdar, K. S., and Ranade, V. V.; CFD modeling of rotary cement kilns. Asia-Pacific Journal of Chemical Engineering, 3, 106-18, 2008.

Nielsen, A. R.; Combustion of large solid fuels in cement rotary kilns. Ph.D. thesis, Technical University of Denmark, Department of Chemical and Biochemical Engineering, 2012. ISBN: 978-87-92481-66-5.

Nunn, R., Howard, J. B., Longwell, J. P., and Peters, W. A.; Product Compositions and Kinetics in the Rapid Pyrolysis of Sweet Gum Hardwood. Industrial & Engineering Chemistry Process Design and Development, 24, 836-844, 1985.

Nørskov, L. K.; Combustion of solid alternative fuels in cements kiln burners. Ph.D. thesis, Technical University of Denmark, Department of Chemical and Biochemical Engineering, 2012. ISBN: 978-87-92481-98-6.

Paschedag, A. R.; Computational Fluid Dynamics. Ullmann's Encyclopedia of Industrial Chemistry. 2005.

Pershing, D. W., Lighty, J. S., Silcox, G. D., Heap, M. P., and Owens, W. D.; Solid waste incineration in rotary kilns. Combustion Science and Technology, 93, 245-76, 1993.

Ramakrishnan, V., and Sai, P. S. T.; Mathematical modeling of pneumatic char injection in a direct reduction rotary kiln. Metallurgical and Materials Transactions B-Process Metallurgy and Materials Processing Science, 30, 969-77, 1999.

Ranade, V. V., and Mujumdar, K. S.; A CFD tour of a cement kiln. Tce, 39-41, March 2006. Available at www.tcetoday.com/.

Reina, J., Velo, E., and Puigjaner, L.; Kinetic study of the pyrolysis of waste wood. Industrial & Engineering Chemistry Research, 37, 4290-5, 1998.

Sadighi, S., Shirvani, M., and Ahmad, A.; Rotary cement kiln coating estimator: Integrated modelling of kiln with shell temperature measurement. Canadian Journal of Chemical Engineering, 89, 116-25, 2011.

Silcox, G. D., and Pershing , D. W.; The effects of rotary kiln operating conditions and design on burden heating rates as determined by a mathematical model of rotary kiln heat transfer. Journal of the Air & Waste Management Association, 40, 337-344, 1990.

Spang, H. A.; Dynamic model of a cement kiln. Automatica, 8, 309-323, 1972.

Stadler, K. S., Poland, J., and Gallestey, E.; Model predictive control of a rotary cement kiln. Control Engineering Practice, 19, 1-9, 2011.

Sullivan, J. D., Maier, C. G., and Ralston, O. C.; Passage of solid particles through rotary cylindrical kilns. US Bureau of Mines, Technical Paper 384, 1-42, 1927.

Svedin, K., Ivarsson, C., and Lundborg, R.; Lime kiln modelling. CFD & one-dimensional simulations. ÅFORSK and VÄRMEFORSK, 2009. Available at http://www.aforsk.se and http://www.varmeforsk.se/

Wang, S., Lu, J., Li, W., Li, J., and Hu, Z.; Modeling of pulverized coal combustion in cement rotary kiln. Energy & Fuels, 20, 2350-6, 2006.

Witsel, A. C., Renotte, C., and Remy, M.; New dynamic model of rotary cement kiln. 17th IMACS World Congress Scientific Computation, Applied Mathematics and Simulation, Paris, France, 2005.

Xiao, R., and Song, Q.; Characterization and kinetics of reduction of $CaSO_4$ with carbon monoxide for chemical-looping combustion. Combustion and Flame, 158, 2524-39, 2011.

Yang, Y., Pijnenborg, M. J. A., Reuter, M. A., and Verwoerd, J.; Combustion modeling of a rotary-kiln hazardous waste incinerator. 23rd Proceedings of the Annual International Conference on Incineration and Thermal Treatment Technologies, United States, 2004.

8. Model on Build-ups Tendency in the Kiln System

A model to predict the tendency of build-ups of a kiln system caused by sulfur and chlorine evaporation and condensation will be described in this chapter. The description of the system is explained in section 8.1, followed by the assumptions, and the model development. Two cases are considered; first when the kiln system operates with fuel in the calciner and kiln burner, and secondly, when the kiln system operates with alternative fuels substitution in the kiln inlet and the corresponding sulfur evaporation factor, calculated in Chapter 7, will be combined in this model.

8.1 Introduction

When partially converted or unburned alternative fuels drop into the material bed in the inlet of the rotary kiln, the sulfur may be released from the material bed contributing to a higher internal recirculation of sulfur. Deposit build-ups, which negatively affect the process stability of the kiln system, are a consequence of the internal recirculation of volatile constituents, as explained in Chapter 4.

The aim of the model of the build-up tendency in the kiln system is to predict the content of sulfur and chlorine in the hot meal, which is subsequently used to evaluate the risk of build-up formations in the calciner according to Figure 4-12 in Chapter 4.

The model is based on a mass balance of sulfur and chlorine around the preheater tower and the calciner. The input sources of sulfur and chorine are the raw meal, and the fuel fired in the calciner and in the kiln burner. In the burning zone of the kiln, chlorine and sulfur evaporation from the raw materials takes place due to thermal degradation. The fraction evaporated and the input from the kiln burner can partly be absorbed in the kiln and the remaining part is absorbed in the calciner by *fresh* raw meal. Then the concentrations of SO_3 and Cl in the hot meal are calculated which re-enters the rotary kiln and the calculation steps are repeated until these concentrations do not change from iteration to iteration, reaching a steady-state. When considering alternative fuel substitution in the kiln inlet, sulfur evaporation takes place both in the kiln inlet due to reducing conditions and in the burning zone due to thermal decomposition.

The input and output solid mass flows in the kiln system are specified in Figure 8-1. The solid mass flows can be from raw material (black), dust transported with the gas flow (red), and fuel ashes (green) that can be incorporated in the material.

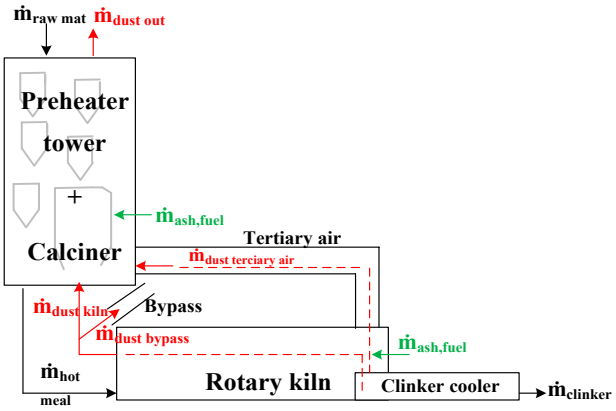

Figure 8-1: Schematic kiln system with the mass flows of raw material (black), dust (red) and the ashes introduced by the fuel (green) specified.

In order to simplify the mass flow system, it is assumed that the sulfur and chlorine of the fuel is included in the model as inputs to the gas phase. Furthermore, the mass contribution of the dust from the tertiary air is already included in the calculations of the hot meal mass flow. A simple scheme of the considered model system with the gas and solid flows is therefore illustrated in Figure 8-2, where the control volume of the model is indicated by the green dotted line.

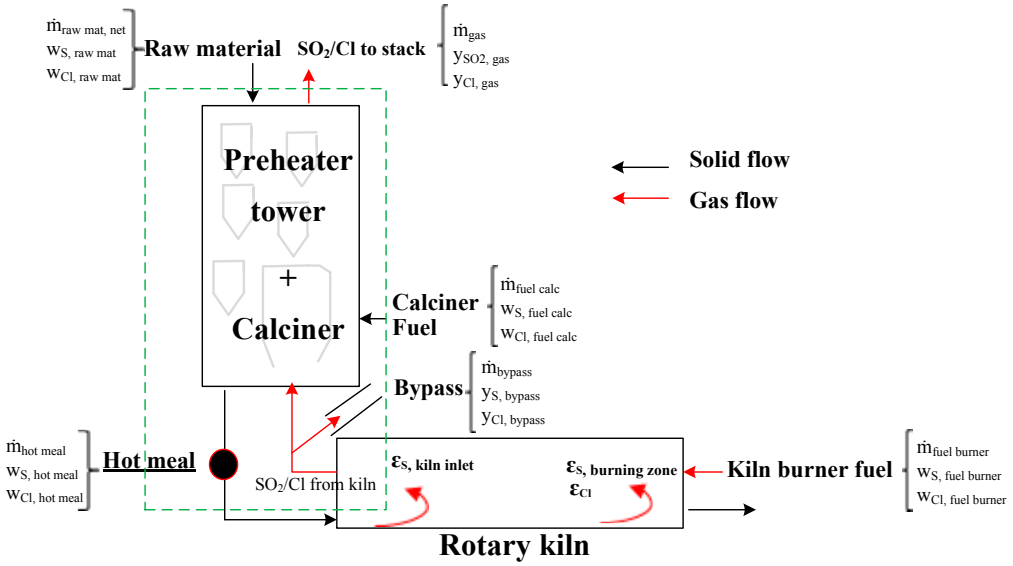

Figure 8-2: Simplified scheme of the kiln system with the gas and solid flows and the concentrations of S and Cl that enters and exist the system. The boundaries of model are indicated by the green dotted line.

8.2 Kiln System without Alternative Fuel Substitution in the Kiln Inlet

8.2.1 Model Development

The model can be schematically summarized in different steps, as illustrated in Figure 8-3.

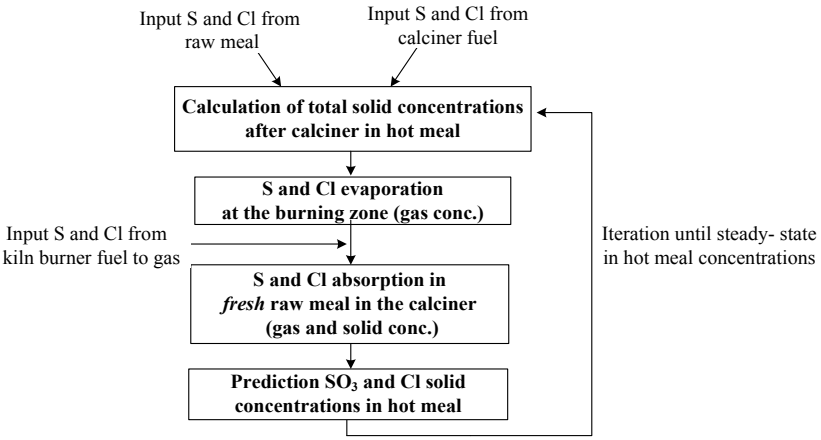

Figure 8-3: Scheme of the modeling steps for determining the SO_3 and Cl concentrations in the hot meal when the kiln system does not have alternative fuel substitution in the kiln inlet.

The input sulfur and chlorine concentrations of the raw meal are recalculated on basis of loss on ignition (LOI) free according to equation 8.1.The weight fraction on basis of loss of ignition free, $w_{i,LOIfree,\ raw\ mat}$, allows their comparison at different locations, after and before calcination.

$$w_{j,LOI\,free,raw\,mat} = \frac{w_{j,raw\,mat} \cdot 100}{(100 - LOI_{raw\,mat})} \qquad \text{where } j\text{= S or Cl} \qquad [8.1]$$

where $w_{j,raw\ mat}$ is the sulfur or chlorine concentration in the raw meal in wt. %, and $LOI_{raw\ mat}$ is the percentage of loss on ignition of the raw meal.

It is considered that a fraction of the sulfur present in the raw meal leaves the preheater tower and is emitted through the stack. In a preheater kiln, it has been estimated that SO_2 emissions from the stack will count 15-30 % of the sulfur entering with the raw materials in the form of non-sulfates, i.e. pyrite and organic sulfur (Nielsen and Jepsen, 1990). Chlorine can also be released in the stack as HCl, however, due to a lack of reported values in the literature a fraction of 10 % of the chlorine entering with the raw materials is assumed.

The total sulfur and chlorine input, $\dot{m}_{S,total\ input}$ and $\dot{m}_{Cl,total\ input,}$ from the raw materials and calciner fuel are determined, by equations 8.2 and 8.3, taking into account the respective mass flows and the fractions that leaves the preheater tower as SO_2 or HCl.

$$\dot{m}_{S,total\,input} = \dot{m}_{raw\,mat,LOI\,free} \cdot \frac{\left(w_{S,LOI\,free,raw\,mat}(1-\gamma_s)\right)}{100} + \dot{m}_{fuel,calc} \cdot \frac{w_{S,fuel}}{100} \quad [8.2]$$

$$\dot{m}_{Cl\,total\,input} = \dot{m}_{raw\,mat,LOI\,free} \cdot \frac{\left(w_{Cl,LOI\,free,raw\,mat}(1-\gamma_{Cl})\right)}{100} + \dot{m}_{fuel,calc} \cdot \frac{w_{Cl,fuel}}{100} \quad [8.3]$$

where $w_{S,fuel}$ and $w_{Cl,fuel}$ are the sulfur and content of the calciner fuel in wt. %, respectively, $\dot{m}_{rawmat,\,LOI\,free}$ is the net mass flow of the raw meal LOI free when introduced in the preheater in kg/h, $\dot{m}_{fuel,\,calc}$ is mass flow of the fuel introduced in the calciner in kg/h, and γ_S and γ_{Cl} are the fraction of sulfur and chlorine, respectively, which leaves the preheater tower.

The net raw meal mass flow is calculated by the difference of the feed raw meal flow and the flow of dust loss out of the preheater. In order to this be valid, it is assumed that the same concentration of sulfur and chlorine that enters with the feed raw meal flow is the same in the flow of dust loss.

The recirculation of volatiles from the rotary kiln is included in the model by defining a sulfur evaporation factor, ε_S, a chlorine evaporation factor, $\varepsilon_{Cl,}$ and a kiln sulfur absorption factor, β_S. The iteration process starts by calculating the sulfur that evaporates in the kiln, $\dot{n}_{Sevap,\,i}$, that enters the model system by the gas stream. For the first iteration (i=1), the sulfur and chlorine molar flows correspond to the raw meal and for the following iterations ($i \geq 2$), the molar flows corresponds to the hot meal. This is mathematically expressed as following where *i* is the number of iterations and N is the total number of iterations.

For $i = 1$ $\quad \dot{n}_{S,\,i=1} = \dot{n}_{S,\,raw\,meal} = \dot{n}_{S,tota\,linput}$ and $\dot{n}_{Cl,\,i=1} = \dot{n}_{Cl,total\,input}$

For $i \geq 2$ to N $\quad \dot{n}_{S,\,i\geq2} = \dot{n}_{S,\,hot\,meal} = \dot{n}_{S,i}$ and $\dot{n}_{Cl,\,i\geq2} = \dot{n}_{Cl,i}$

The sulfur that evaporates in the burning zone is calculated according to equation 8.4 by taking into account the sulfur evaporation factor, the sulfur input from the kiln burner fuel, $\dot{n}_{S,burner}$, which is calculated by the sulfur content and the mass flow of the fuel, and the kiln absorption of sulfur.

$$\dot{n}_{Sevap,i} = \left(\dot{n}_{S,i} \cdot \varepsilon_S + \dot{n}_{S,burner}\right) \cdot (1-\beta_S) \qquad \text{for } i = 1 \text{ to N} \quad [8.4]$$

For chlorine, it is assumed that there is no absorption in the kiln inlet due to its high volatility, however, this phenomena has not been reported and may be difficult to quantify it due to the inaccessibility of the rotary kiln during operation. The chlorine that evaporates is thereby determined by equation 8.5.

$$\dot{n}_{Clevap,i} = \dot{n}_{Cl,i} \cdot \varepsilon_{Cl} + \dot{n}_{Cl,burner} \qquad \text{for } i = 1 \text{ to N} \quad [8.5]$$

In the calciner, the sulfur in the kiln gas stream is fully absorbed by *fresh* calcined raw meal (Rasmussen, 2011), and the chlorine fully condenses in the *fresh* calcined raw meal (Jøns et al., 2008). The *fresh* calcined

raw meal refers to raw meal that contains the total input of sulfur and chlorine from the raw materials and calciner fuel. Subsequently, the molar concentration of sulfur and chlorine in the hot meal (for i≥2) can be calculated by equation 8.6 and 8.7.

$$\dot{n}_{S,i+1} = \dot{n}_{S,total\,input} + \dot{n}_{S\,evap,i} \qquad \text{for } i = 1 \text{ to N} \qquad [8.6]$$

$$\dot{n}_{Cl,i+1} = \dot{n}_{Cl,total\,input} + \dot{n}_{Cl\,evap,i} \qquad \text{for } i = 1 \text{ to N} \qquad [8.7]$$

Then, the iteration process will continue by recalculating the $\dot{n}_{S,evap}$ and $\dot{n}_{Cl,evap}$ (equation 8.4 and 8.5) followed by determining a new molar concentration of sulfur and chlorine in the hot meal (equation 8.6 and 8.7). When this sulfur and chlorine concentration in the hot meal do not change from iteration to iteration, the system has reached steady-state and hot meal concentrations are determined by converting into mass flows multiplying by the molar mass of SO_3 and Cl, respectively.

Finally, the SO_3 and Cl concentrations in the hot meal, $w_{SO3,hot\,meal,\,LOI\,free}$ and $w_{Cl,hot\,meal,\,LOI\,free}$, in wt. % LOI free basis, are determined by equation 8.8 and 8.9.

$$w_{SO_3,hot\,meal,LOI\,free} = \left(\frac{\dot{m}_{SO_3,hot\,meal}}{\dot{m}_{hot\,meal}} \cdot 100 \right) \cdot \left(\frac{100}{100 - LOI_{hot\,meal}} \right) \qquad [8.8]$$

$$w_{Cl,hot\,meal,LOI\,free} = \left(\frac{\dot{m}_{Cl,hot\,meal}}{\dot{m}_{hot\,meal}} \cdot 100 \right) \cdot \left(\frac{100}{100 - LOI_{hot\,meal}} \right) \qquad [8.9]$$

where $\dot{m}_{SO3,hot\,meal}$ and $\dot{m}_{Cl,hot\,meal}$ are the molar flows of SO_3 and Cl in the hot meal in kg/h, $\dot{m}_{hot\,meal}$ is the mass flow of the hot meal in the bottom cyclone in kg/h, and $LOI_{hot\,meal}$ is the percentage of loss on ignition of the hot meal. Finally, the tendency of build-ups can be evaluated by using these concentrations.

The effect of chlorine removal by a bypass can also be included in the model by including a calculation step. The bypass, as mentioned in Chapter 4, is installed with the main purpose to remove chlorine, however, SO_2 may also be extracted with the kiln gases removed. Assuming a uniform concentration of the gas phase, the model also includes that the sulfur as SO_2 is removed by the bypass. The sulfur and chlorine that evaporate, calculated by equation 8.7 and 8.8, respectively, are used to determine the chlorine that condenses and the sulfur that absorbs in the hot meal by equation 8.10 and 8.12, respectively, taking into account that a gas fraction will be removed with a bypass. A bypass absorbed factor, ϕ, is defined, which is directly related to the bypass size that is normally specified as a percentage of the kiln gases removed. Subsequently, the sulfur and chlorine in the hot meal, calculated according to equations 8.11 and 8.13, expresses the chlorine condensation and the sulfur absorption in the hot meal. These steps are repeated in each iteration process to

achieve the SO_3 and Cl concentration in the hot meal. When the system reaches steady-state, the SO_3 and Cl concentrations in the hot meal are determined by equation 8.8 and 8.9, respectively.

$$\dot{n}_{Cl\,\mathrm{conds},i} = \dot{n}_{Cl\,evap,i} \cdot (1-\phi) \qquad \text{for } i\text{= 1 to N} \qquad [8.10]$$

$$\dot{n}_{\mathrm{Cl},\,i+1} = \dot{n}_{Cl,\mathrm{totalinput}} + \dot{n}_{Cl\,cond,i} \qquad \text{for } i\text{= 1 to N} \qquad [8.11]$$

$$\dot{n}_{S\,abs,i} = \dot{n}_{S\,evap,i} \cdot (1-\phi) \qquad \text{for } i\text{= 1 to N} \qquad [8.12]$$

$$\dot{n}_{\mathrm{S},\,i+1} = \dot{n}_{S,\mathrm{totalinput}} + \dot{n}_{S\,abs,i} \qquad \text{for } i\text{= 1 to N} \qquad [8.13]$$

8.2.2 Results

A cement plant with a clinker production of 3500 tons per day with an energy consumption of 2.993 MJ/kg clinker is considered the base for the calculations. The input parameters used for the model are specified in Table 8-1. The sulfur and chlorine content in the calciner and kiln burner fuel is typical for a low sulfur petcoke, however, it could also represent another fuel.

The fuel flows in the calciner and in the kiln burner, in kg/h, are determined by the energy required in each place, which is 60 % in the calciner and 40 % in the kiln burner, and the lower heating value of the fuel. The raw materials and hot meal flow and loss of ignition are chosen to be typical values in the cement industry; however, these values can vary depending on the type and origin of the different raw materials.

The sulfur and chlorine inputs in the raw materials are the recommended upper limits to introduce in the kiln system. The sources specify these limits are normally specified in loss of ignition free based, but these values have been converted to use as defined in this model.

The sulfur and the chlorine evaporation factors can vary between 0.3 and 0.7 and from 0.90 to 0.99, respectively, as previously mentioned in Chapter 4. The values of these parameters have been assumed in their typical range, however, the parameters depend significantly on other process variables, such as temperature in the burning zone and oxygen content in the kiln and this is not considered in the present model.

In order to check the mass balance, the mass flows of the raw meal and hot meal are calculated in loss of ignition free based, which allows their comparison at different locations, after and before calcination. In Figure F-1 in Appendix F, the typical material feed, hot meal and dust loss are specified.

Table 8-1: Input parameters for the model on build-ups tendency in the kiln system.

Parameter	Symbol	Value	Reference
Sulfur in raw materials [wt. %]	$w_{S,raw\ mat}$	0.05	(Hewlett, 1998)
Chlorine in raw materials [wt. %]	$w_{Cl,raw\ mat}$	0.01	(Norbom, 1973)
Raw materials flow [kg/kg clinker]	$F_{raw\ mat}$	1.602	Industrial relevant value
LOI of raw meal, 975 ^{o}C [wt. %]	$LOI_{raw\ mat}$	36.1	Industrial relevant value
Sulfur fraction that leaves the preheater [-]	γ_S	0.3	(Nielsen and Jepsen, 1990)
Chlorine fraction that leaves the preheater [-]	γ_{Cl}	0.1	Assumed
Fuel lower heating value [MJ/kg]	LHV	30	(Milenkova et al., 2003)
Sulfur in calciner fuel [wt. %]	$w_{S,fuel\ calc}$	5.00	(Milenkova et al., 2003)
Chlorine in calciner fuel [wt. %]	$w_{Cl,fuel\ calc}$	0.001	Assumed
Calciner fuel flow [kg/h]	$\dot{m}_{fuel,calc}$	8725	Calculated
Sulfur in kiln burner fuel [wt. %]	$w_{S,fuel\ burner}$	5.00	(Milenkova et al., 2003)
Chlorine in kiln burner fuel [wt. %]	$w_{Cl,fuel\ burner}$	0.001	Assumed
Kiln burner fuel flow [kg/h]	$\dot{m}_{fuel\ burner}$	5816	Calculated
Sulfur evaporation factor [-]	ε_S	0.60	(Bhatty et al., 2011)
Chlorine evaporation factor [-]	ε_{Cl}	0.95	(Jøns et al., 2008)
Kiln sulfur absorption factor [-]	β_S	0.1	Assumed
Hot meal flow [kg/kg clinker]	$F_{hot\ meal}$	1.27	Industrial relevant value
LOI of hot meal, 975 ^{o}C [wt. %]	$LOI_{hot\ meal}$	5	Industrial relevant value
Bypass absorbed factor [-]	Φ	0.15	(Jøns et al., 2008)

The output of the model is the predicted SO_3 and Cl content in the hot meal. For the parameters in Table 8-1, the SO_3 and Cl content are 2.45 and 0.83 wt. %, respectively. Figure 8-4 shows the result obtained, indicated by a blue cross in the diagram for predicting the tendency of build-ups. Furthermore, when the bypass absorbed factor is introduced for a new calculation, the chlorine condensation and the sulfur absorption in the calciner are reduced as illustrated by a red star in Figure 8-4. With bypass, the SO_3 and Cl concentrations in the hot meal obtained are 1.98 and 0.19 wt. %, respectively.

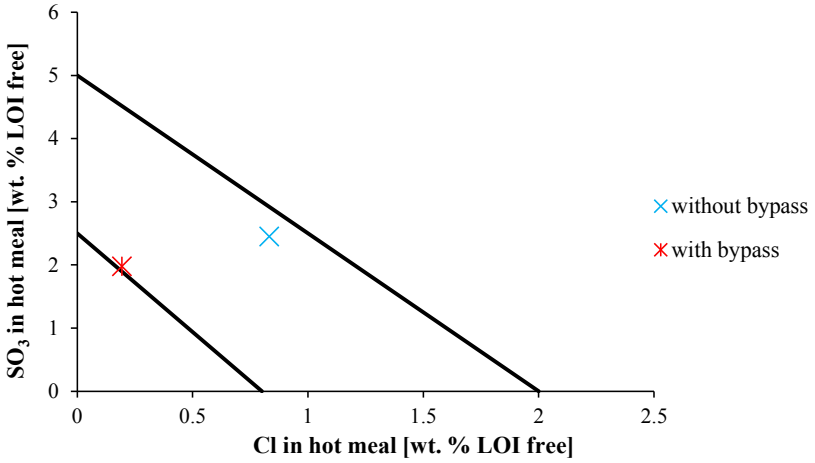

Figure 8-4: Prediction of SO_3 and Cl content in the diagram of build-up tendency for the initial conditions (without bypass) and with bypass operation (ϕ=0.15).

According to the definitions of the zones in the graph, the cement plan without bypass will have a medium tendency of build-up and with bypass a medium build-up tendency, quite close to the low tendency area.

A sensitivity analysis of the individual parameters has been carried out in order to investigate the effect of the parameters on the SO_3 and Cl content of the hot meal. The sulfur and chlorine input concentrations and evaporation factors have been investigated. Each input parameter is changed with +/- 25 % while keeping the remaining parameters constant, except for the chlorine evaporation, which has tested for the interval limits of its variation. Table 8-2 summarizes the variation input values and the output results obtained in each case specifying SO_3 and Cl concentration in hot meal and in which zone of the build-up tendency diagram that scenario belongs. Furthermore, the deviation from the output results obtained by the initial case is determined in order to evaluate the influence of the parameter.

The results show that chlorine evaporation factor has the largest influence on the output variables with 400 % deviation on the Cl concentration compared to the reference case when the chlorine evaporation factor was 0.99. The variation of the sulfur evaporation factor greatly influences the SO_3 concentration with -23 % and 42 % deviation when the input is varied -/+ 25 %. The ranking is followed by the sulfur concentration in the calciner fuel (with almost +/- 14 % deviation) and in the kiln burner (with -/+ 8 % deviation). On the contrary, the chlorine input in the calciner fuel and the sulfur content in the raw materials content do not influence significantly to output results. The bypass reduces significantly the chlorine circulation even when the chlorine evaporation factor is maximum. The actual uncertainty of the sulfur and chlorine in the fuels may be higher than -/+ 25 % variation, depending on the homogeneity of the used fuel. The uncertainty of the sulfur and

chlorine evaporation factor may also be higher if there is high variations on the process conditions, such as the oxygen concentration in the kiln and the burning zone temperature.

Table 8-2: Sensitivity analysis of the build-up tendency model on the SO_3 and Cl concentrations in the hot meal. Note:* +/-25 % variation of the initial value has not applied, the interval limits of the chlorine evaporation factor has been chosen.

Input parameters		**Output variables**			**Deviation [%]**	
	Variation +/- 25 %	SO_3 [wt. % LOI free]	Cl [wt. % LOI free]	Build-up tendency zone	SO_3 conc.	Cl conc.
Sulfur in raw materials [wt. %]	0.0375	2.37	0.83	Medium	-2.98	0.00
	0.0625	2.52	0.83	Medium	2.98	0.00
Chlorine in raw materials [wt. %]	0.0075	2.45	0.77	Medium	0.00	-7.46
	0.0125	2.45	0.89	Medium	0.00	7.46
Sulfur in calciner fuel [wt. %]	3.75	2.11	0.83	Medium	-13.76	0.00
	6.25	2.78	0.83	Medium/High	13.76	0.00
Chlorine in calciner fuel [wt. %]	0.0008	2.45	0.83	Medium	0.00	-0.03
	0.0013	2.45	0.83	Medium	0.00	0.03
Sulfur in kiln burner [wt. %]	3.75	2.25	0.83	Medium	-8.26	0.00
	6.25	2.65	0.83	Medium	8.26	0.00
Chlorine in kiln burner fuel [wt. %]	0.0008	2.45	0.69	Medium	0.00	-17.5
	0.0013	2.45	0.98	Medium/High	0.00	17.5
Sulfur evaporation factor	0.45	1.89	0.83	Medium	-22.69	0.00
	0.75	3.46	0.83	High	41.54	0.00
Chlorine evaporation factor*	0.9	2.45	0.42	Medium	0.00	-50.0
	0.99	2.45	4.16	High	0.00	400
When Φ=0.15						
Sulfur evaporation factor	0.45	1.63	0.19	Low	-17.50	0.00
	0.75	2.51	0.19	Medium	26.92	0.00
Chlorine evaporation factor*	0.90	1.98	0.16	Low/Medium	0.00	-18.1
	0.99	1.98	0.23	Medium	0.00	21.5

8.3 Kiln System with Alternative Fuel Substitution in the Kiln Inlet

8.3.1 Model Modification

When alternative fuels are fired in the kiln inlet, sulfur evaporation also takes place in the kiln inlet and thereby the steps needed to determine the SO_3 concentration in the hot meal can be summarized in Figure 8-5. The model steps for the calculation of the Cl concentration in the hot meal are not modified, since the chlorine is not affected by the combustion of alternative fuels in contact with the kiln bed material.

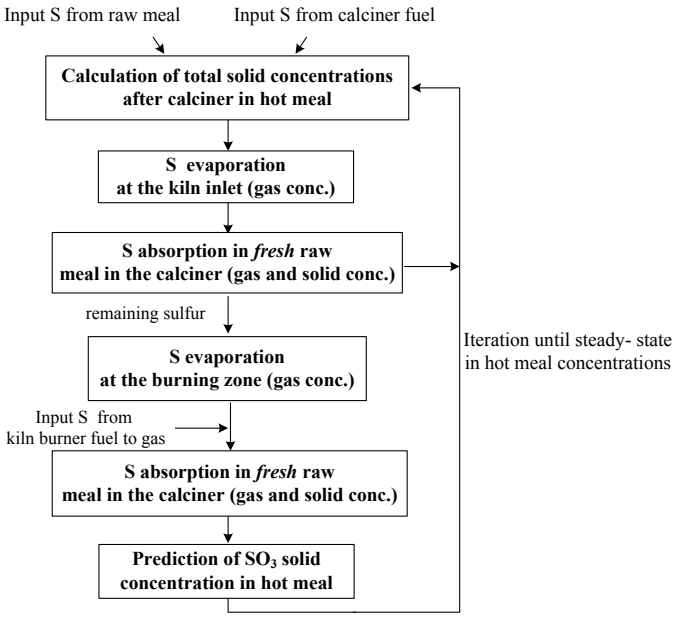

Figure 8-5: Scheme of the modeling steps for determining the SO_3 concentration in the hot meal when the kiln system has alternative fuel substitution in the kiln inlet.

The total sulfur from the raw materials and fuel are determined using the same procedure explained in section 8.2.1 (equations 8.1, and 8.2). Due to alternative fuels firing in the kiln inlet, the sulfur evaporation at the kiln inlet, $\dot{n}_{S,evap\ inlet}$, is described for each iteration according to equation 8.14, where $\varepsilon_{S,\ inlet}$ is the sulfur evaporation factor in the kiln inlet obtained in Chapter 7. The sulfur evaporated in the kiln inlet is assumed that cannot be absorbed along the rotary kiln because the gas will flow towards the calciner.

$$\dot{n}_{S\,evap\,inlet,i} = \dot{n}_{S,i} \cdot \varepsilon_{S,inlet} \qquad \text{for } i\text{= 1 to N} \qquad [8.14]$$

The remaining sulfur in the solid bed material inside the rotary kiln, $\dot{n}_{S,remaining}$, is calculated by the difference of the sulfur input in the raw meal (i =1) or hot meal ($i \geq 2$) and the sulfur evaporated in the kiln inlet (equation 8.15).

$$\dot{n}_{S remaining,i} = \dot{n}_{S,i} - \dot{n}_{S\,evap\,inlet,i} \qquad \text{for } i\text{= 1 to N} \qquad [8.15]$$

The remaining sulfur can evaporate in the burning zone of the rotary kiln and the sulfur from the kiln burner fuel also contributes to the gas phase SO_2. The sulfur evaporated in the burning zone may also be absorbed along the kiln. Therefore, the sulfur evaporation at the burning zone, $\dot{n}_{S\ evap\ end}$, is mathematically determined by equation 8.16.

$$\dot{n}_{S\,evap\,end,i} = (\dot{n}_{S\,remaining,i} \cdot \varepsilon_S + \dot{n}_{S,burner}) \cdot (1 - \beta_S) \qquad \text{for } i\text{= 1 to N} \qquad [8.16]$$

The sulfur in the hot meal can finally be determined by equation 8.17. Then, equations 8.14, 8.15, 8.16, and 8.17 are recalculated until the system reach steady-state by reaching a stable value of the sulfur molar flow.

$$\dot{n}_{S,i+1} = \dot{n}_{S,totalinput} + \dot{n}_{S\,evap\,inlet,i} + \dot{n}_{S,evap\,end,i} \qquad \text{for } i\text{= 1 to N} \qquad [8.17]$$

A large number of iterations are needed to reach a stable sulfur concentration in the hot meal since the sulfur recirculation is increased significantly in the initial iterations.

8.3.2 Results

It is considered that 10 % of the energy required for cement production from the calciner is substituted fuel fired in the kiln inlet. The fuel used consist of wood particles of 1 g each, which does not contain neither sulfur nor chlorine. In Chapter 7, a sulfur evaporation factor of 0.04 was obtained for this scenario. Using the initial input parameters specified in Table 8-1 and the sulfur evaporation factor in the kiln inlet, the SO_3 and Cl concentrations in the hot meal are 2.55 and 0.83 wt. %, respectively. A cement plant operating under these conditions will experience a high build-up tendency, as shown in Figure 8-6.

When firing alternative fuels in the kiln inlet, the calciner fuel flow is typically reduced in order to avoid too high calciner temperature. Then, a 10 % of the calciner fuel flow is reduced, from 8725.4 kg/h to 7852.8 kg/h, and the SO_3 and Cl concentrations in the hot meal correspond to 2.41 and 0.83 wt. %, respectively.

Introducing the bypass absorbed chlorine factor, ϕ=0.15 and using 7852.8 kg/h calciner fuel, the SO_3 and Cl concentrations in the hot meal obtained are 1.94 wt. % and 0.19 wt. %, respectively. Figure 8-6 shows that the results of these scenarios are in the medium tendency zone in the diagram of build-up tendency.

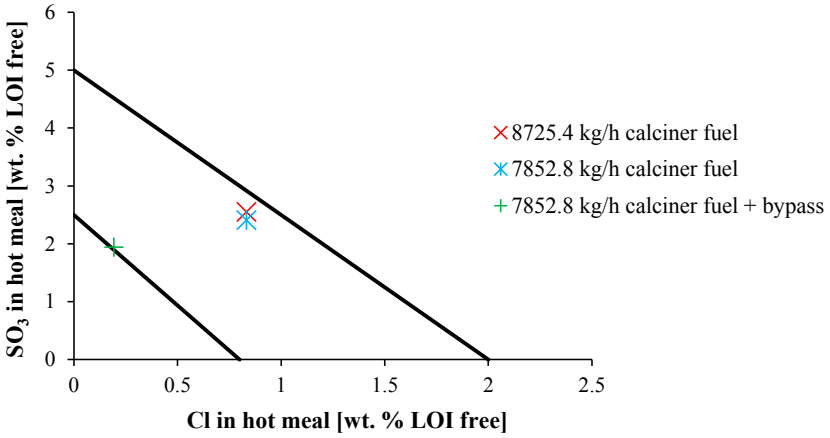

Figure 8-6: Prediction of SO_3 and Cl content in the diagram of build-up tendency for the initial conditions (without bypass) plus firing alternative fuels in the kiln inlet causing a sulfur evaporation factor of 0.04, when the calciner fuel flow is reduced 10 % and when bypass is included.

A sensitivity analysis of the SO_3 and Cl content of the hot meal, when the calciner fuel flow is reduced 10 % (7852.8 kg/h), is conducted using the same procedure as in section 8.2.2 by changing one parameter at the time with +/- 25 % and compare it with the initial case. However, only the sulfur input parameters are studied since the alternative fuels firing in the kiln inlet does not modify the chlorine cycle.

Table 8-3: Sensitivity analysis of the build-up tendency model on the SO_3 concentration in the hot meal when firing alternative fuels in the kiln inlet causing sulfur evaporation.

Input parameters		**Output variables**		**Deviation [%]**
	Variation +/- 25 %	SO_3 [wt. % LOI free]	Build-up tendency zone	SO_3 conc.
Sulfur in raw materials [wt. %]	0.0375	2.33	Medium	-3.15
	0.0625	2.49	Medium	3.15
Sulfur in calciner fuel [wt. %]	3.75	2.09	Medium	-13.1
	6.25	2.73	Medium	13.1
Sulfur in kiln burner fuel [wt. %]	3.75	2.20	Medium	-8.74
	6.25	2.62	Medium	8.74
Kiln inlet sulfur evaporation factor	0.03	2.40	Medium	-0.26
	0.05	2.47	Medium	2.40
Burning zone sulfur evaporation factor	0.45	1.86	Medium	-22.7
	0.75	3.41	High	41.5

The sensitivity analysis show that the sulfur evaporation factor at the burning zone is the most influencing parameter to the SO_3 concentration in the hot meal with a -23 % and 41 % deviation to the reference case when the input is changed -/+ 25 % of its value. The ranking is followed by the sulfur input in the calciner fuel (with

+/- 13 % deviation) and in the kiln burner fuel (with almost +/- 9 % deviation). The variation of the kiln inlet sulfur evaporation factor does not give a significant variation in the SO_3 in the hot meal. However, the actual uncertainty of this input parameter may depend on the fuel type, particle size and degree of coverage and may contributed with higher kiln inlet sulfur evaporation factor value.

8.4 Model Limitations

The model developed for prediction of the build-up tendency in the kiln system does not consider the interaction of alkali with sulfur and chlorine, which may influence the volatile cycles.

The dust recirculation in the preheater tower and the efficiency of each cyclone are taken into account indirectly by the material flows in the inlet and outlet of the preheater tower. Furthermore, the sulfur and chlorine content in the dust may be different than in the material flow in each cyclone stage, and this effect is not included in the model.

The model does not included that the alternative fuel fired in the kiln inlet contributes with sulfur and chlorine inputs. These contributions may need to be further implemented because many of alternative fuels contain sulfur and/or chlorine, as showed in Table 3-2. Furthermore, it was assumed that the mass flow and that the sulfur and chlorine in the calciner and burner fuels are inputs to the gas phase, and thereby the fuel ash is not accounted in the mass balance. To use a solid fuel in the model, it is necessary to take into account the fuel ash contribution to the hot meal flow and subsequently to the clinker. However, this limitation will not influence so much the model results because if it is assumed that the used calciner fuel has 0.5 wt. % ash, the ash mass will contribute to 4362.5 kg/h, which is a 2.92 % of the raw material flow.

The model does not determine either the clinker quality in respect to SO_3 and Cl or the emissions in stack or bypass, because the gas flow is normally used in the mill and it is out of the purpose of this model.

8.5 Conclusions

A model to predict the tendency of build-ups of a kiln system based on the SO_3 and Cl concentrations in the hot meal has been developed. The model gives realistic results because the output concentrations are in the range expected.

Results are obtained specifying the sulfur and chlorine content in the raw material and calciner fuel, and the sulfur and chlorine evaporation factors. For a cement plant with 3500 tons per day without bypass using raw materials with 0.05 wt. % S and 0.01 wt. % Cl and fuel with 5 wt. % S and 0.001 wt. % Cl, the tendency of build-ups predicted was in the medium/high line, while using bypass the tendency of build-ups was medium, close to the low region. A sensitivity analysis was performed in order to investigate the effect of the parameters on the SO_3 and Cl content of the hot meal and showed that the chlorine evaporation factor has the largest

influence with almost 400 % deviation on the Cl concentration when the evaporation factor was 0.99 as opposed to the reference case of 0.95. On the contrary, the modification on the chlorine content in the calciner fuel did not varied the output results and sulfur content in the raw material influenced only with -/+ 4 % deviation at a 25 % input variation.

When alternative fuels are fired in the kiln inlet, sulfur evaporation at the kiln inlet is taken into account as well as the sulfur evaporation at the burning zone. The results showed that the plant will experience medium tendency build-ups, except when operating with bypass. The sensitivity analysis results show that the sulfur evaporation factor at the burning zone is the most influencing parameter to the SO_3 concentration in the hot meal with a -23 % and 41 % deviation at an input variation of 25 %, while the variation of the kiln inlet sulfur evaporation factor has a small effect on the output.

When the bypass chlorine absorption factor is considered in the model, the chlorine concentration in the hot meal is significantly reduced both with and without firing alternative fuels in the kiln inlet.

The model is limited by not taking the alkali interaction, dust recirculation in the preheater tower, and the sulfur and chlorine input from the fuel fired in the kiln inlet into account.

8.6 References

Bhatty, J. I., Miller, F. M., and Kosmathka, S. K.; Innovations in Portland cement manufacturing. Illinois, USA. 2011. ISBN: 978-0893122713.

Hewlett, P. C.; Lea's chemistry of cement and concrete. Fourth edition. New York. 1998. ISBN: 978-0-7506-6256-7.

Jøns, E., Hundebol, S., and Clausen, K.; New reasons for installing a chloride by-pass. Interaction between chloride and sulphur. IEEE Cement Industry Technical Conference Record, 178-92, 2008.

Milenkova, K. S., Borrego, A. G., Alvarez, D., Xiberta, J., and Menendez, R.; Devolatilisation behaviour of petroleum coke under pulverised fuel combustion conditions. Fuel, 82, 1883-91, 2003.

Nielsen, P. B., and Jepsen, O. L.; An overview of the formation of SO_x and NO_x in various pyroprocessing systems. IEEE Cement Industry Technical Conference XXXII, 255-76, 1990.

Norbom, H.R.; Application of Suspension Preheater Kilns versus Other Kilns in North America, Proceedings of the IEEE, Cement Industry Technical Conference, Miami, USA, 1973.

Rasmussen, M. H.; Low SO_2 emission preheaters for cement production. Ph.D. thesis, Technical University of Denmark, Department of Chemical and Biochemical Engineering, 2011. ISBN: 978-87-92481-59-7.

9. Industrial Experience on Sulfur Release

The purpose of this chapter is to study the sulfur release in the kiln inlet on an industrial plant, which fires alternative fuels in the calciner and the kiln riser.

The aim of the industrial study was to investigate the relationship between organic carbon in the last cyclone (bottom stage cyclone) and SO_2 in the gas phase in the kiln inlet, because the organic carbon from the hot meal is believed to be directly related to unburned calciner fuel. Unburned light fuel particles can be carried upwards with the gas flow through the calciner and transported into the bottom stage cyclone. The char particles may arrive to the kiln inlet and their subsequently combustion may cause the release of sulfur.

The investigation was carried out by analysis of hot meal samples and process data from an industrial cement plant. Multicomponent gas measurements were compared with the stationary measurement equipment of the cement plant in order to support the investigations of sulfur release during combustion in the kiln inlet.

The chapter starts with a description of the plant, such as the system design, the fuels used, and a description of the tests performed. Section 9.2 describes the two gas measurements systems used in the kiln inlet and compares their results. The investigation of sulfur evaporation from the process is explained in section 9.3, which includes the organic carbon results from the hot meal samples and analyses of the calciner fuel conversion, the tendency of build-ups, and the sulfur volatility. Finally, the conclusions of the industrial experience and the challenges encountered in the sulfur release study are described.

9.1 Background

The cement plant, where the investigation was carried out, has two separate line calciners. The strings, named string A and B, are identical and consist of a calciner and three cyclones, as shown schematically in Figure 9-1. The raw materials used are wet and form a slurry, which is introduced into the dryer crusher of each stream where the slurry is dried and ground. The dry raw materials are then carried upwards to the top cyclone by the gas stream. The gases in the preheater tower are bypassed from the second cyclone to the dryer crusher before going to the top cyclone, which works as gas/dust separator. The hot air from the clinker cooler goes to the calciner and the rotary kiln gases are mixed with the calciner outlet gases. The plant produces mineralized clinker, which means that 0.13 wt. % fluoride on clinker basis is added in the kiln inlet, which allows lowering the burning temperature in the kiln.

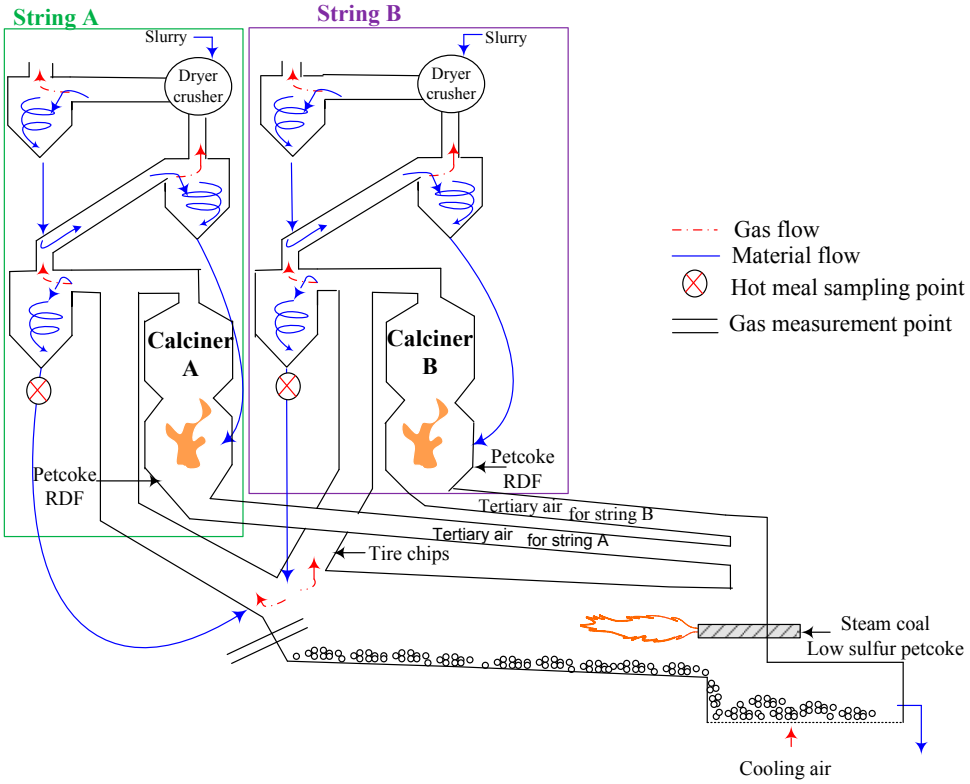

Figure 9-1: Scheme of the industrial cement plant where the investigation took place. Not to scale.

The fuels used in both calciners are petcoke and plastic/paper-based refused derived fuel (RDF). Sometimes, tire chips are fired in the riser duct from 2 meters above the kiln inlet. The fuel analyses of petcoke, RDF, and tire chips are specified in Table 9-1, where a.r. denotes as received.

Table 9-1: Fuel analyses and lower heating values (LHV) of petcoke, RDF, and tire chips that the cement plant used in the calciner and riser duct. Notes: [1]Volatile matter, [2] Fixed carbon.

Fuel	Moisture [wt. % a.r.]	Proximate analysis [wt. % a.r.]			Ultimate analysis [wt. % a.r.]					LHV [MJ/kg]
		VM[1]	FC[2]	Ash	C	H	N	Cl	S	
Petcoke	1.1	13.0	84.9	1.0	86.9	3.71	-	-	5.85	35.183
RDF	24.1	61.6	6.6	7.7	45.8	6.31	0.67	0.54	0.40	19.330
Tire chips	-	64	3.5	2.5	80.5	7.01	0.20	-	1.47	34.199

The cement plant controls the calciner temperature by adjusting the flow of petcoke fired. In order to estimate the amount of RDF fired, the percentage of fuel input to each calciner originating from petcoke is calculated by to equation 9.1. The percentage remaining of fuel input corresponds to RDF.

$$petcoke\% = \frac{F_{petcoke} \cdot LHV_{petcoke}}{E_{calc} \cdot F_{produc}} \cdot 100 \qquad [9.1]$$

where $F_{petcoke}$ is the flow of petcoke in t/h fired into the calciner, $LHV_{petcoke}$ is the lower heating value of the petcoke, which is approx. $33.5 \cdot 10^6$ J/kg (the lower heating value for petcoke is $35.183 \cdot 10^6$ J/kg according to the analysis, but the fired petcoke is mixed with unspecified fuels), E_{calc} is the energy consumption of the calciner, which is estimated to be $29.3 \cdot 10^5$ J/kg clinker, and F_{produc} is the production of each string in t/h.

The tire chips are assumed not to contribute to the calciner energy consumption, because the amount of fuel fired in the main burner is reduced when tire chips are fired. Figure 9-2 qualitatively illustrates the flows of mixture fuel fired in the main burner and tire chips. The temperature in the hot zone can be lowered, because the gas temperature in the kiln inlet will increase due to the combustion of tire chips. The tire chips fired in the kiln inlet contribute therefore to the energy consumption of the main burner. The fuel in the main burner consists of a mixture of 50 wt. % steam coal and 50 wt. % low sulfur petcoke, and the overall sulfur content in the mixture is 2.7 wt. %.

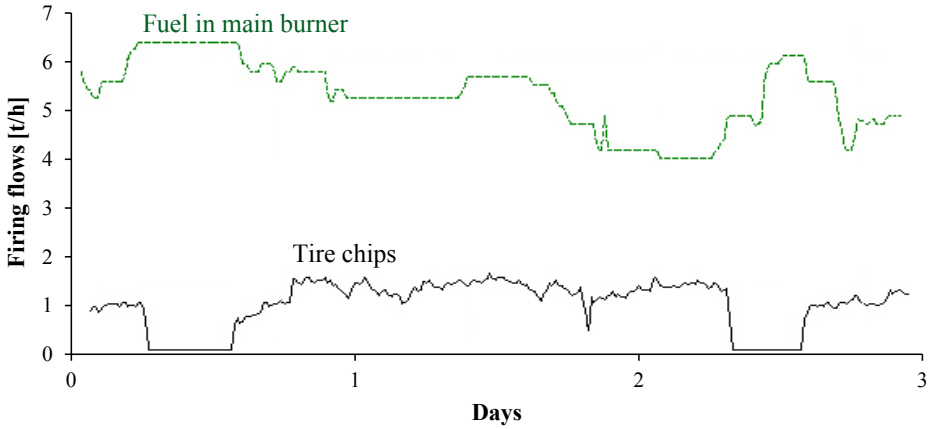

Figure 9-2: Qualitative representation of the firing flows of tire chips and mixture fuel in the main burner.

Hot meal samples were taken from the bottom cyclone of strings A and B during a period of one month in 8 different sampling days. The hot meal samples were taken with a sampler provided by FLSmidth A/S to ensure a homogenous cooling and to avoid oxidation of the carbon. Multicomponent gas measurements with focus on

SO_2, CO, and O_2 in the kiln inlet were performed on sampling day 3 and 4 using a hot Fourier transform infrared spectroscopy (FTIR) measurement system with a heated self-cleaning probe and samples were also taken during these days.

The two tests performed consisted of:

- Test 1: Increase of RDF firing in calciner A (from 37 to 85 % RDF of calciner fuel input). Petcoke flow was decreased from 4.6 to 1.1 t/h. No tire chips were fired in the kiln inlet.
- Test 2: Increase of tire chips injection in the kiln inlet from 1 to 1.5 t/h.

9.2 Gas Measurements

During the visit to the cement plant, a hot FTIR gas measurement system was used and compared to a cold gas measurement system, typically used in the cement industry. The main difference between the systems is that the hot FTIR system measures the components in the analyzer using the hot gases, while the fixed installation of the plant (cold gas system) needs to cool the gas before the measurement. The cooling of the gas can affect the measurements because condensed moisture can absorb SO_2. The measurement principle of both techniques can be found in Appendix G.

9.2.1 Comparison between Two Measurements Systems

The fixed equipment (the cold gas measuring system) logs the data every 60 seconds and purges the probe (to remove the dust that may enter) every 10 minutes. The FTIR equipment was set to log data every 5 seconds, and a self-purge cleaning mechanism was set up to purge every 5 minutes. Therefore, the FTIR equipment was sampling more frequently and it was also cleaned more frequently in order to avoid the SO_2 absorption. Furthermore, the detection limits of the FTIR system were lower than for the fixed equipment.

The probe used for the hot FTIR equipment had smaller dimensions than the one used for the fixed equipment. This was an advantage because the gas residence time in the probe and the filter was shorter than normal, which means, that the gases had less time to react or be absorbed inside the probe.

The FTIR equipment was placed on a level 3-4 meters above the fixed equipment. Therefore, the fixed equipment was measuring more directly into the kiln gasses. Figure 9-3 illustrates representatively the location of the hot FTIR gas measurement system and the fixed cold gas measurement system in the kiln system.

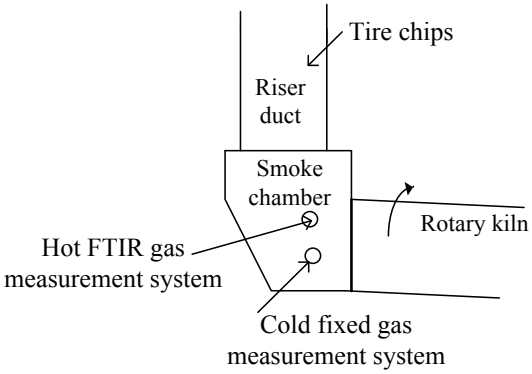

Figure 9-3: Scheme of the location of the hot FTIR gas measurement system and the fixed cold gas measurement system.

The FTIR equipment recorded concentrations of CO and SO_2 when the fixed equipment showed lower concentrations than 0.02 vol. % of CO and 0 ppm SO_2. The CO and SO_2 spikes were observed in brief periods during test 1 and 2. It was noticed that the O_2 levels measured by the FTIR equipment were at least 1 vol. % higher than the kiln inlet probe position from the fixed equipment.

The fixed gas analyzer recorded 0 ppm SO_2 in the kiln inlet, even though the fuel mixture in the main burner has 2.7 wt. % of sulfur. Assuming that the fuel mixture has a composition of 86.9 wt. % C, 3.71 wt. % H, 3.15 wt. % N, and 2.7 wt. % S and that it is combusted in 6 vol. % O_2 (which is the approximate level observed in Table 9-2), the SO_2 concentration at the kiln inlet coming from main burner should be approx. 1400 ppm SO_2 assuming no SO_2 absorption by the dust or clinker. However, this high SO_2 concentration is not seen in the kiln measurements, which means that the sulfur has been absorbed by the clinker or by the dust in the cement kiln.

Figure 9-4 and Figure 9-5 show the O_2, CO, and SO_2 measurements with the fixed equipment and the FTIR equipment for normal operation, test 1, and the addition of 1 t/h tire chips during the sampling day 3.

The CO measurements by the fixed equipment cannot be trusted because the uncertainty of this measurement is usually 2 % of the full range of the equipment, which is from 0 to 5 vol. % CO, therefore the uncertainty is ± 0.1 % CO.

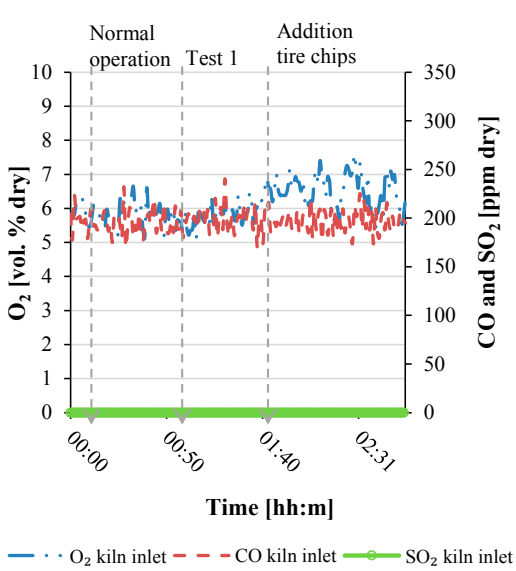

Figure 9-4: O_2, CO and SO_2 concentrations in the kiln inlet measured by the fixed equipment for normal operation, test 1 and the addition of tire chips (1 t/h). Probe cleaning effects have been removed.

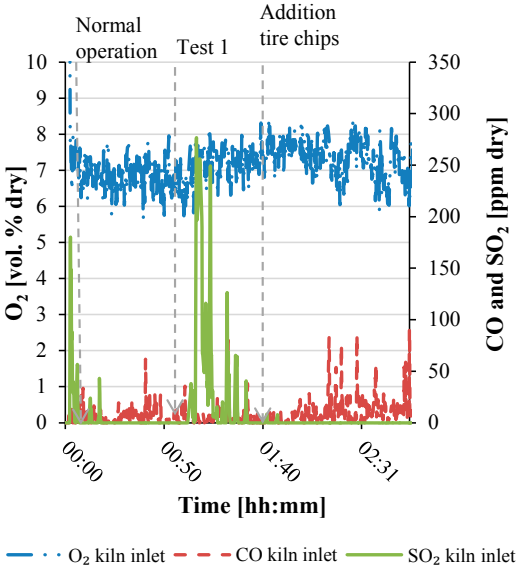

Figure 9-5: O_2, CO and SO_2 concentrations in the kiln inlet measured by the FTIR equipment for normal operation, test 1 and the addition of tire chips (1 t/h). Probe cleaning effects have been removed.

Some spikes of CO and SO_2 were briefly observed with the FTIR equipment, while with the fixed equipment very small CO spikes were recorded and the SO_2 concentration did not change. Table 9-2 summarizes the averages, maximum and minimum concentrations of O_2, CO, and SO_2 during the different periods. The FTIR equipment measured 80 and 277 ppm as maximum concentration of CO and SO_2, respectively.

Table 9-2: Summary of the average (avg), maximum and minimum concentrations of O_2, CO and SO_2 measured by the FTIR equipment and the fixed equipment during normal operation, test 1 and addition of tire chips.

Measurements of Sampling day 3

FTIR equipment	**O_2 [vol. %]**			**CO [ppm]**			**SO_2 [ppm]**		
	avg	max	min	avg	max	min	avg	max	min
Normal Production	6.8	8	5.6	4.9	61.6	0	1	56.6	0
Test 1	7.1	8.3	5.7	5.3	79.9	0	23.8	276.6	0
Addition tire chips 1 t/h	7.2	8.4	5.7	12.6	91.2	0	0	0	0
Fixed equipment	**O_2 [vol. %]**			**CO [vol. %]**			**SO_2 [ppm]**		
	avg	max	min	avg	max	min	avg	max	min
Normal Production	5.9	6.6	5.1	0.019	0.019	0.019	0	0	0
Test 1	5.7	6.5	5.1	0.020	0.024	0.016	0	0	0
Addition tire chips 1 t/h	6.5	7.6	5.4	0.020	0.022	0.017	0	0	0

Figure 9-6 shows an enlargement of the O_2, CO, and SO_2 concentration profiles in the kiln inlet measured by the FTIR equipment during test 1. It can be seen that the O_2 concentration increases when the probe is purged. This means that no dust is present inside the probe, subsequently higher concentrations of SO_2 are measured, which is the SO_2 concentration present in the kiln inlet. Afterwards, the SO_2 concentration slowly decreases, because the SO_2 is absorbed in dust or/and on the probe filter. The O_2 concentration is around 6 vol. %, which is the level present in the kiln gas. This cycle is repeated for each purge.

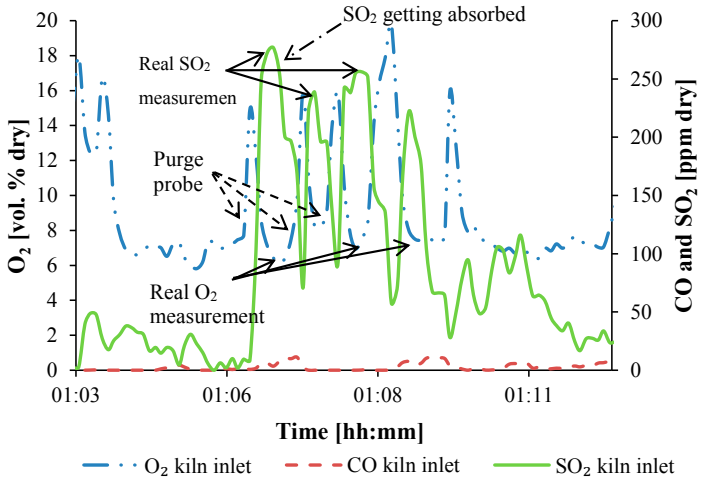

Figure 9-6: O_2, CO and SO_2 concentrations obtained by the FTIR equipment during test 1. The blowing cleaning effects on the signals have been removed.

It can be seen that the dust from the kiln constitute a challenge when measuring the "real" SO_2 concentration in the kiln.

Figure 9-7 and Figure 9-8 show the O_2, CO, and SO_2 concentration profiles obtained with the fixed equipment and the FTIR equipment during normal operation and during test 2 at sampling day 4. When the tire chips were increased from 1 to 1.5 t/h, spikes of CO and SO_2 were only seen with the FTIR equipment.

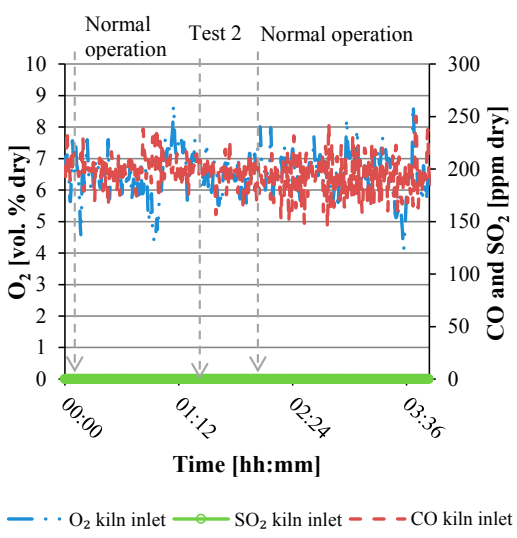

Figure 9-7: O_2, CO and SO_2 concentrations in the kiln inlet measured by the fixed equipment during normal operation and test 2. Probe cleaning effects have been removed.

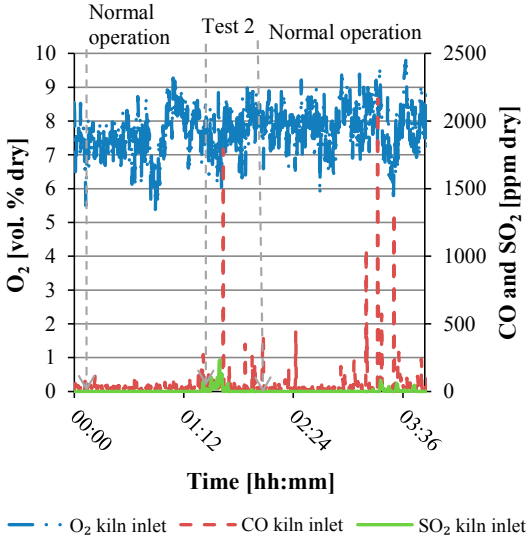

Figure 9-8: O_2, CO and SO_2 concentrations in the kiln inlet measured by the FTIR equipment during normal operation and test 2. Probe cleaning effects have been removed.

The average concentrations, the maximum and minimum concentrations of O_2, CO and SO_2 for the measurements performed on day 4 are listed in Table 9-3. The maximum concentration of CO and SO_2 detected with the FTIR equipment were 1792 ppm and 233 ppm, respectively.

Table 9-3: Summary of the average (avg), maximum and minimum concentrations of O_2, CO and SO_2 measured by the FTIR equipment and the fixed equipment during normal operation and test 2.

Measurements of Sampling day 4

FTIR equipment	**O_2 [vol. %]**			**CO [ppm]**			**SO_2 [ppm]**		
	avg	max	min	avg	max	min	avg	max	min
Normal Production	7.4	8.5	5.5	30.2	112.8	1	0	0	0
Test 2	7.5	8.9	6	55.5	1791.6	1	30.7	232.6	0
Normal Production	7.9	9.9	5.8	54.8	2164.8	1	1.9	83.4	0
Fixed equipment	**O_2 [vol. %]**			**CO [vol. %]**			**SO_2 [ppm]**		
	avg	max	min	avg	max	min	avg	max	min
Normal Production	6.5	8.7	4.3	0.020	0.024	0.015	0	0	0
Test 2	6.2	7	5.5	0.019	0.022	0.016	0	0	0
Normal Production	6.5	8.7	4.1	0.019	0.024	0.014	0	0	0

In general, the SO_2 concentration levels were low and the spikes were brief, so the fixed installation had difficulties to measure the process changes which occurred so briefly. The purge function and sampling

conditioning of the FTIR equipment did improve the measurements, but the dust in the probe also quickly started to absorb SO_2.

In conclusion, there is a good agreement of the oxygen concentration levels measured by the two measurement equipments, but the hot FTIR gas measurement equipment is able to measure changes in CO and SO_2 concentrations that were not detected by the cold gas measurement equipment. The CO concentration measured by the cold gas measurement equipment cannot be trusted because the CO concentration levels are below the uncertainty. The SO_2 concentration cannot be either trusted because the data log and purge time is quite long, which makes that the analyzer is not detecting the fast variations. Furthermore, the lack of frequent maintenance (meaning that the dust in filters may not been removed) may have influence the results, obtaining no detection of SO_2.

9.3 Investigation of Sulfur Evaporation on the Process

Hot meal samples were taken from the bottom cyclone of strings A and B at 8 separate days during a month period. During this period, one sample from each calciner string was taken during normal operation, but on sampling days 5 and 6 only one sample was taken from B string because the A-string was out of operation. During the visit on sampling day 3 and 4, the following samples were taken:

- Sampling day 3: two samples during normal operation and three samples (two from string A and one from B) during a period where the RDF was increased in calciner A.
- Sampling day 4: two samples (one from string A and one from B) during a period with increased tire chips injection in the kiln inlet.

The samples were sent to the FLSmidth A/S laboratory for analyses of the chemical composition (by X-Ray diffraction) and organic carbon. The organic carbon was determined by an instrument, which incinerates the sample in an oxygen flow and an IR cell, subsequently analyses the CO_2 generated during the incineration.

The O_2, CO, and SO_2 concentrations in the kiln inlet, CO and O_2 out of the preheater, the flows of petcoke and tire ships and the temperatures in the calciners were recorded as process data corresponding to the days of the samples. Table 9-4 shows the concentration range of the O_2, CO and SO_2 measurements in the kiln inlet and preheater, and the production rate and the calciner temperatures during the period of sampling.

Table 9-4: Concentration range of the gas measurements (O_2, CO and SO_2) in the kiln inlet and preheaters, the production range and the temperature of the calciner for normal operation. Target calciner temperature: 875 °C.

O_2 kiln inlet [vol. %]	CO kiln inlet [vol. %]	SO_2 kiln inlet [ppm]	O_2 preheater [vol. %]	CO preheater [vol. %]	Production each string [t/day]	T calciner [°C]
5-9	≤ 0.02	0	4-10	0-0.2 spikes to 0.4	2000-2500	881-1013

During the sampling period the cement plant operated with high concentration of oxygen, which varied from 4 to 10 vol. %, and subsequent low CO concentrations, below 0.02 vol. %, both in the kiln inlet and in the preheater.

Table 9-5 summarizes the hot meal analysis of the all samples taken for this investigation and it can be seen that the content of minor components, such MgO, Mn_2O_3, TiO_2, P_2O_5, and SrO, have a small variation (less than 0.05 wt. % in standard deviation) in the 19 hot meal samples. However, SiO_2 and CaO, which are important components for the clinker, are having large standard deviations of 1.66 and 3.32 wt. %, respectively. The Al_2O_3 and Fe_2O_3 content, which are the other main oxides in the clinker, vary to less extent with a standard deviations of 0.5 and 0.25 wt. %, respectively. The Cl, K_2O and SO_3 contents present similar standard deviations as the main oxides, giving 0.62, 0.56 and 0.26 wt. %, respectively. The greatest variation is in the loss on ignition (LOI), which range from 1.87 to 17.9 wt. %. The loss on ignition indicates how incomplete the calcination was. The organic carbon from the hot meal samples during normal operation varies from 0.03 to 0.12 wt. % with an average of 0.06 wt. %. When RDF firing was increased the organic carbon varied from 0.03 to 0.07 wt. %, and when the firing of tires chips in the kiln inlet was increased the organic carbon varied from 0.05 to 0.1 wt. %.

The fixed installation of the cement plant recorded always a SO_2 concentration of 0 ppm in the kiln inlet during the sampling period, as shown in Table 9-4. Therefore, the organic carbon variation from the hot meal samples cannot be related to the SO_2 in the kiln inlet. However, it may be possible that the content of organic carbon measured in the hot meal under those conditions provokes a minor SO_2 release that the analyzer was unable to detect.

Table 9-5: Summary of the hot meal samples analysis for each sample taken during normal operation, test 1 and test 2. Note: [1]Loss on ignition.

Chemical composition [wt. %]	**Pre-test** Process instability		**Sampling day 1** Normal operation		**Sampling day 2** Normal operation		**Sampling day 3** Normal operation		Test 1			**Sampling day 4** Test 2		**Sampling day 5** Normal operation	**Sampling day 6** Normal operation	**Sampling day 7** Normal operation		**Sampling day 8** Normal operation	
	A	B	A	B	A	B	A	B	A	A	B	A	B	B	B	A	B	A	B
SiO_2	19.2	17.97	19.76	20.38	19.49	19.74	17.09	20.78	18.57	18.58	20.68	16.10	20.20	23.83	20.24	20.28	21.59	20.24	19.51
Al_2O_3	5.11	4.77	4.82	5.52	4.82	5.45	4.37	5.76	4.83	4.77	5.87	4.02	5.63	5.31	5.36	5.06	5.58	5.76	5.49
Fe_2O_3	3.71	3.63	4.16	3.59	4.29	3.59	3.6	3.64	3.93	3.96	3.64	3.47	3.58	4.14	3.91	4.02	3.87	4.25	3.72
CaO	58.3	54.9	63.5	58.29	62.24	55.24	61.03	62.13	64.29	64.12	60.46	52.33	59.74	58.96	62.83	63.31	60.48	62.44	61.88
MgO	0.74	0.73	0.8	0.78	0.79	0.75	0.71	0.79	0.77	0.78	0.81	0.63	0.78	0.82	0.78	0.82	0.79	0.81	0.78
Mn_2O_3	0.03	0.03	0.03	0.03	0.03	0.03	0.03	0.03	0.03	0.03	0.03	0.02	0.03	0.03	0.03	0.03	0.03	0.03	0.03
TiO_2	0.25	0.24	0.26	0.29	0.27	0.29	0.23	0.31	0.26	0.25	0.31	0.20	0.28	0.26	0.27	0.27	0.30	0.31	0.29
P_2O_5	0.28	0.33	0.5	0.3	0.5	0.29	0.26	0.31	0.35	0.38	0.28	0.21	0.25	0.24	0.24	0.37	0.25	0.28	0.26
K_2O	2.17	3.0	1.1	1.48	1.38	2.22	1.28	0.92	1.38	1.49	1.22	2.31	1.20	0.92	1.07	1.14	0.93	1.05	1.44
Na_2O	0.44	0.51	0.36	0.4	0.43	0.54	0.37	0.38	0.42	0.46	0.47	0.56	0.42	0.84	0.41	0.45	0.44	0.43	0.45
SrO	0.14	0.12	0.15	0.14	0.14	0.13	0.13	0.14	0.14	0.14	0.14	0.11	0.13	0.14	0.15	0.14	0.14	0.15	0.14
SO_3	1.90	1.325	1.9	1.52	1.85	1.94	1.52	1.87	1.73	1.88	1.99	1.75	1.63	2.11	2.4	1.35	1.92	1.85	2.04
Chlorine	1.60	2.82	0.47	0.85	0.93	1.72	0.89	0.47	0.95	0.93	0.79	2.06	0.67	0.50	0.61	0.80	0.45	0.59	0.99
LOI[1] 975 °C	7.10	12.21	2.12	6.74	2.4	8.76	9.60	2.5	3.13	2.92	3.28	17.9	5.73	2.04	2.72	2.64	2.98	1.87	3.21
TOTAL	97.49	98.44	99.46	99.46	98.63	98.97	100.22	99.56	99.83	99.76	99.18	99.61	99.6	99.64	100.41	99.88	99.3	99.47	99.24
Organic Carbon	0.09	0.07	0.03	0.1	0.03	0.05	0.07	0.2	0.04	0.03	0.07	0.05	0.1	0.07	0.12	0.07	0.04	0.04	0.05

When RDF in calciner A was increased from 37 to 85 % RDF of fuel input (test 1), the organic carbon in the samples corresponded to the lower range of the organic carbon content during normal operation. According to this observation and the fuel analysis, the RDF contains 90 % of combustible material and it was well combusted in the calciner.

The organic carbon from the hot meal samples correlates to the percentage of fuel input to the each calciner coming from petcoke as shown in Figure 9-9, calculated according to equation 9.1.

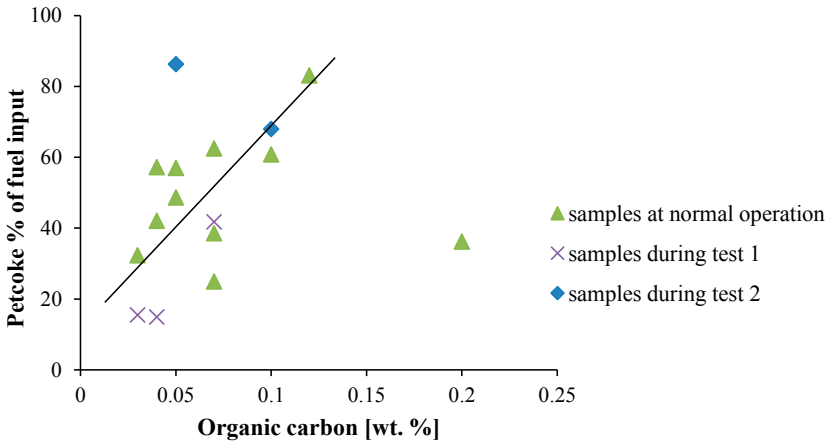

Figure 9-9: Relationship between the percentage of petcoke as fuel input in the calciner and the organic carbon of hot meal samples.

The results show that the organic carbon increased when higher petcoke and lower RDF were fired. As such, it may be concluded that the organic carbon is the unconverted carbon coming from the petcoke, since it has higher content of fixed carbon than RDF. According to Figure 9-9, it would be advantageous to fire higher content of RDF. However, the cement plant have found by experience that the limitation for firing large amounts of RDF is the CO emissions in the stack, where the daily accumulated limit of CO, which is 350 mg/Nm^3 CO @ 10 vol. % O_2, cannot be exceeded.

9.3.1 Fuel Conversion in the Calciner

Table 9-6 summarizes the gas concentrations in the kiln inlet, the preheater, the fuel flows in the calciner, the production flow, the content of organic carbon in the hot meal, the degree of char conversion, and the total conversion in the calciner to the corresponding time when the hot meal sample was taken.

The CO concentration measured in the preheater gives an indication of the combustion in the calciner. The high content of O_2 and the low content of CO in the kiln inlet and in the preheater ensured a good combustion.

Table 9-6: Summary of the process data in the kiln inlet, the preheater, the fuel flows in the calciner, the production flow, the organic carbon in the hot meal, the degree of char conversion and the total conversion in the calciner when the hot meal sample was taken. Note:*Calculated using equation 9.1 from the RDF % fuel input and its lower heating value.

			Kiln inlet concentrations			Preheater concentrations		Fuel in calciner				Hot meal	**Production**	**Degree char**	**Total degree**
			O_2 [vol.%]	**SO_2 [ppm]**	**CO [vol.%]**	**O_2 [vol.%]**	**CO [vol.%]**	**Petcoke [t/h]**	**RDF* [t/h]**	**Petcoke [%]**	**RDF [%]**	**Organic Carbon [wt. %]**	**[t/day]**	**conversion [%]**	**conversion [%]**
Sampling day 1	Normal operation	A	9.47	0	0.021	8.46	0.052	7.10	0.68	92.99	7.01	0.03	2095	99.5	99.6
		B	8.89	0	0.013	5.24	0.129	5.20	4.28	60.8	39.2	0.10	2345	97.7	98.6
Sampling day 2	Normal operation	A	7.85	0	0.017	8.63	0.018	2.43	6.51	32.31	67.69	0.03	2066	98.9	99.6
		B	7.27	0	0.02	6.94	0.043	4.86	4.68	57.01	42.99	0.05	2339	98.8	99.3
Sampling day 3	Normal operation	A	6.36	0	0.02	6.46	0.105	4.66	3.59	62.54	37.46	0.07	2061	98.4	99.0
		B	6.07	0	0.018	4.55	0.044	3.23	7.09	36.23	63.77	0.20	2389	93.7	97.4
	Test 1	A	5.90	0	0.021	5.26	0.038	1.12	8.17	14.9	85.1	0.04	2061	97.6	99.4
		A	5.89	0	0.021	5.07	0.417	1.16	8.11	15.5	84.5	0.03	2061	98.3	99.6
		B	6.25	0	0.020	4.09	0.042	3.64	6.48	41.75	58.25	0.07	2389	97.9	99.1
Sampling day 4	Test 2	A	6.55	0	0.020	7.01	0.031	6.22	1.26	86.28	13.72	0.05	1978	99.0	99.2
		B	6.65	0	0.019	5.13	0.056	5.84	3.51	68.02	31.98	0.10	2357	98.0	98.7
Sampling day 5	Normal operation	B	9.14	0	0.010	4.58	0.025	2.20	8.44	24.93	75.07	0.07	2415	97.0	99.0
Sampling day 6	Normal operation	B	8.89	0	0.020	4.83	0.022	6.97	1.8	83.16	16.84	0.12	2299	98.0	98.5
Sampling day 7	Normal operation	A	6.49	0	0.001	5.37	0.035	3.17	6.46	38.54	61.46	0.07	2256	97.8	99.1
		B	6.49	0	0.009	5.68	0.035	3.28	5.76	42.1	57.9	0.04	2135	98.8	99.4
Sampling day 8	Normal operation	A	5.39	0	0.01	6.91	0.037	4.68	4.47	57.23	42.77	0.04	2244	99.1	99.5
		B	6.02	0	0.01	9.37	0.069	4.06	5.47	48.68	51.32	0.05	2289	98.7	99.3

The degree of char conversion is calculated from the carbon introduced by the petcoke and the RDF and the organic carbon determined in the samples taken in the bottom stage cyclone. The degree of char conversion in the calciner varies from 93.7 to 99.5 % with an average of 98.2 %. Figure 9-10 shows the relationship between the percentage of petcoke as fuel input and the degree of char conversion in the calciner.

The total degree of conversion is based on the total conversion of combustible material, which comprises the volatiles and the fixed carbon of both RDF and petcoke fired. Figure 9-11 shows the total degree of conversion of the combustible material as function of the petcoke percentage of fuel input in the calciner. The total degree of fuel conversion in the calciner varies from 97.4 to 99.6 % with an average of 99.1 %, which also shows that the combustible material fuel is fully combusted in the calciner.

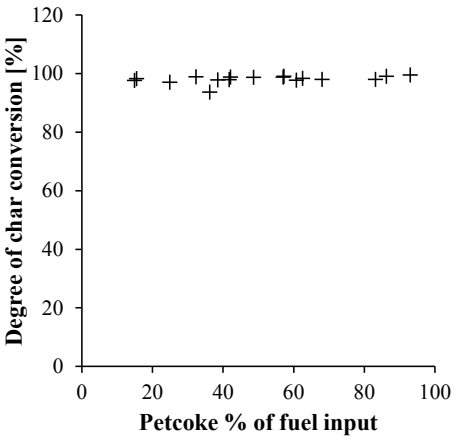

Figure 9-10: Petcoke % of fuel input as function of the degree of char conversion in the calciner.

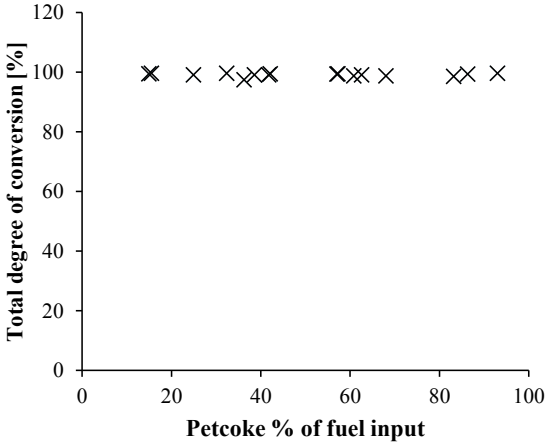

Figure 9-11: Petcoke % of fuel input as function of the total degree of conversion in the calciner.

According to Figure 9-10 and Figure 9-11, f the degree of char conversion and the total degree of conversion are higher than 90 % for the different percentage of petcoke fired, which means that the calciner fuel is fully converted in the calciner.

9.3.2 Tendency of Build-ups

The SO_3 and Cl contents in the hot meal samples were determined because these concentrations may predict the tendency of the build-ups formation in the kiln system according to Figure 9-12. The diagram, previously presented in Chapter 4, is based on industrial experience using fossil fuels and is divided in 3 zones: low, medium, and high build-up tendency. In the graph points corresponding to samples taken during a process instability, normal operation, test 1, test 2, and samples taken from string B while there was a build-up in string A are plotted.

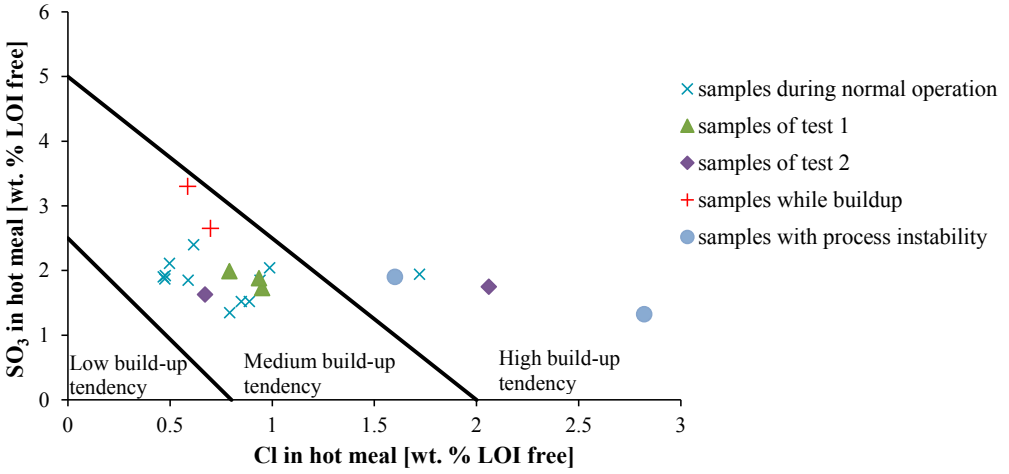

Figure 9-12: Diagram for predicting the tendency of build-ups by the content of SO_3 and Cl in the hot meal when firing fossil fuels.

It can be seen that the samples taken during normal operation are situated in the zone corresponding to medium tendency build-up. The point in the high build-up tendency region from test 2 originates from string A, which experienced a blockage 2 days after sampling, where string A was stopped corresponding to sampling day 5 and 6. The other point in the high build-up tendency region during the normal operation corresponds to string B during the sampling day 2, this string also experienced blockage the following day. The samples taken while the string experiences are very close to the limit of high build-up tendency region, which could indicate the cause of the observed build-ups. The build-ups, which this cement plant experiences, are normally present in the bottom stage cyclone and in the riser duct.

9.3.3 Sulfur Volatility

The volatility of the sulfur in the kiln can be described using an evaporation factor, as described in Chapter 4. The sulfur evaporation factor, ε_s, is defined according to equation 9.2.

$$\varepsilon_s = \frac{w_{SO_3\ hotmeal,LOI\ free} - w_{SO_3\ clinker}}{w_{SO_3\ hotmeal,LOI\ free}} \qquad [9.2]$$

where $w_{SO3\ hotmeal,\ LOI\ free}$ is the content of SO_3 in the hot meal on LOI free basis and $w_{SO3\ clinker}$ is the content of SO_3 in the clinker. The dust circulation from the coolers and the kiln to the bottom stage cyclone has been disregarded. The clinker produced was analyzed every second hour by the cement plant laboratory. It is assumed that the clinker analysis corresponds to the hot meal sample after 30 min from the time of sampling, which corresponds approx. to the residence time of the solid material in the rotary kiln. The SO_3 content in the

clinker is summarized in Table H-1 in Appendix H, which shows the clinker analysis of the corresponding hot meal samples.

Table 9-7 shows the range of the sulfur evaporation factor during the normal operation and for test 1 and 2.

Table 9-7: Sulfur evaporation factor range during normal operation, test 1 and test 2.

	Normal operation	Test 1	Test 2
Sulfur evaporation factor	0.25-0.54	0.38-0.46	0.42- 0.46

It can be seen that the tests performed does not change the sulfur evaporation. Figure 9-13 shows the sulfur evaporation factor as function of the organic carbon of the hot meal samples. It can be seen that there is no clear relationship. This supports the experiments using wood with different degree of devolatilization, presented in Chapter 5, where char caused less much sulfur release than the volatiles.

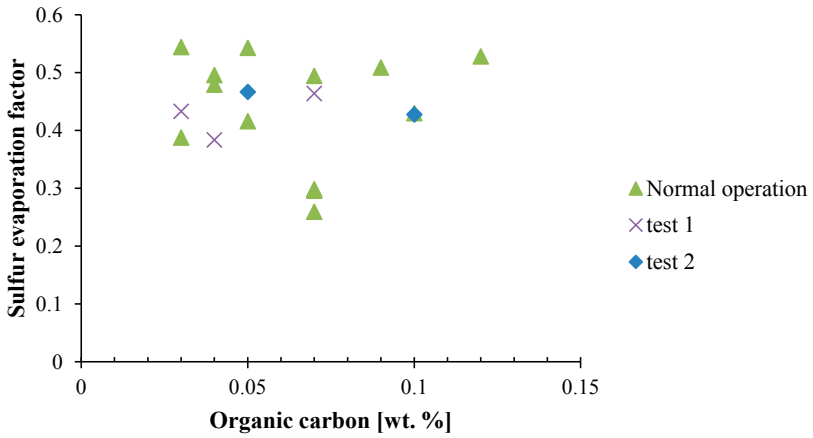

Figure 9-13: Sulfur evaporation factor as function of the organic carbon of hot meal samples during normal operation and for test 1 and test 2.

9.4 Conclusions for the Industrial Experience and Challenges

Hot meal sampling and multicomponent gas measurements with focus on SO_2, CO and O_2 in the kiln inlet were performed in a cement plant with the aim of determining the relationship between organic carbon in the bottom stage cyclone and the SO_2 in the kiln inlet. Two tests were performed: 1) an increase of RDF firing in calciner A and 2) an increase of tire chips injection in the kiln inlet.

There were differences in the CO and SO_2 concentration measured with the hot FTIR gas measurement equipment and the cold gas measurement equipment. The cold gas measurement equipment was not able to detect spikes of SO_2 and CO occurring in brief periods when the two tests were performed.

During the sampling period, the organic carbon from the hot meal samples varied from 0.03 to 0.2 wt. % with an average of 0.06 wt. % and the gas analysis recorded by fixed equipment showed always 0 ppm SO_2 in the kiln inlet. Therefore, it was not possible to identify a relationship between organic carbon and SO_2 in the kiln inlet from these measurements. However, it cannot be excluded that the organic carbon in the hot meal is related to the SO_2 release in the kiln inlet.

A relationship between the organic carbon and the percentage of petcoke fired in the calciner was found. The organic carbon increased when more petcoke (and less RDF) was fired. The degree of char conversion in the calciner and the total degree of fuel were higher than 90 %, which indicate that the calciner fuel was well combusted in the calciner.

Build-ups and process instabilities experienced by the cement plant correspond to SO_3 and Cl levels in the analyzed hot meal in or close to the region of high build-up tendency for fossil fuels. There is a good consistency between the predictions of build-ups by the diagram and the reality, this tool could therefore be potentially used to detect and avoid future build-ups when firing alternative fuels

Nowadays there still exist challenges on the measurements to control process stability and predict instability situations. The SO_2 concentration in the kiln is fast continuous variable used to control the cement plant operation. However, the measurement of SO_2 in the kiln is difficult due to the high content of dust in the gas and the technology used is not always able to measure it because the dust absorbs the SO_2. Analysis of SO_3 and Cl in the hot meal is another indication for process instability but it is time consuming to take the sample, analyze it, and react on the process control. From an economical and practical point of view, it is more convenient for the cement plants to have a fast indication of the process stability by continuous gas measurements instead of the hot meal sampling.

10. Final Conclusions

An improved understanding of sulfur release during fuel combustion in the kiln inlet of cement rotary kilns has been gained through this Ph.D. project through review of the existing literature, pilot and full-scale experimental investigations, and mathematical modeling.

10.1 Main Results and Conclusions

The main conclusions to be drawn from the literature review are:

- Cement production is a very energy-consuming process. There is an interest in replacing fossil fuels with selected waste, biomass and industrial by-products with recoverable calorific value, defined as alternative fuels, in order to minimize production cost, i.e. due to increasing fossil fuel prices and environmental concerns.
- The combustion of alternative fuels is more challenging than combustion of fossil fuels, due to the lack of experience in handling the different and varying combustion characteristics caused by different chemical and physical properties, e.g. higher moisture content and larger particle sizes. New combustion equipments or modifications of existing plant layouts have been developed but alternative fuels are often directly fired in the calciner and/or to the main burner despite the large particle sizes because this requires a minimum of investments.
- Sulfur, chloride, sodium, and potassium, which are volatile elements, evaporate when exposed to high temperature in the burning zone and subsequently condense in colder parts of the plant. High concentrations of volatile elements often cause difficulties in kiln operation and plant stability by causing build-ups, kiln rings and/or shell corrosion.
- When unconverted or partly converted alternative fuels drop into the rotary kiln inlet and are combusted in direct contact with the bed material, local reducing conditions may occur. The volatiles released from the fuels may therefore react with sulfates present in the hot meal and form gaseous SO_2.
- Previous studies of sulfur release during combustion of alternative fuel particles have shown that reducing gases from the fuel devolatilization cause reductive decomposition of $CaSO_4$ and indicated that the fuel particle size is of high importance for the degree of sulfur release.
- Investigations of the reductive decomposition of $CaSO_4$ showed that CaO, CaS, or mixtures of both products are favored depending on the temperature and the type and concentration of the reducing gas. The most influencing parameter to the reaction rate of reduction of $CaSO_4$ is the partial pressure of the gaseous reductive agent.

The main results and conclusions regarding sulfur release in the material inlet of cement rotary kiln are:

- The inorganic chemistry was studied by thermodynamic calculations in order to improve understanding of the chemistry. The reducing agents in the gas phase decreased the stability of $CaSO_4$ and increased the stability of SO_2 in the kiln inlet at temperatures between 900 and 1100 ºC. The volatility of the chlorine was not affected by the gas atmosphere, but was very sensitive to the temperature. Higher levels of alkali compared sulfur reduced the sulfur release to the gas phase, but increased the amount of compounds in liquid phase in the kiln and the alkali species in the gas phase.
- The pilot plant experiments in the high temperature rotary drum using pine wood and tire rubber particles were performed in order to investigate the effect of particle size, fuel conversion degree, sulfur load in the bed and moisture content of the fuel on the release of sulfur. The effect of fuel particle size on sulfur release showed that smaller particles increase the SO_2 release because they were heated faster and thus released the volatile gases faster and with higher concentrations because stronger local reducing conditions were formed. The effect of wood cylinders with different degree of volatiles showed that the sulfur release mainly took place during devolatilization, corresponding to the cases of virgin wood and wood chars made at 300 and 500 °C. This was supported by the findings of the industrial investigation on sulfur released, where no clear relationship was observed between the organic carbon (char) from the fuel entering in the rotary kiln and the sulfur evaporation factor.
- The effect of different concentrations of CO, H_2, and CH_4 on sulfur release was investigated experimentally at different temperatures, oxygen contents and times of exposure. The experiments using a single reducing agent indicated a threshold concentration below which SO_2 release does not occur. The effect of the different concentrations can be related to the effect of gases released from alternative fuels. The concentration of the reducing agent and the time of exposure were of high importance for SO_2 release because it was found that a high concentration of the reducing agent in a short period (representing devolatilization) led to a higher total SO_2 amount compared to the a low concentration during a long period (representing char combustion or devolatilization of large fuel particles).
- The experimental results of binary mixtures when CO was present showed that SO_2 increases with increasing CO concentration in the mixture. Similar SO_2 release was obtained for the different mixtures of CH_4 and H_2.
- A mathematical model, which was able to predict sulfur release caused by volatiles from wood particles fired in the material kiln inlet was developed based on the reaction between the volatiles and $CaSO_4$ in the bed material in CSTR in series. The effect of the fuel degree of coverage, the bed fill degree, and the bed sulfur content and firing degree on sulfur release was investigated. The sulfur evaporation factor increased with decreasing particle mass, sulfur content in the bed and fill degree,

while it decreased with increasing the fuel degree of coverage. The firing degree and the fuel degree of coverage were identified by the sensitivity analysis as the most influencing factors for the total SO_2 release and the sulfur evaporation factor, while the kinetic parameters did not modify the output results. The model evaluation showed that the model follows the experimental data tendency.

- A model to predict the tendency of build-ups of a kiln system based on the SO_3 and Cl concentrations in the hot meal was developed. For a cement plant with 3500 tons per day without bypass using raw materials with 0.05 wt. % S and 0.01 wt. % Cl and fuel with 5 wt. % S and 0.001 wt. % Cl, the tendency of build-ups predicted was in the medium/high line, while using bypass the tendency of build-ups was medium, close to the low region. The model also predicted medium tendency build-ups when alternative fuels are fired in the kiln inlet. A sensitivity analysis was performed in order to investigate the effect of the parameters on the SO_3 and Cl content of the hot meal and showed that the chlorine evaporation factor has the largest influence with almost 400 % deviation on the Cl concentration.

10.2 Recommendations

When considering alternative fuel utilization in the calciner or in the riser duct, the particle size and fuel flow are key parameters to ensure a proper combustion before the particles reach the bed material in the kiln inlet causing sulfur release. Shredding large fuel particles would be the first recommendation to avoid their combustion in contact with the bed material and thereby avoid sulfur release in the kiln inlet. However, if the combustion of small particles in large amounts is not complete, high sulfur release may take place due to the particle size and elevated number of particles. The sulfur release may decrease when operating the kiln with an oxygen concentration above 5 vol. % in the kiln inlet, which is also recommended if the fuel is not downsized. Since no SO_2 release takes place below a threshold concentration of reducing agent/s, a threshold fuel flow for the kiln inlet may exist, giving no sulfur release because the concentration of the reducing agents released are below the threshold. However, each kiln may have its own threshold fuel flow in the kiln inlet, which would depend on the kiln characteristics and raw materials and fuels used. Thereby a general recommendation in this aspect is difficult to make.

Gas stratification in the rotary kiln has been reported by measurements (Hansen, 2002) and predicted by CFD modeling. Figure 10-1 and Figure 10-2, which are cordially provided by Aixergee Process Optimization, show the O_2 and CO_2 gas concentrations, respectively, in the inlet of the rotary kiln for a an ILC-kiln system with 2 string. It can be seen that both concentrations are stratified, meaning that the concentration is increasing/decreasing in layers and is not uniform in the entire freeboard. The model allows the mixing inflow, however, the results show that there is a poor mixing between the gas and the bed material (no gas penetration into the bed material) and the bed material is contact with the lowest concentration of O_2 and the highest of CO_2.

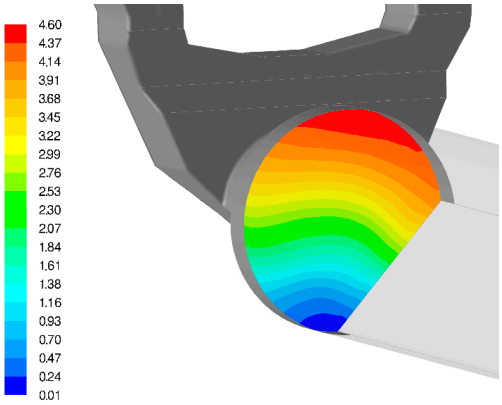

Figure 10-1: CDF modelling of the stratification of the O_2 concentration in vol. % in the kiln inlet of a cement plant, provided by Aixergee Process Optimization.

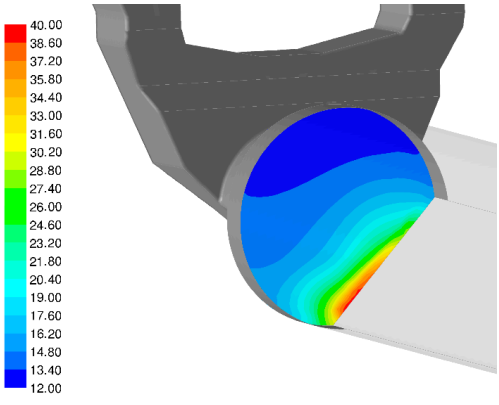

Figure 10-2: CDF modelling of the stratification of the CO_2 concentration in vol. % in the kiln inlet of a cement plant, provided by Aixergee Process Optimization.

This effect may influence the combustion of alternative fuel particles in the kiln inlet and subsequently the sulfur release. In order to prevent or minimize gas stratification, mixing devices can be applied in the kiln inlet to enhance turbulence flow and optimize the fuel combustion. These mixing devices may minimize the sulfur release, because of the uniformity of the gas atmosphere and the time of contact between the fuel and material may be reduced. However, they may have a short service life due to abrasion, thermal stress or mechanical stress. Other ways of breaking the gas stratification may also have a positive effect reducing sulfur release.

The sulfur release in the inlet of the rotary kiln can be avoided when the volatile gases from fuels are not released in contact with the bed material, thereby, only allowing fuel char to be in contact with the kiln bed material. Assuming a cement plant with a production of 3500 tons per day that operates the rotary kiln with 5 vol. % O_2, the maximum char fuel flow introduced into the rotary kiln can be calculated based on the minimum gas flow for the char combustion and the actual gas flow in the kiln inlet, which is 0.5 kg gas/kg clinker. The fuel char is assumed to consist of carbon. For the pine wood with 44.7 wt. % C, the maximum wood char flow is 3377 kg/h. However, this amount of char would consume all the oxygen content in the gas phase, which is undesirable for the process. It would be reasonable to assume that between 1/4 and 1/10 of the maximum char flow could be introduced into the rotary kiln without causing undesired effects, because the oxygen content should not decrease drastically. Thereby, the real char flow into the rotary kiln is between 845 to 340 kg/h wood char, which would correspond to 7500-3000 kg wood/h for a wood with 11.3 wt. % fixed carbon. Considering tire rubber with 87 wt. % C, the maximum char fuel is 1700 kg/h and the real char flow varies between 430 to 170 kg /h tire char, corresponding to 1300-520 kg/h tire (for a tire rubber with 32.6 wt. % fixed carbon). The tire rubber flow fired in the riser duct in the industrial campaign, where 4000-5000 tons of clinker was produced, are around the same order of magnitude as the calculated results.

Sulfur release from the kiln bed material can also be minimized when fuel combustion takes place at temperatures below 800 ºC. This may imply to have a different configuration of the kiln system with the place of fuel combustion, in which the fuel combustion is completed at lower temperatures and the hot flue gas is used for calcination.

10.3 Suggestions for Future Work

The model to predict sulfur release in the kiln inlet due to alternative fuels firing has been successfully developed and evaluated against experimental data. However, the model could be optimized with respect to predicting the SO_2 release when the sulfur concentration in the kiln bed material is varied, which is related to the particle motion in the bed and rotational speed. The particle motion could be relevant to include but also difficult, and CFD tools may be needed.

A comparison between the model and the pilot-scale data implies that the model over-estimates the SO_2 concentration compared to the experiment results at 10 vol. % O_2. Hence, the effect of the oxygen in the freeboard atmosphere should be further implemented. Furthermore, the kiln model and tendency of build-ups model should be validated against full-scale data and thereby, the absorption of SO_2 on the dust carried by the kiln gas could be also included.

The effect of the gas stratification in the high temperature rotary kiln may be difficult to achieve but the effect of the gas atmosphere, i.e. different CO_2 concentrations together with O_2, could be further experimentally investigated.

Experiments with mixing devices in the rotary kiln could be investigated in order to optimize the fuel combustion in direct contact with the kiln bed material, and characterize the effect on sulfur release.

10.4 References

Hansen, E.R.; Staged combustion for NO_x reduction using high pressure air injection. IEEE-IAS/PCA Cement Industry Technical Conference, 2002.

List of Symbols

Abbreviations and acronyms

a.r.	As received
avg	Average
C_2S	Belite
C_3S	Alite
C_4AF	Ferrite
C_3A	Aluminate
CFD	Computational fluid dynamics
CSTR	Continuous stirred tank reactor
ILC	In-Line Calciner
FC	Fixed Carbon
FTIR	Fourier transform infrared spectroscopy
Max	Maximum
MBM	Meat and Bone Meal
Min	Minimum
n.a.	Not available
PE	Polyethylene
PVC	Poly-vinyl-chloride
RDF	Refuse derived fuel
SLC	Separate Line calciner
TDF	Tire-derived fuel
VLS	Vapor-liquid-solid
VM	Volatile matter

Roman nomenclature

a	Activity	[-]
A	Area	[m^2]
A	Pre-exponential factor	[m/s] or [s^{-1}]
C	Concentration	[mol/m^3] or [ppm]
C_p	Heat capacity	[J/kg·K]
D	Diffusion coefficient	[m^2/s]
E_a	Activation energy	[J/mol]
FC	Fixed carbon	[wt. %]
F	Flow	[kg/h] or [t/h]
F	Fill degree	[-] or [%]
G	Free Gibbs Energy	[J/mol]
h	Heat transfer coefficient	[W/m^2·K]
H	Enthalpy	[kJ/kg]
k_p	Thermal conductivity	[W/m·K]
k_g	Mass transfer coefficient	[m/s]
k	Rate constant	[m/s]
L	Length	[m] or [mm]
LHV	Lower heating value	[MJ/kg]
LOI	Loss on ignition	[%]

m	Mass	[g] or [kg]
$\dot{m}$	Mass flow	[kg/h]
M	Molar weight	[g/mol]
n	Moles	[mol]
$\dot{n}$	Molar flow	[mol/s]
P	Pressure	[Pa] or [atm]
Q	Volumetric flow	[m^3/s]
r	Radius	[m]
R	Initial Radius	[m]
R	Universal gas constant	8.314 [m^3·Pa/mol·K]
Re	Reynolds number	[-]
Sc	Schmidt number	[-]
Sh	Sherwood number	[-]
t	Time	[s] or [min]
T	Temperature	[°C] or [K]
v	Velocity	[m/s]
V	Volume	[m^3]
w	Weight percent concentration	[wt. %]
y	Mole fraction	[-]
x	Distance	[m]
X	Degree of conversion	[-]
z	Special atomic diffusion volume	[-]

Greek nomenclature

α	Porosity	[-]
α	Na_2O fraction reacting with SO_3	[-]
β	Absorption factor	[-]
γ	Activity coefficient	[-]
γ	Fraction leaving preheater tower	[-]
ε	Evaporation factor	[-]
ρ	Density	[kg/m^3]
ϕ	Degree of coverage	[-]
ø	Diameter	[m]
τ	Residence time	[s]
τ	Tortuosity	[-]
ω	Rotational speed	[rpm]

Subscripts

avg	Average
abs	Absorbed
b	Bed
burner	Rotary kiln burner
calc	Calciner
cond	Conduction
conds	Condensed
Cl	Chlorine

diff	Diffusion
eff	Effective
end	Hot end of the rotary kiln
f	Final
Fuel	Fuel
g	Gas
hot meal	Calcined cement raw material
in	Inlet
inlet	Material rotary kiln inlet
k	Rotary kiln
LOI free	Loss on ignition free
p	Particle
prod	Production
pyr	Pyrolysis
out	Outlet
raw mat	Raw materials
reac	Reaction
S	Sulfur
Vol	Volatiles
w	Wood
0	Initial conditions or t=0

Appendixes

Appendix A: Equilibrium Calculations

- **Equilibrium between SO_2 and SO_3**

The equilibrium concentration as function of the temperature for reaction (A-1) is shown in Figure A-1.

$$SO_2(g) + \tfrac{1}{2}O_2(g) \rightarrow SO_3(g) \qquad \text{(A-1)}$$

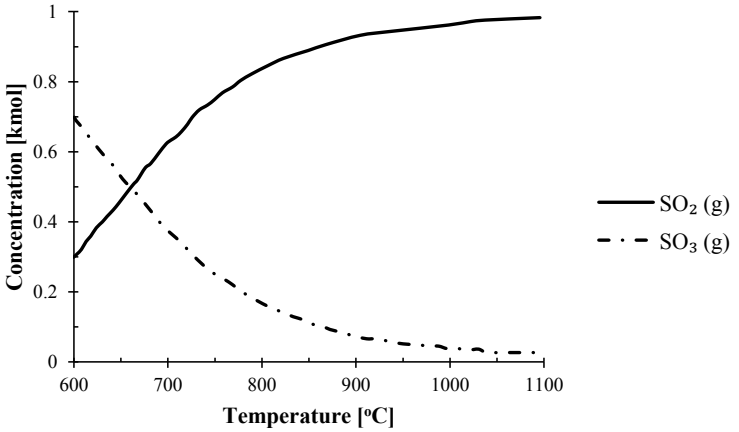

Figure A-1: Equilibrium calculations for the reaction $SO_2 + 0.5\ O_2 = SO_3$, thermodynamic data from HSC chemistry program.

This phenomenon can also be seen by the free Gibbs Energy of the equilibrium reaction (A-1), which is mathematically expressed by equation A.1.

$$\Delta G = \Delta G^0 + R \cdot T \cdot \ln\left(\frac{P_{SO_3}}{P_{SO_2} \cdot P_{O_2}^{1/2}}\right) \qquad \text{[A.1]}$$

where ΔG^o is the free Gibbs energy at standard conditions (298.15 K and 1 atm) , which is -141.8 kJ, R is the universal gas constant (8.314 J/mol·K), T is the absolute temperature in K and P_i is the partial pressure of the component *i*.

- **Gibbs Energy Minimization**

The equilibrium of a closed thermodynamic system is established when its Gibbs energy at constant temperature and pressure has reached its minimum.

$$G'(T,P,n_i') \leq G(T,P,n_i) \quad [A.2]$$

Gibbs Energy of the system of one or more phases is given by equation A.3.

$$G = \sum_k \sum_i n_i^k \cdot \mu_i^k \quad [A.3]$$

where k is the number of different phase, n_i is the molar amount of the phase constituent i, μ_i is the chemical potential of a phase constituent i,

At equilibrium the chemical potential of each element or compound at each phase is equal (equation A.5). The chemical potential is defined by equation A.4.

$$\mu_j^\alpha = \mu_j^\beta = \mu_j^\gamma ... \quad [A.4]$$

$$\mu_i = \mu_i^0 + R \cdot T \cdot \ln a_i = \mu_i^0 + R \cdot T \cdot \ln x_i \gamma_i \quad [A.5]$$

where *ai* is the activity and γ is the activity coefficient. Thereby, expression A.3 can be rewritten as:

$$G = \sum_k \sum_i n_i^k \left(\mu_i^{k0} + R \cdot T \cdot \ln x_i^k \gamma_i^k \right) \quad [A.6]$$

The minim value of Gibbs energy is found also when masses of the system components remain constant (mass balance constraints). This is mathematically expressed by A.7.

$$b_j = \sum_\alpha \sum_i n_i^\alpha \cdot a_{ij}^\alpha \quad [A.7]$$

where b_j is the molar amount of the system component *j*, n_i is the molar amount of the constituent *i* in phase α and a_{ij} is the stoichiometric coefficient of the system component *j* in constituent *i*.

FactStage uses ChemApp library during the process to minimize Gibbs energy.

Appendix B: Species included in the Thermodynamic Calculations

For the equilibrium calculations of Chapter 4, ideal gas phase compounds, pure solid phases, and pure liquid phases were included from the FactSage 6.2 compound database. The species included in the full calculations (section 4.4.1) from the compound database are listed below. For the simplified model (section 4.4.2) these species are also considered, excluding the species marked in bold.

- **Ideal gas phase components**

C	C_2	C_3	C_4	C_5	N	N_2	N_3
CN	C_2N	CNN	CNN (g2)	$(CN)_2$	C_4N_2	O	O_2
O_3	CO	C_2O	CO_2	C_3O_2	NO	N_2O	NO_2
NO_3	N_2O_3	N_2O_4	N_2O_5	NCO	Na	Na_2	NaCN
$(NaCN)_2$	NaO	**Al**	**Al_2**	**AlC**	**AlN**	**AlO**	**AlO**
Al_2O	**$(AlO)_2$**	**Si**	**Si_2**	**Si_3**	**SiC**	**SiC_2**	**Si_2C**
SiN	**Si_2N**	**SiO**	S	S_2	S_3	S_4	S_5
S_6	S_7	S_8	CS	CS_2	NS	SO	SO_2
SO_3	SSO	COS	Na_2SO_4	**AlS**	**Al_2S**	**Al_2S_2**	**SiS**
SiS_2	Cl	Cl_2	CCl	CCl_2	C_2Cl_2	CCl_3	CCl_4
C_2Cl_4	C_2Cl_6	C_6Cl_6	ClCN	ClO	ClO_2	Cl_2O	COCl
$COCl_2$	ONCl	NO_2Cl	NaCl	$(NaCl)_2$	**AlCl**	**$AlCl_2$**	**$AlCl_3$**
Al_2Cl_6	**OAlCl**	**$NaAlCl_4$**	**SiCl**	**$SiCl_2$**	**$SiCl_3$**	**$SiCl_4$**	SCl
S_2Cl	SCl_2	ClSSCl	$SOCl_2$	SO_2Cl_2	K	K_2	KCN
$(KCN)_2$	KO	K_2SO_4	KCl	$(KCl)_2$	**$KAlCl_4$**	Ca	Ca_2
CaO	CaS	CaCl	$CaCl_2$	**Fe**	**FeO**	**$Fe(CO)_5$**	**FeS**
FeCl	**$FeCl_2$**	**$FeCl_3$**	**$(FeCl_2)_2$**	**$(FeCl_3)_2$**	**$NaFeCl_4$**	**$AlCl_6Fe$**	**$FeAl_2Cl_8$**

- **Pure liquids phases**

Na_2O	**Al_2O_3**	**SiO_2**	K_2O	CaO	N_2O_4	Na	C_2Na_2
NaCN	Na_2O	Na_2CO_3	$NaNO_2$	$NaNO_3$	**Al**	**Al_2O_3**	**$NaAlO_2$**
Si	**SiO_2**	**$(Na_2O)(SiO_2)$**	**$(Na_2O)_2(SiO_2)$**	**$(Na_2O)(SiO_2)_2$**	**$Na_6Si_2O_7$**	S	CS_2
SO_3	Na_2S	NaS_2	Na_2S_2	Na_2S_3	Na_2SO_3	Na_2SO_4	AlS
Al_2S_3	SiS_2	CCl_4	C_2Cl_4	NaCl	**$AlCl_3$**	**$NaAlCl_4$**	**$SiCl_4$**
SCl_2	ClSSCl	K	KCN	K_2O	K_2CO_3	KNO_3	$KAlO_2$
K_2SiO_3	**$K_2Si_2O_5$**	**$K_2Si_4O_9$**	K_2S	K_2SO_3	K_2SO_4	KCl	$KAlCl_4$
Ca	CaO	**$CaAl_2$**	**$CaAl_4$**	**$CaAl_2O_4$**	**$CaAl_4O_7$**	$CaSO_4$	$CaCl_2$
Fe	**Fe_3C**	**FeO**	**Fe_3O_4**	**$Fe(CO)_5$**	**FeS**	**$FeCl_2$**	**$FeCl_3$**

- **Pure solid phases**

Na_2O	Na_2O (s2)	Na_2O (s3)	**Al_2O_3**	**Al_2O_3 (s2)**	**Al_2O_3 (s3)**
Al_2O_3 (s4)	**$NaAlO_2$**	**$NaAlO_2$(s2)**	**$NaAl_9O_{14}$**	**$Na_2Al_{12}O_{19}$**	**SiO_2**
SiO_2 (s2)	**SiO_2 (s3)**	**SiO_2 (s4)**	**SiO_2 (s5)**	**SiO_2 (s6)**	**SiO_2 (s7)**
SiO_2(s8)	**Na_2SiO_3**	**Na_4SiO_4**	**$Na_2Si_2O_5$**	**$Na_2Si_2O_5$ (s2)**	**$Na_2Si_2O_5$ (s3)**
$Na_6Si_2O_7$	**$Na_6Si_8O_{19}$**	**$Al_2Si_2O_7$**	**$NaAlSiO_4$**	**$NaAlSiO_4$ (s2)**	**$NaAlSi_2O_6$**
$NaAlSi_3O_8$	**$NaAlSi_3O_8$ (s2)**	K_2O	**$KAlO_2$**	**$KAlO_2$ (s2)**	**KAl_9O_{14}**
$K_2Al_{12}O_{19}$	**K_2SiO_3**	**$K_2Si_2O_5$**	**$K_2Si_2O_5$ (s2)**	**$K_2Si_2O_5$ (s3)**	**$K_2Si_4O_9$**
$K_2Si_4O_9$ (s2)	**$KAlSiO_4$**	**$KAlSiO_4$ (s2)**	**$KAlSi_2O_6$**	**$KAlSi_2O_6$ (s2)**	**$KAlSi_3O_8$**
$KAlSi_3O_8$ (s2)	**$KAlSi_3O_8$ (s3)**	CaO	**$CaAl_2O_4$**	**$CaAl_4O_7$**	**$CaAl_{12}O_{19}$**
$Ca_3Al_2O_6$	**$CaSiO_3$**	**$CaSiO_3$ (s2)**	**Ca_2SiO_4**	**Ca_2SiO_4 (s2)**	**Ca_2SiO_4 (s3)**
Ca_3SiO_5	**$Ca_3Si_2O_7$**	**$Na_4CaSi_3O_9$**	**$Na_2CaSi5O_{12}$**	**$Na_2Ca_2Si_3O_9$**	**$Na_2Ca_3Si_6O_{16}$**
$CaAl_2SiO_6$	**$CaAl_2Si_2O_8$**	**$CaAl_2Si_2O_8$ (s2)**	**$Ca_2Al_2SiO_7$**	**$Ca_3Al_2Si_3O_{12}$**	**Fe_2O_3**
Fe_2O_3 (s2)	**Fe_2O_3 (s3)**	**$Na_2Fe_2O_4$**	**$Al_2Fe_2O_66$**	**$FeSiO_3$**	**$FeSiO_3$ (s2)**
$FeSiO_3$ (s3)	**Fe_2SiO_4**	**Fe_2SiO_4 (s2)**	**Fe_2SiO_4 (s3)**	**$Fe_2Al_4Si_5O_{18}$**	**$Fe_3Al_2Si_3O_{12}$**
$CaFe_2O_4$	**$Ca_2Fe_2O_5$**	**$CaFe_4O_7$**	**$CaFeSi_2O_6$**	**$Ca_2FeSi_2O_7$**	**$Ca_3Fe_2Si_3O_{12}$**
C	C (s2)	N_2O_4	N_2O_5	Na	C_2Na_2
NaCN	NaO_2	Na_2O	Na_2O (s2)	Na_2O (s3)	Na_2O_2
Na_2O_2(s2)	Na_2CO_3	Na_2CO_3 (s2)	Na_2CO_3(s3)	$NaNO_2$	$NaNO_2$ (s2)
$NaNO_3$	$NaNO_3$ (s2)	**Al**	**Al_4C_3**	**AlN**	**Al_2O_3**
Al_2O_3(s2)	**Al_2O_3 (s3)**	**Al_2O_3 (s4)**	**$NaAlO_2$**	**$NaAlO_2$ (s2)**	**$NaAl_9O_{14}$**
$Na_2Al_{12}O_{19}$	**Si**	**SiC**	**SiC (s2)**	**Si_3N_4**	**SiO_2**
SiO_2 (s2)	**SiO_2 (s3)**	**SiO_2 (s4)**	**SiO_2 (s5)**	**SiO_2 (s6)**	**SiO_2 (s7)**
SiO_2 (s8)	**$(Na_2O)(SiO_2)$**	**$(Na_2O)_2(SiO_2)$**	**$(Na_2O)(SiO_2)_2$**	**$(Na_2O)(SiO_2)_2$ (s2)**	**$(Na_2O)(SiO_2)_2$ (s3)**
$Na_6Si_2O_7$	**$Na_6Si_8O_{19}$**	**Al_2SiO_5**	**Al_2SiO_5 (s2)**	**Al_2SiO_5(s3)**	**$(Al_2O_3)(SiO_2)_2$**
$Al_6Si_2O_{13}$	**$NaAlSiO_4$**	**$NaAlSiO_4$(s2)**	**$NaAlSiO_4$ (s3)**	**$NaAlSiO_4$ (s4)**	**$NaAlSi_2O_6$**
$NaAlSi_3O_8$	**$NaAlSi_3O_8$ (s2)**	S	S (s2)	SO_3	Na_2S
NaS_2	Na_2S_2	Na_2S_3	Na_2S_4	Na_2SO_3	Na_2SO_4
Na_2SO_4 (s2)	**AlS**	**Al_2S_3**	**$Al_2(SO_4)_3$**	**SiS**	**SiS_2**
NaCl	$NaClO_4$	$NaClO_4$ (s2)	**$AlCl_3$**	**OAlCl**	**$NaAlCl_4$**
K	KCN	KO_2	K_2O	K_2O_2	K_2CO_3
K_2CO_3 (s2)	KNO_3	KNO_3 (s2)	**$KAlO_2$**	**$KAlO_2$ (s2)**	**KAl_9O_{14}**
$K_2Al_{12}O_{19}$	**K_2SiO_3**	**$K_2Si_2O_5$**	**$K_2Si_2O_5$ (s2)**	**$K_2Si_2O_5$ (s3)**	**$K_2Si_4O_9$**
$K_2Si_4O_9$ (s2)	**$KAlSiO_4$**	**$KAlSiO_4$ (s2)**	**$KAlSi_2O_6$**	**$KAlSi_2O_6$ (s2)**	**$KAlSi_3O_8$**
$KAlSi_3O_8$ (s2)	**$KAlSi_3O_8$ (s3)**	K_2S	K_2SO_3	K_2SO_4	K_2SO_4 (s2)
$K_3Na(SO_4)_2$	$KAl(SO_4)_2$	KCl	$KClO_4$	$KClO_4$ (s2)	K_2ClNO_3
$KAlCl_4$	Ca	Ca (s2)	CaC_2	CaC_2 (s2)	Ca_3N_2
CaO	CaO_2	$CaCO_3$	$CaCO_3$ (s2)	$Ca(NO_3)_2$	**$CaAl_2$**
$CaAl_4$	**$CaAl_2O_4$**	**$CaAl_4O_7$**	**$CaAl_{12}O_{19}$**	**$Ca_3Al_2O_6$**	**CaSi**
$CaSi_2$	**Ca_2Si**	**$CaSiO_3$**	**$CaSiO_3$ (s2)**	**Ca_2SiO_4**	**Ca_2SiO_4 (s2)**
Ca_2SiO_4 (s3)	**Ca_3SiO_5**	**$Ca_3Si_2O_7$**	**$Na_4CaSi_3O_9$**	**$Na_2CaSi_5O_{12}$**	**$Na_2Ca_2Si_3O_9$**
$Na_2Ca_3Si_6O_{16}$	**$CaAl_2SiO_6$**	**$CaAl_2Si_2O_8$**	**$CaAl_2Si_2O_8$ (s2)**	**$Ca_2Al_2SiO_7$**	**$Ca_3Al_2Si_3O_{12}$**
CaS	$CaSO_3$	$CaSO_4$	$CaSO_4$ (s2)	$CaCl_2$	$CaOCl_2$

$K_2Ca(CO_3)_2$	$K_2Ca_2(CO_3)_3$	$K_2Ca_2(SO_4)_3$	$KCaCl_3$	**Fe**	**Fe (s2)**
Fe_3C	**Fe_3C (s2)**	**Fe_2N**	**Fe_4N**	**Fe_4N (s2)**	**FeO**
Fe_2O_3	**Fe_2O_3 (s2)**	**Fe_2O_3 (s3)**	**Fe_3O_4**	**Fe_3O_4 (s2)**	**Fe_3O_4 (s3)**
Fe_3O_4 (s4)	**$FeCO_3$**	**$(Na_2O)(Fe_2O_3)$**	**$FeAl_3$**	**$FeAl_2O_4$**	**$Al_2Fe_2O_6$**
FeSi	**$FeSi_2$**	**Fe_3Si**	**Fe_3Si_7**	**$FeSiO_3$**	**$FeSiO_3$ (s2)**
$FeSiO_3$(s3)	**$(FeO)_2(SiO_2)$**	**$(FeO)_2(SiO_2)$ (s2)**	**$(FeO)_2(SiO_2)$ (s3)**	**$Fe_2Al_4Si_5O_{18}$**	**$Fe_3Al_2Si_3O_{12}$**
FeS	**FeS (s2)**	**FeS (s3)**	**FeS_2**	**FeS_2 (s2)**	**Fe_7S_8**
$FeSO_4$	**$Fe_2(SO_4)_3$**	**$FeCl_2$**	**$FeCl_3$**	**FeOCl**	**$NaFeC_{l4}$**
$FeAl_2Cl_8$	**$KFeCl_3$**	**$KFeCl_4$**	**K_2FeCl_4**	**$CaFe_2O_4$**	**$Ca_2Fe_2O_5$**
$CaFe_4O_7$	**$CaFeSi_2O_6$**	**$Ca_2FeSi_2O_7$**	**$Ca_3Fe_2Si_3O_{12}$**		

Appendix C: Data from the Experiments using Reducing Agents

- **Example of obtained Data**

Original data obtained in the experiments presented in Chapter 6 is exemplified in Figure C-1, which shows the constant SO_2 concentration for different CO concentrations introduced in different experiments. The duration of the period where CO was introduced under the bed material for each concentration was 4 or 5 min in order to reach a steady-state and have a constant SO_2 concentration. The results shown in Chapter 6 are the averages of the constant SO_2 concentrations and the standard deviations of results.

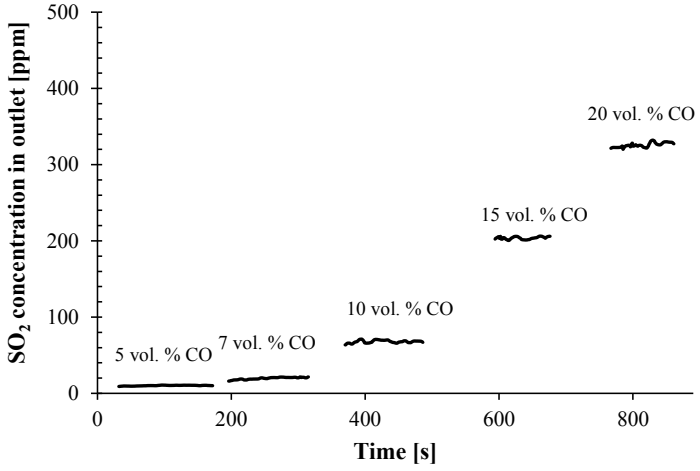

Figure C-1: Effect of different CO concentrations introduced under the bed material on SO_2 concentration. Experimental conditions: flow tube 1NL/min, 900 °C, 5 % fill degree, 2 wt. % $CaSO_4$, 100 NL/min with 5 vol. % O_2, 6 rpm.

- **Carbon Balance**

The carbon mass balance was checked by considering the molar mass flow rate of CO introduced and CO_2 measured by the gas analyzer, according to equation C.1. The deviation of the results is calculated according to equation C.2.

$$\dot{n}_{CO,\text{in}} = \dot{n}_{CO,\text{out}} \qquad [C.1]$$

$$Deviation\,(\%) = \frac{\dot{n}_{C,\text{out}} - \dot{n}_{C,\text{in}}}{\dot{n}_{C,\text{in}}} \cdot 100 \qquad [C.2]$$

The CO_2 concentration measured by the analyzer needed to be corrected for the mass balance because the CO_2 coming from the air of the freeboard atmosphere need to be subtracted. The base lines are 215-248 ppm CO_2 when using 5 vol. % O_2 and 383 ppm CO_2 when using 10 vol. % O_2. The data for the experiments performed

at 900 ºC at 5 and 10 vol. % O_2 are shown in Table C-1 and C-2, respectively, and Table C-3 shows the data for the experiments performed at 1000 ºC.

Table C-1: Carbon balance and deviation for the experiments performed at 900 ºC and 5 vol. % O_2. Note: Base line for CO_2 from the air content of the freeboard atmosphere is 215 ppm.

IN			**OUT**				
Flow	1 NL/min		Flow	101 NL/min			
CO conc. [vol. %]	y_{CO}	kmol CO/min = **kmol C_{in}/min**	CO_2 conc. [ppm]	CO_2 without base line [ppm]	y_{CO2}	kmol CO_2/min= **kmol C_{out}/min**	**Deviation [%]**
5	0.05	$2.23 \cdot 10^{-3}$	683	468	$4.68 \cdot 10^{-4}$	$2.11 \cdot 10^{-3}$	5.46
7	0.07	$3.12 \cdot 10^{-3}$	853	638	$6.38 \cdot 10^{-4}$	$2.87 \cdot 10^{-3}$	7.95
10	0.1	$4.46 \cdot 10^{-3}$	1165	950	$9.50 \cdot 10^{-4}$	$4.28 \cdot 10^{-3}$	4.05
15	0.15	$6.69 \cdot 10^{-3}$	1590	1375	$1.38 \cdot 10^{-3}$	$6.20 \cdot 10^{-3}$	7.42
20	0.2	$8.92 \cdot 10^{-3}$	2101	1886	$1.89 \cdot 10^{-3}$	$8.50 \cdot 10^{-3}$	4.76

Table C-2: Carbon balance and deviation for the experiments performed at 900 ºC and 10 vol. % O_2. Note: Base line for CO_2 from the air content of the freeboard atmosphere is 383 ppm.

IN			**OUT**				
Flow	1 NL/min		Flow	101 NL/min			
CO conc. [vol. %]	y_{CO}	kmol CO/min = **kmol C/min**	CO_2 conc. [ppm]	CO_2 without base line [ppm]	y_{CO2}	kmol CO_2/min= **kmol C/min**	**Deviation [%]**
5	0.05	$2.23 \cdot 10^{-3}$	861	478	$4.78 \cdot 10^{-4}$	$2.15 \cdot 10^{-3}$	3.44
7	0.07	$3.12 \cdot 10^{-3}$	1050	667	$6.67 \cdot 10^{-4}$	$3.01 \cdot 10^{-3}$	3.76
10	0.1	$4.46 \cdot 10^{-3}$	1309	926	$9.26 \cdot 10^{-4}$	$4.17 \cdot 10^{-3}$	6.47
15	0.15	$6.69 \cdot 10^{-3}$	1865	1482	$1.48 \cdot 10^{-3}$	$6.68 \cdot 10^{-3}$	0.21
20	0.2	$8.92 \cdot 10^{-3}$	2297	1914	$1.91 \cdot 10^{-3}$	$8.62 \cdot 10^{-3}$	3.34

Table C-3: Carbon balance and deviation for the experiments performed at 1000 ºC and 5 vol. % O_2. Note: Base line for CO_2 from the air content of the freeboard atmosphere is 248 ppm.

IN			**OUT**				
Flow	1 NL/min		Flow	101 NL/min			
CO conc. [vol. %]	y_{CO}	kmol CO/min = **kmol C/min**	CO_2 conc. [ppm]	CO_2 without base line [ppm]	y_{CO2}	kmol CO_2/min= **kmol C/min**	**Deviation [%]**
5	0.05	$2.23 \cdot 10^{-3}$	780	482	$4.82 \cdot 10^{-4}$	$2.17 \cdot 10^{-3}$	2.64
10	0.1	$4.46 \cdot 10^{-3}$	1240	942	$9.42 \cdot 10^{-4}$	$4.24 \cdot 10^{-3}$	4.86
15	0.15	$6.69 \cdot 10^{-3}$	1785	1543	$1.54 \cdot 10^{-3}$	$6.95 \cdot 10^{-3}$	3.90
20	0.2	$8.92 \cdot 10^{-3}$	2324	2026	$2.03 \cdot 10^{-3}$	$9.1 \cdot 10^{-3}$	2.31

- **CO_2 concentrations of the Different Experiments**

The corresponding CO_2 concentrations measured for each experiment of section 6.3 are plotted as the average of the constant concentrations and the standard deviations of results. Figure C-2 shows the CO_2 concentrations for different CO concentrations used varying the oxygen concentration.

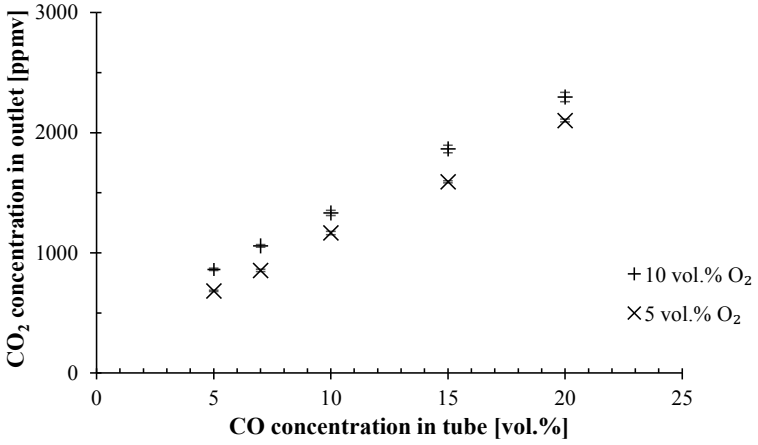

Figure C-1: CO_2 concentration when different CO concentrations were introduced under the bed material with 5 and 10 vol. % O_2. Experimental conditions: flow tube 1NL/min, 900 °C, 5 % fill degree, 2 wt. % $CaSO_4$, 100 NL/min, 6 rpm.

The CO_2 concentrations for different CO concentrations used varying the temperature are shown in Figure C-3.

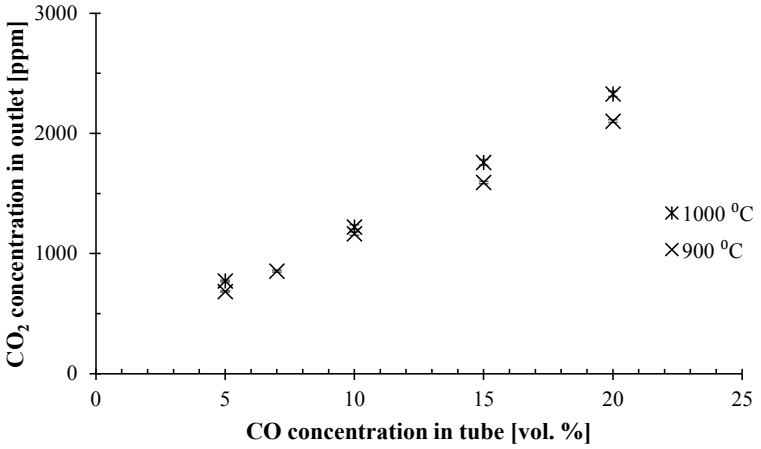

Figure C-2: CO_2 concentration when different CO concentrations were introduced under the bed material at 900 and 1000 °C. Experimental conditions: flow tube 1 NL/min, 5 % fill degree, 2 wt. % $CaSO_4$, 100 NL/min with 5 vol. % O_2, 6 rpm.

The CO_2 concentrations corresponding to the experiments investigating the time of exposure of different CO concentrations at 900 and 1000 ºC are plotted in Figure C-4 and Figure C-5, respectively.

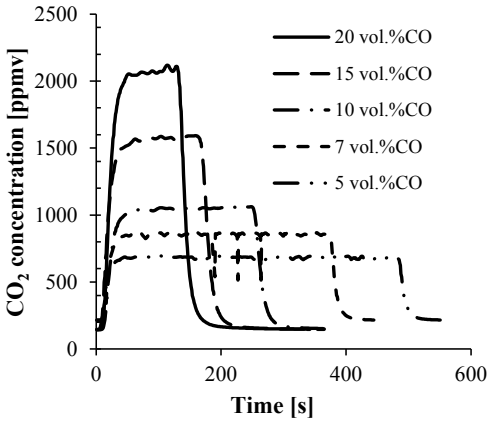

Figure C-3: CO_2 concentrations when a total of 0.4 L of CO was introduced under the bed material with 5, 7, 10, 15, and 20 vol. % CO at 900 °C. Experimental conditions: flow tube 1 NL/min, 5 % fill degree, 2 wt. % $CaSO_4$, 100 NL/min with 5 vol. % O_2, 6 rpm.

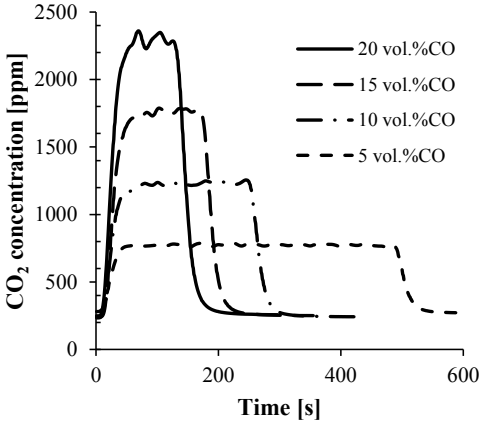

Figure C-4: CO_2 concentrations when a total of 0.4 L of CO was introduced under the bed material with 5, 10, 15, and 20 vol. % at 1000 °C. Experimental conditions: flow tube 1 NL/min, 5 % fill degree, 2 wt. % $CaSO_4$, 100 NL/min with 5 vol. % O_2, 6 rpm.

For the different CH_4 concentrations experiments, the corresponding CO_2 concentrations varying the oxygen concentration are illustrated in Figure C-6.

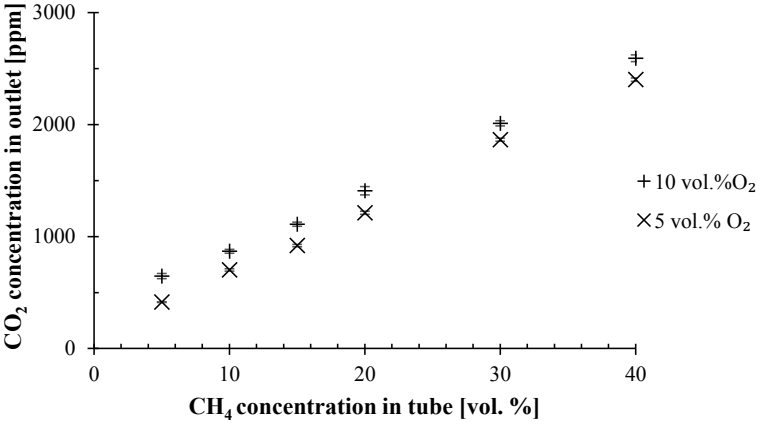

Figure C-6: CO_2 concentration when different CH_4 concentrations were introduced under the bed material with 5 and 10 vol. % O_2. Experimental conditions: flow tube 1NL/min, 900 °C, 5 % fill degree, 2 wt. % $CaSO_4$, 100 NL/min, 6 rpm.

The corresponding CO_2 concentrations for different CH_4 concentrations used varying the temperature are illustrated in Figure C-7.

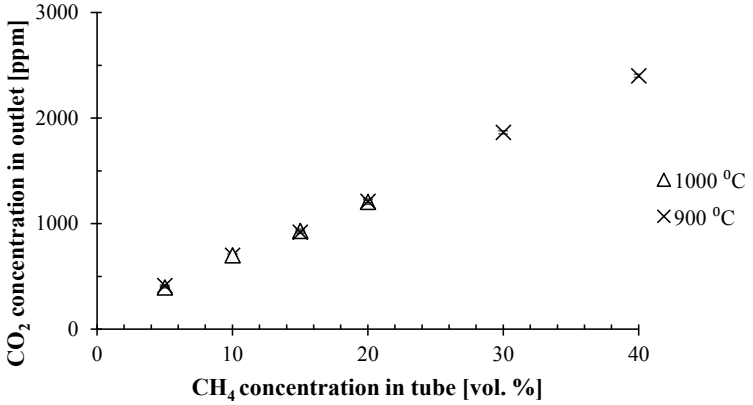

Figure C-5: CO_2 concentration when different CH_4 concentrations were introduced under the bed material at 900 and 1000 °C. Experimental conditions: flow tube 1 NL/min, 5 % fill degree, 2 wt. % $CaSO_4$, 100 NL/min with 5 vol. % O_2, 6 rpm.

The CO_2 concentrations corresponding to the experiments investigating the time of exposure of different CH_4 concentrations at 900 and 1000 °C are plotted in Figure C-8 and Figure C-9, respectively.

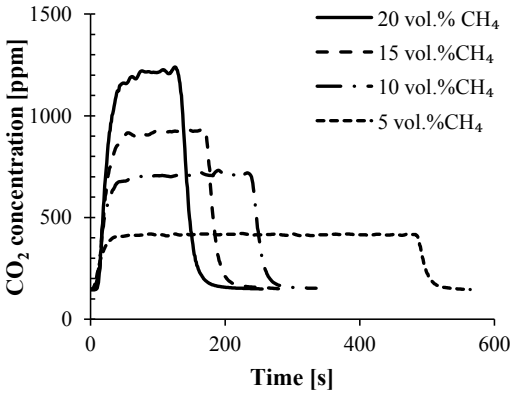

Figure C-6: CO_2 concentrations when a total of 0.4 L of CH_4 was introduced under the bed material with 5, 10, 15 and 20 vol. % CH_4 at 900 °C. Experimental conditions: flow tube 1NL/min, 5 % fill degree, 2 wt. % $CaSO_4$, 100 NL/min with 5 vol. % O_2, 6 rpm.

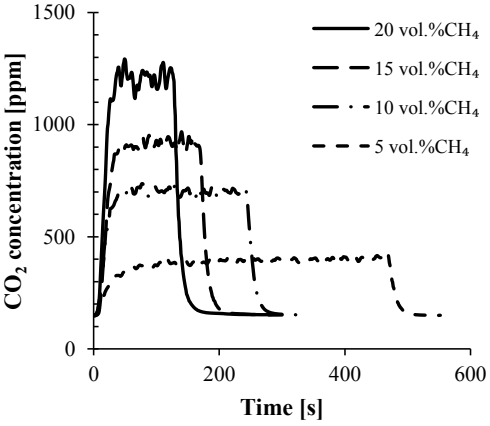

Figure C-7: CO_2 concentrations when a total of 0.4 L CH_4 was introduced under the bed material with 5, 10, 15 and 20 vol. % CH_4 at 1000 °C. Experimental conditions: flow tube 1NL/min, 5 % fill degree, 2 wt. % $CaSO_4$, 100 NL/min with 5 vol. % O_2, 6 rpm.

The corresponding CO_2 concentrations for experiments of the mixtures of CO/CH_4 and CO/H_2 as function of the CO concentration are shown in Figure C-10, and for the experiments of the CH_4/CO and CH_4/H_2 mixtures as function of the CH4 concentration in Figure C-11.

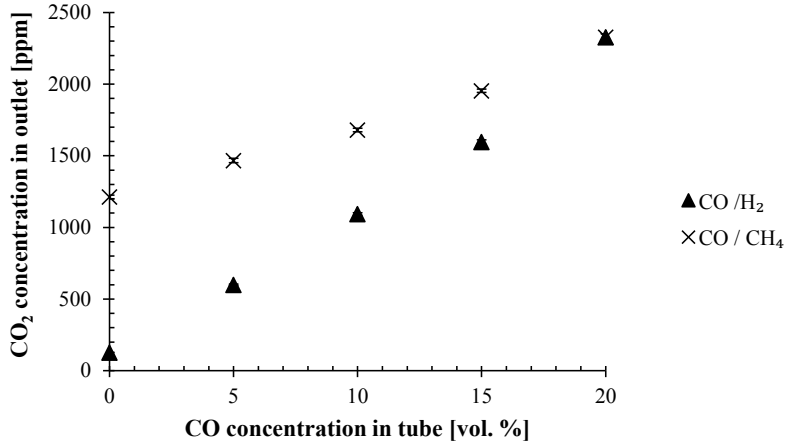

Figure C-8: CO_2 concentrations when mixtures CO/CH_4 and CO/H_2 were introduced under the bed material at 900 °C. Experimental conditions: flow tube 1 NL/min, 5 % fill degree, 2 wt. % $CaSO_4$, 100 NL/min with 5 vol. % O_2, 6 rpm.

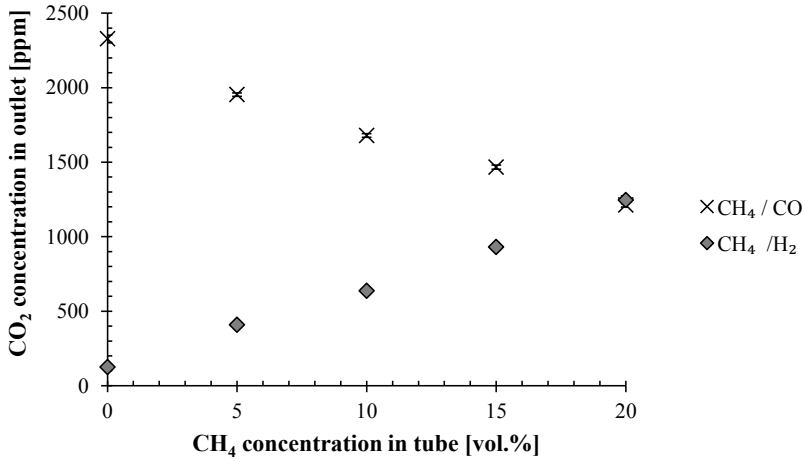

Figure C-9: CO_2 concentrations when mixtures of CH_4/CO and CH_4/H_2 were introduced under the bed material at 900 °C. Experimental conditions: flow tube 1 NL/min, 5 % fill degree, 2 wt. % $CaSO_4$, 100 NL/min with 5 vol. % O_2, 6 rpm.

Appendix D: Kinetic Studies of $CaSO_4$ Reductive Decomposition

Kinetic studies of the reductive decomposition of $CaSO_4$ with CO and H_2 have been performed at different concentrations and temperature ranges by many authors (Diaz-Bossio et al., 1985; Xiao and Song, 2011; Zheng et al., 2011; Kim and Sohn, 2002; Talukdar et al., 1996). The activation energy and the pre-exponential factor found for the reductive decomposition of $CaSO_4$ with CO and H_2 according to reactions (D-1) and (D-2) are summarized in Table D-1. No kinetic parameters for the reductive decomposition of $CaSO_4$ with CH_4 have been reported.

$$CaSO_4(s) + CO\,(g) \rightarrow CaO(s) + SO_2(g) + CO_2(g) \quad \text{(D-1)}$$

$$CaSO_4(s) + H_2(g) \rightarrow CaO(s) + SO_2(g) + H_2O\,(g) \quad \text{(D-2)}$$

Table D-1: Summery of the reported kinetic parameters for reductive decomposition of $CaSO_4$ by CO and H_2.

Reaction	Reducing agent	Conditions	T range [°C]	Ea [kJ/mol]	A [m/s]	Equipment	Reference
(D-1)	CO	variation 1-6 vol. % CO with 24 vol. % CO_2	900-1180	242 ± 33	$7.4 \cdot 10^4$	TGA	(Diaz-Bossio et al., 1985)
(D-1)	CO	variation 0.1-1 vol. % CO	750-950	251.7	$6.964 \cdot 10^7$	Circulating fluidized bed reactor	(Talukdar et al., 1996)
(D-1)	CO	20, 40 and 70 vol. % CO in N_2	880-950	145.3	$1.89 \cdot 10^3$	Isothermal bed reactor	(Xiao and Song, 2011)
(D-2)	H_2	variation 1-6 vol. % H_2 with 24 vol. % CO_2	900-1180	288 ± 44	$6.1 \cdot 10^6$	TGA	(Diaz-Bossio et al., 1985)

The kinetic parameters for the reductive decomposition of $CaSO_4$ by CO found by Xiao and Song (Xiao and Song, 2011) are the ones used for the model because no CO_2 was introduced and the temperature range is relevant.

Appendix D References

Diaz-Bossio, L. M., Squier, S. E., and Pulsifer, A. H.; Reductive decomposition of calcium sulfate utilizing carbon monoxide and hydrogen. Chemical Engineering Science, 40, 319-24, 1985.

Kim, B., and Sohn, H. Y.; A novel cyclic reaction system involving CaS and $CaSO_4$ for converting sulfur dioxide to elemental sulfur without generating secondary pollutants. 3. Kinetics of the hydrogen reduction of the calcium sulfate powder to calcium sulfide. Industrial & Engineering Chemistry Research, 41, 3092-6, 2002.

Talukdar, J., Basu, P., and Greenblatt, J. H.; Reduction of calcium sulfate in a coal-fired circulating fluidized bed furnace. Fuel, 75, 1115-23, 1996.

Xiao, R., and Song, Q.; Characterization and kinetics of reduction of $CaSO_4$ with carbon monoxide for chemical-looping combustion. Combustion and Flame, 158, 2524-39, 2011.

Zheng, M., Shen, L., Feng, X., and Xiao, J.; Kinetic model for parallel reactions of $CaSO_4$ with CO in chemical-looping combustion. Industrial & Engineering Chemistry Research, 50, 5414-27, 2011.

Appendix E: $CaSO_4$ Particle Analysis

The particle size of $CaSO_4$ has been characterized by a Malvern with a repetition of 5 samples. The statistical results are listed below.

Results Statistics:

Distribution type: Volume	Concentration= 0.0066 vol. %	Density= 1.000 g/ cm^3	Specific S.A. = 3.2264 m^2/g
Mean diameters:	D (v, 0.1)= 0.97 µm	D (v, 0.5)= 6.49 µm	D (v, 0.9)= 28.74 µm

The cumulative particle distribution is shown in Figure E-1 and the raw data obtained is presented in Table E-1.

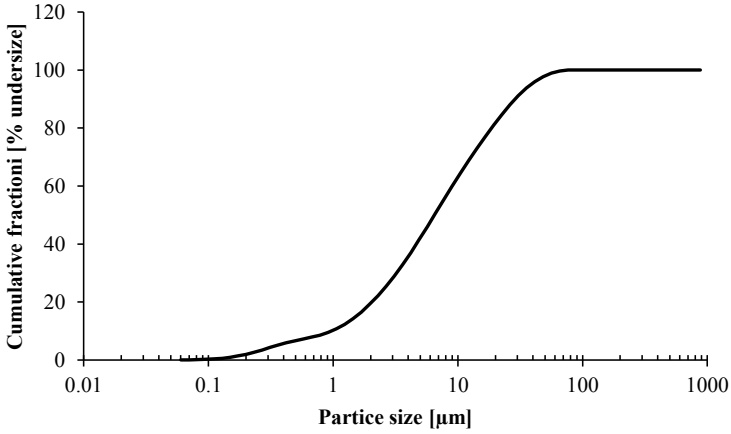

Figure E-1: Cumulative particle distribution of the used $CaSO_4$.

Table E-2: Low and high particle size interval corresponding to the cumulative fraction for the $CaSO_4$ particle distribution.

Size low [µm]	Size high [µm]	Cumulative fraction [% undersize]	Size low [µm]	Size high [µm]	Cumulative fraction [% undersize]
0.05	0.06	0.02	6.63	7.72	55.33
0.06	0.07	0.05	7.72	9.00	59.94
0.07	0.08	0.11	9.00	10.48	64.44
0.08	0.09	0.21	10.48	12.21	68.80
0.09	0.11	0.36	12.21	14.22	73.01
0.11	0.13	0.59	14.22	16.57	77.06
0.13	0.15	0.92	16.57	19.31	80.95
0.15	0.17	1.36	19.31	22.49	84.65
0.17	0.20	1.93	22.49	26.20	88.08
0.20	0.23	2.64	26.20	30.53	91.18
0.23	0.27	3.45	30.53	35.56	93.86
0.27	0.31	4.31	35.56	41.43	96.05
0.31	0.36	5.15	41.43	48.27	97.74
0.36	0.42	5.91	48.27	56.23	98.93
0.42	0.49	6.60	56.23	65.51	99.68
0.49	0.58	7.24	65.51	76.32	100.00
0.58	0.67	7.87	76.32	88.91	100.00
0.67	0.78	8.57	88.91	103.58	100.00
0.78	0.91	9.53	103.58	120.67	100.00
0.91	1.06	10.76	120.67	140.58	100.00
1.06	1.24	12.31	140.58	163.77	100.00
1.24	1.44	14.23	163.77	190.80	100.00
1.44	1.68	16.51	190.80	222.28	100.00
1.68	1.95	19.13	222.28	258.95	100.00
1.95	2.28	22.08	258.95	301.68	100.00
2.28	2.65	25.35	301.68	351.46	100.00
2.65	3.09	28.93	351.46	409.45	100.00
3.09	3.60	32.82	409.45	477.01	100.00
3.60	4.19	37.00	477.01	555.71	100.00
4.19	4.88	41.41	555.71	647.41	100.00
4.88	5.69	46.00	647.41	754.23	100.00
5.69	6.63	50.66	754.23	878.67	100.00

Appendix F: Mass balance in basis of loss of ignition free

The solid mass flows of the raw meal and hot meal are calculated in loss of ignition free based according to equation F.1. The basis of loss of ignition free allows their comparison at different locations, after and before calcination.

$$\dot{m}_{j,LOI\,free} = \frac{\dot{m}_j \cdot (100 - LOI_j)}{100} \qquad \text{where } j\text{= raw meal or hot meal} \qquad [F.1]$$

In Figure F-1, the typical material feed and hot meal (in black) and dust loss (in red) are specified. The net flows are calculated in order to check that at the different locations of the plant there is approximately 1 kg of material LOI free per kg of clinker. The dust from the rotary kiln is assumed to have 0 % LOI in order to calculate the net flow of the hot meal, and 15 % of the kiln dust is removed by the bypass.

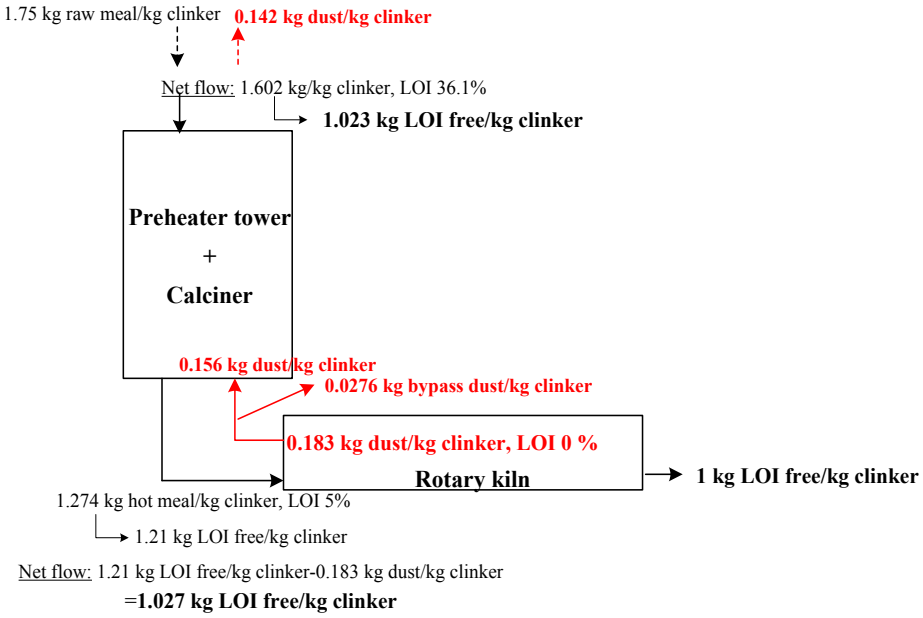

Figure F-1: Solid mass flows material feed and hot meal (in black) and dust loss (in red) in basis of loss of ignition free in order to check that there is no formation or loss of material.

Appendix G: Industrial gas measurement system principles

- **Cold gas measurement system principle**

The fixed gas measurement system is located in kiln inlet. The gas measurement system can be divided in three main blocks as illustrated in Figure G-1.

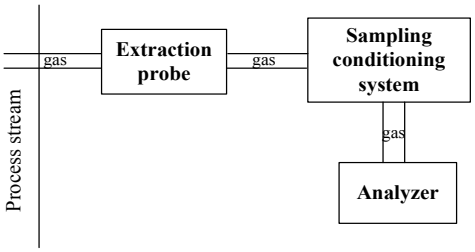

Figure G-1: Measuring principle of the process gas analysis system.

The gas measurement system consists of:

- An extraction probe. The design of the extraction probe is identical for the cold gas measurement system and the hot FTIR measurement system. It consists of a tube with a steel cooling jacket with circulating water to keep the probe cool, so it can resist the high temperature in cement plants. The inner tube is heated to 200-210 ^{o}C.

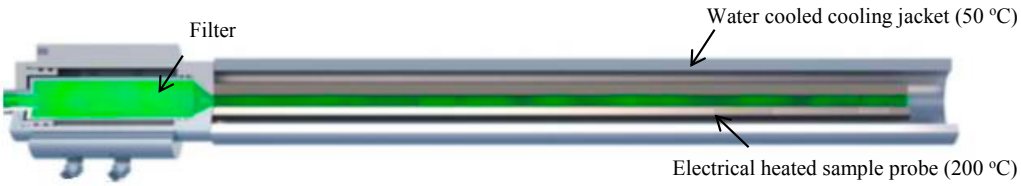

Figure G-2: Schematic drawing of the applied extraction probe (FSLmidth A/S 2012a).

- Sampling conditioning system. It consists of a gas cooler, a gas pump, a condensation pump, a flow meter and a filter with humidity sensor. The sample gas pump sucks the gas which is cooled to 5 ^{o}C in the gas cooler to remove condensate water (FLSmidth A/S, 2012b).
- Analyzer. This cement plant has an infrared system to analyze SO_2, CO, and NO, and paramagnetic for O_2.

- **Hot FTIR measurement system principle**

The FTIR measurement system consists of the blocks shown in Figure G-1. The sampling conditioning system differs between the two techniques. In the FTIR measurement system the gas is not cooled. The heated pump contains a zirconium cell for analyzing the oxygen. The analyzer consists of an FTIR spectometer, where the rest of the gas components, are analysed.

FTIR analyzes the gas composition by measuring the absorbance at different frequencies. The structure of the FTIR spectrometer is shown in Figure G-3. The spectrometer measures all the IR wavelengths simultaneously. FTIR has the advantage of being able to measure continuously and multicomponents simultaneously, such as NO_x, SO_2, CO_2, CO, H_2O, NH_3, HCl, and hydrocarbons from single measurement and interferences are automatically resolved. NH_3, HCl and hydrocarbons can be measured by the FTIR because the gas has not been cooled and these componends have not condensed.

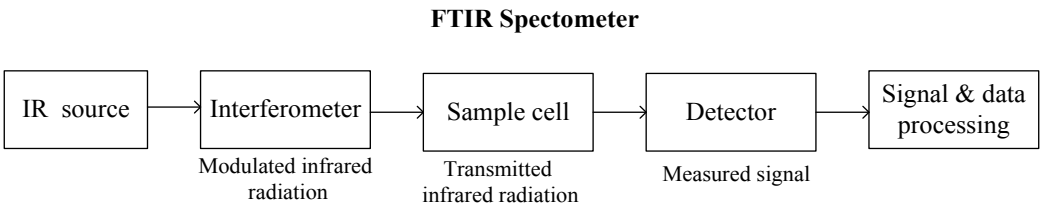

Figure G-3: Scheme of the structure of FTIR spectrometer (Gasmet, 2013).

Appendix G References

FLSmidth A/S; Kiln inlet gas analysis for a competitive edge. 2012a. Available at http://www.flsmidth.com/en-us/Gas+Analysis+Technology/Applications/Gas+Analysis+in+Cement/Kiln+Inlet/Kiln+Inlet+Gas+Analysis.

FLSmidth A/S; Gas conditioning system. 2012b. Available at http://www.flsmidth.com/en-US/Gas+Analysis+Technology/Products/Gas+Analysis+Systems/Gas+Conditioning+Systems.

Gasmet; FTIR gas analysers. 2013. Available at http://www.gasmet.com/products/ftir_gas_analyzers/.

Appendix H: Clinker composition for the industrial investigation

In order to calculate the sulfur evaporation factor, SO_3 content in the clinker is needed. The clinker analysis, which corresponds to the hot meal sample after 30 min from the time of sampling is summarized in Table H-1.

Table H-1: Summary of the clinker analysis corresponding to the hot meal samples taken.

	Clinker composition [wt. % clinker based]									
	Free CaO	Alite	Aluminate	Ferrite	SO_3	Na_{eq}	Fluoride	Cl	P_2O_5	MgO
Sampling day 1	0.8	65.8	7.5	12.3	1.3	0.5	0.1	0	0.4	0.9
Sampling day 2	1.2	67.5	7.3	12.6	1.7	0.6	0.2	0	0.4	0.9
Sampling day 3	2.0	72.7	8.0	12.1	1.6	0.6	0.1	0	0.3	0.9
Sampling day 3 (test 1)	1.8	78.7	7.9	12.1	1.6	0.6	0.1	0	0.4	0.9
Sampling day 4 (test 2)	1.3	63.2	7.5	12.5	1.4	0.6	0.1	0	0.3	0.8
Sampling day 5	1.0	64.6	7.6	12.6	1.6	0.6	0.2	0	0.2	0.9
Sampling day 6	1.1	67.7	7.4	12.6	1.7	0.6	0.2	0	0.2	0.8
Sampling day 7	2.1	70.9	7.4	11.8	1.5	0.6	0.1	0	0.3	0.9
Sampling day 8	1.2	69.5	8.2	12.1	1.4	0.6	0.1	0	0.3	0.9

Publication

Maria del Mar Cortada Mut,[1] Linda Kaare Nørskov,[2] Peter Glarborg[1] and Kim Dam-Johansen[1]
[1] Technical University of Denmark, [2] FLSmidth A/S, Denmark

Sulphur release from alternative fuel firing

The cement industry has long been dependent on the use of fossil fuels, although a recent trend in replacing fossil fuels with alternative fuels has arisen.[1,2] However, when unconverted or partly converted alternative fuels are admitted directly in the rotary kiln inlet, the volatiles released from the fuels may react with sulphates present in the hot meal to form SO_2. Here Maria del Mar Cortada Mut and associates describe pilot and industrial scale experiments focusing on the factors that affect SO_2 release in the cement kiln inlet.

In the cement industry alternative fuels are often fired directly in the calciner and/or the main burner despite the large particle sizes because this requires the lowest investment. A consequence of firing large alternative fuel particles is that the partially converted or unburned solid fuels may fall into the material charge and affect the process stability. Solid fuels can end up in the material charge in the rotary kiln in four different ways if the fuels are fired in the calciner, main burner or directly into the material inlet of the kiln (Figure 1):[3]

1. Large solid fuel particles of a considerable weight, which cannot be carried upwards with the gas flow, when fired in the calciner, may drop through the riser duct into the rotary kiln.
2. Large solid fuel particles fired through the kiln burners may not be completely combusted in the flame of the main burner and fall into the material charge.
3. Small and unconverted solid fuel particles, which are light enough to be carried upwards with the gas flow through the calciner and transported into the bottom cyclone stage, may flow into the kiln inlet with calcined raw meal.
4. Coarse solid fuels may be fired directly into the rotary kiln material inlet end.

Consequences of the combustion of alternative fuels in the rotary kiln can include:

- Direct physical contact between the fuels and the cement raw materials;
- Local reducing conditions in the bed material of the rotary kiln;
- Potential increase of internal circulation of sulphur, chlorine and alkali metal species.

These consequences result in modified process conditions and may affect the clinker quality and the process operation, causing build-ups, blockages and/or corrosion. The formation of build-ups and blockages is a consequence of high internal circulation in the kiln of the volatile elements, which are sulphur, chlorine and alkali metals. This article focuses on the kiln inlet of the rotary kiln and sulphur recirculation.

Sulphur recirculation

Sulphur can be introduced to cement rotary kilns by the cement raw materials and/or by the fuels. Biomass fuels such as wood waste and straw contain between 5-10 times less sulphur than fossil fuels. A large difference in sulphur content between fossil fuels also exists. The gaseous SO_2 coming from burner fuel and thermal decomposition in the rotary kiln flows to the calciner, where good gas-solid mixing and the temperature favours nearly 100% capture of the SO_2 with free lime (CaO), forming calcium sulphate ($CaSO_4$). Calcium sulphate, whether sourced from the raw materials or formed in the calciner, will be incorporated in the hot meal entering the rotary kiln.

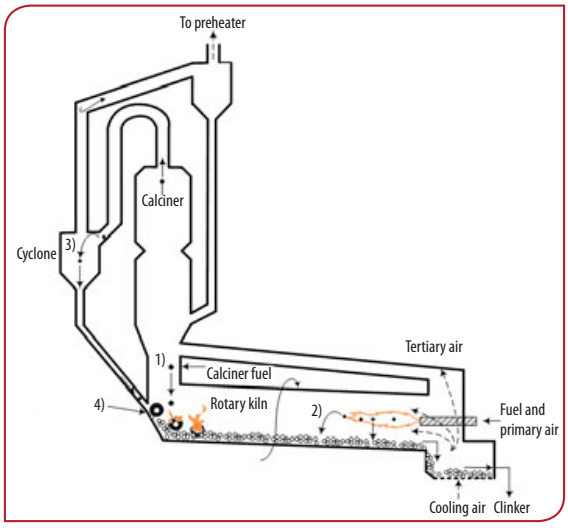

Right - Figure 1: The four scenarios whereby solid fuels can drop into the material charge in the rotary kiln.[3]

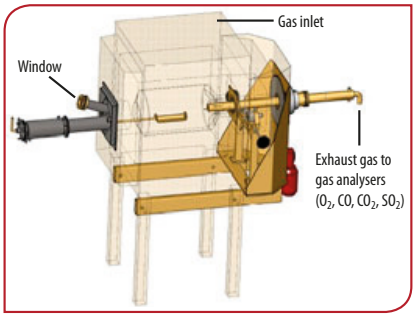

Left - Figure 2: 3D view of the high temperature rotary drum.

The combustion of alternative fuels in direct contact with the bed material in the kiln inlet may result in SO_2 release resulting from the decomposition of $CaSO_4$ by reducing gases released by the fuels. The main volatile compounds released from the fuels are CO(g), CH_4(g) and H_2(g). Consequentially, $CaSO_4$(s) decomposes according to reactions **1**, **2** and **3**, resulting in the release of SO_2(g). In the calciner, the SO_2 can again be absorbed on the CaO to form $CaSO_4$. Thus, an internal sulphur cycle is established in the rotary kiln and the calciner, which increases the intensity of the sulphur cycle in the kiln.

1. $CaSO_4 + CO \rightarrow CaO + SO_2 + CO_2$
2. $CaSO_4 + ¼CH_4 \rightarrow CaO + SO_2 + ¼CO_2 + ½H_2O$
3. $CaSO_4 + H_2 \rightarrow CaO + SO_2 + H_2O$

High levels of SO_2(g) increase the risk of deposit build-ups and corrosion. The deposits typically accumulate in the material inlet end of the rotary kiln or in the riser duct between the calciner and rotary kiln, where they cause blockages. In severe cases, it may be necessary to shut down the cement plant to remove the deposits.

Pilot plant experiments

Sulphur release from the raw material due to combustion of alternative fuels has been studied on a pilot scale setup that simulates the cement kiln material inlet. Investigations of the effect of fuel particle size and the degree of fuel devolatilisation have been made. The industrial scenarios presented in Figure 1 were used as guides for the experiments where non- or partly converted alternative fuels may fall into the rotary kiln.

Equipment

The experiments were performed in a high temperature rotary drum, which simulates the process conditions at the material inlet end of an industrial rotary kiln (Figure 2).[3] The rotary drum is electrically heated by a furnace. Gas can be introduced into the chamber furnace through a hole in the roof in order to have a controlled atmosphere. An externally placed gas pump transports the gas through the rotating drum and the steel tube, after which the gas exiting the reactor, which includes SO_2, CO, CO_2, and O_2, is cooled and analysed. The chamber furnace door is equipped with a window for visual inspection, two holes for thermocouples and a centrally placed water-cooled tube for the introduction of solid fuels. The solid fuels are placed in a sample container which can be pushed into the hot rotary drum or pulled out to the water cooled tube.

The experiments were performed with a constant flow of 100NL/min of air mixed with N_2 at 900°C. The cement raw materials were based on a synthetic mixture of coarse quartz sand with a particle size ranging from 0.5-0.71mm and 2wt% $CaSO_4$. The mixture was placed in the rotary drum in the desired volumetric filling degree of 5%.

Fuels

Pine wood cylinders with diameters of 19, 13, and 8mm were used as fuels. All cylinders had a length of 25mm. The fuel analysis and the lower heating value (LHV) are shown in Table 1. All experiments used the same energy input of 55kJ. This means the mass of the wood cylinders was kept constant, therefore five cylinders of 8mm diameter, two cylinders of 13mm diameter and one cylinder of 19mm were used. Wood char made from the pine wood cylinders was pyrolised in a horizontal tube reactor under a nitrogen atmosphere for 20min at 300, 500, 700, and 900°C in order to obtain wood char with different degree of volatiles. The degree of devolatilisation was calculated on the basis of the volatile concentration before and after pyrolysis, which is 25% for the wood char at 300°C, 90% for the wood char at 500°C and 100% for the wood char made at 700°C and 900°C.

Proximate analysis (wt% a.r.)			Ultimate analysis (wt% a.r.)				LHV (MJ/kg a. r.)
VM	FC	Ash	C	H	N	S	
76.8	22.7	0.5	44.7	5.54	0.04	-	15.97

Left - Table 1: Fuel analysis and lower heating value (LHV) for pine wood cylinders.
a.r. = as received
VM = volatile matter
FC = fixed carbon (char)

The total release of SO_2 was calculated for each experiment and quantified by integration of the SO_2 concentration in the gas over the relevant time interval according to Equation 1.

$$n_{Sulphur\ release} = \int_0^t y_{SO_2} dt \cdot 10^{-6} \cdot \frac{PV}{RT}$$

$n_{sulphur\ release}$ = total SO_2 release (mol)
y_{SO2} = SO_2 concentration (ppmV)
R = The Ideal Gas Constant (8.314J/molK),
P = Atmospheric pressure (Pa)
T = Temperature (K)
V = Gas flow (m^3/s)

Left - Equation 1: Total SO_2 release is quantified by integration of the SO_2 concentration over time.

Results

The influence of the pine wood particle size and oxygen content on SO_2 release from the synthetic raw materials at conditions corresponding to the kiln inlet is illustrated in Figure 3. For all particle sizes, SO_2 release decreases with increasing oxygen concentration. The high oxygen concentration in the atmosphere may react with the reducing agent and thereby lower its concentration. Another possibility is that the oxygen may influence the reductive decomposition reactions.

The experiments performed with the wood char at different temperatures showed that only the non-pyrolised wood and wood char made at 300 and 500°C caused SO_2 release. No SO_2 was measured during the experiments with wood char made at 700 and 900°C. Figure 4 presents the total SO_2 release from the raw materials as a function of the particle size of the combusted non-pyrolised wood and wood char made at 300 and 500°C. The results show that the SO_2 release decreases with decreasing degree of devolatilisation.

Scan the QR code below or enter the bit.ly code into your web-brower to read the industrial scale results and conclusion....

See more http://bit.ly/1q9LrUo

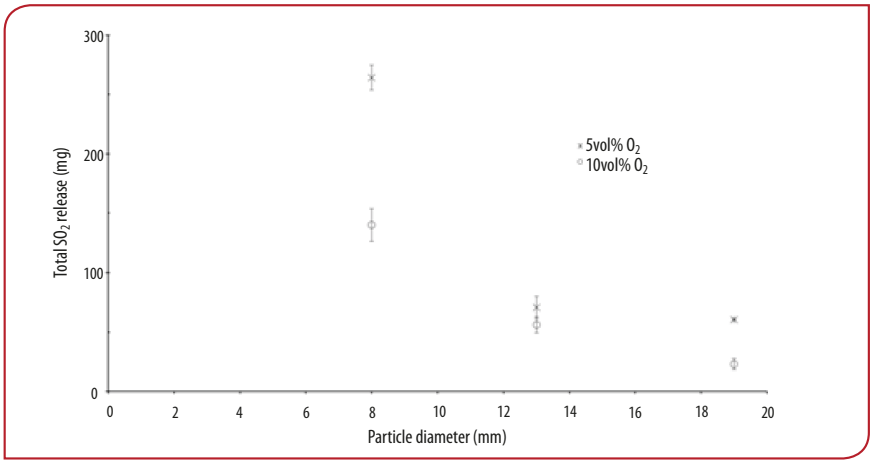

Right - Figure 3: Effect of particle diameter of pine wood cylinders and oxygen content on SO_2 release from the raw materials due to combustion. Energy input of 55kJ in each experiment. Experimental conditions: 900°C, 5% fill degree, 2wt% $CaSO_4$, 100NL/min, 6rpm.

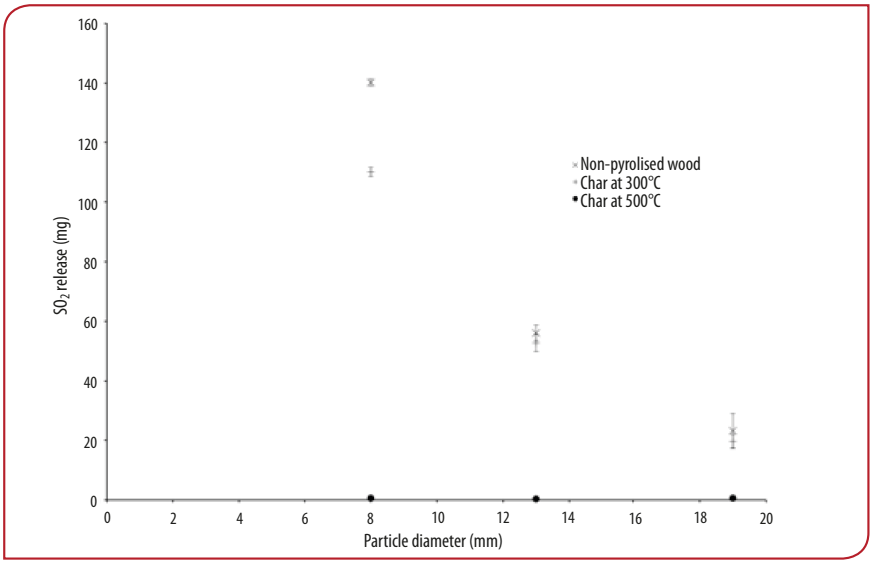

Right - Figure 4: SO_2 release from the raw materials due to the combustion of different particle size wood and wood char at 300 and 500°C. Experimental conditions: 900°C, 5% fill degree, 2wt% $CaSO_4$, 100NL/min, 10vol% O_2 in N_2, 6rpm.

Additionally, the char combustion step for the wood chars does not provoke SO_2 release. This is contradictory to the general experience when unburned petcoke is admitted to the kiln inlet causing a dramatic increase in sulphur circulation.[4]

It was also observed that SO_2 release increases with decreasing particle size. For example, the SO_2 concentration peak reached higher values for the 8mm pine wood particles than for the larger particle dimensions under the same conditions (Figure 5). This is because the smallest particles are heated faster and release the volatile gases faster and in higher concentrations. Consequently, stronger local reducing conditions are formed. The total SO_2 release increases, as previously discussed, with decreasing particle size of non-pyrolised wood and wood char made at 300°C. There is a big difference in the SO_2 release for wood char made at 300 and 500°C due to the degree of fuel conversion at these temperatures. The total SO_2 release for the wood char made at 500°C is below 1mg for all of the different fuel particle sizes. This is due to the high degree of devolatilisation, 90%, whereby few volatile gases are released.

Industrial investigation of SO_2 release

Industrial scale measurements that investigate the relationship between organic carbon in the bottom stage cyclone and SO_2 in the kiln inlet were conducted. Organic carbon from the hot meal is believed to be directly related to unburned calciner fuel. Unburned fuel particles may be carried upwards with the gas flow through the calciner and transported into the bottom stage cyclone. The char particles may therefore arrive in the kiln inlet and their subsequent combustion may cause the release of SO_2.

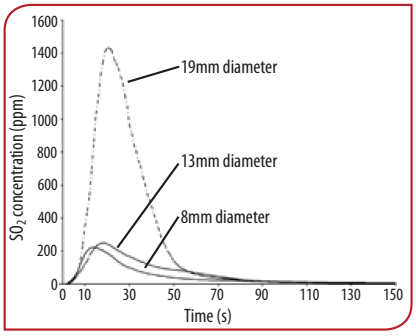

Left - Figure 5: SO_2 concentrations from the raw materials due to combustion of the different dimensions of pine wood cylinders. Energy input of 55kJ in each experiment. Experimental conditions: 900°C, 5% fill degree, 5vol% O_2 in N_2, 2wt% $CaSO_4$, 100NL/min, 6rpm.

The investigation was carried out at a cement plant with two separate line calciners. The strings, named A and B, are identical and consistent with a calciner and three cyclones (Figure 6).

The raw materials are wet and form a slurry that is introduced into the dryer crusher where it is dried and ground. The dry raw materials are then carried upwards to the top cyclone by a gas stream. The gases in the preheater tower are bypassed from the second cyclone to the dryer crusher before going to the top cyclone, which works as gas/dust separator. The hot air from the clinker cooler goes to the calciner and the rotary kiln gases are mixed with the calciner outlet gases.

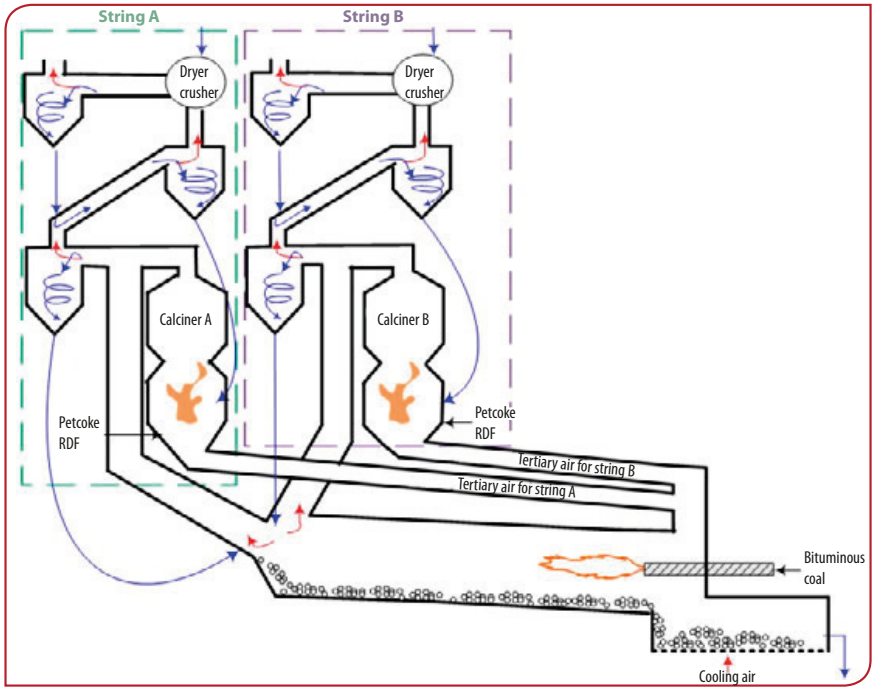

Left - Figure 6: Scheme of the industrial cement plant where the investigation took place.

Right - Table 2: Fuel analyses and lower heating values (LHV) of petcoke, RDF and tyre chips that the cement plant used in the calciner and riser duct.
a.r. = As received
VM = Volatile matter
FC = Fixed carbon (char)

	Moisture (wt% a.r.)	Proximate analysis (wt% a.r.)			Ultimate analysis (wt% a.r.)					LHV (MJ/kg a.r.)
		VM	FC	Ash	C	H	N	Cl	S	
Petcoke	1.1	13.0	84.9	1.0	86.9	3.71	-	-	5.85	34.779
RDF	24.1	61.6	6.6	7.7	45.8	6.31	0.67	0.54	0.40	19.330
Tyre chips	-	64	3.5	2.5	80.5	7.01	0.20	-	1.47	34.199

Right - Table 3: O_2, CO and SO_2 concentration range of the gas measurements in the kiln inlet and preheaters, the production range, the energy consumption of the calciner and the temperature of the calciner for normal operation. Target calciner temperature: 875°C.

O_2 kiln inlet (vol%)	CO kiln inlet (vol%)	SO_2 kiln inlet (ppm)	O_2 preheater (vol%)	CO preheater (vol%)	Production each string (t/day)	Energy calciner (MJ/kg clinker)	T calciner (°C)
5-9	≤0.02	0	4-10	0-0.2 spikes to 0.4	2000-2500	2.93	881-1013

The fuels used in the calciners are petcoke, plastic and paper-based refused derived fuel (RDF). Sometimes tyre chips are fired in the riser duct from 2m above the kiln inlet. The fuel analyses of petcoke, RDF and tyre chips are specified in Table 2.

The cement plant controlled the calciner temperature by adjusting the flow of petcoke. In order to estimate the amount of RDF fired, the percentage of fuel input to each calciner originating from petcoke is calculated by Equation 2. The percentage remaining in the calciner after firing corresponds to RDF.

Two tests were performed at the plant:

- **Test 1**: Increase of RDF firing in calciner A (from 37 to 85% RDF of calciner fuel input, while petcoke flow was decreased from 4.6t/hr to 1.1t/hr). No tyre chips were fired.
- **Test 2**: Increase tyre chips injection in the kiln inlet from 1 to 1.5t/hr.

Hot meal samples were taken from the bottom cyclone of strings A and B during eight sampling days over a one month period. The hot meal samples were taken with an FLSmidth sampler to ensure homogeneous cooling and to avoid oxidation of the carbon. The O_2, CO and SO_2 concentrations in the kiln inlet, CO and O_2 out of the preheater, the petcoke and tyre chips flows and the calciner temperatures were recorded (Table 3).

Below - Equation 2: The estimated amount of RDF fired was calculated according to the percentage of fuel input to each calciner that originated from the petcoke.

$$petcoke\,\% = \frac{F_{petcoke} \cdot LHV_{petcoke}}{E_{calciner} \cdot P} \cdot 100$$

$F_{petcoke}$ = Flow of petcoke (t/hr) fired into the calciner
$LHV_{petcoke}$ = Lower heating value of the petcoke, which is approximately 33.5MJ/kg (the lower heating value for petcoke is 34.78MJ/kg according to the analysis, but the fired petcoke is mixed with unspecified fuels)
$E_{calciner}$ = Calciner energy consumption, which is estimated to be 2.93MJ/kg clinker
P = Production of each string (t/hr)
petcoke % = Petcoke fired as fuel input (%)

The SO_2 gas measurement in the kiln inlet always recorded 0ppm of SO_2 during the sampling period (Table 3). Therefore, the organic carbon variation from the hot meal samples cannot be related to the SO_2 in the kiln inlet. However, it may be possible that the content of organic carbon measured in the hot meal under such conditions provokes minor SO_2 release that the analyser was unable to detect.

The organic carbon from the hot meal samples correlates to the percentage of fuel input to each calciner coming from the petcoke (Figure 7). The results show that the levels of organic carbon increased when the petcoke content was increased and the RDF content was reduced. As such, it may be concluded that the organic carbon in the unconverted carbon comes from the petcoke, since it has a higher concentration of fixed carbon than RDF. According to Figure 7, it would be advantageous to fire higher content of RDF, however, the cement plant found that firing large amounts of RDF caused process control problems.

The volatility of the SO_2 in the kiln was assessed using the sulphur evaporation factor $\varepsilon_{sulphur}$ (Equation 3). The dust circulation from the coolers and the kiln to the bottom stage cyclone was disregarded. The clinker was analysed every second hour. It was assumed that the clinker analysis corresponds to the hot meal sample after 30min from the time of sampling, which correlates approximately to the residence time of the solid material in the rotary kiln. Figure 8 shows $\varepsilon_{sulphur}$ as a function of the organic carbon of the hot meal samples. There is no clear relationship between organic carbon and $\varepsilon_{sulphur}$ in the kiln. This supports the observation in the wood char experiments where the SO_2 volatility was not affected by char combustion.

Conclusions

The combustion of alternative fuels in direct contact with the kiln bed increases sulphur recirculation when they are fired directly into the kiln inlet or when they end up in the kiln inlet because they have not reached full conversion in the calciner.

The experimental work shows that SO_2 release from the raw materials takes place primarily during devolatilisation and not during char combustion when firing biomass as an alternative fuel. The industrial scale observations did not show any correlation between $\varepsilon_{sulphur}$ and the organic carbon content in the hot meal samples, the fraction of the calciner fuel fired as RDF, or tyre chip firing in the kiln inlet.

The pilot plant experiments indicate that SO_2 release decreases with increasing oxygen concentration. Smaller particles in the kiln charge increase SO_2 release because they are heated faster and thus release the volatile gases faster and in higher concentrations. However, when admitted to the calciner, fine RDF particles will generally burn in suspension, thereby never reaching the kiln charge, whereas larger particles will. When firing fuel directly into the back end of the kiln the experimental results explain why it may be more advantageous to use coarse chips or whole tyres rather than finer particles.

References

1. Cembureau, *"Sustainable cement production: Co-processing of alternative fuels and raw materials in the cement industry,"* 2009.

2. Mokrzycki, E. and Uliasz-Bochenczyk, A., *"Alternative fuels for the cement industry,"* Appl. Energy, 74, 95, 2003.

3. Nielsen, A.R., *"Combustion of large solid fuels in cement rotary kilns,"* PhD Thesis, Technical University of Denmark, Kgs. Lyngby, Denmark, 2012. ISBN: 978-87-92481-66-5.

$$\varepsilon_{sulphur} = \frac{[SO_3]_{hot\,meal,\,LOI\,free} - [SO_3]_{clinker}}{[SO_3]_{hot\,meal,\,LOI\,free}}$$

$\varepsilon_{sulphur}$ = Sulphur evaporation factor
$[SO_3]_{hot\ meal,\ LOI\ free}$ = SO_3 concentration in hot meal on loss on ignition (LOI) free basis (wt%)
$[SO_3]_{clinker}$ = SO_3 concentration in the clinker (wt%)

Left - Equation 3: The volatility of the SO_2 in the kiln is assessed using the sulphur evaporation factor $\varepsilon_{sulphur}$.

4. Nielsen, P. B. and Jepsen, O.L., *"An overview of the formation of SO_x and NO_x in various pyroprocessing systems,"* IEEE Cement Industry Technical Conference, 1990.

Acknowledgments

This project is established within the framework of the advanced technology platform 'New Cement Production Technology,' founded by the Danish National Advanced Technology Foundation, FLSmidth A/S and the Technical University of Denmark.

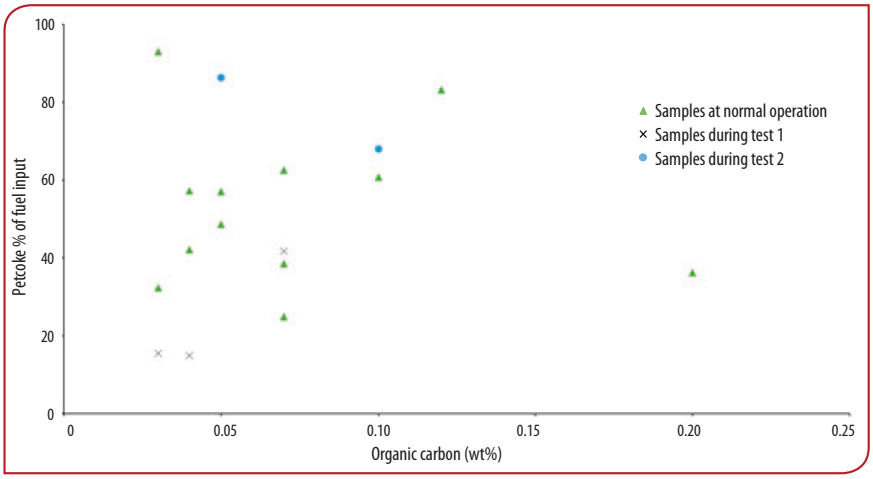

Left - Figure 7: Relationship between the percentage of petcoke as fuel input in the calciner and the organic carbon of hot meal samples.

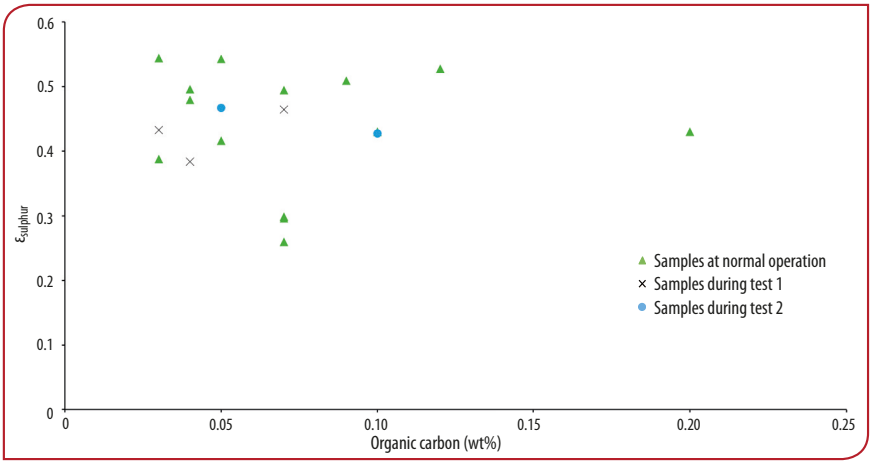

Left - Figure 8: Sulphur evaporation factor $\varepsilon_{sulphur}$ as a function of the organic carbon of hot meal samples during normal operation and for tests 1 and 2.

Centre of Combustion and Harmful Emission Control
Department of Chemical and
Biochemical Engineering
Technical University of Denmark
Søltofts Plads, Building 229
DK-2800 Kgs. Lyngby
Denmark

Phone: +45 4525 2800
Fax: +45 4525 4588
Web: www.chec.kt.dtu.dk

ISBN : 978-87-93054-48-6